

## Copyright Undertaking

This thesis is protected by copyright, with all rights reserved.

**By reading and using the thesis, the reader understands and agrees to the following terms:**

1. The reader will abide by the rules and legal ordinances governing copyright regarding the use of the thesis.
2. The reader will use the thesis for the purpose of research or private study only and not for distribution or further reproduction or any other purpose.
3. The reader agrees to indemnify and hold the University harmless from and against any loss, damage, cost, liability or expenses arising from copyright infringement or unauthorized usage.

### IMPORTANT

If you have reasons to believe that any materials in this thesis are deemed not suitable to be distributed in this form, or a copyright owner having difficulty with the material being included in our database, please contact [lbsys@polyu.edu.hk](mailto:lbsys@polyu.edu.hk) providing details. The Library will look into your claim and consider taking remedial action upon receipt of the written requests.

**DEVELOPMENT OF PRESSURE MONITORING  
UNDERGARMENT FOR SCOLIOTIC BRACE  
TREATMENT**

LEE KA PO

PhD

The Hong Kong Polytechnic University

2024

The Hong Kong Polytechnic University

School of Fashion and Textiles

**Development of Pressure Monitoring Undergarment  
for Scoliotic Brace Treatment**

Lee Ka Po

A thesis submitted in partial fulfilment of the requirements for the  
degree of Doctor of Philosophy

August 2023

## **CERTIFICATE OF ORIGINALITY**

I hereby declare that this thesis is my own work and that, to the best of my knowledge and belief, it reproduces no material previously published or written, nor material that has been accepted for the award of any other degree or diploma, except where due acknowledgement has been made in the text.

\_\_\_\_\_ (Signed)

\_\_\_\_\_Lee Ka Po\_\_\_\_\_ (Name of student)

## ABSTRACT

Monitoring force and pressure are critical for effective compression therapy, such as bracing, which is the most prevalent type of treatment for adolescent idiopathic scoliosis (AIS) patients with a Cobb's angle greater than  $25^{\circ}$ . The goal of this treatment is to passively correct spinal abnormalities by exerting pressure. However, because of ambiguous brace effectiveness, the applied pressure depends on the judgment of the orthotist. Not only can result in physical injury, excessive pressure also negatively impacts compliance and quality of life. A variety of sensors is available to measure the force and pressure exerted by braces, but they have some limitations, including inflexibility, small measuring ranges, time delays, and difficulty in application. To prevent these issues, a pressure monitoring undergarment is developed by inserting 14 fibre bragg gratings (FBG) sensors into a knitted undergarment. The primary objective of this pressure monitoring undergarment is to deliver reliable sensor readings while placing a paramount emphasis on optimizing wearer comfort.

This study consists of four main components including (a) a review of the development of textile-based fibre optic sensors (TFOSs) for health monitoring, in regard of their features, applications, and integration methods, (b) an examination of the main factors affecting the wear comfort of undergarments, (c) the design and development of a flexible pressure monitoring undergarment, (d) the formulation of a simulation model to examine the how the spine response to brace pressure.

TFOSs is one of the most appropriate means of obtaining close-to-body measurements because they are very flexible and lightweight and have electromagnetic immunity while maintaining high strain sensitivity. Although they have gained increasing receptivity in health monitoring, there is a lack of comprehensive understanding of the knowledge structure and research trends

in this field. This study stands out by providing an objective and systematic literature review on TFOs for health monitoring, coupled with a citation network analysis (CNA). The study brings attention to the largest research cluster, "Flexible sensors for vital signs monitoring," with a specific emphasis on respiratory monitoring. This insight has the potential to shape future research directions and contribute to advancements in health monitoring technologies. Additionally, one of the most popular methods was to embed fibre Bragg grating (FBG) sensors into a flexible silicone with a curvilinear shape, which enhanced the fibre flexibility, robustness, and compatibility of the sensor with the skin's surface. Therefore, the pressure monitoring undergarment is also developed by using this method.

To create an undergarment with high comfort, it is necessary to investigate the main factors that affect wear comfort in terms of tactile and thermal sensations. A series of experiments including physical experiments, KES-FB measurements, and a wear trial were conducted on seven conventional undergarments. The results indicated that lighter, thinner, and low stitch density fabrics constructed with uniform filaments increased breathability and enhanced moisture wicking. Additionally, lighter and thinner materials with a higher percentage of elastane, finer yarn, and uniform and long fibres offered a softer, smoother, and cooler hand feel. Moreover, the pure cotton material appeared to more regulate body temperature as the resultant undergarment facilitated a higher rate of perspiration despite clinging. These results serve as a useful reference for developing the pressure-monitoring undergarment.

To investigate the relationship between normal force and strain sensed by using FBG sensors, the protocol of pressure-monitoring undergarment was developed by inserting four silicone-embedded FBG sensors into a knitted undergarment via the inlay method. The proposed design offers several advantages over existing methods, including ease of use and adaptability to adolescents with different body shapes, without requiring any additional procedures prior to

treatment. Additionally, the instant data acquisition and overall pressure distribution allow the tightness to be adjusted and monitored during the fitting process. After conducting a bracing stimulation on artificial skin, the experimental results showed that the sensors embedded in the silicone membranes achieved enhanced sensitivity to force, as well as flexibility and softness. Additionally, by assessing the degree of FBG response to a range of standardised forces, the linearity ( $R^2$ ) between the shift in the Bragg wavelength and force was found to be above 0.95, with an ICC of 0.97, when tested on a soft surface. The implications of this study are particularly relevant in healthcare, specifically in the fitting processes for bracing treatment in AIS patients because it offers a more objective approach to determine the optimal bracing pressure.

The formulation of a biomechanical model that simulates the forces exerted by a brace can aid in the examination of how the spine responds to brace pressure. Therefore, a FE model based on Fok (2020)'s FE model was constructed, which consisted of a body torso, ribs, a spine, and a sternum that corresponded to the X-rays of the recruited subject. Unlike Fok (2020)'s FE model, the loading condition was increased from 2 to 14 to study how the overall pressure distribution affects the spinal corrective effect. Since it is impossible to recruit the same AIS subject to do the brace pressure measurement, a validated soft mannequin was employed to the pressure test by using the pressure monitoring undergarment with 14 FBG sensing points. To validate the model, the in-brace vertebrae position and Cobb's angle on the FE model were compared to that on X-rays. Their correlation coefficient is found to be 0.90, which is highly correlated. In addition, both the X-ray image and the FE model show a reduction in the Cobb's angles in the thoracic (T5 to T11) and lumbar (T11 to L3) regions. These results are comparable to the clinical study that conducted by Fok (2020). Therefore, it is believed that the

implementation of the biomechanical model in this study effectively overcomes the challenges associated with conducting human wear trials to assess the efficacy of bracing.

The research results in this study provided valuable insights into the research domains and trends in TFOSs for health monitoring purposes. This understanding is crucial for researchers and practitioners to navigate the existing knowledge and identify areas for further investigation. Additionally, the study suggests desired properties of summer undergarment. The identified relationships between fabric specifications offer insights for developing summer underwear that prioritizes breathability, moisture-wicking, and a cooler feel. Moreover, the study stands out for its originality and novelty in developing a pressure monitoring undergarment using silicone-embedded FBG sensors and warp-inlay method. It overcomes the limitations of existing sensors, such as lack of elasticity and inconvenience, absence of instant and overall pressure distribution. In addition, the simulation model could be used to examine how the spine responds to the exerted brace pressure and predict the degree of in-brace correction. The research output could be further extended to determine ideal bracing pressure levels, thus preventing AIS patients from having to endure excessive pressure, while maintaining an appropriate amount of bracing force in order to halt curve progression and reduce the risk of pressure-related injuries.



## PUBLICATIONS ARISING FROM THE THESIS

### Journal papers

Lee, K.-P., Yip, J., Yick, K.-L., Lu, C., & Lo, C. K. (2022). Textile-based fiber optic sensors for health monitoring: A systematic and citation network analysis review. *Textile research journal*, 92(15-16), 2922-2934.

Lee, K.-P., Yip, J., Yick, K.-L., Lu, C., Lu, L., & Lei, Q.-W. E. (2023). A Novel Force-Sensing Smart Textile: Inserting Silicone-Embedded FBG Sensors into a Knitted Undergarment. *Sensors*, 23(11), 5145. <https://doi.org/10.3390/s23115145>

Lee, K.-P., Lu C., L., Hui K.-T., Zhang J., Yick, K.-L., & Yip, J. (2024). Morphing Torso Mannequin for Pressure Measurement and Scoliotic Brace Efficacy Evaluation. *Fashion and Textiles*. (In submission).

### Conference papers

Lee, K.-P., Yip, J., Yick, K.-L., & Lu, C. (2021). *Development of Pressure Monitoring Undergarment for Scoliotic Brace Treatment (Poster Presentation)*. Postgraduate Conference on Interdisciplinary Learning: Re-Imagining Postgraduate Studies in the 21st Century and Beyond. Lingnan University. Hong Kong, 26-27, March.

Lee, K.-P., Yip, J., & Yick, K.-L. (2022). Investigating the Factors Affecting the Thermal and Tactile Comfort of Summer Undergarments. *Human Factors for Apparel and Textile Engineering*, 32, 46.

Lee, K.-P., Yip, J., Yick, K.-L., & Lu, C. (2023). *Development of a smart force-sensing undergarment for the Adolescent Idiopathic Scoliosis Patients (Poster Presentation)*. 14th International Conference on Applied Human Factors and Ergonomics, California, USA. 20-24 July.

## **ACKNOWLEDGEMENTS**

I would like to express my utmost appreciation and heartfelt gratitude to my Chief Supervisor, Prof. Joanne YIP, at the School of Fashion and Textiles, The Hong Kong Polytechnic University. Her unwavering support, patient guidance, invaluable advice, and profound insight have left a lasting impression on me. Prof. Joanne YIP has been instrumental in providing me with trust, support, and the freedom to explore my research while offering constructive feedback that has been indispensable to the completion of my postgraduate studies. Without her inspiration, mentoring, and encouragement, this study would have been an arduous undertaking.

Additionally, I would like to extend my deepest thanks to my co-supervisors, Prof. Kit-Lun YICK at the School of Fashion and Textiles, The Hong Kong Polytechnic University, and Prof. Chao LU at the Department of Electronic and Information Engineering, The Hong Kong Polytechnic University. Their continuous support, insightful comments, and encouragement have played a vital role in shaping my research journey. Their expertise and guidance have been invaluable, and I am truly grateful for their contributions.

I am also grateful to Dr. Alice Zhang and Dr. Cynthia Liang at the School of Fashion and Textiles, The Hong Kong Polytechnic University, for their invaluable advice on mechanical and finite element analysis and for providing a conducive research environment throughout my postgraduate studies. Moreover, I am greatly indebted to Mr. Linyue LU at Department of Electrical Engineering, The Hong Kong Polytechnic University for providing professional advice and technical support on manufacturing the fibre Bragg grating sensors.

I would like to extend my heartfelt gratitude and appreciation to my research colleagues and teammates, namely Dr. Queenie Fok, Dr. Jess Chan, Ms. Lily Kwan, Ms. Hallie Cheung, Ms. Karolyn, Ms. Claire Chung, Ms. Charlotte Wong, and Ms. Linda Sit. Their immeasurable help, continuous encouragement, and unwavering support have been instrumental in my research journey. Their dedication, expertise, and camaraderie have made this experience truly meaningful and rewarding.

I would also like to express my deepest appreciation to my family members and friends for their unconditional love and unwavering support throughout the years of my study. Their encouragement and belief in my abilities have been a constant source of motivation, and I am truly grateful for their presence in my life.

Furthermore, I would like to acknowledge the financial support provided by the Departmental Grant from the School of Fashion and Textiles at The Hong Kong Polytechnic University. This support has played a crucial role in the successful completion of my research project, and I am sincerely grateful for the opportunity it has afforded me.

In conclusion, I would like to express my profound gratitude to all those who have contributed to my research and thesis. The collective support and encouragement I have received have been invaluable, and I am humbled by the generosity and kindness shown to me throughout this journey.

# TABLE OF CONTENTS

<b>ABSTRACT .....</b>	<b>I</b>
<b>PUBLICATIONS ARISING FROM THE THESIS .....</b>	<b>V</b>
<b>ACKNOWLEDGEMENTS.....</b>	<b>VI</b>
<b>TABLE OF CONTENTS.....</b>	<b>VIII</b>
<b>LIST OF FIGURES .....</b>	<b>XIV</b>
<b>LIST OF TABLE.....</b>	<b>XIX</b>
<b>LIST OF ABBREVIATIONS.....</b>	<b>XXI</b>
<b>CHAPTER 1 INTRODUCTION .....</b>	<b>1</b>
<b>1.1 Research background .....</b>	<b>1</b>
<b>1.2 Problem statement.....</b>	<b>4</b>
1.2.1 Ambiguous brace effectiveness without standardised pressure .....	4
1.2.2 Ambiguous overall pressure distribution.....	5
1.2.3 Absence of instant pressure distribution.....	5
1.2.4 Issues with the use of an additional procedure .....	6
<b>1.3 Aim and research objectives.....</b>	<b>6</b>
<b>1.4 Project originality and significance .....</b>	<b>7</b>
<b>1.5 Outline of the thesis.....</b>	<b>9</b>

<b>CHAPTER 2 LITERATURE REVIEW .....</b>	<b>12</b>
<b>2.1 Introduction .....</b>	<b>12</b>
<b>2.2 Introduction to adolescent idiopathic scoliosis .....</b>	<b>12</b>
2.2.1 Definition.....	12
2.2.2 Types of spinal curvatures .....	13
2.2.3 Trends and potential problems of AIS.....	15
<b>2.3 Scoliotic treatments for AIS patients.....</b>	<b>16</b>
2.3.1 Types of scoliotic braces .....	19
2.3.2 Three-point pressure system .....	27
<b>2.4 Bracing compliance .....</b>	<b>28</b>
2.4.1 Correlation between bracing compliance and effectiveness.....	28
2.4.2 Correlation between brace compliance and quality of life .....	30
<b>2.5 Existing force/pressure sensors and their limitations .....</b>	<b>33</b>
2.5.1 Time-recording pressure sensor.....	34
2.5.2 Wireless force sensor.....	35
2.5.3 Pressurex® pressure film.....	36
2.5.4 Teksens® .....	37
2.5.5 BodiTrak® pressure mat.....	38
<b>2.6 Smart textiles .....</b>	<b>39</b>
2.6.1 Advantages of textile-based fibre optic sensors .....	41
2.6.2 Types of optical fibres .....	42

2.6.3 Classification of fibre optic sensors.....	43
2.6.4 Applications.....	46
<b>2.7 Materials for comfortable pressure monitoring undergarments.....</b>	<b>52</b>
2.7.1 Soft and hydrophilic materials.....	52
2.7.2 Cooling material .....	53
<b>2.8 Construction method of finite element model.....</b>	<b>55</b>
<b>2.9 Summary.....</b>	<b>57</b>
 <b>CHAPTER 3 TEXTILE-BASED FIBRE OPTIC SENSORS FOR HEALTH MONITORING.....</b>	 <b>60</b>
3.1 Introduction .....	60
3.2 Methodology .....	62
3.3 Result.....	68
3.3.1 Descriptive statistics .....	68
3.3.2 Research domains .....	71
3.3.3 Integration methods of fibre optic sensors and textiles .....	80
3.4 Future trends and challenges .....	84
3.5 Limitations .....	86
3.6 Summary.....	87

**CHAPTER 4 FACTORS THAT AFFECT WEAR COMFORT OF SUMMER UNDERGARMENT .....88**

**4.1 Introduction.....88**

**4.2 Materials and methods .....89**

4.2.1 Materials and conditioning .....89

4.2.2 Thermal comfort .....91

4.2.3 Tactile comfort .....93

4.2.4 Wear trial .....96

**4.3 Results .....96**

**4.4 Discussion.....102**

4.4.1 Thermal comfort .....103

4.4.2 Tactile comfort .....107

4.4.3 Total hand value and wear trial .....110

**4.5 Summary.....111**

**CHAPTER 5 SMART TEXTILE: INSETING SILICONE-EMBEDDED FBG SENSORS INTO KNITTED UNDERGARMENT .....112**

**5.1. Introduction.....112**

**5.2. Methodology .....115**

5.2.1 Construction of the smart textile: Inlaying FBG sensors into highly elastic knitted undergarment .....115

5.2.2 Embedding FBG sensors into silicone membranes .....116

5.2.3 Wear trial to simulate bracing .....118

5.2.4 Data analysis.....121

<b>5.3 Result and Discussion .....</b>	<b>122</b>
5.3.1 Smart textile design .....	122
5.3.2 Linearity of silicone-embedded FBG sensors and bare FBG sensors .....	123
5.3.3 Linearity and reliability of silicone-embedded FBG sensors and Pliance®-X pressure sensor .....	125
5.3.4 Challenges of conventional integration methods.....	127
<b>5.4. Limitations of experiment .....</b>	<b>129</b>
<b>5.5. Summary.....</b>	<b>131</b>
 <b>CHAPTER 6 DESIGN AND DEVELOPMENT OF SOFT MANNEQUIN .....</b>	 <b>132</b>
<b>6.1 Introduction.....</b>	<b>132</b>
<b>6.2 Methodology .....</b>	<b>134</b>
6.2.1 Construction of the proposed mannequin .....	134
6.2.2 Validation of the proposed mannequin.....	141
<b>6.3 Result and Discussion .....</b>	<b>144</b>
6.3.1 Body contour of proposed mannequin.....	144
6.3.2 Spinal curvature of proposed mannequin .....	145
6.3.3 Pressure test on proposed mannequin.....	148
6.3.4 Spinal corrective effect on proposed mannequin .....	148
<b>6.4 Challenges and Limitations.....</b>	<b>151</b>
<b>6.5 Summary.....</b>	<b>152</b>



<b>CHAPTER 7 BIOMECHANICAL SIMULATION MODEL .....</b>	<b>154</b>
<b>7.1 Introduction.....</b>	<b>154</b>
<b>7.2 Methodology .....</b>	<b>155</b>
7.2.1 FE model construction.....	155
7.2.2 Pressure measurement on proposed mannequin.....	159
7.2.3 Validation .....	164
<b>7.3 Result and discussion.....</b>	<b>165</b>
7.3.1 Brace force detected by the pressure monitoring undergarment .....	165
7.3.2 Comparison of the spinal corrective effect between FEA and clinical study.....	168
<b>7.4 Limitations.....</b>	<b>173</b>
<b>7.5 Summary.....</b>	<b>174</b>
 <b>CHAPTER 8 CONCLUSIONS AND SUGGESTIONS FOR FUTURE RESEARCH</b>	<b>175</b>
<b>8.1 Conclusions .....</b>	<b>175</b>
<b>8.2 Limitations of the study .....</b>	<b>179</b>
<b>8.3 Suggestions for future research.....</b>	<b>181</b>
<b>References.....</b>	<b>182</b>

## LIST OF FIGURES

<b>Figure 1. 1</b> Study flowchart.....	9
<b>Figure 2. 1</b> Determination of lumbar modifiers (Lenke et al., 2001).....	14
<b>Figure 2. 2</b> Determination of sagittal thoracic modifier: <b>(a)</b> Hypokyphosis (-), <b>(b)</b> Normokyphosis (N) and <b>(c)</b> Hyperkyphosis (+). .....	15
<b>Figure 2. 3</b> Before and after surgery. ....	19
<b>Figure 2. 4</b> Milwaukee brace.....	21
<b>Figure 2. 5 (a)</b> Lyon brace, and <b>(b)</b> Preliminary plaster cast .....	22
<b>Figure 2. 6</b> Boston brace .....	23
<b>Figure 2. 7</b> Chêneau brace.....	24
<b>Figure 2. 8</b> SpineCor .....	25
<b>Figure 2. 9</b> Functional intimate apparel. ....	26
<b>Figure 2. 10</b> Three-point pressure system. ....	27
<b>Figure 2. 11</b> Correlation between TLSO treatment success and brace wear time .....	28
<b>Figure 2. 12</b> Correlation between treatment success and brace wear time .....	29
<b>Figure 2. 13</b> Bracing effects: good vs bad compliance groups .....	30
<b>Figure 2. 14</b> Custom-moulded TLSO with embedded pressure switches and data logger .....	35
<b>Figure 2. 15</b> Wireless sensing system and dimensions of the logger unit .....	36
<b>Figure 2. 16</b> Pressurex® pressure film <b>(a)</b> mechanism, <b>(b)</b> before (left) and after (right) using Topaq® imaging system, and <b>(c)</b> measurement process .....	37
<b>Figure 2. 17</b> The textsens® sensor and loadpad® app.....	38
<b>Figure 2. 18 (a)</b> BodiTrak® system <b>(b)</b> Structure of the BodiTrak® pressure mat, and <b>(c)</b> Pleats created by BodiTrack® pressure mat. ....	39

<b>Figure 2. 19</b> Existing use of smart textiles: <b>(a)</b> Adidas Men's Workout Climalite Pants, <b>(b)</b> Nike Adapt BB sports shoes, and <b>(c)</b> Levi's Google smart jean jacket.....	41
<b>Figure 2. 20</b> Working principles of FBG sensor.....	46
<b>Figure 2. 21</b> Illuminous knitted fabric made with polymer optical fibres .....	47
<b>Figure 2. 22</b> <b>(a)</b> Sensor harness, <b>(b)</b> macro-bending sensor inserted in the crochet fabric, <b>(c)</b> POF OTDR sewn onto elastic textile, and <b>(d)</b> FBG sensor embroidered onto elastic band .....	49
<b>Figure 2. 23</b> <b>(a)</b> Schematic diagram of sensing glove, <b>(b)</b> outer side of sensing glove, and <b>(c)</b> inside of sensing glove.....	50
<b>Figure 2. 24</b> 2 x 2 matrix with four optical fibre intersections .....	51
<b>Figure 2. 25</b> Schematic diagram of silica gel-based smart insole with four FBG sensors.....	52
<b>Figure 2. 26</b> FE models: <b>(a)</b> geometric models of the torso, spine and brace are constructed; <b>(b)</b> material properties and the type of element and meshing are defined; <b>(c)</b> the loading conditions are defined; <b>(d)</b> the boundary conditions are defined; and <b>(e)</b> the FE models are analysed: stress distribution of torso, spine, and brace. ....	57
<b>Figure 3.1</b> Article distribution by year.....	68
<b>Figure 3.2</b> Application of TFOSs.....	69
<b>Figure 3. 3</b> Article distribution by research field. ....	70
<b>Figure 3. 4</b> Citation network of articles in sample.....	71
<b>Figure 3. 5</b> <b>(a)</b> Sensing belt , and <b>(b)</b> sensing harness. ....	73
<b>Figure 3. 6</b> Arrangement of 12 FBG sensors on T-shirt. ....	75
<b>Figure 3. 7</b> <b>(a)</b> Sensing glove with hetero core fibre optical sensor, <b>(b)</b> FBG sensing glove, and <b>(c)</b> sensing glove with micro-bending transducers.....	76
<b>Figure 3. 8</b> <b>(a)</b> SLWOSs applied on gloves, <b>(b)</b> SLWOS attached to fabric, and <b>(c)</b> an FBG sensing glove.....	77

<b>Figure 3. 9 (a)</b> Pressure sensing pad and <b>(b)</b> a skin-like FBG strain sensor .....	78
<b>Figure 3.10 (a)</b> POF intensity-based smart insole, and <b>(b)</b> POF macro-bending based 3D-printed smart insole.....	79
<b>Figure 3. 11 (a)</b> Sewing and <b>(b)</b> embroidering optical fibres onto textiles.....	81
<b>Figure 3. 12</b> Three layered structure sensing glove. ....	82
<b>Figure 3. 13</b> Inserting optical fibres into <b>(a)</b> a woven fabric, and <b>(b)</b> a knitted wrist band. ...	84
<b>Figure 4.1</b> Total hand values of undergarments.....	100
<b>Figure 4. 2</b> Changes in temperature of skin and RH during wear trial. ....	102
<b>Figure 5.1 (a)</b> Three-dimensional illustration of smart textile, <b>(b)</b> structure of optical fibre warp-inlaid into single jersey fabric, <b>(c)</b> cross-section of warp-inlaid structure, and <b>(d)</b> configuration of optical fibre and allocation of FBG sensors 1 to 4.....	116
<b>Figure 5.2</b> Schematic of embedding FBG sensors into a silicone membrane: <b>(a)</b> filling mould with silicone, <b>(b)</b> peeling off resultant silicone membrane, <b>(c)</b> exposing FBG sensing area for embedding, <b>(d)</b> embedding FBG sensor into groove of silicone membrane, <b>(e)</b> covering embedded FBG sensor with silicone, and <b>(f)</b> cross-sectional view of an embedded FBG sensor warp-inlaid into knitted structure. ....	118
<b>Figure 5.3</b> Equipment setup and schematic of transverse force applied to smart textile on artificial skin. ....	119
<b>Figure 5.4</b> Schematic of amplifying string axial and transverse forces. ....	120
<b>Figure 5.5</b> Schematic of transverse force applied to Pliance <sup>®</sup> -X pressure sensor: <b>(a)</b> between two glass clips and <b>(b)</b> on artificial skin. ....	121
<b>Figure 5.6</b> Seamless knitted undergarment created using Shima Seki knitting machine, and silicone-embedded FBG sensor inlaid in the warp direction. ....	122
<b>Figure 5.7</b> Linearity of Bragg wavelength when applying force on (a) silicone-embedded FBG sensors, and (b) bare FBG sensors. ....	124

<b>Figure 5.8</b> Force detected by Pliance®-X pressure sensor: <b>(a)</b> between two glass clips and <b>(b)</b> on artificial skin. ....	126
<b>Figure 5.9</b> Linear regression between Bragg wavelength delta difference and force when applying force to silicone-embedded FBG sensors 1 to 4. ....	127
<b>Figure 6. 1</b> Meshed models of <b>(a)</b> torso, <b>(b)</b> skeletal structure, and <b>(c)</b> FIA .....	134
<b>Figure 6. 2</b> FE modelled torso and 3D moulds for the torso.....	135
<b>Figure 6. 3</b> <b>(a)</b> 3D printed moulds of skin and muscle tissues, and <b>(b)</b> moulded skin. ....	136
<b>Figure 6. 4</b> FE skeletal model based on x-rays of back and side views .....	137
<b>Figure 6. 5</b> Skeletal construction of the proposed mannequin. ....	137
<b>Figure 6. 6</b> Segmented vertebrae for 3D printing. ....	138
<b>Figure 6. 7</b> Ribs for 3D printing.....	139
<b>Figure 6. 8</b> <b>(a)</b> 3D printed vertebrae, <b>(b)</b> ribs, and <b>(c)</b> pelvis.....	139
<b>Figure 6. 9</b> <b>(a)</b> Intervertebral disc, and <b>(b)</b> moulds for sternum for 3D printing. ....	140
<b>Figure 6. 10</b> <b>(a)</b> 3D printed intervertebral disc, <b>(b)</b> the 3D printed mould for the sternum, and <b>(c)</b> the moulded sternum.....	140
<b>Figure 6. 11</b> <b>(a)</b> Rib cage with filled foam, and <b>(b)</b> the moulded muscle.....	141
<b>Figure 6. 12</b> Equipment setup of the experiment. ....	142
<b>Figure 6. 13</b> FIA design and placement of sensors. ....	143
<b>Figure 6. 14</b> Cobb's angle measurement method.....	144
<b>Figure 6. 15</b> Back of mannequin cut open with fluorescent pigment. ....	144
<b>Figure 6. 16</b> <b>(a)</b> Vertebrae position, and <b>(b)</b> comparison of initial spinal curves and Cobb's angles on AIS soft mannequin, 3D vertebrae model, and X-ray image. ....	145
<b>Figure 6. 17</b> Graphical comparison of spinal curves. ....	147
<b>Figure 6. 18</b> <b>(a)</b> Vertebrae position, and <b>(b)</b> comparison of spinal curves and Cobb's angles on AIS soft mannequin and X-ray images. ....	149

<b>Figure 6. 19</b> Comparison of the spinal corrective effects .....	150
<b>Figure 7. 1</b> Models of <b>(a)</b> torso, <b>(b)</b> skeletal structure, <b>(c)</b> textile materials, and <b>(d)</b> hinge material of FIA.....	156
<b>Figure 7. 2</b> Boundary conditions of torso model. ....	158
<b>Figure 7. 3</b> Inter-FBG sensor intervals on an optical fibre. ....	160
<b>Figure 7. 4</b> Placement of the FBG sensors.....	161
<b>Figure 7. 5</b> Equipment setup and schematic of transverse force applied to smart textile on artificial tissue.....	162
<b>Figure 7. 6</b> The functional intimate apparel.....	163
<b>Figure 7. 7</b> Linear regression between Bragg wavelength delta difference and force when applying force to FBG series 1 to 4. ....	166
<b>Figure 7. 8</b> Loading conditions on the surface of the torso.....	167
<b>Figure 7. 9</b> Displacement of skeletal model.....	169
<b>Figure 7. 10</b> <b>(a)</b> Vertebrae position, and <b>(b)</b> spinal curvatures and Cobb's angles on the FE model and X-ray images. ....	170
<b>Figure 7. 11</b> Comparison of the spinal curves. ....	172

## LIST OF TABLE

<b>Table 2. 1</b> Types of spinal curvatures .....	13
<b>Table 2. 2</b> Scoliotic braces for AIS patients .....	20
<b>Table 2. 3</b> Existing pressure sensors and their limitations .....	34
<b>Table 2. 4</b> Fibre optic sensor applications.....	47
<b>Table 3.1</b> Sample publications.....	64
<b>Table 3. 2</b> Article distribution: Top 5 journals.....	70
<b>Table 3. 3</b> Advantages and disadvantages of integration method .....	80
<b>Table 4. 1</b> Specification of sample undergarments.....	90
<b>Table 4. 2</b> Parameters measured with KES FB-Auto system.....	93
<b>Table 4.3</b> Evaluation of thermal comfort. ....	97
<b>Table 4.4</b> KES FB-Auto testing results.....	98
<b>Table 4.5</b> Correlation among THV, tensile, shearing, bending, compression, surface properties, and Qmax .....	100
<b>Table 4.6</b> Correlation between wear comfort and various fabric specifications .....	101
<b>Table 4.7</b> Possible factors that affect thermal comfort.....	103
<b>Table 4. 8</b> Possible factors that affect tactile comfort. ....	107
<b>Table 6. 1</b> Interface pressure exerted by FIA on proposed mannequin and AIS subject.....	148
<b>Table 6. 2</b> Comparison of Cobb's angle on proposed mannequin and X-ray before and after the intervention of FIA.....	151
<b>Table 7. 1</b> Demographic data of the AIS subject and the FEA predicted Cobb's angle. ....	156
<b>Table 7. 2</b> Mechanical properties of the FE models.....	157
<b>Table 7. 3</b> Mesh elements of the FE models. ....	158
<b>Table 7. 4</b> Specifications of the FBG sensors. ....	161
<b>Table 7. 5</b> Force exerted by the FIA.....	166

<b>Table 7. 6</b> Bragg wavelength delta differences of the FBG sensors from 0 N to 10 N.....	168
<b>Table 7. 7</b> Comparison of Cobb's angles on FE modelling and X-ray. ....	173



## **LIST OF ABBREVIATIONS**

### **A**

ACLD                      Anterior-cruciate-ligament-deficient

AIS                        Adolescent idiopathic scoliosis

### **B**

B                            Bending rigidity

BMI                        Body Mass Index

BSSQ                      Bad Sobernheim Stress Questionnaire

### **C**

CAD                        Computer aided design

CAM                        Computer aided manufacturing

CNS                        Central nervous system

CSVL                      Centre of the sacrum vertical line

CTL SO                    Cervico-thoraco-lumbo-sacral orthosis

### **F**

FBG                        Fibre Bragg grating

FE                           Finite element

FEA                        Finite element analysis

FEM                        Finite element method

FIA                        Functional intimate apparel

FSR Force-sensitive resistors

## **G**

GOF Glass optical fibres

## **K**

KES Kawabata Evaluation System of Fabric

## **L**

LC Compression linearity

LED Light-emitting diode

LT Tensile linearity

## **M**

MIU Coefficient of friction

MMD Mean deviation of coefficient of friction

MNF Micro/nanofibres

MRI Magnetic resonance imaging

MT Main thoracic

## **O**

OTDR Optical time-domain reflectometry

## **P**

PDMS	Polydimethylsiloxane
PLA	Polylactic acid
POF	Polymer optical fibres
PT	Proximal thoracic
PU	Polyurethane
PVC	Polyvinyl chloride

## **R**

RC	Compression resilience
RH	Relative humidity
RI	Refractive index
RT	Tensile resilience

## **S**

SLWOS	Skin-like wearable optical sensors
SMD	Surface roughness
SOSORT	Society on Scoliosis Orthopaedic and Rehabilitation Treatment
SSE	Scoliosis-specific exercise

## **T**

T	Thoracic
TFOS	Textile based-fibre optic sensors
THV	Total hand value

TL/L	Thoracolumbar/lumbar
TLSO	Thoraco-lumbo-sacral orthoses
TPU	Thermoplastic polyurethane

## **U**

U	Lumbar
USB	Universal Serial Bus
UV	Ultraviolet

## **W**

WC	Compression energy
WT	Tensile energy
WVT	Water vapour transmission

## **2**

2D	Two-dimensional
2HB	Bending moment
2HG	Elasticity for minute shear
2HG5	Elasticity for large shear

## **3**

3D	Three-dimensional
----	-------------------

# CHAPTER 1 INTRODUCTION

## 1.1 Research background

Adolescent idiopathic scoliosis (AIS) is the three-dimensional (3D) deformity of the spine that arises in children/adolescents between the ages of 10 and 16 years old (Altaf et al., 2013) and is the most common musculoskeletal deformity in children (Schwieger et al., 2017). AIS is determined by measuring the lateral curvature of the spine using Cobb's angle as the standard. A Cobb's angle of at least  $10^{\circ}$  and vertebral rotation means that the spine has abnormally shifted to one side or rotated (Spoonamore, 2023; Weinstein et al., 2013b). Globally, approximately 0.9% to 12% of adolescents are suffering from this problem, and within this population, nearly 10% of them may eventually require treatment (Schwieger et al., 2017).

Treatments for AIS patients include observation, bracing, physiotherapy, and surgery. The prescribed treatment mainly depends on the size of Cobb's angle and skeletal maturity (Dolan et al., 2007; Spoonamore, 2023). Bracing is the most prevalently used type of conservative treatment to stop the progression of the spinal deformity up to the threshold for surgery and restore normal spinal alignment by exerting pressure on the problematic areas of the spine (Bunge et al., 2010; Schwieger et al., 2017; Weinstein et al., 2013b). Rigid and soft braces are the two major types of braces prescribed for AIS patients, with typical examples including the Boston and SpineCor braces, respectively. In most countries, AIS patients with a Cobb's angle between  $20^{\circ}$  to  $40^{\circ}$  are prescribed a rigid brace which they need to wear for at least 18 h each day (Konieczny et al., 2017; Schwieger et al., 2017). The brace is fitted as tightly as it can tolerate because the tightness and effectiveness of the brace are positively correlated (Tessadri et al., 2012; Weiss, 2010). However, no consensus has been reached on the optimal bracing pressure, so the applied pressure mainly depends on the professional judgment of the orthotist

(Chalmers et al., 2012; Lou et al., 2010a). Additionally, although bracing has been used as a form of treatment since the 1950s, its effectiveness and biomechanical actions are still uncertain (Lou et al., 2010b). This suggests that patients may be subjected to excessive pressure with unknown treatment success. Several notable side effects are associated with bracing treatment, such as skin irritation and psychological trauma when the brace is donned. These side effects often result from prolonged exposure to high pressure, as well as the unappealing physical appearance of the brace. Weinstein et al. (2013a) pointed out that extended periods of exerted pressure that exceed the typical capillary pressure (4.3 kPa) may adversely affect blood circulation, skin metabolism, and subcutaneous tissues. These adverse effects may eventually reduce treatment compliance and efficacy. To prevent excessive brace pressure, a more rigorous and scientific approach is required for designing braces, and one of the methods is to monitor the forces exerted by the braces closely.

A variety of sensors are available to measure the force from the braces and the pressure exerted by them, but all of them have some limitations, including inflexibility, small measurement range, time delays, and application difficulties. For example, Lou et al. (2002) developed a battery-powered wireless force sensor that is capable of measuring the force from a Boston brace of up to 6.78 N (60 kPa). However, certain data loggers feature a time delay, so customised braces are necessary to embed the sensors. Krištof et al. (2010a) created a Pressurex® ultra-low pressure film to gauge the relative pressure between an AIS patient and a Boston brace, with the maximum recorded pressure being 361.87 kPa. While this approach provides the overall pressure distribution, the exact amount of pressure exerted on the film requires further analysis using the Topaq® imaging system and a flatbed scanner that is customised for the study (Sensor Products Inc., 2023). Moreover, attaching a large piece of pressure film onto the inside surface of the brace could cause the film to crinkle, thereby

affecting the pressure distribution profile. While both methods can be used to measure pressure, there remains the absence of an instant pressure measurement technique for braces.

Smart textiles that use fibre optic sensors offer a promising solution to address the limitations of conventional sensors in measuring the pressure exerted by braces. Rothmaier et al. (2008a) suggested that fibre optic sensors might be the most suitable material for integration with textiles because they are low in cost, flexible, lightweight, robust and non-toxic, and have high strain sensitivity and immunity to electromagnetic fields (Carmo et al., 2012; Mac-Thiong et al., 2004; Plümpe et al., 2017). Furthermore, they compensate for the limitations of conductive sensors. For instance, during magnetic resonance imaging (MRI), strain fibre optic sensors can be utilised to monitor real-time respiratory activity (Massaroni et al., 2015), which is not feasible with conductive sensors. Moreover, compared to other wearable electronics, smart textiles coupled with fibre optic sensors are more comfortable to wear with more flexible physical properties like strain and pressure, so body temperature can be measured in real-time. Moreover, a single optical fibre can have more than ten sensing points. Therefore, the overall pressure can be monitored if several sensing fibres are utilised.

Fibre Bragg grating (FBG) sensors offer a significant advantage over other optical sensors in that they do not disrupt the fluctuations of the optical source. This is because the signals they produce are based on wavelength, rather than optical power. As a result, they can detect displacement, making them useful for a variety of physical measurements, including strain, pressure, force, temperature, and motion analyses. FBG sensors are particularly popular in the textile industry because they are easy to produce, lightweight, flexible, stable, and non-conductive. They are also self-calibrated and portable, which eliminates the need for loose connections during transport. Overall, the advantages of FBG sensors make them a popular choice for a wide range of measurement applications.

In view of the above, a pressure monitoring undergarment that addresses the inadequacies of conventional sensors is developed in this study. Aside from an evaluation of the existing sensors that are used to detect the force from a brace and measure the pressure that it exerts, this study also elaborates on the design and development of this novel pressure monitoring undergarment for scoliosis brace treatment. The primary intention of this new undergarment is to provide reliable sensor readings while prioritising wear comfort.

## **1.2 Problem statement**

### **1.2.1 Ambiguous brace effectiveness without standardised pressure**

The effectiveness of different bracing treatments is still controversial due to the uncertainty regarding the brace load and the wear time (Périé et al., 2004). Also, no current standardised pressure is prescribed for braces (Rigo et al., 2006), so the applied pressure mainly relies on the judgment of the orthotist (Chalmers et al., 2012). However, prolonged pressure from a brace has been known to cause both physical and mental discomfort, thus resulting in significant impacts on the quality of life of the affected individuals (Chan et al., 2014). In severe cases, bracing can cause the development of pressure ulcers and trigger epileptic seizures or asthma attacks (Brigham & Armstrong, 2016; Martínez-Llorens et al., 2010). Patients who are unable to tolerate the pressure may resort to self-adjustment or reduce the wear time, which can ultimately reduce the effectiveness of the treatment, given that its efficacy depends on the duration of wear (Weinstein et al., 2013b). In this study, the utilisation of a pressure monitoring undergarment is hypothesised to prevent excessive pressure on AIS patients. As a result, this approach may enhance their treatment compliance and quality of life.



### **1.2.2 Ambiguous overall pressure distribution**

The overall pressure distribution and the changes in instant pressure exerted onto AIS patients have not yet been clarified in the literature (Lou et al., 2010a; Morton et al., 2008) due to the complexities of patient-specific spinal curvatures and different levels of patient tolerance of the treatment. Many sensors can only detect pressure at specific sites. However, measuring the applied force at a few points that are subjected to high levels of pressure cannot provide an understanding of the overall pressure distribution resultant of the bracing treatment. This dilemma is because some areas are intended to be those of relief while others are subjected to concentrated loads, but both affect spinal correction (Chalmers et al., 2012; Périé et al., 2003). Therefore, only conducting measurements on high pressure areas may result in unreliable predictions because the expected treatment result may vary from the real result (Lou et al., 2010b).

### **1.2.3 Absence of instant pressure distribution**

It is difficult to understand how the body responds to the force of different levels by using pressure sensors without a instant pressure profile. Additionally, fitting scoliotic braces could be difficult because the initial correction, if any, can only be identified through X-rays. To avoid redundant efforts, several studies have utilised pressure sensors to investigate the correlation between pressure and corrective outcomes. The findings from these studies have demonstrated that increased strap tension or pad pressure is associated with greater spinal correction (Lou et al., 2010a). Nevertheless, when a high level of pressure is exerted onto the body, skin injuries result which affect treatment compliance with the brace (Weinstein et al., 2013b). Therefore, instant pressure distribution could help orthotists to adjust the tightness of the brace straps and the location of the pads in a more scientific and straightforward way. X-rays can reflect the immediate corrective results of bracing treatment, but the amount of applied pressure can also be used to predict the tolerance of the patient. This suggests that compliance

is just as important as the initial degree of spinal correction, and both factors should be considered when evaluating the effectiveness of bracing treatment.

#### **1.2.4 Issues with the use of an additional procedure**

It is recognised that the occurrence of sensor shifting issues can result in inaccurate and unpredictable outcomes. In the view of this, some sensors can be embedded in the high-pressure areas of customised rigid braces to measure the force applied by a brace. For instance, the battery-powered wireless force sensor in Lou et al. (2002), but the sensor can be used for a specific user only. Moreover, pre-cutting the film and scanning are required when using the Pressurex® ultra-low pressure film to assess the overall pressure distribution (Krištof et al., 2010), which is inconvenient. On the contrary, the pressure monitoring undergarment in this study can be easily adapted to adolescents with different body shapes, without requiring any additional procedures prior to treatment.

### **1.3 Aim and research objectives**

The aim of this thesis is to develop a pressure monitoring undergarment that offers comfortable wear, is capable of providing instant signal profiles, and can provide an overview of the pressure distribution exerted by a scoliotic brace. Additionally, it should be able to easily accommodate adolescents of various body shapes without requiring any pre-treatment procedures. To evaluate the accuracy of the pressure monitoring undergarment, a proposed mannequin with dimensions similar to those of a child with moderate scoliosis was created. The following are the objectives of this thesis:

- i. To review the development of textile-based fibre optic sensors (TFOSs) for health monitoring purposes regarding their features, applications, and integration methods,
- ii. To investigate the main factors that affect the wear comfort of health-monitoring undergarments in terms of tactile and thermal comfort by conducting physical experiments;
- iii. To investigate the relationship between normal force and strain sensed by using FBG sensors;
- iv. To develop a flexible pressure monitoring undergarment by inserting FBG sensors into the knitted garment, so the overall and instant pressure exerted by braces on AIS patients can be measured; and
- v. To formulate a biomechanical model that simulates the forces from a brace and examine how the spine responds to the exerted pressure.

#### **1.4 Project originality and significance**

AIS is the most common musculoskeletal deformity affecting children, and bracing is a common treatment used to correct the scoliotic spine through an external constraint. Prolonged high levels of pressure exerted by a brace, however, could have both mental and physical repercussions. Yet there is no consensus on the optimal bracing pressure. Hence, it is crucial to monitor the forces applied by a brace during its fitting process, with the objective of optimising wear comfort while minimising any significant impacts on the initial corrective outcomes. A number of different pressure sensors are available in the market, however, not all of them are deemed suitable for measuring the pressure exerted by a brace due to three major limitations: absence of an overall pressure distribution and instant pressure profile, and lack of user-friendliness. These issues can lead to unpredictable results or failed bracing treatment.

The pressure monitoring undergarment in this study offers a promising solution to address the limitations of conventional sensors in measuring the pressure exerted by scoliosis braces. This pure cotton knitted undergarment is highly elastic, so it can easily accommodate the different body shapes of adolescents without requiring any supplementary procedures prior to treatment. Additionally, 14 FBG sensors are inlaid into a knitted undergarment, so that both the instant and overall pressure data can be visualised in this study. These benefits highlight the pressure monitoring undergarment as a valuable tool for monitoring the forces applied by a brace during the fitting process in a streamlined and scientifically rigorous manner.

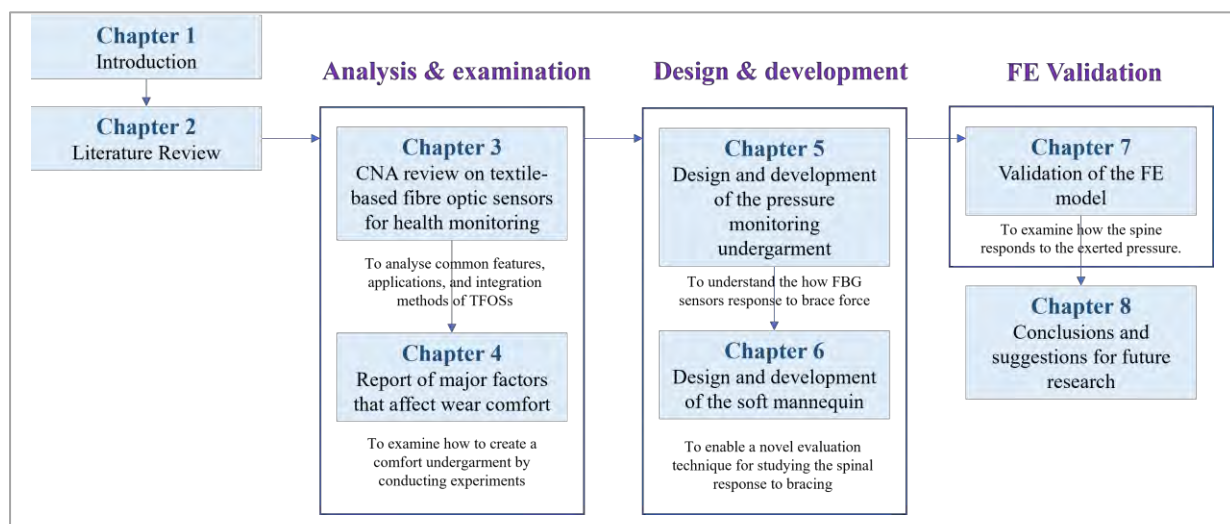
The scope of this project extends to include: (1) reviewing the development of TFOSs for health monitoring, in terms of their features, applications, and integration methods, (2) constructing a comfortable undergarment by examining the main factors that affect its wear comfort, (3) studying the relationship between normal force and strain sensed by the FBG sensors, (4) integrating FBG sensors that have a high degree of compatibility into the undergarment, and (5) formulating a simulation model to examine how the spine responds to the pressure from the brace. These provide useful information for the development of related products, especially in terms of identifying the problems and applying the optimal amount of corrective forces.

The output of the project can be further extended to determine the ideal level of pressure from bracing, which can provide the right amount of load to stop the progression of the spinal curvature while reducing the risk of pressure-related injuries. This means that the pressure monitoring undergarment can help orthotists to adjust the tightness of the brace straps and the placement of padding based on the objective statistics. As a result, AIS patients do not need to suffer from excessive pressure and are more likely to increase their compliance with treatment, thus increasing the likelihood of treatment success. Furthermore, a deeper understanding of the brace biomechanics can be achieved by utilising it in conjunction with MRI. This enables the

simultaneous observation of both the immediate pressures exerted by the brace and the resulting corrected spinal curvature. Additionally, it could be used for continuous health monitoring. For instance, monitoring the pressure distribution on a wheelchair seat when the textile is used as a sitting mat, and tracking plantar pressure for clinical evaluation. Moreover, academia and clinicians are expected to benefit from the formulated biomechanical model, which provides a radiation-free method to understand how the spine responds to applied pressure, thus predicting bracing effectiveness.

## 1.5 Outline of the thesis

There are a total of eight chapters in this thesis as shown in the flowchart in Figure 1. 1.



**Figure 1. 1** Study flowchart.

Chapter 1 provides the background information, problem statement, and objectives, as well as the originality and significance of the thesis work.

Chapter 2 is the literature review, which discusses the background information and non-invasive treatments for AIS, bracing compliance issues and adverse effects, the limitations of conventional sensors for measuring pressure from braces, advantages of smart textiles with

embedded fibre optic sensors, construction of a finite element analysis (FEA), and the appropriate materials for fabricating the undergarment to be worn underneath a brace.

Chapter 3 provides an objective and systematic literature review on TFOSs that are used for monitoring health issues in regard to their features, applications, and integration methods. A citation network analysis (CitNetExplorer) is used to analyse and identify the research domain of textile based-fibre optic sensors (TFOSs) and their trends.

Chapter 4 reports on the main factors that affect the wear comfort of the undergarment in terms of tactile and thermal sensations through a series of experiments, including physical experiments, Kawabata Evaluation System of Fabric (KES-FB) measurements, and a wear trial with seven different undergarments.

Chapter 5 presents the design and development process of the novel pressure monitoring undergarment based on Chapters 2, 4, and 5, which involves embedding FBG sensors into silicone membranes, selecting the undergarment materials, and integrating sensors into the undergarment. Moreover, an experiment is presented to simulate the bracing treatment and gain insights into the correlation between the forces exerted and the strain detected by the FBG sensors.

Chapter 6 elaborates on the development of a soft mannequin, which is designed to provide a novel evaluation method for studying the spinal response to force from a brace in three dimensions. The validation methodology employed is a comparison of the spinal curvature of the proposed mannequin to that of radiographic images of a female subject when she is donning and doffing a textile brace called the functional intimate apparel (FIA).

Chapter 7 reports on the validation results of the pressure monitoring undergarment, which applied the amount of force detected by the FBG sensors in the finite element (FE) model,

which consists of a human model, a functional intimate apparel model, and artificial models of the bones, vertebrae, and intervertebral discs. Also, the predicted spinal curvature from the FE analysis is compared to that of measurements taken from the soft mannequin in three dimensions.

Chapter 8 serves as the concluding chapter of the thesis, wherein a comprehensive summary of the research work is presented. Furthermore, the chapter also includes a discussion of the limitations and provides recommendations for future studies.

## **CHAPTER 2 LITERATURE REVIEW**

### **2.1 Introduction**

This chapter is a literature review with eight goals that include: (1) providing background information on AIS, which includes the definition of AIS, types of spinal curvatures, and potential problems; (2) providing an introduction on scoliotic treatments and describing the designs and mechanisms of rigid and soft braces in detail; (3) studying the correlations among brace compliance, treatment effectiveness and quality of life; (4) comparing different types of commonly used sensors and their limitations; (5) studying the advantages of using textile-based fibre optic sensors; (6) providing recommendations to construct a comfortable undergarment; and (7) studying the construction methods of FE models and their applications.

### **2.2 Introduction to adolescent idiopathic scoliosis**

#### **2.2.1 Definition**

Scoliosis is a 3D spinal deformity associated with a Cobb's angle  $>10^\circ$  and vertebral rotation (Schlösser et al., 2014; Weinstein et al., 2013b). The condition can be classified into three types, namely, idiopathic (no known cause), congenital (from birth), and syndromic (due to syndromes) (Altaf et al., 2013). Although idiopathic scoliosis is the most common type of scoliosis, no early precautionary therapy is available because it is caused by a multifactorial aetiology (Altaf et al., 2013; Hresko, 2013; Lonstein, 1994; Negrini et al., 2012; Rigo et al., 2010; Schlösser et al., 2014). However, there are several risk factors that affect the progression of spinal curvatures, which include rapid growth, skeletal immaturity, gender, genetic heterogeneity, metabolic disorders, and spinal dysraphism (Altaf et al., 2013; Shmerling, 2017; Orlando Liposuction Specialty Clinic, 2023).



### 2.2.2 Types of spinal curvatures

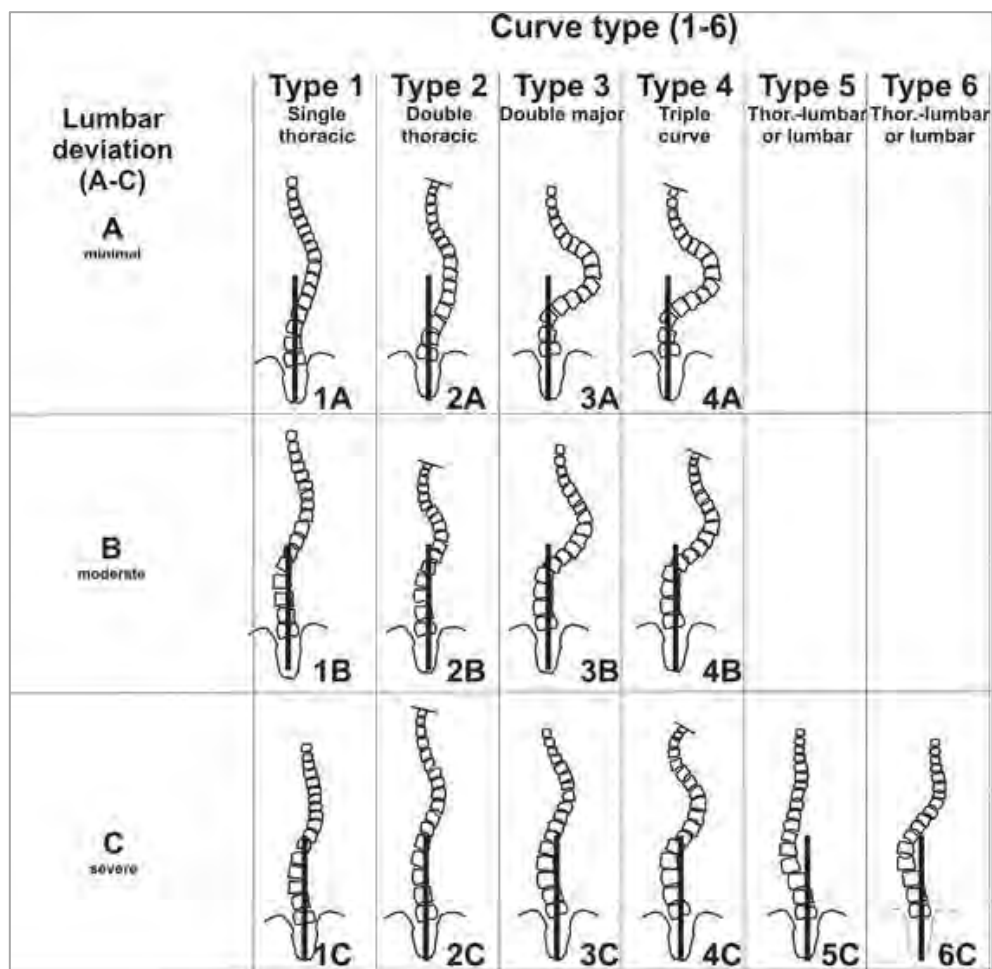
There are several different classification systems that are used to categorise spinal curvatures, such as the Lenke, Rigo and Society on Scoliosis Orthopaedic and Rehabilitation Treatment (SOSORT) classifications. Among them, the Lenke classification system, which is based on the anatomical site of the spinal deformity is commonly used (Smith et al., 2008). This system is a reliable tool that helps doctors to choose the best scoliotic treatment (Ovadia, 2013). According to the Lenke classification system, there are 6 main types of scoliosis, three lumbar spine modifiers (A, B, C) and three sagittal thoracic modifiers (-, N, +) (Kim et al., 2013; Lenke et al., 2001). Also, the structural criteria for the proximal thoracic (PT), main thoracic (MT) and thoracolumbar/lumbar (TL/L) curves is a side bending Cobb's angle  $\geq 25^\circ$ , and T2 to T5 kyphosis  $\geq 20^\circ$ . Table 2.1 summarises the 6 types of curves in the Lenke classification system as follows: (1) **MT**: only MT is the structural curve; (2) **Double thoracic**: MT\* and PT are structural curves; (3) **Double major**: MT\* and TL/L are structural curves; (4) **Triple major**: MT\*, PT, and TL/L\* are structural curves; (5) **TL/L**: only TL/L\* is a structural curve; and (6) **TL/L-MT**: TL/L\* (major curve if  $> 5^\circ$  than MT) and MT are structural curves.

**Table 2. 1** Types of spinal curvatures

Type	Curvature	PT (T3, T4, T5)	MT (T6 -T11 or T12)	TL/L (T12-L1 / L1-2 to L4)
1	MT	-	Structural*	-
2	Double thoracic	Structural	Structural*	-
3	Double major	-	Structural*	Structural
4	Triple major	Structural	Structural*	Structural* /Structural
5	TL/L	-	-	Structural*
6	TL/L-MT	-	Structural	Structural*

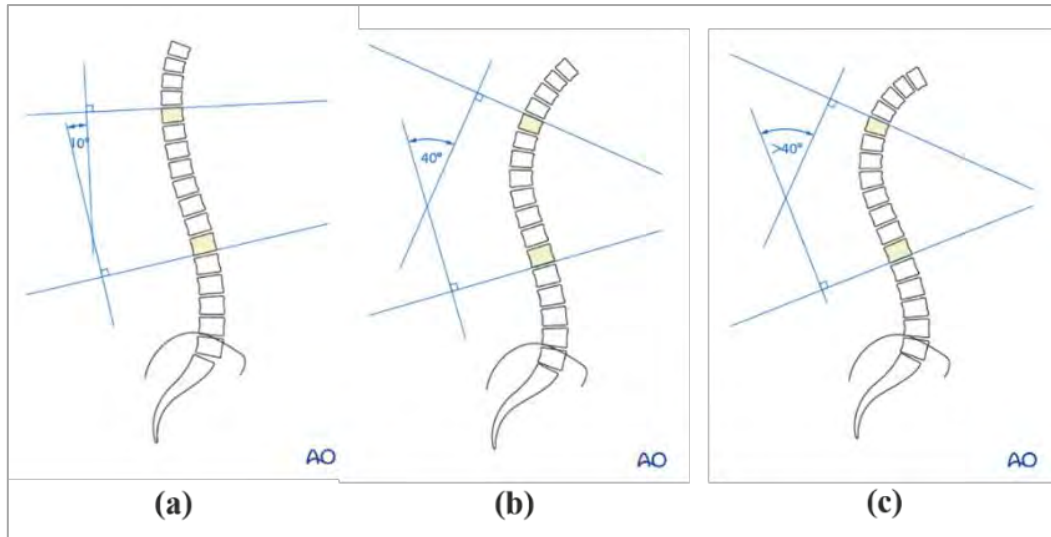
*\*Major curve*

Lenke et al. (2001) stated that the lumbar modifiers, which are used to understand the severity of the curvature, can be determined by drawing a vertical line from the centre of the sacrum (CSVL). Modifier A, which denotes minimal lumbar deviation, is defined as a line between pedicles; Modifier B, which denotes moderate lumbar deviation is defined as a line that touches the apical vertebral pedicle; and Type C, which denotes severe lumbar deviation, is defined as a line that does not touch any part of the vertebral body or pedicle (Figure 2.1).



**Figure 2. 1** Determination of lumbar modifiers (Lenke et al., 2001).

Moreover, determining the sagittal thoracic modifier is dependent on lateral radiographs from T5 to T12. Hypokyphosis (-), normokyphosis (N), and hyperkyphosis (+) refer to angles of the thoracic spine that are  $< 10^\circ$ ,  $10^\circ$  to  $40^\circ$ , and  $> 40^\circ$  respectively (Figure 2.2).



**Figure 2. 2** Determination of sagittal thoracic modifier: **(a)** Hypokyphosis (-), **(b)** Normokyphosis (N) and **(c)** Hyperkyphosis (+) (Kim et al., 2013).

Although the Lenke system is more comprehensive and reliable than the King's classification, which is a widely accepted and traditional system used for AIS, Ovadia (2013) noted that the Lenke system does not include the axial rotation of the apical vertebra. Therefore, advanced technology, stereo-radiographic measurements were introduced, so spinal deformity in the 3D form can be measured (Stokes et al., 2009). This implies that besides the coronal and sagittal planes, future classification systems can also depend on the axial plane to develop a truly 3D scoliotic classification.

### 2.2.3 Trends and potential problems of AIS

Also, girls have a higher incidence of AIS during puberty and around 80% to 90% of AIS patients are female (Busscher et al., 2010; Negrini et al., 2015).

In most cases, adolescents may not be aware that they have a scoliosis problem because the spinal deformity does not cause any health problems during growth (Altaf et al., 2013; Negrini et al., 2015). The most common symptom is apparently abnormal posture, such as asymmetric shoulders and pelvis, rib prominence or shifted trunk (Altaf et al., 2013). These indications are

usually first discovered by the patients themselves, family members or friends, who probably do not consider their physical abnormality as a critical issue of urgency. They might be more alarmed if their case is more extreme; for example, they lose their balance more easily or have abnormal gait due to shifts in head and torso positions (Spoonamore, 2023). Yet, it may be too late when they recognise that they have a problem because the spinal curvature may increase dramatically within a short period of time. If left untreated, the progression of the spinal curvature may escalate, and AIS patients will eventually need surgery. According to Weinstein et al. (2013), 58% of the observed subjects (no bracing) in their study with a Cobb's angle between  $20^{\circ}$  to  $40^{\circ}$  experienced a progression to  $50^{\circ}$ . Besides aesthetic problems, this long-term condition may also affect the quality of life of patients in their adulthood because severe trunk deformity may cause pain, disability, and cardiac and pulmonary problems (Dewald, 2003; Harvard Medical School, 2016; Negrini et al., 2015). Therefore, early detection and scoliotic treatment effectiveness are significantly related.

### **2.3 Scoliotic treatments for AIS patients**

Scoliotic treatments include observation (for a Cobb's angle  $<25^{\circ}$ ), exercise, bracing (for a Cobb's angle of  $25^{\circ}$  to  $45^{\circ}$ ) as well as surgical treatment (for a Cobb's angle  $>45^{\circ}$ ) (Altaf et al., 2013; Busscher et al., 2010; Płaszewski & Bettany-Saltikov, 2014), and the decision mainly depends on the progression of the scoliotic curve and skeletal maturity (Busscher et al., 2010; Dolan et al., 2007; Spoonamore, 2023). Among them, bracing is the most common treatment to reduce the threshold for surgery and restore normal spine alignment by actively exerting pressure (Bunge et al., 2010; Negrini et al., 2015; Schwieger et al., 2017; Weinstein et al., 2013b). Negrini et al. (2015) indicated that the success rate of bracing ( $\sim 72\%$ ) is higher than just observation ( $\sim 48\%$ ), and the success rate could reach 80% if bracing is carried out in conjunction with exercise.

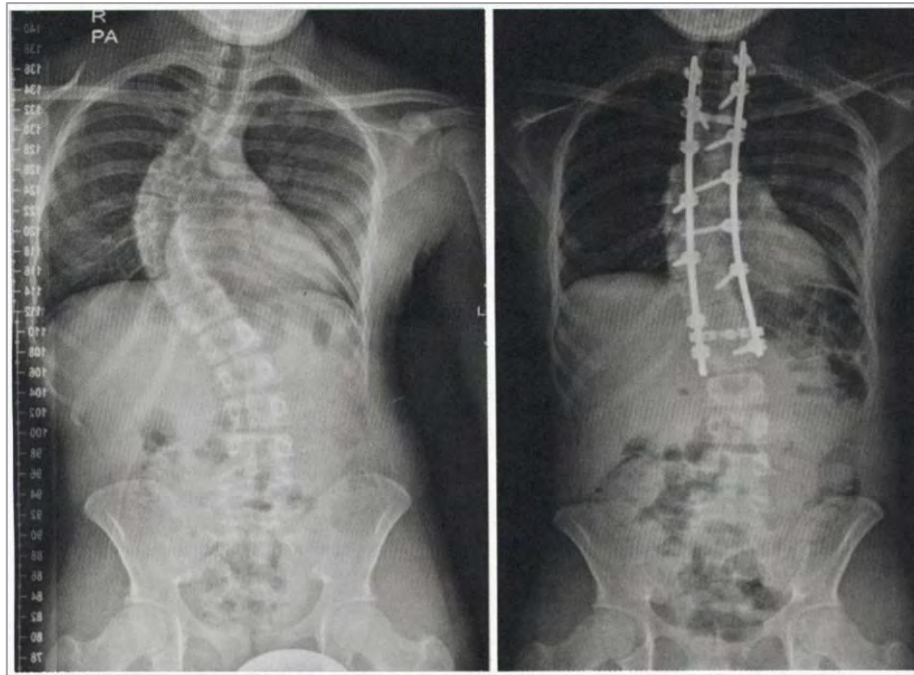
Observation is the first step to treat AIS patients with a mild curvature. Diagnosed patients are assigned to regular clinical evaluations. The follow-up period ranges from 2 to 60 months depending on their specific clinical situations (Negrini et al., 2012). Also, X-rays are not required every time.

Bracing is recommended if the Cobb's angle increases to  $25^{\circ}$  or more and observed at Risser stage 0, 1, or 2 (Lonstein, 2006). The external force applied by the brace can reduce unnatural loading and asymmetrical movement, so as to facilitate proper spinal growth. There are mainly two types of braces; namely, hard, and soft braces (Negrini et al., 2012). In most countries, patients are prescribed rigid braces which they have to wear for more than 18 hours each day to prevent the progression of their curvature (Bunge et al., 2010; Konieczny et al., 2017; Schwieger et al., 2017; Weinstein et al., 2013b), and the treatment usually lasts for 2 to 5 years until full skeletal maturity (Landauer et al., 2003). However, some studies indicate that bracing can only slow down the progression because the spinal curvature may still increase to  $45$  to  $50^{\circ}$  (Negrini et al., 2012). Also, bracing likely triggers adverse impacts that reduce their quality of life, such as causing skin irritation, back pain, and psychological and aesthetics impacts (Negrini et al., 2015).

Scoliosis-specific exercise (SSE) is another early type of conservative treatment, and often coupled with bracing. The aim of SSE is to improve the flexibility and function of the body as well as reduce the spinal deformity by teaching patients to use the correct trunk posture and do exercises (Weiss et al., 2006). There are two types of SSEs; namely, neurophysiological and biomechanical approaches, which treat AIS that originates from the central nervous system (CNS) and skeletal muscle imbalance, respectively (Smania et al., 2008). Both are performed with physiotherapists, and the frequency of therapy sessions are in accordance with the technique, cooperation, and ability of the patients (Negrini et al., 2012). Besides outpatient

treatment, special exercises (rehabilitation) are specially designed for in-patients too. Although bracing is the most common method to treat AIS patients, more researchers are now turning to scoliosis-specific physical therapy exercises (Zaina et al., 2015), such as the Schroth method which was founded by Katharina Schroth in Germany in 1921 (International Schroth Three-Dimensional Therapy, 2023). The Schroth method can reduce spinal deformity by retraining the muscles and nerves for muscular symmetry, reshaping the rib cage and the soft tissues that surround the rib cage, and being aware of posture so as to maintain a straight spine and help the trunk rotate and gain flexibility through deep breathing (Weiss, 2003).

Surgery could be considered if conservative treatments do not help the patient. The aim of surgery is to stop curve progression through spinal fusion so that the affected areas are fused together, thus improving the spinal deformity and physical aesthetics (Altaf et al., 2013). Usually, posterior correction is carried out with AIS patients, which means that pedicle screws are inserted into the spine for support and between the vertebrae to be fused. Subsequently, 2 metal rods are used to connect these screws to prevent movement while allowing the healing of the bone graft (Figure 2.3). Anterior fusion is another approach that is used on patients with thoracolumbar or lumbar curves or in conjunction with posterior correction in special cases. Surgeons access the front of the spine through the abdomen, and then fuse the vertebrae of concern in the lower back together. Non-union with surgical treatment is low, and the incidence of neurological complications is  $< 1\%$  (Diab et al., 2007). However, it is found that patients who have undergone surgery versus those who did not have surgery have similar functional status and pain after a minimum follow-up of 10 years (Bartie et al., 2009). This means that patients may still suffer from back pain after surgery.



**Figure 2. 3** Before and after surgery (Altaf et al., 2013).

### **2.3.1 Types of scoliotic braces**

Traditionally, rigid braces are prescribed for AIS patients, and have proven to effectively reduce spinal curvature or slow down the progression of the curvature (Weinstein et al., 2013b). Nevertheless, they have 3 main shortcomings, namely movement restriction, discomfort, and skin irritation (Bunge et al., 2010; Wong et al., 2008). Therefore, flexible braces have been developed to alleviate these issues. They can improve patient compliance and quality of life as well as bracing efficacy (Chan, 2019; Fok, 2020). Their design, physiological and biomechanism mechanisms are described in this section. Table 2.2 summarises the specifications of commonly used rigid and flexible textile braces.

**Table 2. 2** Scoliotic braces for AIS patients

	Origin	Construction	Rigidity	Material	Mechanism
<b>Milwaukee</b>	USA	-	Rigid	Polyethylene, Aluminium, Steel	Passive & Active
<b>Lyon</b>	France	-	Very rigid	Polymethacrylate, Radiolucent Duralumin	Passive & Active
<b>Boston</b>	USA	Prefabricated model	Rigid	Polyethylene	Passive & Active
<b>Chêneau</b>	France- Germany	CAD/CAM- hand made	Rigid	Polyethylene	Passive & Active
<b>SpineCor</b>	Canada	Prefabricated model	Elastic	Textiles and plastic	Active
<b>Flexible intimate apparel</b>	Hong Kong	Hand made	Semi-rigid	Textiles, artificial bone, silicone pads	Passive & Active

### 2.3.1.1 Rigid braces

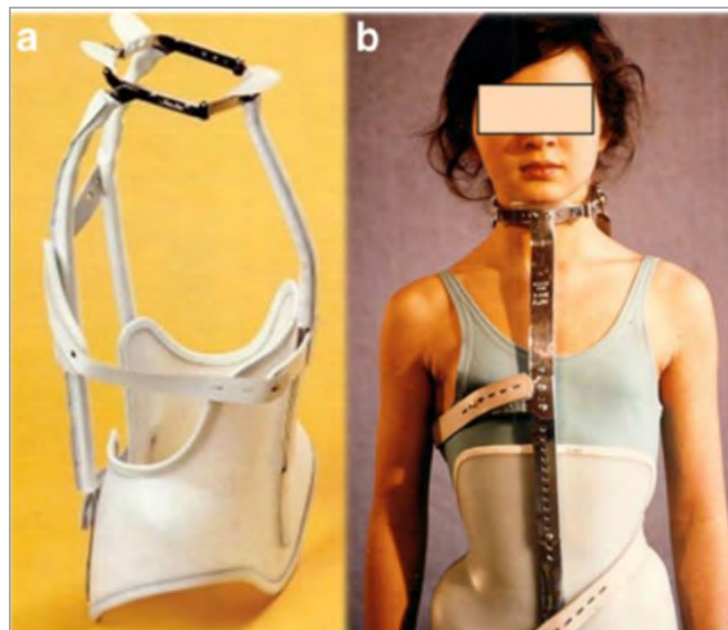
The rigid braces are discussed in the following sections include the Milwaukee, Lyon, Boston, and Chêneau braces.

#### 2.3.1.1.1 Milwaukee brace

The Milwaukee brace, scientifically referred to as a cervico-thoraco-lumbo-sacral orthosis (CTL SO), is a full torso brace that was originally designed by Walter Blount and Albert Schmidt in 1945 (Canavese & Kaelin, 2011) (Figure 2.4). The brace was originally designed for patients after surgery and required long periods of immobilisation. However, due to aesthetics concerns and emotional impacts, the brace is only recommended for treating Scheuermann's kyphosis and high thoracic curves (Zaina et al., 2014). The Milwaukee brace consists of anterior and posterior bars that are linked to a contoured pelvis girdle and neck ring. Also, lateral pressure and trapezius pads, and axillary slings are placed according to the curve.



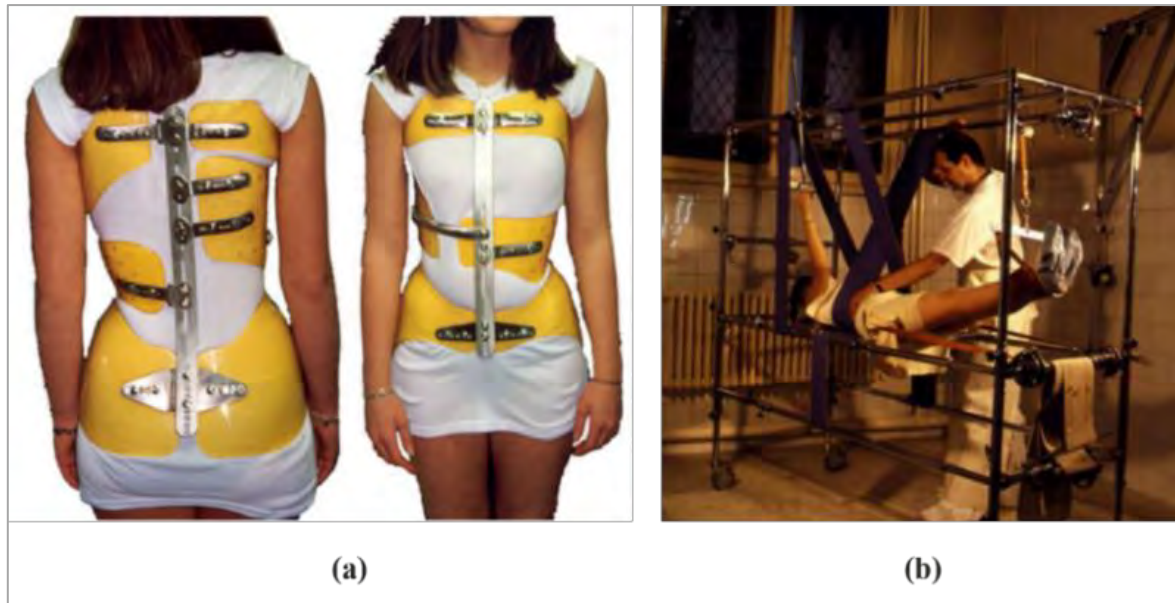
The applied force depends on the tightness of the axillary slings, while active correction is induced by the throat ring or lateral pads because patients are intentionally away from them.



**Figure 2. 4** Milwaukee brace (Zaina et al., 2014).

#### **2.3.1.1.2 Lyonnaise (Lyon) Brace**

The Lyon brace was developed by Pierre Stagnara in France in 1947 (Figure 2.5 (a)). The design of the brace was based on the Lenke classification with 14 types of scoliosis (Zaina et al., 2014). This brace is not suitable for patients who are younger than 11 with a mild curvature ( $<30^\circ$ ) to avoid tubular thorax deformity (Canavese & Kaelin, 2011; Zaina et al., 2014). A preliminary plaster cast is used to stretch the deep ligaments, and then the patient will don the Lyon brace which is adjusted accordingly (Grivas et al., 2018; Zaina et al., 2014) (Figure 2.5 (b)). The brace is divided into different sections: thoracic and lumbar sections are linked by 2 vertical aluminium rods, and the pelvis section is coupled with 2 lateral valves that connect to the aluminium rods (Canavese & Kaelin, 2011). A 3-point pressure system (passive mechanism) is used, in which external forces from the brace push the convex side of the curvature while allowing the concave side to expand.



**Figure 2. 5 (a) Lyon brace, and (b) Preliminary plaster cast (Grivas et al., 2018).**

#### **2.3.1.1.3 Boston Brace**

The Boston brace was jointly designed by John Hall and William Miller in 1972 at the Boston Children's Hospital and is often used in North America (Fayssoux et al., 2010; Grivas et al., 2018; Zaina et al., 2014) (Figure 2.6). The Boston brace is not custom-moulded or fabricated based on a cast. It is instead created by selecting the appropriate prefabricated modules based on the Milwaukee brace and then modified to fit the individual (Emans et al., 2003). Therefore, the Boston brace saves a lot of time and cost. Nowadays, Boston braces are constructed based on body surface scanning and computer aided design-computer aided manufacturing (CAD-CAM) (Zaina et al., 2014). In-brace correction is achieved by placing small pads underneath the brace to push against the curvature of the spine. Also, a window is provided opposite the thoracic pad for active shifting of the trunk and improving ventilation (Zaina et al., 2014). Since the pads are normally placed at the back, the trunk is pushed forward against the front of the brace and held upright (Canavese & Kaelin, 2011).



**Figure 2. 6** Boston brace (North Orthotics & Prosthetics Inc., 2020).

#### **2.3.1.1.4 Chêneau brace**

The Chêneau brace is an asymmetrical rigid brace created by Jacques Chêneau in 1979 (Weiss, 2003; see Figure 2.7). This brace is often used for scoliosis and thoracic hypokyphosis patients of all degrees of severity and maturity in European countries, such as Poland (Zaborowska-Sapeta et al., 2011). For the brace design, large and sweeping pads are used to push the body against the curve (Zaina et al., 2014). A 3-point pressure system is used to correct scoliosis in a variety of dimensions to correct the spinal curvature, elongate the trunk, and unload the deforming forces, as well as de-rotate the thorax (Zaina et al., 2014). The active mechanism is based on vertebral growth as a corrective factor, asymmetrically guiding rib cage movement during respiration, training the muscles to provide physiological action, as well as offering an anti-gravitational effect (Kotwicki et al., 2002). Although this brace is rigid, lateral and longitudinal rotation and movement can still be facilitated (Canavese & Kaelin, 2011). The Chêneau brace is commonly used along with Schroth exercises because this brace helps to perform the exercises correctly.



**Figure 2. 7** Chêneau brace (Zaborowska-Sapeta et al., 2011).

### **2.3.1.2 Flexible textile brace**

Flexible textile braces which will be discussed in the following sections are the SpineCor brace and flexible intimate apparel.

#### **2.3.1.2.1 SpineCor brace**

The SpineCor brace was jointly created by Christine Coillard and Charles Rivard in the 1990s (Canavese & Kaelin, 2011; Fayssoux et al., 2010; Zaina et al., 2014) (Figure 2.8). This strap-based brace is supposedly the most flexible among commonly used braces. However, the brace appears to be only suitable for younger users with a mild curve ( $\sim 15^\circ$ ) because the applied forces are far less intensive than those of rigid braces (Canavese & Kaelin, 2011; Fayssoux et al., 2010). The brace is made of a plastic pelvis section and strong elastic bands that wrap around the trunk and apply corrective forces that pull against the curve and derotation forces onto the trunk. However, its corrective mechanism differs from that of traditional rigid braces because Spinecor primarily relies on active correction, so no passive forces are applied (Zaina et al., 2014). Active correction improves spinal alignment by correcting incorrect posture, muscular dysfunction, and unsynchronised spinal growth (Coillard et al., 2003; Zaina et al.,

2014). Also, Spinecor only performs when the patients move, and therefore high compliance with treatment is needed. Moreover, the brace needs to be used along with the SpineCor® exercise program to enhance the brace efficacy (Fung, 2020).



**Figure 2. 8** SpineCor (Fayssoux et al., 2010).

#### **2.3.1.2.2 Flexible intimate apparel**

The flexible intimate apparel (FIA) as a soft brace was developed by Fok (2020), which is a semi-rigid textile brace that covers the body from the shoulders to the thighs (Figure 2.9). The brace is composed of a bra top, pants, pelvis belt, artificial bones, semi-rigid silicon pads, and elastic straps. Although the artificial bones are rigid, the joints between the hinges are flexible, so that patients can still bend or twist their bodies easily. Since a bra top is attached, the patients do not need to wear extra underwear underneath the brace, so it is more convenient to wear and reduces bulkiness. Moreover, its breathability and softness are much better than that of rigid plastic braces. Therefore, it is comfortable to wear. As a result, mental health is not affected by using the FIA, which can be reflected by the stress level of the users. It has been found that the

stress level of FIA users is lower than that of the Cheneau brace users, which is 14 and 11.04, respectively (Weiss et al., 2007; Fok, 2020).

Like traditional rigid braces, the FIA uses a 3-point pressure system, and the in-brace corrective mechanism is facilitated by carbon fibre artificial bones and silicone pads. The bones and pads at the back push the trunk forward against a high-tension elastic band at the front, and thus hold the body upright. After wearing the FIA for 3 months, it is found that the recruited subjects showed an average of a  $6.1^\circ$  reduction in their spinal curvature. Besides, the use of the FIA showed that the shoulder balance and rotation, as well as posterior trunk balance of the subjects have improved after 3 months of wear.

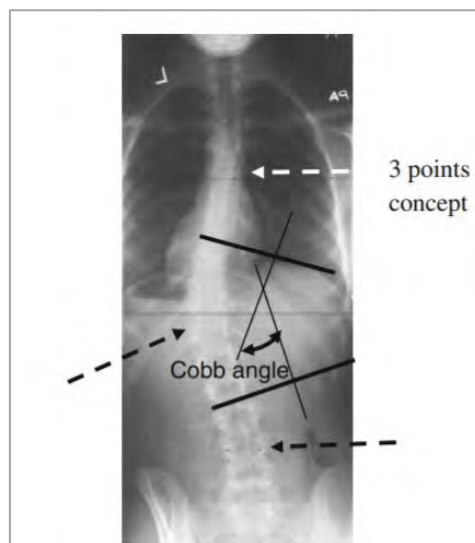


**Figure 2. 9** Functional intimate apparel (Fok, 2020).



### 2.3.2 Three-point pressure system

Although a number of orthoses have been developed, there is no consensus on how to apply forces to the body to correct the spinal curvature because many orthotists mainly rely on their experience and judgment when fitting braces onto AIS patients (Rigo et al., 2006). However, the 3-point pressure concept is believed to be the most acceptable principle (Lou, et al., 2010b; Rigo et al., 2006). The 3-point pressure system is defined as applying force and counterforces at the apex and two ends of the curve, respectively (Figure 2.10). Generally, the passive forces are exerted by pressure pads, slings, or elastic straps, such as the Boston and Chêneau braces. Also, there is consensus that the spinal curvature correction in the coronal plane is the most significant way to de-rotate the major curve. However, more than half of the SOSORT members express doubts as this system may overcorrect shoulder balance (Rigo et al., 2006).



**Figure 2. 10** Three-point pressure system.

#### **Knowledge gap 1:**

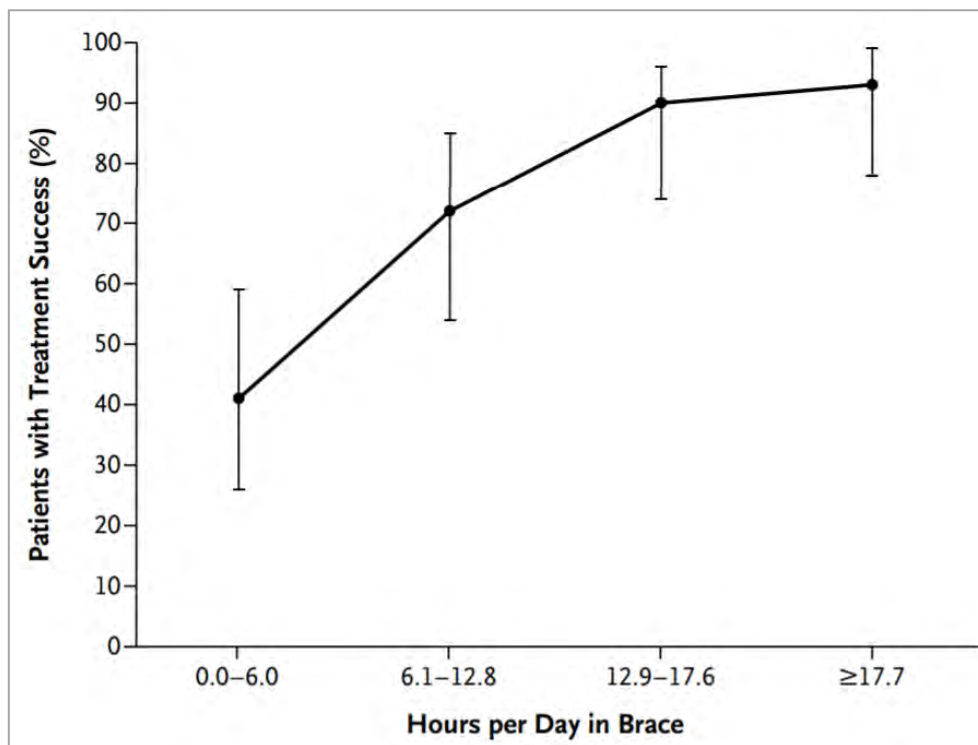
No standardised degree of brace pressure.

AIS subjects may suffer from excessive pressure from bracing when the brace over-corrects their shoulder balance.

## 2.4 Bracing compliance

### 2.4.1 Correlation between bracing compliance and effectiveness

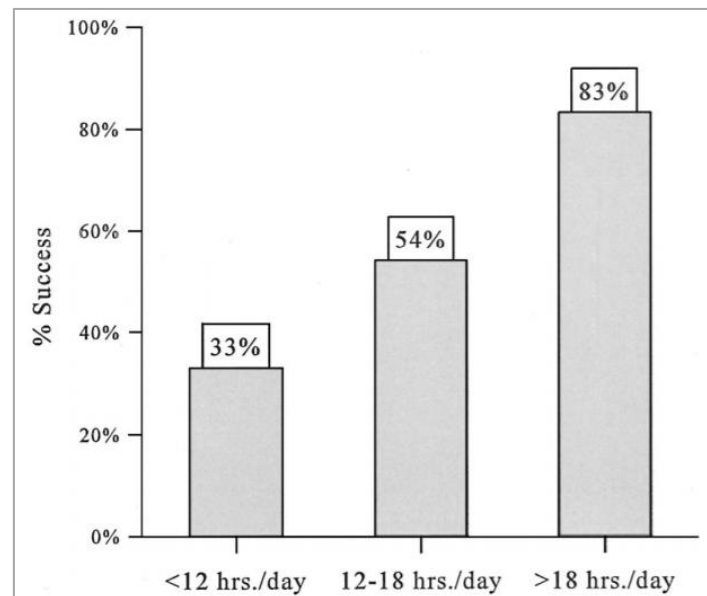
Bracing effectiveness is significantly and positively correlated to length of time that a brace is worn. Effectiveness here is defined as the reduction of the risk of surgical intervention. In Weinstein et al. (2013b), 242 subjects who range from 10 to 15 years old were recruited and assigned to either the observation or one of the bracing groups (Boston or Wilmington brace, or other TLSOs). The rate of success (Cobb's angle  $< 50^\circ$ ) of the braced and observed patients is 72% and 48%, respectively. Also, they reported that a longer brace-wear time results in a higher rate of treatment success. Figure 2.11 is a plot which shows that a wear time that exceeds 12.9 hours results in a 90-93% treatment success rate, while a wear time less than 6 hours only has a 42 % success rate.



**Figure 2. 11** Correlation between TLSO treatment success and brace wear time (Weinstein et al., 2013b).

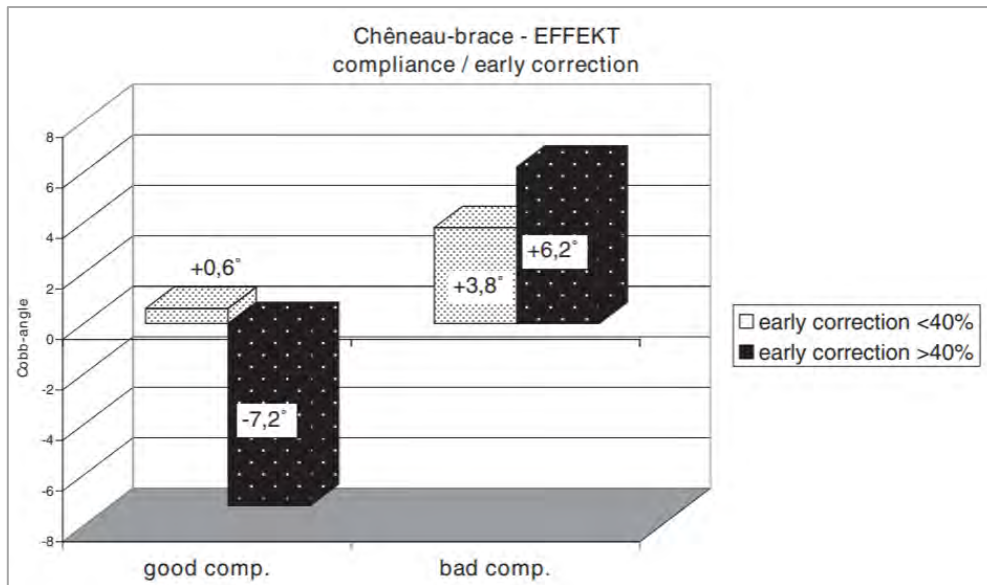


Katz and Durrani (2001) also obtained similar results. They found that wearing a Boston brace for > 18 hours per day results in nearly a 83% success rate (Figure 2.12). This proves that bracing is an effective method to reduce spinal deformity, and compliance is the key factor that determines the treatment success.



**Figure 2. 12** Correlation between treatment success and brace wear time (Katz & Durrani, 2001).

Moreover, Landauer et al. (2003) pointed out that the Cobb's angles could be reduced by 7° if patients comply well with brace use and show a high initial correction. In Figure 2.13, the high compliance group shows a much better result than the low compliance group. The former shows a 7.2° correction in their Cobb's angle while the latter are predisposed to curvature progression. Moreover, the figure shows that even for the subjects with a higher initial correction (> 40%), if they do not comply with the treatment, the result is treatment failure. This shows the importance of compliance. Other factors that affect the bracing effectiveness include age, gender, skeletal maturity, curvature pattern, initial Cobb's angle, applied pressure, placement of pads and fit of brace (Aulisa et al., 2014; Katz & Durrani, 2001; Landauer et al., 2003).



**Figure 2. 13** Bracing effects: good vs bad compliance groups (Landauer et al., 2003).

#### 2.4.2 Correlation between brace compliance and quality of life

Patients may not fully comply with brace wear even if they understand the importance of wearing the brace for extended periods of time because bracing may seriously disrupt their normal life. It is believed that the quality of life is positively correlated to brace compliance in three main aspects, namely physical, emotional, and social well-being (Chan et al., 2014). Although bracing has been proven to reduce the progression of spinal curvature to the threshold for surgery and align the spine correctly (Bunge et al., 2010; Schwieger et al., 2017; Weinstein et al., 2013), prolonged high levels of pressure exerted onto the torso may result in undesirable effects, such as skin irritation and lung volume reduction as well as depression. Chan et al. (2014) showed that patients who experience more pain, and weaker emotional and physical functions tend to comply less with bracing because they face more limitations in their daily life. This shows that both adverse physical and psychological effects are possibly affecting acceptance of bracing as a treatment.

#### **2.4.2.1 Adverse physical effects**

AIS patients with a Cobb's angle of 20° to 40° are asked to don the orthosis for at least 18 hours each day (Canavese & Kaelin, 2011; Konieczny et al., 2017; Schwieger et al., 2017; Weinstein et al., 2013b), and the average pressure from the brace to the primarily padded areas is  $7.1 \pm 1.8$  kPa (Wong et al., 2016). However, a high level of pressure applied for a prolonged period of time to the body may cause physical discomfort, like pain, temporary vital capacity reduction, mild chest wall and inferior rib deformation, and skin irritation (Canavese & Kaelin, 2011). If the problem is left unattended, pressure ulcers may be triggered, which is a deep-tissue injury that often develops on the surface of the skin around the bony prominences.

Skin irritation often occurs in warm climates and the summer due to a higher perspiration rate (Canavese & Kaelin, 2011). Not only is it uncomfortable to wear the brace, but the brace may cause a clinging feeling because it is difficult to wick away sweat. To alleviate this problem, it is recommended that the patient wears cotton undergarment and changes the undergarment frequently. Besides contact friction, brace tightness also causes discomfort and even skin injuries. According to Mak et al. (2010), prolonged exposure to pressures surpassing the typical capillary blood pressure (4.3 kPa) may have implications for blood circulation, skin metabolism, and the underlying subcutaneous tissues. Also, a high level of pressure exerted onto the skin for a prolonged period of time may even lead to tissue ischemia or pressure ulcers because the underlying microvasculature isolates the injured area from healthy tissue, thus the supply of oxygen and nutrients to the tissues is inhibited.

In addition, orthoses may have adverse effects. For instance, thoraco-lumbo-sacral orthoses (TLSOs) may affect the lung volume and growth of AIS patients. Kennedy et al. (1987) indicated that the remaining functional capacity of the lungs of patients is reduced by an average of 26% when they are wearing a brace, and 18% of them even experience a reduction

of 40%. Also, the total lung capacity and forced vital capacity are reduced by 16% and 18% respectively. The reduction of lung capacity may impose a higher risk for other disorders, namely asthma and diaphragmatic weakness. It is believed that lung function is highly correlated to brace tightness; that is, a tighter brace lowers the lung volume. Therefore, the force exerted by the orthosis should be carefully accessed.

Moreover, mild chest wall and inferior rib deformation are commonly found in AIS patients at a younger age because their chest is undeveloped (Canavese & Kaelin, 2011). When corrective force is applied onto the rib convexity, the chest may deform for a short period of time or even permanently depending on the duration of orthosis use. If bracing is adopted at a very young age for many years, the chest wall and rib deformations may be irreversible.

#### **2.4.2.2 Adverse psychological effects**

Bracing may negatively affect the self- and body-images, social life as well as quality of life (Asher et al., 2003). The importance of peer approval escalates during puberty, and peer acceptance may be influenced by appearance, especially for girls (An & Lee, 2015; Forney et al., 2019). This means that physical differences may constitute as social barriers and cause self-devaluation. Therefore, some of the patients may feel fear and distress towards bracing treatment because they are worried that their social life would be affected (Misterska et al., 2018). Their asymmetrical profile may cause loss of confidence but bracing likely further intensifies feelings of inferiority which affects their quality of life, thus reducing compliance with bracing.

Botens-Helmut et al. (2006) stated that bracing treatment increases the level of stress over trunk deformation alone. The Bad Sobernheim Stress Questionnaire (BSSQ) scores are 12.5/24 (moderate stress) and 20/24 (little stress) for the bracing and observation groups, respectively in their study. Similarly, Kotwicki et al. (2007) reported that patients who use a brace in their

study feel more stressed. The BSSQ score of patients who wear a brace and those who do not is 9/24 (moderate stress) and 17/24 (little stress), respectively. Furthermore, Weinstein et al. (2013) mentioned that a patient was sent to the hospital due to depression during bracing treatment. This shows that patients who receive bracing as a treatment may experience additional stress and bracing may even have serious psychological impacts.

The many problems with rigid braces mean that textile braces could be one of the solutions to reduce the problems with the exerted stress because they are much more flexible and thinner, so they are comfortable to wear and undetectable underneath clothing. Textile braces can greatly enhance compliance with bracing and the rate of treatment success. For example, Fung (2020) developed an ergonomic brace, which comprises both soft textiles and hard components (e.g. resin bones and plastic paddings), so that it is comfortable to wear and maintains efficacy at the same time. However, this brace is only suitable for AIS patients with a mild curvature.

#### **Knowledge gap 2:**

Some studies focus on the initial corrective result but ignore pressure tolerance.

Excessive pressure may increase the risk of physical and psychological impacts, thus lowering treatment compliance and treatment success rate.

### **2.5 Existing force/pressure sensors and their limitations**

A large number of force/pressure sensors are available in the market, but not all of them are able to directly obtain close-to-body measurements. Besides high accuracy and precision, they should be flexible, lightweight, small, and safe to use. Also, portable sensors are value-added because they are convenient to use, avoid loose connection problems, and allow ease of movement (Mac-Thiong et al., 2004; Rothmaier et al., 2008a). Some sensors have been used to measure the force/pressure exerted by orthoses, but have various limitations, such as absence

of instant data, time delay, distance limitations between the sensor and system, and can only be used for a particular user. Table 2.3 compares the different sensors used for pressure measurement or monitoring.

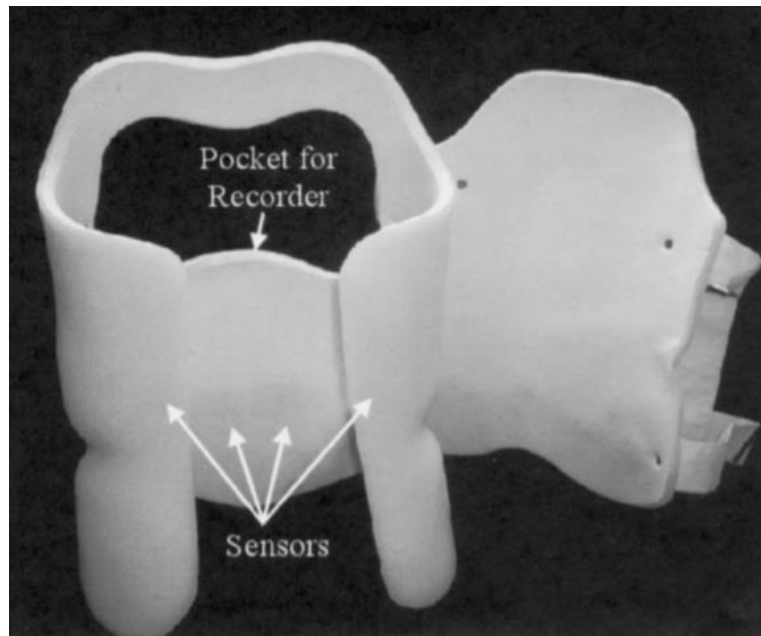
**Table 2. 3** Existing pressure sensors and their limitations

	<b>Sensor location</b>	<b>Function</b>	<b>Limitation</b>
<b>Time-recording pressure sensor</b>	Embedded at designated locations to determine on–off brace-wear	Measure wear time	Cannot measure applied load; no overall and instant pressure; only obtains measurements when the brace is worn properly; and meant for specific users
<b>Wireless force sensor</b>	Placed underneath the pads in the primary pressure areas	Measures load pattern (N) and wear time	8 m limitation in distance; time-delay problem; no overall pressure distribution; and meant for specific users
<b>Pressurex® pressure film</b>	Placed in between any two contact or impact faces	Shows overall pressure distribution profiles in greyscale	Easily pleats and wrinkles; no instant data; and cannot be reused
<b>Texsens®</b>	Inserted underneath textiles	Measures and visualises instant compressional forces on mobile device	Damages easily; sensor shifting problem; and no overall pressure distribution
<b>BodiTrak® pressure mat</b>	Placed on flat surface	Measures and visualises instant overall pressure profiles	Easily pleats and wrinkles, and suitable for flat surfaces only

### 2.5.1 Time-recording pressure sensor

The time-recording pressure sensor is mainly used for monitoring the compliance of brace use (Havey et al., 2002) (Figure 2.14). Force-sensitive resistors (FSRs) and a data logger are embedded in the brace. The logger starts to acquire and records the brace-wear time when at least two switches are turned on. FSRs are thin polymer devices with dimensions of 2 x 2 x 0.5 cm, and their electrical resistance decreases when compressional forces are applied. Therefore, when subjects are donning the brace, the FSR sensors will turn and start to record the wear time. Moreover, a customised Windows software is utilised to display the wear time

and show the on-off status of each FSR sensor in instant. Although the network is simple and easy to use, it can only measure the wear time, and the applied force is unknown. Also, the measurement is only performed when the orthosis is worn properly.

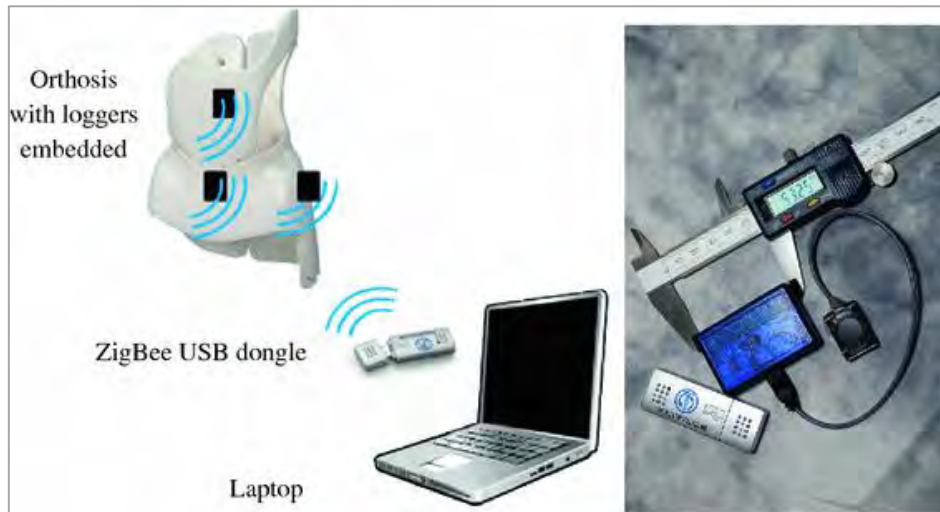


**Figure 2. 14** Custom-moulded TLSO with embedded pressure switches and data logger

### **2.5.2 Wireless force sensor**

Battery-powered wireless force sensors are specially designed for measuring and monitoring the forces exerted by hard braces during daily activities (Lou et al., 2010b) (Figure 2.15). The system consists of a base station (ZigBess USB dongle), a master logger, and 15 slave loggers (each consisting of a Honeywell force sensor that is 4 mm in thickness), which can measure pressure up to 6.78N (60 kPa) per minute. Also, once the batteries are fully charged, they could be used for 4 months continuously. The brace in Lou et al. (2010b) contains 8 sensors, and their location depends on where the pressure pads are placed, which are commonly in the underarm and pelvis regions. However, the results showed that some loggers have a time delay, and this problem becomes worse if there is no further synchronisation. The problem affects the data analysis as the applied forces are not collected at the same time. Also, data may not be recorded

if the distance between the loggers and the base station is more than 8 metres. Moreover, the sensing system appears to be made for a particular user in mind because they are embedded in a tailor-made Boston brace.



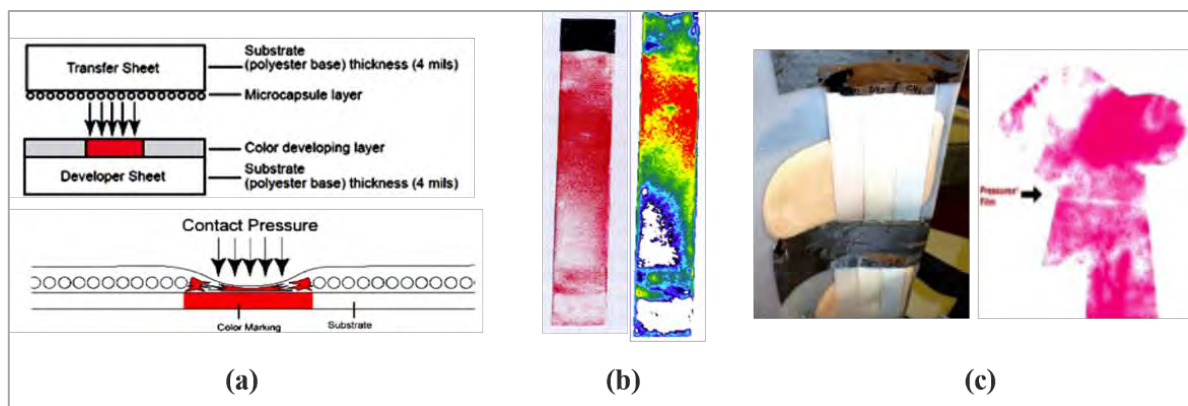
**Figure 2. 15** Wireless sensing system and dimensions of the logger unit (Lou et al., 2010b).

### **2.5.3 Pressurex® pressure film**

Pressurex® is a sensor film that measures the relative pressure between two contact faces within 20 psi (Sensor Products Inc., 2023). Since the sensor is very thin (~0.2 mm) and flexible, it can conform to curved surfaces, and thus favourable for taking close-to-body measurements or used in tight spaces where traditional electronic transducers cannot access. Pressurex® pressure film is made of a polyester base and a layer of tiny microcapsules (Krištof et al., 2010), so that when pressure is applied, the sensor film changes colour (Figure 2.16 (a)). When compression forces are applied, the microcapsules break and produce a greyscale pressure distribution profile immediately. The amount of applied force can be determined by observing the darkness and density of the marked areas. The darker areas denote a greater amount of force. Moreover, the resultant images can be analysed by using a Topaq® imaging system and a specific scanner, so that the exact amount of pressure at every marked point on the film can be determined. The output images are high in resolution in full colour (Figure 2.16 (b)).



Although using this sensor film is a quick and effective method to observe the overall pressure distribution, the results can only be shown when the film is removed, so that the instant pressure exerted by the brace would remain unknown. Also, the large film is not suitable for directly wrapping the human torso because many pleats and wrinkles will be created, which affect the pressure profile. Krištof et al. (2010) used Pressurex® to measure the overall interface pressure distribution between scoliotic patients and their orthosis. To address the pleating, the pressure film was cut into several segments and then attached to the inner side of the orthosis (Figure 2.16 (c)). This provided good results, and the overall pressure could be viewed as a picture. Nevertheless, the sensor film does not provide instant data and is inconvenient to use.



**Figure 2. 16** Pressurex® pressure film (a) mechanism, (b) before (left) and after (right) using Topaq® imaging system, and (c) measurement process (Krištof et al., 2010).

#### 2.5.4 Textsens®

The Textsens® is a flexible and lightweight sensor that is used to measure the compression force applied by textiles (Novel GmbH, 2020) (Figure 2.17). This sensor can obtain highly accurate measurements under a garment because even low contact pressure caused by body movement can be detected. The scanning rate and pressure range are 50 Hz and 1-10 kPa, respectively. The instant compression force can be visualised on a mobile device via Bluetooth and the loadpad® app. Also, the data can be stored on a mobile, uploaded onto the Cloud or

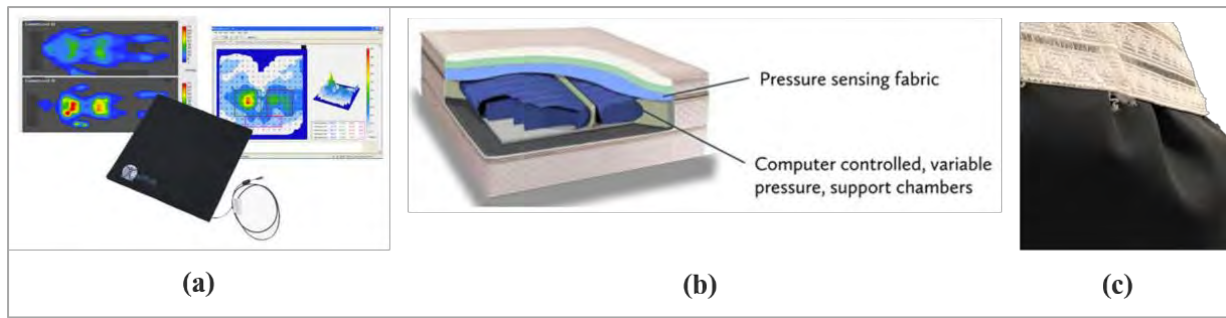
exported to a computer for further analysis. Although this sensor is highly sensitive and precise, it is also thin and flexible, and might be easily damaged or shift due to the friction between clothing and skin.



**Figure 2. 17** The textsens® sensor and loadpad® app (Novel GmbH, 2020).

### **2.5.5 BodiTrak® pressure mat**

The BodiTrak® pressure mat is a multilayer stretchable and breathable smart fabric with built-in smart USB electronics (Health Care & Co., 2020) (Figure 2.18 (a)). Also, its core consists of pressure-sensing fabric and computer-controlled support chambers (Health Care & Co., 2020), which allows the mat to scan the applied force over a hundred times per second (BodiTrak, 2023 (Figure 2.18 (b))). Aside from rapidly acquiring data, the overall pressure distribution can be visualised in instant in a matrix format because the pressure mat modifies the current that passes through the exact location where the force is applied. The mat is normally used on a flat surface, such as on a bed, chair, or the floor to see how the tested objects adapt to the applied force or how athletes apply pressure. However, when wrapped around the body, the results may be influenced by the pleats, which therefore leads to inaccurate data (Figure 2.18 (c)).



**Figure 2. 18 (a)** BodiTrak® system (Health Care & Co., 2020) **(b)** Structure of the BodiTrak® pressure mat (Health Care & Co., 2020), and **(c)** Pleats created by BodiTrack® pressure mat.

### Knowledge gap 3:

No sensor is available that can be easily detached without shifting and pleating to monitor the overall pressure exerted by a brace in instant.

## 2.6 Smart textiles

Smart textiles are defined as textiles that are capable of sensing, responding and adapting to stimuli in the environment through electronic devices that are integrated into the textile structures (Van Langenhove et al., 2005). Therefore, they show significant changes when subjected to different parameters, such as mechanical, thermal, electrical, and optical changes. Also, compared to other wearable electronics, smart textiles are more comfortable to wear and allow ease of movement (Rothmaier et al., 2008a). Nevertheless, even though smart textiles are highly competitive, they still cannot replace current wearable electronics at this moment because they are less robust (Castano & Flatau, 2014).

There are three types of smart textiles, namely passive, active, and very smart textiles (Stoppa & Chiolerio, 2014). The main difference between passive and active smart textiles is their ability to react to the environment. Passive smart textiles have sensors that can only sense the environment or users, while active smart textiles can sense a stimulus and react to them. Very

smart textiles are a higher level of smart textiles; not only are they able to sense and react, but also capable of adapting their abilities to the environment. The first intelligent garment is the Georgia Tech Wearable Motherboard™ (Jayaraman & Park, 2010). Plastic optical fibres are inserted into the woven smart shirt to identify bullet wounds on soldiers as well as monitor their vital signs.

Recently, smart textiles have seemingly become a new trend in the textile technology field because they hold enormous potential and have high demand. Besides applying them in the military area, they have become more common and being used in various sectors now, such as health care and retail (Ameri Research Inc., 2017). Also, it is believed that more smart textiles will be produced and even become a part of our lives in the future. For instance, Adidas created a series of smart sportswear like Climalite and Climachill, which claim to keep wearers cool and dry even when exercising in a hot environment (Adidas, 2023; Philippine Daily Inquirer, 2016) (Figure 2.19 (a)). Also, Nike offers the Nike Adapt BB self-lacing trainers, with a custom motor and gear train that are capable of sensing the required foot tension and then adapting accordingly to accommodate the foot snugly (Bell, 2019) (Figure 2.19 (b)). Moreover, Levi partnered with Google to develop a smart jean jacket that can control music and answer phone calls. The jacket cuff can act as a touchpad when the phone is connected to the jacket (Hartmans, 2019) (Figure 2.19 (c)). According to a news reported by Dublin in 2023, smart textiles were predicted to generate nearly US\$4.5 billion in the year of 2022, and may reach US\$20.6 billion by 2030. Also, they would evolve from passive to active to ultra-smart textiles (Dublin, 2023).



**Figure 2. 19** Existing use of smart textiles: **(a)** Adidas Men's Workout Climalite Pants (Adidas, 2023), **(b)** Nike Adapt BB sports shoes (Bell, 2019), and **(c)** Levi's Google smart jean jacket (Hartmans, 2019).

### 2.6.1 Advantages of textile-based fibre optic sensors

Fibre optic sensors are fibres that are capable of generating, transmitting, modulating, and detecting photons (Tao, 2005). They can measure different parameters, like force, pressure, electrical current, humidity, and temperature variations (Castano & Flatau, 2014). Fibre optical sensors are a crucial application of optics technology, and their applications have been studied for more than 30 years (Plümpe et al., 2017). When incorporated with textiles to provide a sensing function, the resultant product is considered to be a smart textile, which can be directly used on the body.

Optical fibre sensors are perhaps the most appropriate devices for integration with textiles (Rothmaier et al., 2008a) because they are low in cost, flexible, lightweight, robust and non-toxic, and have high strain sensitivity as well as immunity to electromagnetic fields and (Carmo et al., 2012; Mac-Thiong et al., 2004; Plümpe et al., 2017). These advantages have caught the attention of scientists in different fields, especially those in the field of clinical biomechanics because optical fibre sensors are non-toxic, lightweight, and small enough for insertion into the body for examination of various conditions that is not possible with conventional sensor

devices. Also, compare to other wearable electronics, TFOSs are more comfortable to wear and have ease of movement (Rothmaier et al., 2008a).

### **2.6.2 Types of optical fibres**

Optical fibres consist of three parts – the core, cladding and outer coating or buffer. The core which carries light, is glass or plastic, so it is transparent. The core has a high index of refraction and is wrapped with a cladding material which confines light to the core. The cladding material has a lower index of refraction than the core. The difference in the indexes allows total internal reflection to take place at the core and cladding boundaries, so that light can be transmitted down the fibre and not escape through its sides (Schwarz-Pfeiffer et al., 2015). Finally, the outer coating serves to protect the core and cladding from damage. As stated, the core can be glass or plastic, hence optical fibres can be classified into two categories, namely glass optical fibres (GOFs) and polymer optical fibres (POFs). Both are lightweight, flexible, and robust; have high sensitivity and immunity to electromagnetic interference; and produce no heat (Allsop et al., 2012; Mac-Thiong et al., 2004; Rothmaier et al., 2008a; Zheng, 2014). However, they are not very elastic compared to textiles, so special fibre arrangements may be needed when making smart textiles, such as bending the optical fibres in a curvilinear shape continuously to increase the range of movement. POFs usually have a lower Young's modulus (1.6 GPa to 5.0 GPa) and are less stiff, as well as larger breaking strain (6% to 38%) than GOFs (Peters, 2011; Zheng, 2014). This means that POFs are more compatible with the fabric manufacturing process where high tension and friction will be applied.

However, POFs have higher attenuation than GOFs, so they can be used for short-distance communication only (Zubia & Arrue, 2001). Also, stiff POFs, like polycarbonate and polystyrene, are probably not suitable for insertion into fabric because they may induce a stiff hand feel (Rothmaier et al., 2008a). In addition, POFs may lose their original properties after

repeated use. Chen et al. (2011) found that the loss of the properties of commercially available conventional SI POFs could reach 18.3% after 100 cyclic loadings. Other factors may also lead to loss of light, such as the wavelength, curvature radius, wrapping turns, temperature, and the presence of protective layers (Zendehnam et al., 2010).

### **2.6.3 Classification of fibre optic sensors**

Optical fibre sensors can be categorized into two main subgroups, namely extrinsic and intrinsic sensors. The key function of the former is to deliver the measured data to and from a transducer at a remote location, while the latter are sensitive to external stimulus so they can transport and modify light to perform as a sensor (Da Silva et al., 2013; Zheng, 2014). Since intrinsic sensors are the focus of the thesis, and light intensity and FBG is commonly used to construct intrinsic sensors, more information about them are provided below.

#### **2.6.3.1 Light-intensity based fibre optic sensors**

Micro and macro-bending sensors depend on light intensity variations (Zheng, 2014), and provide the optical effects when the fibres are bent from a straight axis (Corning Incorporated, 2013). Micro-bending sensors have optical fibres that are bent with a small curvature radius (Zendehnam et al., 2010), and the attenuation will increase with higher frequencies and a smaller radius bend along the length of the fibre (Corning Incorporated, 2013). Although micro-bending sensors usually have good sensitivity, nevertheless they are associated with a low measurement range (Zheng, 2014). Macro-bending sensors on the other hand, are similar to micro-bending sensors with the main differences being the sensor dimensions and bending range (Zheng, 2014). They have a bending radius that is much larger than that of the fibre radius (Zendehnam et al., 2010), and the attenuation is caused by bending and wrapping. These sensors have a wider measurement range, but lower resolution compared to the micro-bending

sensors (Zheng, 2014). Nevertheless, excessive bending may cause fibre breakage and signal loss for both micro and macro-bending sensors.

### **2.6.3.2 Fibre Bragg grating sensors**

FBG sensors are intrinsic sensors used for a variety of sensing applications and most commonly for measuring strain and temperature. These sensors contain FBGs which are embedded in optical fibres by using ultraviolet (UV) lithography. The optical fibres are characterised by periodical modulations of the refractive index along the fibre axis (Schwarz-Pfeiffer et al., 2015). FBG sensors can perform as a reject-band filter that is capable of reflecting selected Bragg wavelengths while transmitting others (Da Silva et al., 2013) (Figure 2.20). To install FBGs into the fibre, the core is doped with germanium to increase the refractive index and photosensitivity, and then the coating will be removed for inscription (Witt et al., 2012). Next, the refractive index of the core will be modulated along the fibre with pitch ( $\Lambda$ ) by illuminating UV light. Also, by making use of an appropriate phase mask, more than one FBG sensor can be inscribed onto a single optical fibre with the required spacing arrangement. After that, the fibres will be recoated to protect the weak points.

FBG sensor is commonly used for measuring strain and temperature. However, when FBG sensors are associated with the proper interface, the shift of the Bragg wavelength can act as a parameter transducer to measure many other mechanical parameters, like pressure and vibration (Werneck et al., 2013). As the broad light source is launched, the Bragg wavelength ( $\lambda_B$ ) will be reflected by grating and can be expressed by using Equation (2.1) (Hill & Meltz, 1997). The shift is the sum of changes in the refractive index and the pitch that is caused by the dependent variables, like strain, and the equation can be expressed as Equation (2.2). The sensitivity of the Bragg wavelength with strain and temperature can be calculated by using Equations (2.3) and (2.4), respectively.



$$\lambda_B = 2n_{eff}\Lambda \text{ ----- (2.1)}$$

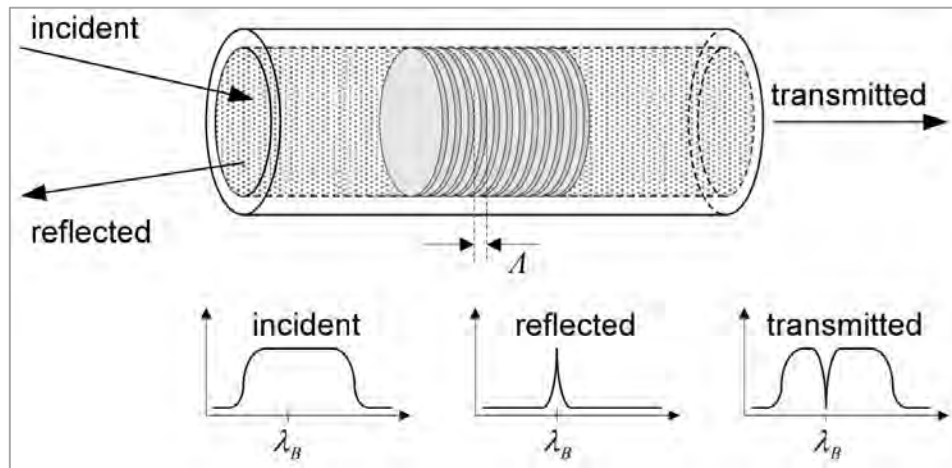
$$\frac{\Delta\lambda_B}{\lambda_B} = \frac{\Delta\Lambda}{\Lambda} + \frac{\Delta n_{eff}}{n_{eff}} \text{ ----- (2.2)}$$

$$\frac{\Delta\lambda_B}{\Delta T} = 2n_{eff}\frac{\partial\Lambda}{\partial T} + 2\Lambda\frac{\partial n_{eff}}{\partial T} \quad OR \quad \frac{\Delta\lambda_B}{\lambda_B} = \frac{1}{\Lambda}\frac{\partial\Lambda}{\partial T}\Delta T + \frac{1}{n_{eff}}\frac{\partial n_{eff}}{\partial T}\Delta T \text{ ----- (2.3)}$$

$$\frac{\Delta\lambda_B}{\Delta L} = 2n_{eff}\frac{\partial\Lambda}{\partial L} + 2\Lambda\frac{\partial n_{eff}}{\partial L} \quad OR \quad \frac{\Delta\lambda_B}{\lambda_B} = \frac{1}{\Lambda}\frac{\partial\Lambda}{\partial L}\Delta L + \frac{1}{n_{eff}}\frac{\partial n_{eff}}{\partial L}\Delta L \text{ ----- (2.4)}$$

Besides,  $N_{eff}$ , the fibre effective refractive index (RI), can also be used as a parameter transducer (Werneck et al., 2013). Effective RI refers to the average RI of the core and cladding. The parameter depends on the penetration of the evanescent field of the core to cladding. As the cladding diameter is much larger than the evanescent field, the effective RI is not affected by external influence. However, if the fibre cladding is corroded and reaches the evanescent field, the RI of the surrounding media, such as gas, air, and liquid, should be considered too.

The major advantage of FBG sensors is that they do not interfere with the fluctuations of the optical source because the signals are dependent on the wavelength instead of optical power (Da Silva et al., 2013). This makes displacement possible, and therefore FBG sensors are suitable for physical measurements, like strain, pressure, force, temperature, and motion analyses (Da Silva, 2013). They are popular for measurements associated with textiles because they are easy to manufacture, low in cost, lightweight, flexible, non-conductive, and stable (Da Silva et al., 2013; Jonghun, 2011; Lakho et al., 2019; Schwarz-Pfeiffer et al., 2015). Moreover, they are self-calibrated and portable, so there are no loose connection problems with ease of transport.



**Figure 2. 20** Working principles of FBG sensor (Da Silva et al., 2013).

#### 2.6.4 Applications

Apart from being used in data transmission like telecommunication systems, optical fibres also have enormous potential in lighting technology and sensing applications (Plümpe et al., 2017). When the sensors are integrated into textiles, they become smart textiles which are now being used in healthcare.

Previously, the integration of optical fibres into textiles was purely for visual enjoyment. For example, Thiele (2003) recommended that optical fibres could be intertwined into mesh to produce luminous fabric (Figure 2.21). However, the light loss is probably much higher than their insertion into a woven structure because the curvature radius is much smaller, and angles may even form. This also implies that only extrinsic sensors are suitable for knitting into a mesh for emitting light because a stable signal transmission is not required. Conversely, intrinsic sensors that require high accuracy are apparently not suitable for directly replacing knitting yarn. Not only does this cause extreme losses in signals, but the small curvature radius of the knitted loops and tightly packed structure may easily cause mechanical failure or breakage (El-Sherif, 2005; Rantala et al., 2011). Moreover, the superior characteristics of

knitted fabric may be lost after integration with low-flexibility optical fibres, such as its elasticity and drapability.



**Figure 2. 21** Illuminous knitted fabric made with polymer optical fibres (Thiele, 2003).

Nowadays, the outstanding performance of fibre optical sensors is gaining more acceptance, especially for health monitoring. Thus, more scientists and researchers are focusing on smart textiles for monitoring respiration, motion, heartbeat, blood pressure, pulse oximetry and temperature. Table 2.4 shows the integration methods of several different types of TFOs, types of fibres and sensors as well as their functions. All of them can be recognised as passive smart textiles as they can sense and react to stimuli from the environment.

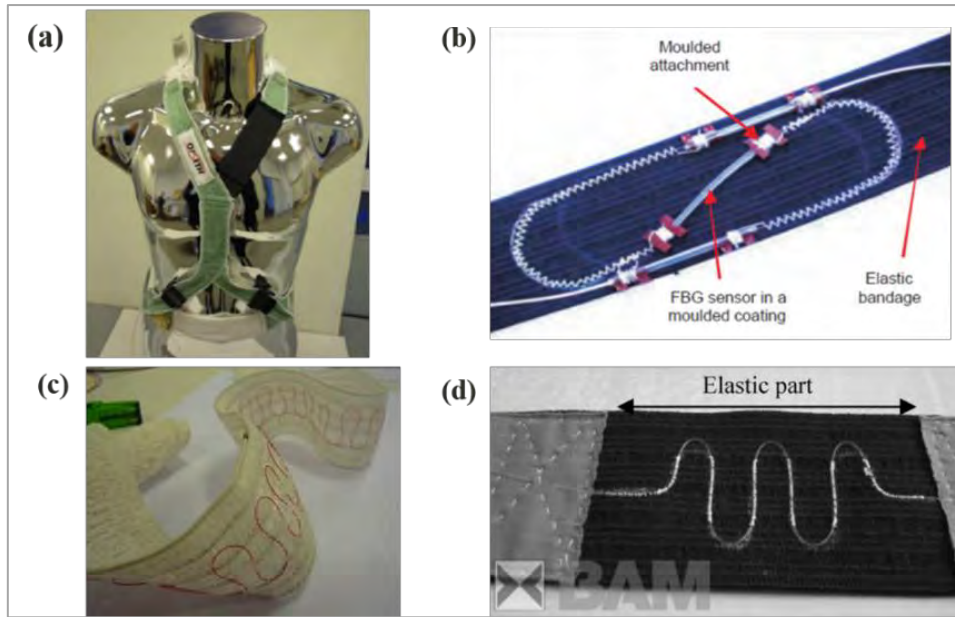
**Table 2. 4** Fibre optic sensor applications.

	Integration method	Type of fibre and sensor	Function
<b>Sensor harness</b>	Sewn & adhered	GOF, FBGs	Monitors respiratory movement during MRI
	Knitted	POF, macro-bending,	
	Sewn	POF, OTDR	
<b>Sensing glove</b>	Embedded	GOF, FBGs	Monitors hand motions and functional abilities
<b>Pressure sensor</b>	Woven	POF, micro-bending	Measures pressure
<b>Smart insole</b>	Embedded, adhered	GOF, FBGs	Monitors plantar pressure distribution

#### **2.6.4.1 Sensor harness for respiratory monitoring**

Witt et al. (2012) designed a sensor harness to monitor the respiratory movement of patients during MRI by sewing optical fibre sensors onto the fabric (Figure 2.22 (a)). Three types of fibre optic sensors were used, namely macro-bending, POF optical time-domain reflectometry (OTDR) and FBG sensors.

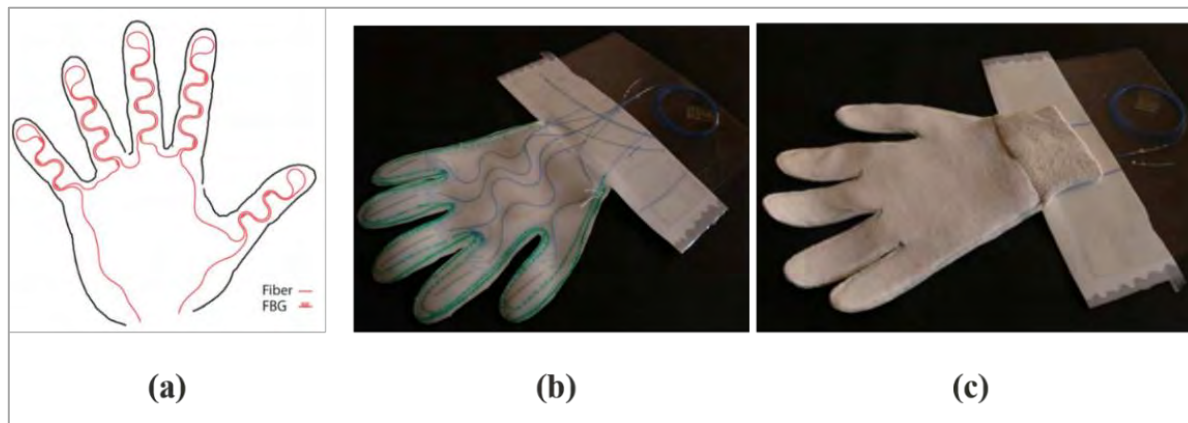
A silica FBG sensor was applied to the thoracic region because it has high accuracy but a low strain limit (Figure 2.22 (b)). To enhance its elasticity, the sensor was bent into a curvilinear shape. Also, a silicone coating was applied and the 2 ends of the FBG were fixed with glue to enhance the robustness of the sensor. Also, both POF OTDR and macro-bending sensors were applied at the abdomen area because they are flexible enough to support the abdominal surface movement, which is normally elongated by 1-3% during breathing. For the macro-bending sensor, the high elasticity and breakdown strain of the POFs make it possible to insert this sensor into the crochet fabric during the manufacturing process (Figure 2.22 (c)). Moreover, the POF OTDR sensors were sewn onto elastic textile and bent into a curvature (Figure 2.22 (d)). Since instant strain is based on time and intensity, the instant strain at different locations could be measured. Although the sensor harness showed good sensing ability, the measurement equipment may be expensive and complex to use. Also, data processing may be complicated and time-consuming because three different types of fibre optic sensors are used.



**Figure 2. 22** (a) Sensor harness, (b) macro-bending sensor inserted in the crochet fabric, (c) POF OTDR sewn onto elastic textile, and (d) FBG sensor embroidered onto elastic band (Witt et al., 2012).

#### 2.6.4.2 Customised wearable sensing glove

Da Silva et al. (2011) developed a customised wearable sensing glove to monitor hand movements and functional abilities by embedding FBG sensors into a three-layer glove (Figure 2.23). As the finger joints can stretch the glove to around 14% of its size, if the fibres lie straight on the glove, finger joint movement is limited. Therefore, the optical fibres were continuously bent into a curvilinear shape to ensure enough elasticity when the glove was tested. In total, 14 FBG sensors were inscribed onto a single optical fibre and assigned specific distances to match the finger phalanx locations. Then, they were fixed onto a thin and flexible polymeric laminate, and embedded between the glove and top layer, which is made of polyvinyl chloride (PVC) to minimise the movement of the sensing fibres. When wearing the gloves, the angle of the finger joint can be estimated because the hand movements are converted into numerical data in instant.

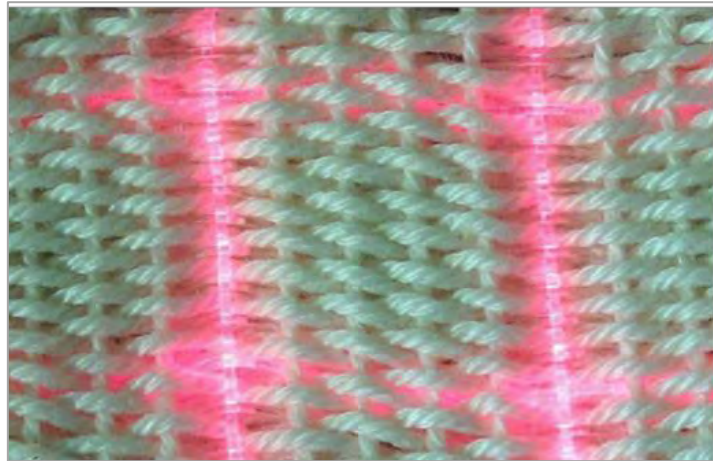


**Figure 2.23**(a) Schematic diagram of sensing glove, (b) outer side of sensing glove, and (c) inside of sensing glove (Da Silva et al., 2011).

#### 2.6.4.3 Woven pressure sensor

Rothmaier et al. (2008a) created a pressure sensor by inserting polymer optical fibres into a woven structure (Figure 2.24 (a)). Due to their elastomeric property, the cross-section of the optical fibres changes when subjected to external pressure, so the transmitted light intensity would also change and be detectable. An applied pressure between 0 to 30 N can be measured. A twill structure, Atlas pattern with a 1/4 repeat, was used to incorporate the pressure sensor because it only shows a few dislocations, and thus light attenuation can be minimised. A 2x2 matrix on 1.5 cm<sup>2</sup> of textile with 4 optical fibre intersections was created (Figure 2.24 (b)). The equipment set-up included a light-emitting diode (LED), 4 phototransistors, and an analogue/digital converter board for recording the detected signals. The results showed that the thicker POFs (0.98 mm in diameter) have a lower signal resolution with smaller forces, but can measure pressure up to 30 N, while thinner POFs (0.51 mm in diameter) can measure up to 15 N only. Nevertheless, regardless of whether the sensors are thick or thin optical fibre sensors, the sensing fibres on the top are more sensitive than those on the bottom when measuring smaller forces. This may be because the bottom fibres cannot bend as much as the top fibres when smaller forces are applied. Zheng (2014) integrated pressure sensors into a woven

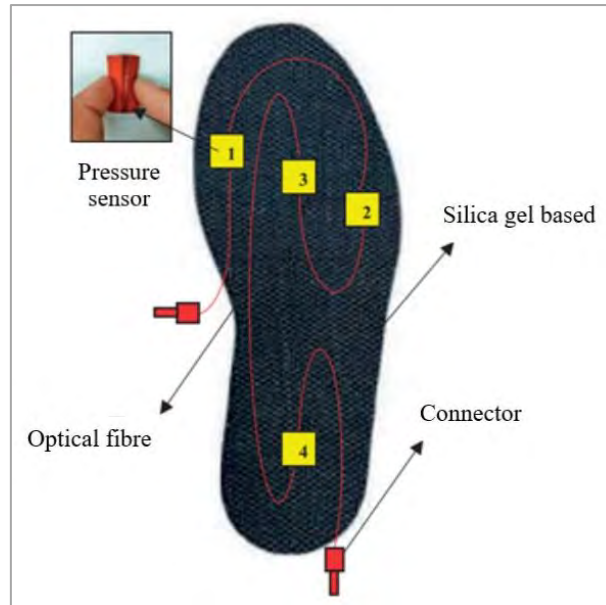
structure, as optical fibres inserted into woven structures have always been intended to only emit light. However, in doing so, the resultant product appears to be suitable for measuring relatively high forces only. Moreover, due to the elastomeric property of POFs, it is predicted that the accuracy and precision will degrade when pressure sensors are used frequently, and they cannot be easily repaired.



**Figure 2. 24** 2 x 2 matrix with four optical fibre intersections (Rothmaier et al., 2008a).

#### **2.6.4.4 Smart insole**

Lakho et al. (2019) developed a smart insole to monitor the plantar pressure distribution, analyse biomechanical gait and evaluate the body posture by embedding FBG sensors into the insole (Figure 2.25). Four FBG sensors with different wavelengths were placed at different locations: the first, third, and fifth metatarsals, and the heel. Synthetic silica gel was used for making the insole and sensors because it is flexible, easy to apply, and comfortable to wear. A path was engraved for the optical fibre, and then the pre-stressed FBG sensors were embedded and glued in the grooves by using epoxy resin. After that, four rectangular holes were cut at the sensing locations on the insole to embed the pressure sensors. The sensitivity of the FBG sensors is approximately 0.000412 nm/kPa.



**Figure 2. 25** Schematic diagram of silica gel-based smart insole with four FBG sensors  
(Lakho et al., 2019).

#### **Knowledge gap 4:**

There are few studies and research efforts on TFOSs that not only monitor pressure applied to the torso but are also comfortable to wear.

## **2.7 Materials for comfortable pressure monitoring undergarments**

### **2.7.1 Soft and hydrophilic materials**

As pressure monitoring undergarments directly come into contact with skin, they should be soft and smooth in hand feel. Also, bracing causes feelings of physical warmth easily because many of them are made of thermoplastic, which has poor thermal conductivity and breathability. This problem becomes worse in the summer as perspiration may be trapped inside the brace (Canavese & Kaelin, 2011). In terms of textile braces, if they cannot absorb sweat quickly, the result is a clinging feeling. Besides discomfort, the clinging may also cause body odour, which may intensify the negative psychological impact on AIS patients.



Cotton is one of the most suitable materials to fabricate a pressure monitoring undergarment because it has very good water absorbency, and is breathable and strong (Rathore, 2018). Moreover, it is a natural fibre with a soft hand feel, so there is less chance of this material causing skin irritation. However, pure cotton undergarments dry slowly, and wrinkle and mildew easily. When blended with other materials, this problem can be reduced and provide more wear comfort. For example, the Boston T made of CoolMax/lycra is wrinkle-resistant and wicks moisture away quickly (Boston Orthotics & Prosthetics, 2017). Also, a scoliosis brace T-shirt with exterior seams made of organic cotton, bamboo rayon and spandex blend is soft, highly elastic, and more comfortable to wear (Embraced in Comfort, 2021).

Modal is a semi-synthetic material and a variation of viscose rayon, but its properties are more cotton-like (Krishna, 2017). Compared to rayon, it is stronger when wet, and has higher resilience and dimensional stability, but poorer water absorbency. When compared to cotton, modal has a similar stability and strength, but is softer and lustrous, so the material gives a silkier feeling than cotton (Tencel, 2020). Its comfortable feeling and good water absorbency make modal favourable for producing intimate apparel. However, it is more expensive and has a higher tendency to pile due to the long fibres used (Verma, 2010).

### **2.7.2 Cooling material**

Yip and Chan (2020) pointed out that thermal conductivity, moisture wicking, and breathability are the three main factors that regulate heat and moisture. Therefore, pressure monitoring undergarments should be breathable, and able to transfer body heat and wick moisture away into the environment efficiently, to keep the body cool and dry. However, some of the hard braces are nearly unbreathable, which prevents body thermoregulation and thus increases the body temperature. Cooling materials may help to improve thermal comfort because of their excellent thermal conductivity (Cao et al., 2016). For instance, the Boston Silver T is one of

the solutions for Boston brace wearers. This garment is made of CoolMax and X-static pure silver fibres, which provide a cooling and anti-microbial effect (Boston Orthotics & Prosthetics, 2017).

Besides, CEO $\alpha$ <sup>TM</sup> is a comfortable deviation of “Shingosen”, a synthetic fibre that is made of highly water-absorptive polyester filament yarns (TORAY Group, 2020a). Its manufacturer claims that the fibres provide a cool feeling, and their water absorption is better than pure cotton due to its capillary absorption structure. Also, the garments made of CEO $\alpha$ <sup>TM</sup> are soft, drape well, lightweight, and dry quickly due to the cross-section of the fibres and fibre-blending. SPORTINGTEX<sup>®</sup> cooling textile is a knitted fabric made of polyester/nylon and consists of naturally low-temperature minerals (SportingTex, 2021). Since minerals have higher thermal conductivity than traditional fibres, they can transfer heat faster. The company claims that body heat can be transferred quickly to the fabric when the body and material come into contact, yet the fabric remains cool after leaving the skin or moving away from the heat source. These advantages make SPORTINGTEX<sup>®</sup> favourable for underwear and sportswear.

### **2.7.3 High elasticity materials**

Pressure monitoring undergarments should be elastic and offer a tight fit to avoid pleats created underneath the brace, otherwise, the optical fibre sensor may break or become damaged easily. LYCRA<sup>®</sup> fibres are a thin and transparent synthetic spandex fibre. They have excellent elasticity, which can be stretched 4 to 7 times their original length (TORAY Group, 2020b). Even a small amount of LYCRA<sup>®</sup> fibre can change the performance of a fabric. Therefore, they are blended with natural or human-made fibres to produce stretchy fabrics with better fit and shape retention as well as offer ease of movement. For example, the Boston Silver T is made of CoolMax/lycra with some antibacterial fibres. It can be stretched over 150% and therefore fits the body perfectly (Boston Orthotics & Prosthetics, 2017). Generally, garments that require

a better fit, shape retention, durability and ease of movement are usually made of LYCRA<sup>®</sup>, such as activewear, swimwear and intimate apparel.

Besides the raw material properties, the fabric structure can also improve fabric elasticity. Generally, knitted garments are more elastic than woven fabrics due to the yarn configuration. Each knit loop forms an “Ω” shape while the weave yarns are in a predominantly straight alignment (Behera & Hari, 2010; Behera et al., 2010). The knit loops can be stretched easily in all directions, and able to recover to their original shape after relaxing, but weave yarns cannot because they are intersected with each other (Chong, 2013). Moreover, the high porosity of knitwear allows more air to pass through, so it has better breathability.

## **2.8 Construction method of finite element model**

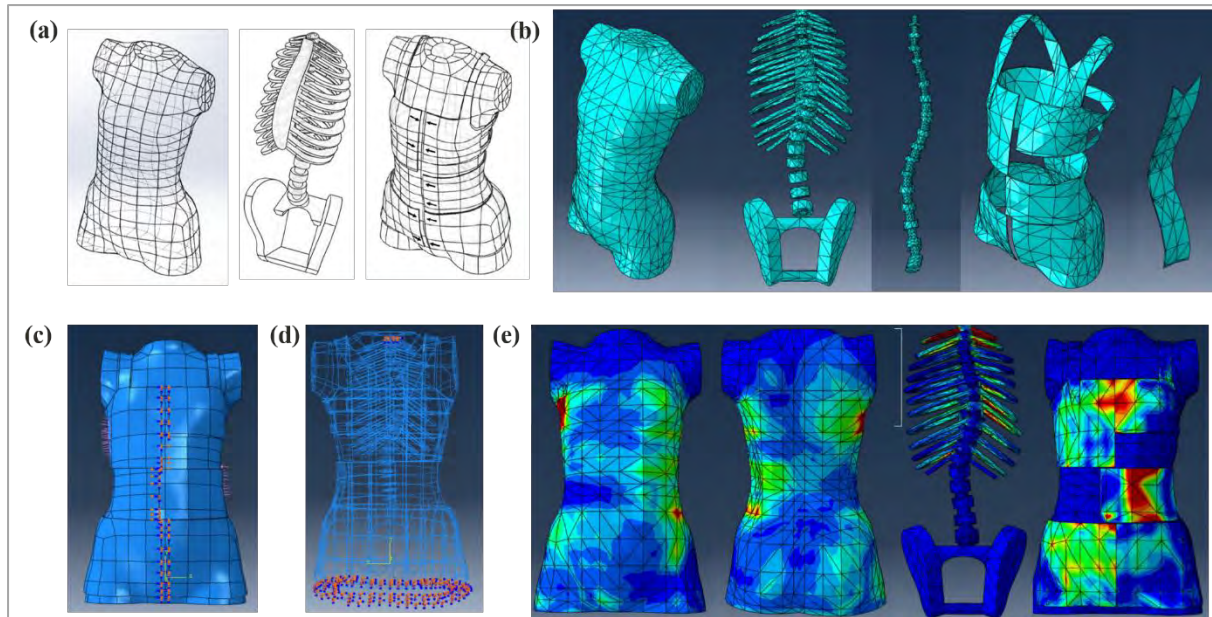
FE simulation is used to evaluate the amount of applied brace force without the needs for repetitive experiments and wear trials (Chan, 2019). This method saves a lot of time and protects subjects from unpredictable risks.

Nowadays, finite element analysis (FEA) methods are not limited to the engineering field; many researchers also use the methods to predict the performances of products and systems. Therefore, it is not surprising that FEA has been widely utilised in orthopaedic biomechanics (Yahyaiee Babil & Rouhi, 2020). FE analysis can be used to simulate the bracing, evaluate the brace treatment efficiency as well as estimates and predicts the pressure exerted by the brace. For example, Périé et al. (2004) compared the pressure applied by simulated and real braces; Chan (2019) created an FEA to show the stress distribution of a brace (posture correction girdle) on the torso and spine; Khoddam-Khorasani et al. (2018) used an FEA to estimate the trunk muscle forces in vivo loads (muscle exertions and gravity loads); Gignac et al. (2000) employed an FEA to determine the optimal load to correct both spine and rib cage deformities in 3D formats; and Clin et al. (2010) utilised FEA to compare the biomechanical 3D efficiency of

12,288 braces, so as to determine the most influential design factors. The results showed that there were 5 main attributes, namely brace opening position, strap tension, trochanter extension side, lordosis design and the rigid shell shape. Moreover, Clin et al. (2010) proved that the long-term result of bracing can be predicted by the immediate in-brace correction by using an FEA. These studies show that an FEA can provide a better understanding of the brace biomechanics and optimise their designs.

According to Chan (2019) and Fok (2020), there are 6 major steps in the analysis of FE models: 1) construct a geometric model; 2) define the material properties; 3) define the types of elements and meshing; 4) define the boundaries and loading conditions; 5) validate the model by comparing the spinal curvatures with x-rays; and 6) analyse the models (Figure 2.26).

The easiest way to construct a geometric model is to input the 3D geometry of the brace and human body into diagnostic tools. The 3D geometry of the brace and body is obtained through computed tomography (CT), MRI or multiview radiographic reconstruction (Clin, et al., 2010). However, these measurement methods are risky when repeated many times due to ionizing radiation. Therefore, AIS patients are required to take x-rays only. Nevertheless, it is challenging to create 3D models from 2D x-rays are because multiple views are required, and it is time-consuming. Three-dimensional body scanning is an alternative method although it can only capture the body surface contours (Lu, 2017). However, combining the 3D body scanned images and x-rays can provide an entire geometric model of the torso with bones by using Solidworks (Chan, 2019). Then, the pre-processed 3D images can be imported into the FE model to continue Steps 2 to 4.



**Figure 2. 26** FE models: **(a)** geometric models of the torso, spine and brace are constructed; **(b)** material properties and the type of element and meshing are defined; **(c)** the loading conditions are defined; **(d)** the boundary conditions are defined; and **(e)** the FE models are analysed: stress distribution of torso, spine, and brace (Fok, 2020).

## 2.9 Summary

AIS is a 3D spinal deformity that arises in children aged 10-16 for unknown reasons. The diagnosed patients have a lateral spinal curvature greater than  $10^\circ$ . When the Cobb's angle increases to  $20^\circ$ - $40^\circ$ , patients are prescribed a scoliotic brace, which is a common device used to stop or slow down the progression of the curvature. However, the brace effectiveness is unclear, and no standardised brace pressure has been established (*Knowledge gap 1*). Therefore, AIS subjects may suffer from the excessive pressure exerted by their brace, which over corrects their shoulder balance.

There are primarily 2 types of braces, namely hard and soft braces. Generally, the former is uncomfortable to wear due to inhibition of mobility and materials that are largely unbreathable, and sometimes the prolonged pressure may also induce pressure-related injuries. Moreover, the awkward and bulky appearance may have negative psychological effects on AIS patients and therefore reduce their compliance with the bracing treatment. On the other hand, soft braces usually have a more aesthetically pleasing appearance and are comfortable to wear due to less restriction, their lighter weight, and use of soft materials. Although they do not cause psychological issues, pain may be induced by high-tension straps or elastic bands. Also, the applied forces are not consistent or as effective as rigid braces because the fabric recovery deteriorates with time. The success of treatment depends on their initial corrective forces and compliance with treatment. However, some bracing treatments focus on the initial forces but neglect the importance of pressure tolerance, which affects compliance with treatment (*Knowledge gap 2*).

To improve compliance with treatment, it is important to monitor the amount of pressure exerted by the brace because excessive pressure tends to cause pain or injury. However, existing sensors for measuring brace pressure have 4 main inadequacies, namely no overall pressure distribution, no instant profile, shifting problem with shifting, and only designed for specific users (*Knowledge gap 3*). Smart textiles which comprise integrated fibre optic sensors into fabric could be one of the solutions. Fibre optic sensors are flexible, have high strain sensitivity, and capable of showing instant information. When incorporated with enough FBG sensors or transducers, the overall pressure distribution can also be known. There are several different methods to integrate sensors and textiles, and the key to success is probably their compatibility. This means that the sensor should have high sensitivity while maintaining the properties of the fabric, such as its elasticity and softness. Otherwise, the original intention for the integration of these two items would be futile. However, there are few studies and research

efforts on TFOs that monitor pressure applied on the torso and offers wear comfort (*Knowledge gap 4*).

A biomechanical model needs to be constructed to understand the relationship between applied pressure and spinal correction. This means that an FE model should be employed to simulate vertebral movement when donning a brace with different amounts of corrective forces. Therefore, the success of bracing as a treatment can be predicted based on the applied pressure.

## **CHAPTER 3 TEXTILE-BASED FIBRE OPTIC SENSORS FOR HEALTH MONITORING**

### **3.1 Introduction**

The idea of using wearable textile sensing devices for health monitoring purposes is gaining wider acceptance among scientists (Abro et al., 2019). This area of research is particularly important for patients who require continuous medical support and treatment. However, several critical considerations have to be addressed, such as sensor functionality and accuracy, user safety, wear comfort, and mobility.

Textile-based fibre optic sensors (TFOSs) are considered one of the most suitable tools for obtaining close measurements of the body. Their popularity is because they have high strain sensitivity, electromagnetic immunity, lightweight construction, affordability, non-toxicity, portability, and robustness (Carmo et al., 2012; Mac-Thiong et al., 2004; Plümpe et al., 2017). These features enable them to measure different parameters that cannot be obtained through conventional sensor devices. For instance, optical sensors can be used in magnetic resonance imaging (MRI) to monitor instant respiratory activity and heartbeat, thereby ensuring patient safety (Massaroni et al., 2015). Additionally, flexible and portable sensors can prevent issues with loose connections and allow ease of movement (Mac-Thiong et al., 2004; Rothmaier et al., 2008a), which make them ideal for remote monitoring and measuring physical movement. The data collected can be used to evaluate rehabilitation progress, detect diseases, prevent accidents, assess athletic performance, and act as a training device. The superior performance and advantages of fibre optic sensors have significantly increased their popularity in healthcare (Lam, 2007; Leal-Junior et al., 2019a; Massaroni et al., 2015). Therefore, it is believed that TFOSs are promising tool for health monitoring.



TFOSs belong to the smart textiles family, which are designed to integrate functionality into textile structures to enable them to sense and respond to their environment (Das et al., 2013; Koncar, 2016; Schneegass, 2017). Previously, the application of smart textiles was mainly confined to the military domain, but nowadays, they are available to the general public with a significant expansion in everyday health monitoring applications (Van Langenhove, 2015), such as the Adidas Bluetooth Smart Heart Rate Monitor with Textile Strap (Ameri Research Inc., 2017). Furthermore, the global smart textile market is projected to reach US\$ 13.63 billion by 2025 (The Insight Partners, 2020), which highlighted the rising trend in the adoption of smart textiles.

While the origination of smart textiles can be traced back to 1989 with the invention of a shape memory silk thread (Das et al., 2013; Van Langenhove, 2015), the application of TFOSs for health monitoring purposes was first introduced by Grillet et al. (2008), making them a relatively recent innovation. Therefore, it is unsurprising that many of them are in the research and development (R&D) stage, with enormous potential for future exciting applications. Thus, it is crucial to investigate existing research on TFOSs to analyse the latest paths of development to predict their trends.

It is unfortunate that only seven systematic reviews on TFOSs for health monitoring purposes have been found, and all of them employ a subjective approach to classify the reviewed articles, and focus exclusively on a subset of the available TFOSs. For instance, Leal-Junior et al. (2019a) primarily focused on studying polymer fibre optic sensors, while Massaroni et al. (2015) conducted a review of smart textiles based on fibre optics for monitoring vital signs but did not incorporate studies on instant body motion monitoring. Quandt et al. (2015) reviewed studies that focused on textile-based fibre optic force and strain sensors; however, they did not address other types of sensors, such as temperature sensors. Both Vanegas et al. (2020) and

Roudjane et al. (2018) reviewed papers that only focused on TFOSs for respiratory movement. Additionally, Costa et al. (2019) evaluated various kinds of flexible sensors but did not specifically target TFOSs. Although Gong et al. (2019) investigated photonic textiles for wearable and medical applications, their emphasis was on the working principles and integration methods. Apparently, the development and future trends of TFOSs for health monitoring purposes have received little attention in the scholarly literature. Although a manual literature review offers flexibility, the process is time-consuming to identify the research domain and knowledge development of the target studies (Fan et al., 2014). This is owing to the need for the individual examination of their relevance and correlation, and manually determining the linkages. Therefore, inconsistencies may arise because of variations in classification criteria.

To address the inadequacies of previous review studies, this chapter presents an objective and more thorough investigation of TFOSs, and an analysis of the trends through a citation network analysis (CNA). The objectives of this chapter are: (1) to describe the characteristics of TFOS-related articles based on the published journal, year of publication, type of article and research field, country of origin of the first author, as well as sensor application; (2) to identify the research domain of TFOSs by using CitNetExplorer; and (3) to recommend and conclude on future research opportunities of TFOSs.

### **3.2 Methodology**

Traditionally, researchers conducted systematic literature reviews manually to determine the research domain and knowledge structure of related studies. However, this approach could be time-consuming because it requires reading all of the relevant journal articles, sorting, and classifying them, as well as summarising the trends. With the advent of CNA, the literature review process has significantly evolved, although the tool may not completely capture the

semantics of the field (Zhuge, 2016). CNA is an objective method that enables researchers to identify the research domain, highlight the advancements, and demonstrate the evolving patterns of a specific area of study (Colicchia & Strozzi, 2012; Fan et al., 2014; Hummon & Dereian, 1989). The application of CNA enhances the efficiency of the classification process, provides clear illustrations of the linkages, and improves the consistency of the results. The process works by utilising the bibliographic data of journals, such as cited references and research areas, to establish linkages among different publications. Therefore, the research focuses and achievements over time can be easily organised and presented. By employing this method, researchers can gain a more efficient understanding of the work and outcomes of other researchers, thus enabling them to identify potential research areas and advance the field (Colicchia & Strozzi, 2012).

This study utilises a CNA in conjunction with a full-text search of journal articles on the Web of Science (WoS) Core Collection. The timeframe spans from 1959 to 2020, and the chosen keywords were extracted from relevant studies, which encompasses four primary categories: "textiles", "optical fibres", "sensors", and "health monitoring". To prevent the omission of relevant studies, related phrases were also included, such as "smart textiles" and "healthcare". Since this study focuses on TFOSs designed for human health monitoring, other applications of such sensors were not considered, such as for structural and marine health monitoring.

The inclusion terms were “TS=(weaving OR knitting OR woven OR knitted OR textile OR fabric OR clothing OR smart textile OR wearable electronic OR E-textile OR electric textile OR interactive textile OR wearable OR undergarment OR intimate OR clothing OR apparel OR fashion OR functional garment) AND TS=(fibre optic OR fibre Bragg grating OR FBGs OR optical device OR photosensitivity OR Bragg wavelength shift OR flexible optical fibres technology OR optical fibre OR optical) AND TS=(sensor array OR sensor OR pressure sensor

OR strain sensor OR strain measurement OR embedded sensor OR pressure OR strain OR embedded OR embedding OR insert OR insertion OR fibre optic sensor OR sensing) AND TS=(vital bio OR health OR medical OR health care OR health monitoring OR body OR clinic OR MRI OR human).”

A total of 47 studies published between 2008 and 2020 were selected to create the sample, which met all of the criteria in the keyword list. CitNetExplorer was employed to cluster the studies and show the development of the literature over time. Table 3.1 summarises their features and integration methods, along with the different textiles and applications.

**Table 3.1** Sample publications.

Source	Main feature/Title	Integration method; placement	Application
<b>Group 1 Flexible sensors for vital signs monitoring</b>			
(Abro et al., 2019)	FBG sensor is prestressed and placed in rectangular silica to provide higher sensitivity	Adhered onto an elastic belt by using silica gel; knee	Knee joint posture monitoring for sports and stroke patients
(Bennett et al., 2020)	Multimode fibres	Attached on a strap and wrist band; chest and wrist	Respiratory and heartbeat, pulse wave velocity and blood pressure monitoring for home & ambulatory health care improvement
(Costa et al., 2019)	Flexible Sensors-From Materials to Applications	<i>Review</i>	/
(Dziuda et al., 2013)	Ballistocardiography system with an FBG sensor	Attached on a mattress; underneath subject	Respiratory and heartbeat monitoring during MRI
(Vanegas et al., 2020)	Sensing Systems for Respiration Monitoring: A Technical Systematic Review	<i>Review</i>	/
(Fajkus et al., 2017)	Multichannel hybrid fibre optic sensor based on FBGs	Embedded in PDMS membranes and attached onto an elastic strap; chest	Respiratory and heartbeat and temperature monitoring
(Gong et al., 2019)	Wearable Fibre Optic Technology Based on Smart Textile: A Review	<i>Review</i>	/
(Grillet et al., 2008)	POF OTDR, FBGs, macro-bending sensors	Sewn and glued on elastic bandages in curvilinear layout; abdomen	Respiratory monitoring during MRI
(Katayama et al., 2020)	FBG sensor to trace sudden blood pressure changes	Adhered onto subject with medical tape (can be attach onto textile easily); wrist	Blood pressure monitoring to prevent and treat diseases

(Koyama et al., 2017)	FBG sensor covered with silk yarns by using braiding machine	Inserted into knitted wristband by inlay method	Blood pressure monitoring
(Krehel et al., 2014a)	POFs	Sewn on a polyester strap in U-shape; chest	Respiratory monitoring
(Krehel et al., 2013)	Co-POFs; applied force is based on light deflection in fibre waveguides.	Sewn on a woven sheet in U-shape; underneath subjects	Force sensor for monitoring immobile patients to prevent decubitus
(Krehel et al., 2014b)	Luminous sensor; 3 embroidered rings act as a light collector, a 3D ring is embroidered with black polyester yarn	Embroidered on woven and non-woven sheets in form of concentric rings; fingertip	Pulse oximetry measurement
(Leal-Junior et al., 2019a)	POFs; enhanced sensitivity done by laterally sectioning fibres	Attached on an elastic band in curvilinear shape; chest	Respiratory and heartbeat monitoring when performing periodic movements
(Li et al., 2012)	FBG, temperature sensitivity is 150 pm/°C	Inserted into woven fabric; trunk	Body temperature monitoring in clinics
(Li et al., 2020)	A POF sensor that consists of an etched grating fibre and a D-shape side-polished fibre	Sewn on a polyamide wrist brace; wrist	Wrist joint motion monitoring for exercise rehabilitation
(Lo Presti et al., 2019)	2 FBGs; VELCRO® fastener for adjusting the tightness	Attached on 2 elastic bands; thoracic spine and abdomen	Respiratory and heartbeat monitoring of archers to stabilise chest wall excursion with beating of heart and breathing
(Massaroni et al., 2016)	Placed 6 FBGs on the pulmonary and abdominal rib cages, and abdomen	Glued onto fabric sheet; trunk	Respiratory monitoring during MRI
(Massaroni et al., 2018)	12 FBGs	Adhered onto T-shirt with silicon rubber; trunk	Trunk motion and respiratory monitoring during sporting activities
(Massaroni et al., 2015)	Medical Smart Textiles Based on Fibre Optic Technology: An Overview	<i>Review</i>	/
(Nedoma et al., 2019)	Ballistocardiography system with FBG optic sensor embedded in 4-layer fibre glass fabric	Attached on an elastic band; chest	Respiratory and heartbeat monitoring during MRI
(Qu et al., 2018)	Stretchable multi-material optical fibre sensors via thermal drawing	Attached on knitted fabric; multi-purpose	Strain measurement, can be used as medical textile
(Quandt et al., 2015)	Body-Monitoring and Health Supervision by Means of Optical Fibre-Based Sensing Systems in Medical Textiles	<i>Review</i>	/
(Quandt et al., 2017)	Bi-component POFs by melt-spinning; reusable and washable	Embroidered onto bed sheet; underneath subject	Heartbeat and blood flow monitoring for wound healing and ulcer prevention
(Quandt et al., 2018)	POFs	<i>Overview on POF</i>	/

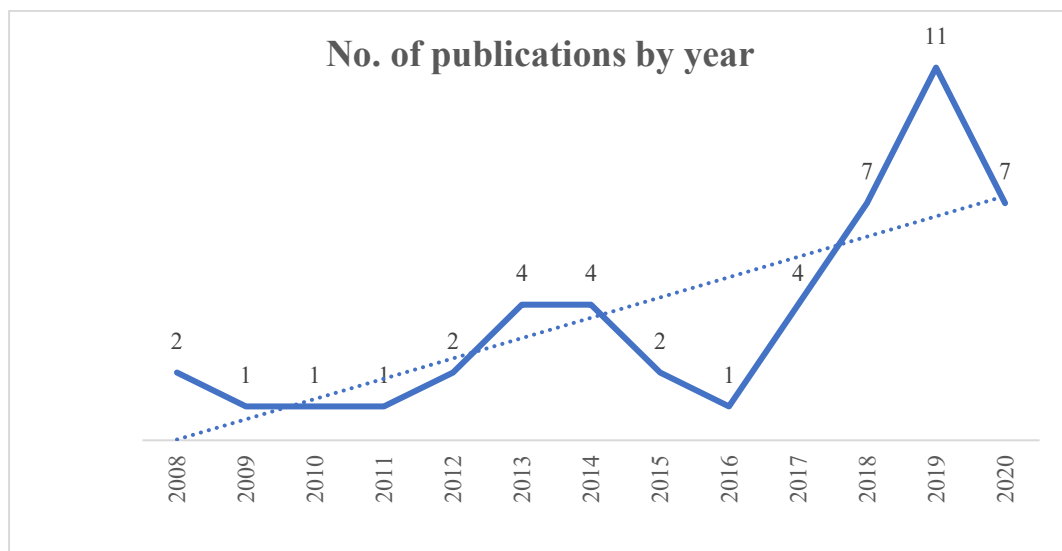
(Rothmaier, et al., 2008b)	Intensity-based POF sensor	Embroidered on a PET woven sheet; fore fingertip	Pulse oximetry measurement
(Roudjane et al., 2018)	New Generation Wearable Antenna Based on Multimaterial Fibre for Wireless Communication and Real-Time Breath Detection	<i>Review</i>	/
(Silva et al., 2013)	Macro-bending fibre optic sensor	Embedded on textile in curvilinear shape; joint	Joint angle measurement for rehabilitation
(Sirkis et al., 2017)	Device based on single mode in-fibres Mach-Zehnder interferometer	Attached onto a cotton shirt; trunk	Respiratory and heartbeat and pulse wave velocity monitoring
(Witt et al., 2012)	POF OTDR, FBGs, macro-bending sensors	Sewn and glued onto harness in curvilinear shape; thoracic and abdomen	Respiratory monitoring during MRI
(Zheng et al., 2014)	V-shaped notches are made on the sides of POFs to enhance sensor sensitivity	Sewn and adhered onto elastic woven belt in the form of circular loops; chest	Respiratory monitoring
<b>Group 2 Strain sensors for motion monitoring</b>			
(da Silva et al., 2011)	14 FBGs at the finger joint locations; works with 3D virtual reality system to enable game-like exercises	Embedded into 3-layered structures in curvilinear shape; hand	Hand posture monitoring for rehabilitation
(Fujiwara et al., 2014)	5 micro-bending transducers; silica optical fibre sensor is inserted into bending transducer in U-shape to increase sensitivity	Attached onto a glove; hand	Hand posture monitoring for human-robot interaction
(Guo et al., 2019b)	Skin-like POF sensors made of thermal-sensitive upconversion nanoparticles and stretchable POFs	Embedded in thin PDMS membranes (wearable); mouth, nose, and hand	Interior and surface temperature monitoring for healthcare, human-machine interfaces and robotics
(Jha et al., 2019)	FBG sensor that offers a very high angular resolution of $0.1^\circ$ with a very high sensitivity of 18.45 pm/degree	Attached onto glove; hand	Hand posture monitoring for rehabilitation and detecting Parkinson's tremor of stroke survivors
(Koyama et al., 2013)	Single-mode hetero-core fibre optical sensor	Sewn and glued onto sportswear; elbow and back	Trunk and elbow joint motion monitoring, used as teaching device in sports and rehabilitation fields
(Koyama et al., 2018)	16 intensity-based hetero-core fibre optical bending sensors; embedded in smart silicone pressure sheet	Attached onto strap; shoulder, elbow, thigh and knee	Motion and shape monitoring
(Leber et al., 2019)	Stretchable step-index optical fibre sensors; works with visual motion capture; 2 thermoplastic elastomers are coextruded by melt-	Attached on knee brace & glove; knees & hand	Knee and hand motion monitoring for sports and rehabilitation

flow method to form high index core and low index cladding			
(Li et al., 2018)	Hybrid plasmonic microfibre knot resonator	Embedded into thin PDMS membranes (wearable); wrist and hand	Wrist pulse, respiration, and finger pulse monitoring during MRI, military, aerospace
(Nishiyama & Watanabe, 2009)	Unconstrained hetero-core fibre-optic nerve sensors; works with 3D virtual reality system	Embedded into a nylon glove; hand	Hand posture monitoring
(Pan et al., 2020)	Skin-like silica MNF optical sensor	Embedded in thin PDMS membrane and attached onto fabric; elbow and forehead	Motion, respiratory and temperature monitoring to gauge athletic performance
(Zhang et al., 2020)	Ultrasensitive skin-like glass MNF sensors	Embedded into thin PDMS membranes and glove; throat, finger and wrist	Pressure, high-frequency vibrations, human voice and wrist pulse monitoring
<b>Group 3 TFOSs embedded in polymer substrate for lower limb monitoring</b>			
(Guo et al., 2019a)	Finite element analysis on skin-like FBG sensor interrogated by a free-running fibre laser with dual-comb output	Embedded into thin PDMS membrane and attached onto kneepad and glove; knees and hand	Respiratory, phonation, facial expression and motion monitoring for sports, rehabilitation, human-machine interfaces and virtual reality
(Kanellos et al., 2010)	4 FBGs; Finite element analysis	Embedded into insole (PDMS membranes) in curvilinear shape; underneath subjects	Pressure sensor, used in shoes, wheelchair seating-system, hospital-bed monitoring
(Leal-Junior et al., 2018)	4 curvature intensity-based POF sensors; laterally sectioned fibres through a polishing process; finite element analysis	Attached onto insole; foot	Gait monitoring
(Leal-Junior et al., 2019c)	15 POF macro-bending sensors	Embedded into 3D-printed PLA and TPU insole in curvilinear shape; foot	Plantar pressure and gait monitoring for clinical evaluation and remote health monitoring
(Leal-Junior et al., 2019b)	Polymer Optical Fibre Sensors in Healthcare Applications: A Comprehensive Review	<i>Review</i>	/

### 3.3 Result

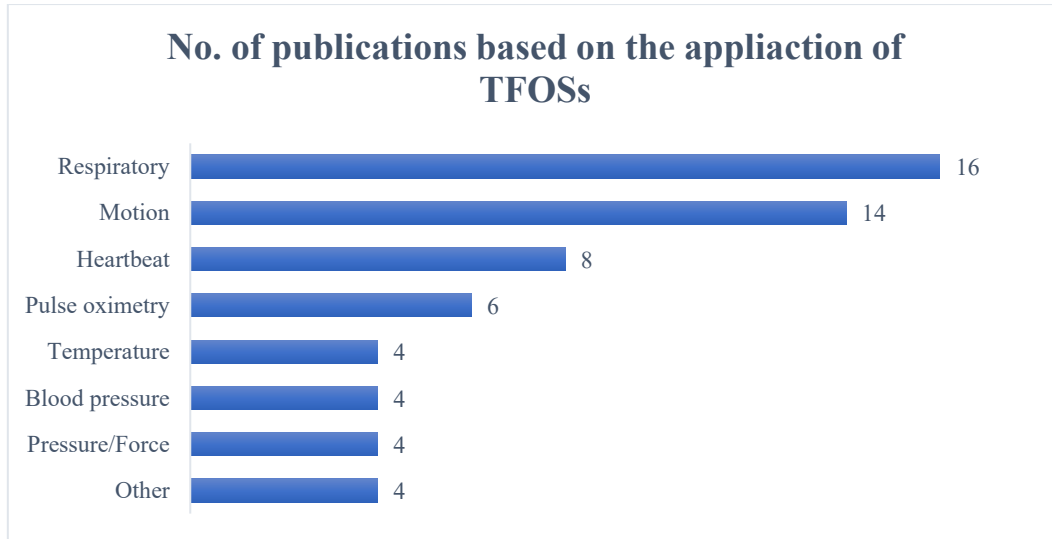
#### 3.3.1 Descriptive statistics

This section describes the characteristics of the samples based on the published journal name, year of publication, type of article and research field, country of origin of the first author, and sensor application. As depicted in Figure 3.1, there is an increasing trend in the application of TFOSs for health monitoring purposes from 2008 to 2019. Moreover, at the time of writing of this thesis, more than half of the articles in the sample (53%) were published within the period of 2017-2019. This indicates growing interest among researchers in advancing work in this domain, particularly concerning the application of TFOSs for monitoring body motion and respiration (Figure 3.2).



**Figure 3.1** Article distribution by year.





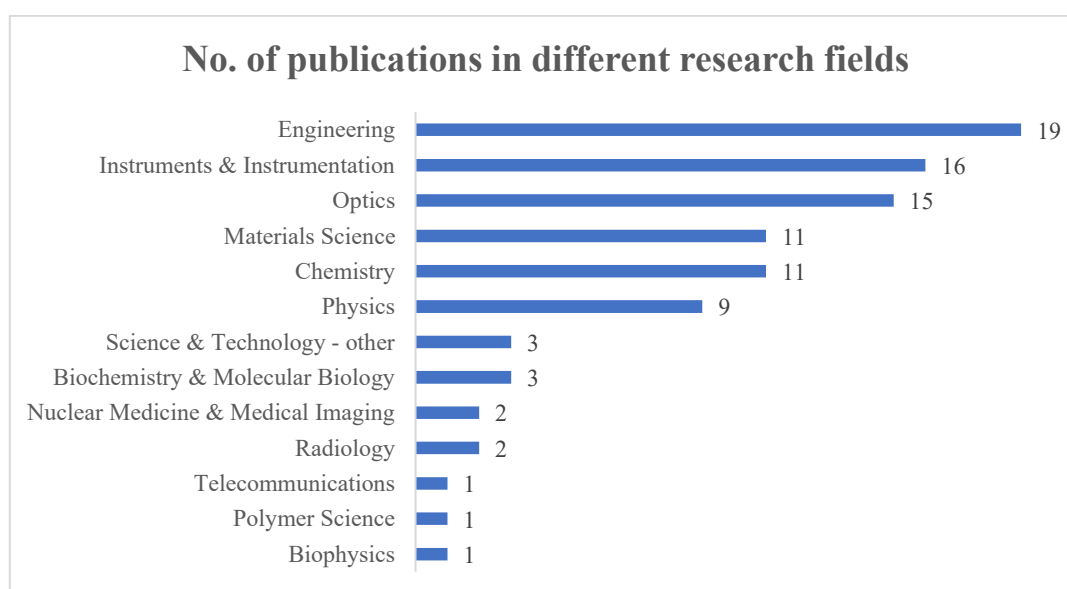
*Note:* The application is classified based on the stated research focus; 9 publications are excluded, and some sensors may have more than one type of application; and Other refers to facial expression, phonation, and high frequency vibrations.

**Figure 3.2** Application of TFOSs.

The articles included in the sample were distributed among 27 journals. As shown in Table 3.2, the majority of articles that examine the application of TFOSs for health monitoring purposes were published in *Sensors* (15%), with *IEEE Sensor Journal* (13%) and *Optics Express* (9%) ranking second and third, respectively. Only a small number of articles were published in textile-related journals. Furthermore, according to the research areas in the WoS, the majority of articles were classified as related to engineering (40%), instruments and instrumentation (34%), and optics (32%) (Figure 3.3). Although a small number of articles identified themselves as textile-related, the data suggested that the researchers were predominantly focused on enhancing the performance of optical sensors by leveraging the unique characteristics of textiles, such as their flexibility and softness.

**Table 3. 2** Article distribution: Top 5 journals.

Rank	Journal	No. of publications
1	Sensors	7
2	IEEE Sensors Journal	6
3	Optics Express	4
4	IEEE Transactions on Instrumentation and Measurement	3
5	Advanced Functional Materials	2
5	Journal of Fiber Science and Technology	2
5	Materials	2
5	Optics & Laser Technology	2
5	Textile Research Journal	2



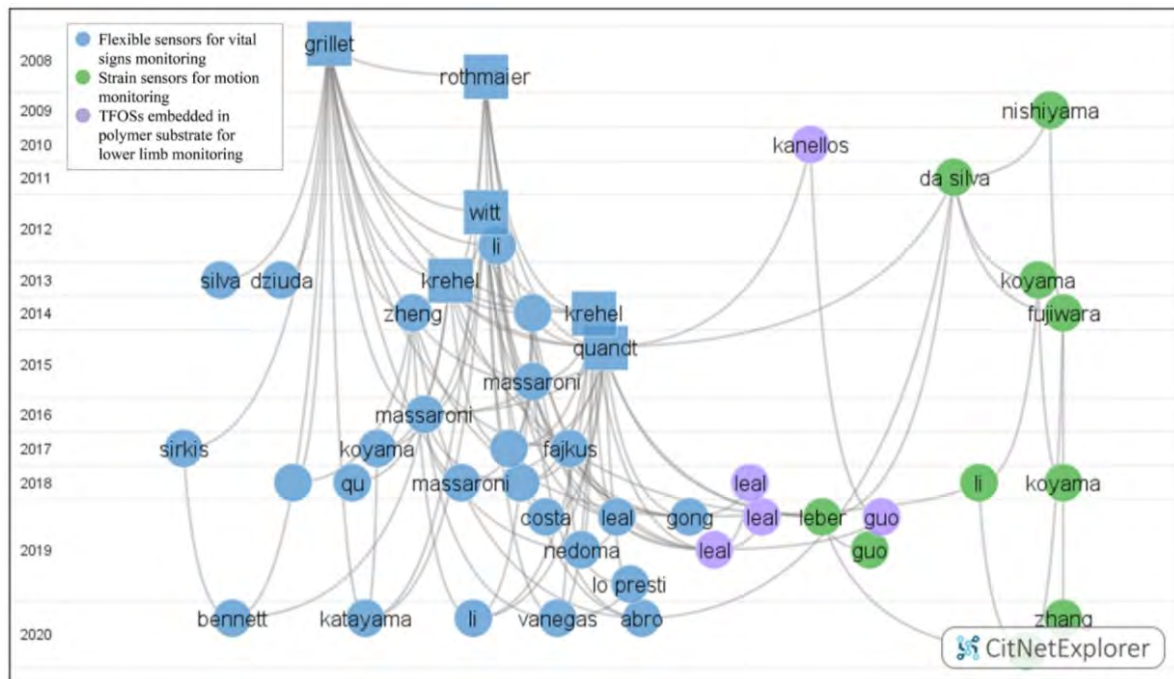
*Note: Articles may be relevant to more than one field*

**Figure 3. 3** Article distribution by research field.

Regarding the type of article, 85% of the articles in the sample were categorised as research articles, while 15% are reviews. With respect to the country of origin of the first author, the top five countries represented among authors who had published papers on TFOSs for health monitoring purposes were China (21%), Switzerland (17%), Brazil (11%), Japan (11%), and Italy (9%).

### 3.3.2 Research domains

The selected articles were categorised into Groups 1 to 3, denoted by blue, green, and purple circles in Figure 3.4, respectively. Publications within the same group have strong connections, thus forming a group that can be considered a domain in the literature (Van Eck & Waltman, 2014). The domains are labelled according to the articles with the highest number of internal citations in each group in terms of the application and used materials. Specifically, the domains are denoted as "Flexible sensors for vital signs monitoring" (31 publications), "Strain sensors for motion monitoring" (11 publications), and "TFOSs embedded in polymer substrate for lower limb monitoring" (5 publications) for Groups 1 to 3, respectively.



*Note: Squares represent top 5 articles with the highest internal citation scores*

**Figure 3. 4** Citation network of articles in sample.

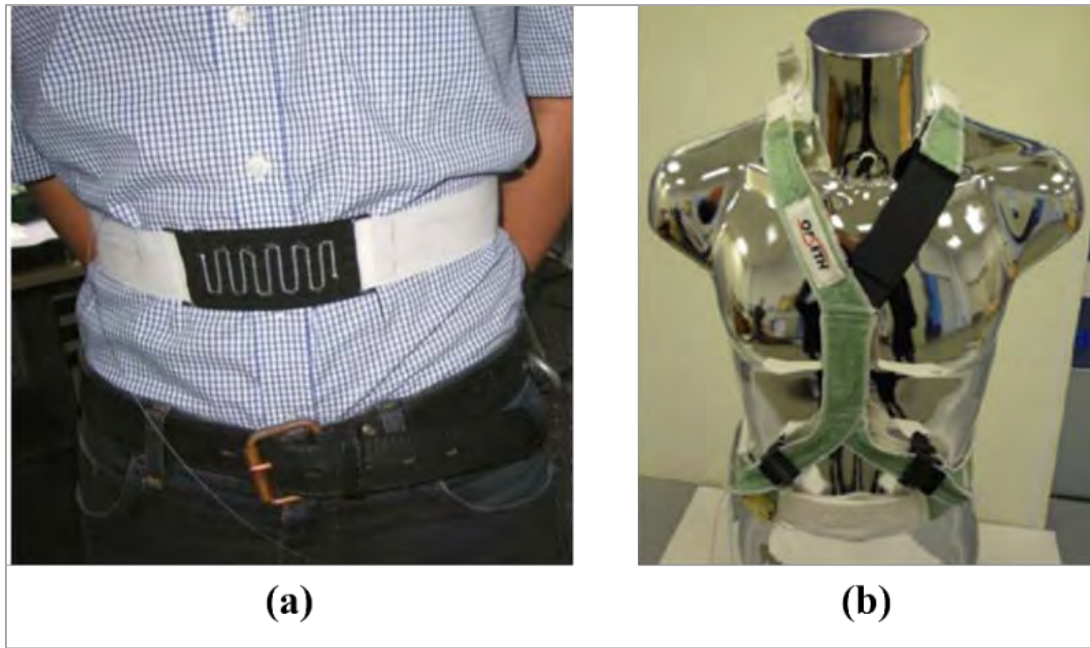
The top five publications with the highest internal citation scores show a significant correlation and are all in Group 1. The internal citation score refers to the frequency in which a publication is cited by others within the same field (Van Eck & Waltman, 2014). Among these publications,

Grillet et al. (2008) have the highest internal citation score of 17, which is regarded as the most remarkable article in this area. Additionally, the findings suggested that researchers prioritise the monitoring of the vital signs of patients over their movements. This may be attributed to the fact that even though TFOSs can be applied to obtain body measurements during MRI, they can be easily substituted with other electrical sensors when monitoring body movement, even though the electrical sensors potentially offer less flexibility or convenience.

### **3.3.2.1 Group 1: Flexible sensors for vital signs monitoring**

The most extensively researched domain is "Flexible sensors for vital signs monitoring", which comprises 66% (31) of the publications in the sample. This domain primarily involves the integration of fibre optic sensors into textiles, thereby enhancing the capabilities of medical textiles for monitoring vital signs, such as respiratory movement, cardiac activity, oxygen saturation, and body temperature.

The earliest study in this domain is Grillet et al. (2008), who developed sensing belts by sewing optical fibre sensors onto elastic bandages to monitor respiratory movement during MRI (Figure 3.5(a)). The sensors utilised include macro-bending, polymer optical fibre (POF) and silica fibre Bragg grating (FBG) sensors and an optical time domain reflectometer (OTDR). The sensing mechanism relied on the elongation of the abdominal circumference resultant of breathing. Witt et al. (2012) employed a comparable methodology to fabricate a sensing harness by affixing fibre optic sensors onto the surface of the fabric, (Figure 3.5(b)). Although they used the same types of sensors and materials as those employed in Grillet et al. (2008), Witt et al. (2012) applied them in both the thoracic and abdominal regions to obtain a comprehensive view of the respiratory movement. The design in Witt et al. (2012) appears to be an enhanced iteration of that in Grillet et al. (2008).



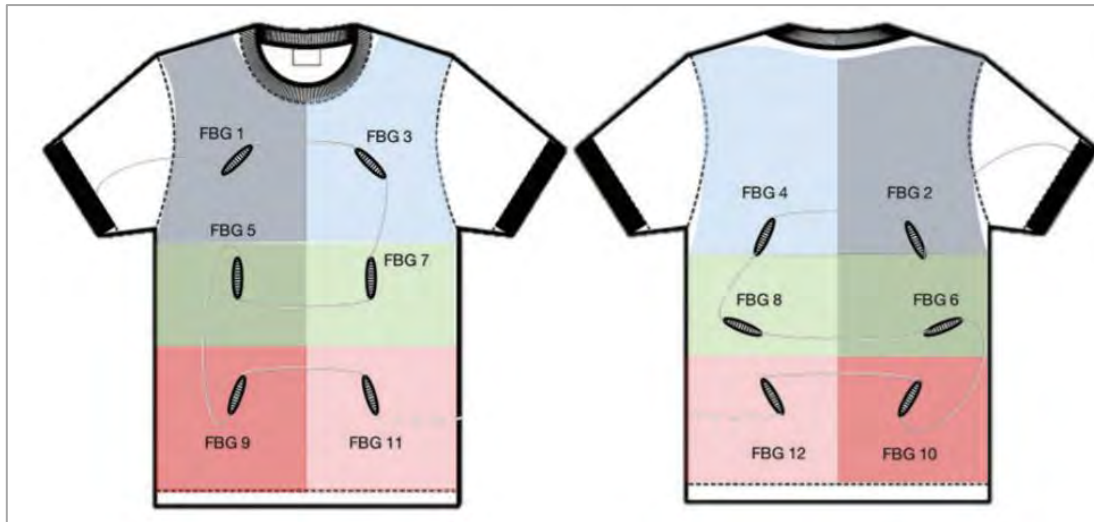
**Figure 3. 5 (a)** Sensing belt (Grillet et al., 2008), and **(b)** sensing harness (Witt et al., 2012).

Additionally, it is noteworthy that Krehel et al. (2014a, 2014b), Quandt et al. (2015, 2017), and Massaroni et al. (2015, 2016, and 2018) are the most influential authors in this field, owing to their multiple publications within the same group and relatively high internal citation scores. Their respective highest internal scores are 10, 10, and 5. This indicates that their works have been instrumental in advancing the field and inspiring other scholars to pursue related research. Krehel et al. (2014a, 2014b) developed three types of TFOSs: two types of strain sensors were sewn and embroidered onto textiles to measure respiratory activity and pulse oximetry, respectively, while a force sensor was created to monitor immobile hospitalised patients to prevent decubitus ulcers (Krehel et al., 2013). Quandt et al. (2015, 2017) contributed to this field with two publications. The first article discussed the application of POF sensors integrated into a moisture-wicking fabric to detect heartbeat and blood pressure for preventing pressure ulcers and monitoring wound healing (Quandt et al., 2017). The second article provided a comprehensive review of existing sensing techniques and explored the potential of employing TFOSs for body monitoring (Quandt et al., 2015). Massaroni et al. (2015, 2016, 2018)

published three articles that pertain to smart textiles, and the mentioned TFOSs were primarily employed for vital signs monitoring. For instance, they developed a sensing fabric sheet by adhering six FBG sensors onto the pulmonary and abdominal rib cages and abdomen to monitor respiratory movement during MRI (Massaroni et al., 2016).

Other scholars were inspired by their studies and subsequently endeavoured to develop sensors to monitor vital signs. For instance, Dziuda et al. (2013) and Zheng et al. (2014) developed a ballistocardiography system with an FBG sensor and V-shaped notches POF fabric strain sensors to monitor respiratory movement, respectively. In addition, Fajkus et al. (2017) and Li et al. (2012) developed a multichannel hybrid fibre optic sensor based on FBG and a temperature sensitive FBG sensor to measure the body temperature, respectively.

Furthermore, CitNetExplorer provides insights into the technological evolution of TFOSs. Previously, most TFOSs were sewn onto elastic bands to measure chest or abdomen movements (Abro et al., 2019; et al., 2020; Fajkus et al., 2017; Krehel et al., 2014a; Leal-Junior et al., 2019b; Lo Presti et al., 2019; Zheng et al., 2014). However, Massaroni et al. (2018) recently demonstrated the feasibility of using sensing apparel to capture full-body measurements by integrating 12 FBG sensors into a T-shirt. which could be used to monitor respiratory movement and evaluate thoraco-abdominal movement patterns during physical activities (Figure 3.6). These TFOSs provide instant data that can be used to assess athletic performance and detect vital sign abnormalities. Additionally, most of the publications in this field use POF sensors instead of traditional glass optical fibre sensors, primarily due to their higher elasticity (Grillet et al., 2008; Krehel et al., 2013, 2014a; Li et al., 2020; Quandt et al., 2017; Rothmaier et al., 2008b; Witt et al., 2012; Zheng et al., 2014). This suggests that the integration of POF sensors into apparel is likely to become a new trend.



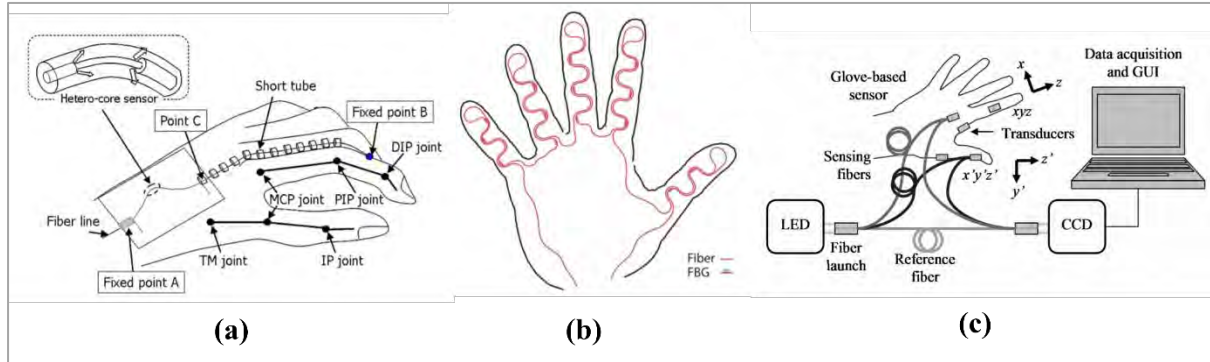
**Figure 3. 6** Arrangement of 12 FBG sensors on T-shirt (Massaroni et al., 2018).

### **3.3.2.2 Group 2: Strain sensors for motion monitoring**

The second research category, "Strain sensors for motion monitoring", comprised 23% (11) of the publications in this field. The beginnings of the work in this group can be traced back to Nishiyama and Watanabe (2009), who pioneered the development of the first wearable sensing glove with a 3D virtual reality system for capturing instant hand motions (Figure 3.7(a)). The sensing mechanism was realised by incorporating hetero-core fibre-optic sensors in the back of the gloves, which makes it possible to detect finger joint angles by using only a few sensors without any constraints. Drawing inspiration from Nishiyama and Watanabe (2009), da Silva et al. (2011) developed sensing gloves for monitoring hand gestures and posture. However, in contrast to the hetero-core fibre-optic sensors used in the former, the latter used 14 FBG sensors at the finger joints (Figure 3.7(b)). The decision to use FBG sensors was motivated by their inherent self-referencing and multiplexing capabilities, as well as their resistance to fragility issues that arise from splicing fibres with varying diameters. In addition, a curvilinear layout of optical fibres was used instead of a straight layout to ensure that the gloves had sufficient elasticity. While these two gloves minimised fragility issues and maximised flexibility, Fujiwara et al. (2014) chose to simplify their design approach by incorporating only five micro-



bending transducers that were embedded with U-shaped silica optical fibres (Figure 3.7(c)). This approach eliminated the need for complex setups and measurements typically required by FBG sensors, which made the design more user-friendly.

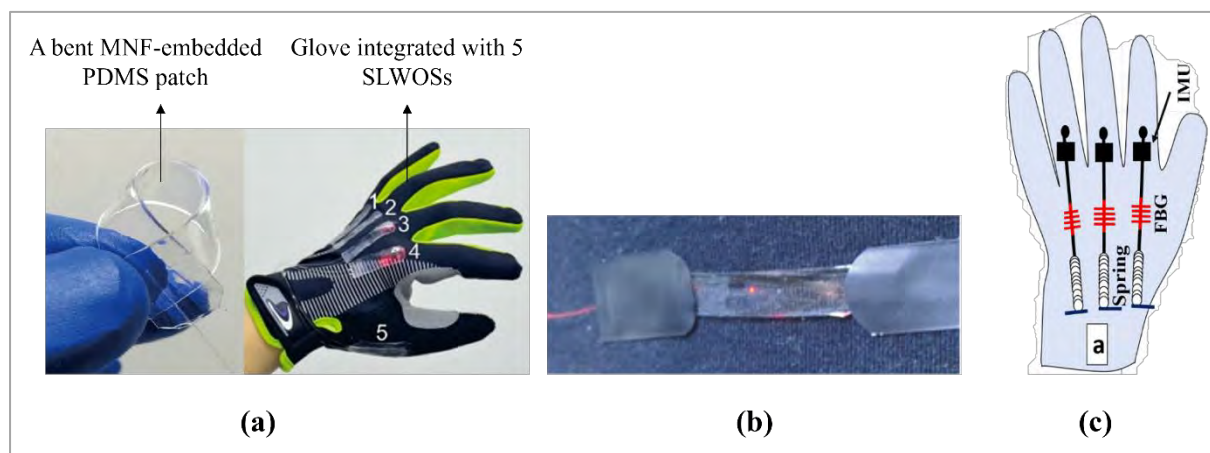


**Figure 3. 7 (a)** Sensing glove with hetero core fibre optical sensor (Nishiyama & Watanabe, 2009), **(b)** FBG sensing glove (da Silva et al., 2011), and **(c)** sensing glove with micro-bending transducers (Fujiwara et al., 2014).

The progress made in biotechnology and nanotechnology has led to the emergence of skin-like wearable optical sensors as a new trend in healthcare, robotics, and bioelectronics. Using conventional optical fibres to construct wearable sensors has been challenging due to their large diameter (125  $\mu\text{m}$ ) and rigidity. However, the advent of optical micro/nanofibres (MNFs) with a diameter of 1  $\mu\text{m}$  made the construction of such sensors possible. These MNFs offer superior flexibility and mechanical strength and exhibit lower waveguide losses because of their precise geometric uniformity. For example, Zhang et al. (2020) developed ultrasensitive skin-like wearable optical sensors (SLWOSs) by embedding glass MNFs into thin layers of polydimethylsiloxane (PDMS) (Figure 3.8(a)). The SLWOSs can be placed onto gloves for monitoring the flexion and extension of the finger joints and offer a superior performance in terms of higher angular resolution when compared to standard optical fibre sensors and stretchable conductive strain sensors. Likewise, Pan et al. (2020) created SLWOSs by attaching MNFs onto fabric for the instant monitoring of respiration, arm motion, and body temperature,



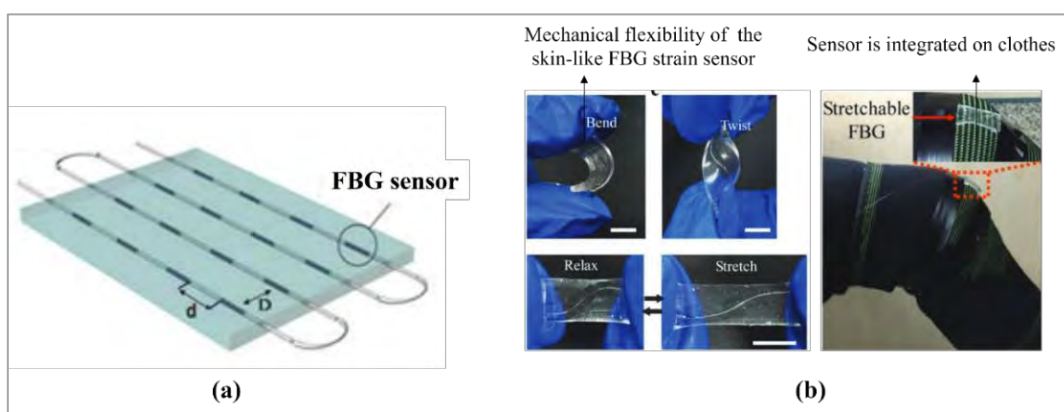
with the aim of evaluating athletic performance in instant (Figure 3.8(b)). Both Zhang et al. (2020) and Pan et al. (2020) applied sensitive silica optical fibres instead of highly flexible POFs. However, the latter improves the fibre arrangement from a straight to a slightly bent layout to enhance the stretchability of the SLWOS. The data collected by these flexible sensors can be utilised to evaluate sports activity performance or the degree of rehabilitation (da Silva et al., 2011; Koyama et al., 2013; Leber et al., 2019). For instance, Jha et al. (2019) developed a sensing glove by integrating FBG sensors to monitor hand movements for rehabilitation and detecting Parkinson's tremor in stroke survivors (Figure 3.8(c)). Additionally, a single-mode hetero-core fibre optical sensor can be incorporated into smart sportswear as a teaching device to monitor trunk and elbow joint movements (Koyama et al., 2013), which facilitate posture correction. This indicates that these technologies can also be utilised to evaluate the effectiveness of treatment and sports training.



**Figure 3. 8 (a)** SLWOSs applied on gloves (Zhang et al., 2020), **(b)** SLWOS attached to fabric (Pan et al., 2020), and **(c)** an FBG sensing glove (Jha et al., 2019).

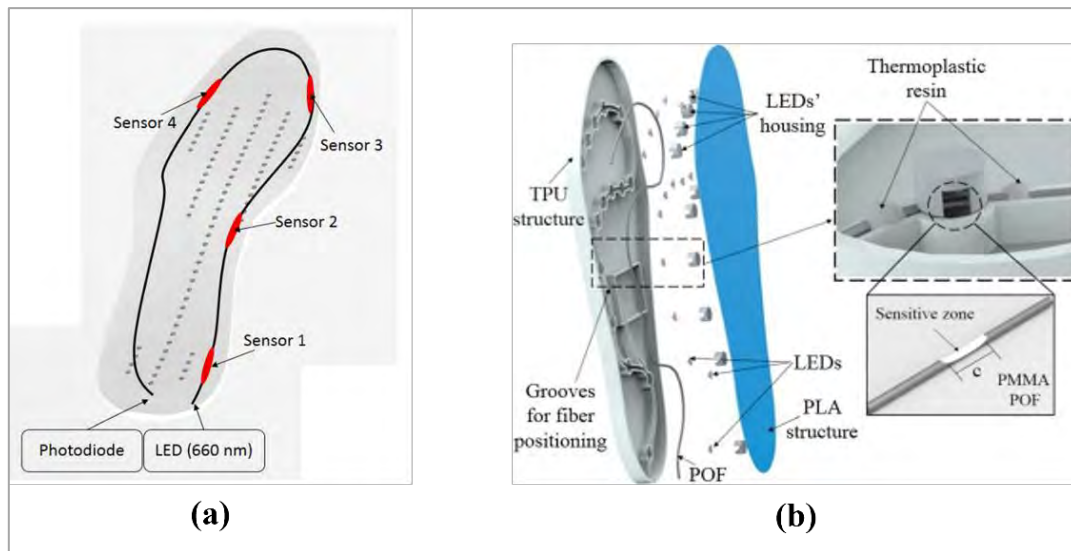
### 3.3.2.3 Group 3. TFOSs embedded in polymer substrate for lower limb monitoring

Group 3 which focuses on "TFOSs embedded in polymer substrate for lower limb monitoring" comprises five studies that include, for example, Kanellos et al. (2010), who developed a flexible 2D optical fibre-based pressure sensing pad by embedding FBG sensors into a thin polymer sheet ( $2 \times 2 \text{ cm}^2$  with a thickness of 2.5 mm) (Figure 3.9(a)). Also, the sensing pad exhibited a maximum fractional pressure sensitivity of  $12 \text{ MPa}^{-1}$  in instant. Due to its thin and flexible properties, the sensing pad is well-suited for intimate contact with human skin and different biomedical applications that require skin pressure to be measured such as shoes, wheelchair seats, and hospital beds. Moreover, Guo et al. (2019) developed a skin-like FBG strain sensor that can be directly applied to the skin surface for monitoring respiratory movement, facial expression, joint movement, and phonation (Figure 3.9(b)). The fibre optic sensor was embedded into a PDMS substrate with a curvilinear-shaped configuration that enables the fibres to elongate as the PDMS is stretched. Although both Kanellos et al. (2010) and Guo et al. (2019) created a skin-mountable sensor, the sensor of the latter exhibits higher flexibility, owing to its curvilinear-shaped configuration and utilisation of PDMS.



**Figure 3. 9 (a)** Pressure sensing pad (Kanellos et al. 2010) and **(b)** a skin-like FBG strain sensor (Guo et al. 2019a).

Leal-Junior et al. (2018, 2019b and 2019c) published three articles that focused on the application of POF sensors. Their first study involved a smart insole for gait monitoring by using intensity-based POF curvature sensors with enhanced sensitivity, which was achieved by laterally sectioning the fibres through a polishing process (Leal-Junior et al., 2018) (Figure 3.10(a)). After that, a 3D-printed smart insole was developed by encapsulating 15 POF macro-bending sensors in a two-layered insole made of thermoplastic polyurethane (TPU) and polylactic acid (PLA) (Leal-Junior et al., 2019c) (Figure 3.10(b)). When pressure is applied onto the insole, the pressure distribution can be visualised and measured. Their third study reviewed the application of POFs in healthcare, where all TFOSs were incorporated with thin polymer substrates to enhance their softness and elasticity. The previous studies in the literature were particularly useful for constructing insoles or pressure pads that are subjected to compressional forces. Furthermore, they disclosed that TFOSs are remarkably proficient in detecting facial expression, phonation, or other minimal movements of the human skin, due to their capability to be directly applied onto the skin, and they typically offer a higher resolution.



**Figure 3.10** (a) POF intensity-based smart insole (Leal-Junior et al., 2018), and (b) POF macro-bending based 3D-printed smart insole (Leal-Junior et al., 2019c).

### 3.3.3 Integration methods of fibre optic sensors and textiles

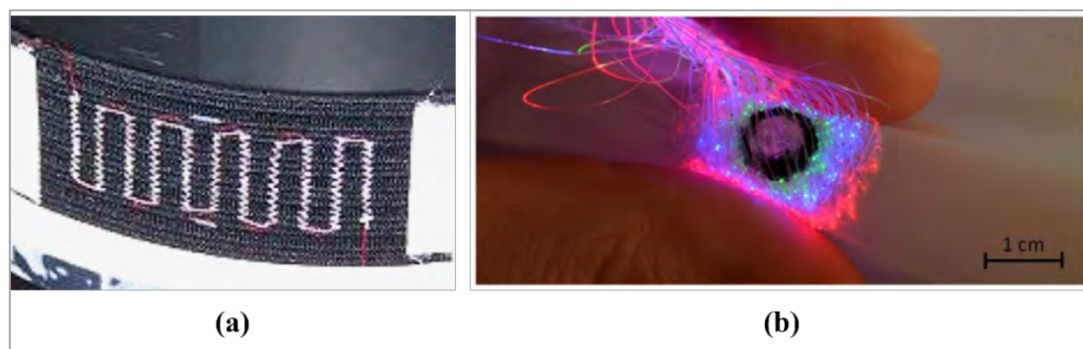
In general, there are five methods that can be utilised to integrate fibre optic sensors into textiles, namely adhering, sewing, embroidering, embedding/layering, and inserting. Given their unique properties, compatibility is the most critical factor that should be considered before integrating these sensors. This requires careful consideration of their configurations, flexibility, materials, and structures to prevent the loss of exceptional fabric properties, such as elasticity, when the rigid fibre optic sensors are inserted. Although bending the sensors in a continuous U-shape enhances the elasticity of the fabric, doing so could lead to signal loss (Schrack et al., 2017). On the contrary, a straight alignment ensures stable signal transmission, but may result in increased stiffness of the fabric. Therefore, an appropriate TFOS should have outstanding functionality while preserving the unique properties of the textile. Table 3.3 provides an evaluation of the advantages and disadvantages associated with each of the five methods (Selm et al., 2010; Zheng, 2014).

**Table 3. 3** Advantages and disadvantages of integration method (Selm et al., 2010; Zheng, 2014).

	<b>Fibre arrangement</b>	<b>Advantages</b>	<b>Disadvantages</b>
<b>Adhering</b>	Straight	Easy to apply, very secure; low signal loss	Affects fabric softness and elasticity
<b>Sewing</b>	Macro-bending	Maintains fabric elasticity	Suitable for thin fibre optic sensors only; high signal loss
<b>Embroidering</b>	Arbitrarily twined	Fibre arrangement is the most versatile	High signal loss
<b>Embedding/layering</b>	Straight or macro-bending	Low signal loss	Inhibits ease of mobility due to increased bulkiness
<b>Inserting (weaving)</b>	Straight with little undulation	Obscures sensors perfectly; low signal loss	Affects elasticity of fabric
<b>Inserting (Inlaid knitting)</b>	Straight lying	Obscures sensors perfectly; low signal loss	Affects fabric elasticity and thickness

Adhering is the simplest approach for integrating fibre optic sensors because they can be attached to various textile types with minimal signal loss. The integration process does not require consideration of the fabric structure or properties, and hence, offers the most flexibility among the five methods (Rantala et al., 2011). Adhering can be employed as the sole integration method or used in conjunction with other techniques to secure the sensor. For instance, an FBG sensor can be adhered to a fabric sheet to monitor vital signs in an MR environment (Massaroni et al., 2016), and a POF strain sensor with notches can be sewn and attached to an elastic woven fabric for monitoring respiratory movement (Zheng et al., 2014). However, excessive fixation may result in the loss of fabric softness and elasticity.

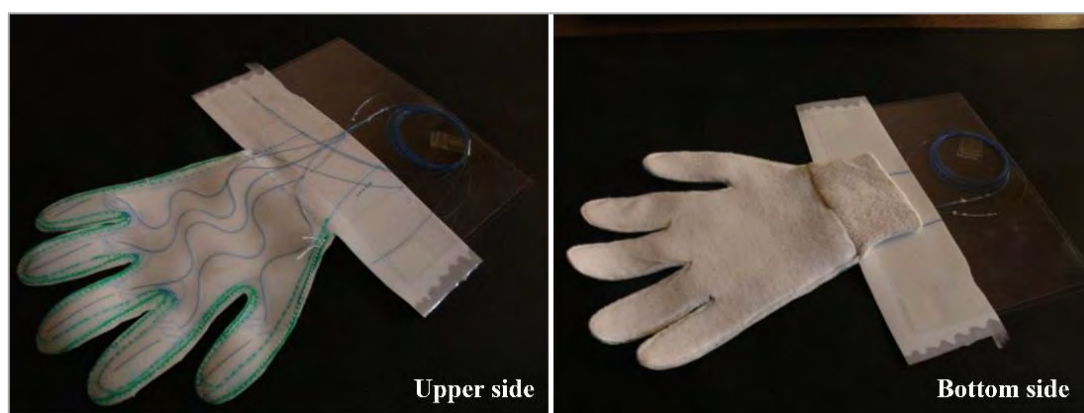
Sewing is an alternative method for attaching sensors to a 2D substrate (Figure 3.11(a)). This method is superior to adhering because of the comparative elasticity of the sewing threads. Sewing has been employed as a fixation technique for various applications, such as a sensing belt and harness for respiratory movement monitoring in an MRI environment (Grillet et al., 2008; Witt et al., 2012); sensing sportswear for tracking trunk and elbow joint movements (Koyama et al., 2013); and sensing fabric for detecting heartbeat and blood flow (Quandt et al., 2017). Nevertheless, sewing is only appropriate for thin fibre optic sensors only, otherwise, the stitched yarns may be subjected to significant mechanical stress.



**Figure 3. 11 (a) Sewing (Grillet et al., 2008) and (b) embroidering optical fibres onto textiles (Krehel et al., 2014b).**

In contrast to sewing, embroidering commonly employs optical fibres as the yarn for the textile (Figure 3.11 (b)). For example, Krehel et al. (2014b) and Rothmaier et al. (2008) embroidered sensors onto woven sheets to measure pulse oximetry. Embroidering is widely regarded as the most versatile method because it bends optical fibres into the desired shape, thereby providing the broadest range of possibilities. Consequently, this technique is frequently employed to enhance the visual appeal of luminous sensors. However, this method is also linked to the most substantial signal loss due to small bending radius (Schränk et al., 2017). Therefore, embroidering may not be ideal for producing sensors that necessitate high precision and resolution.

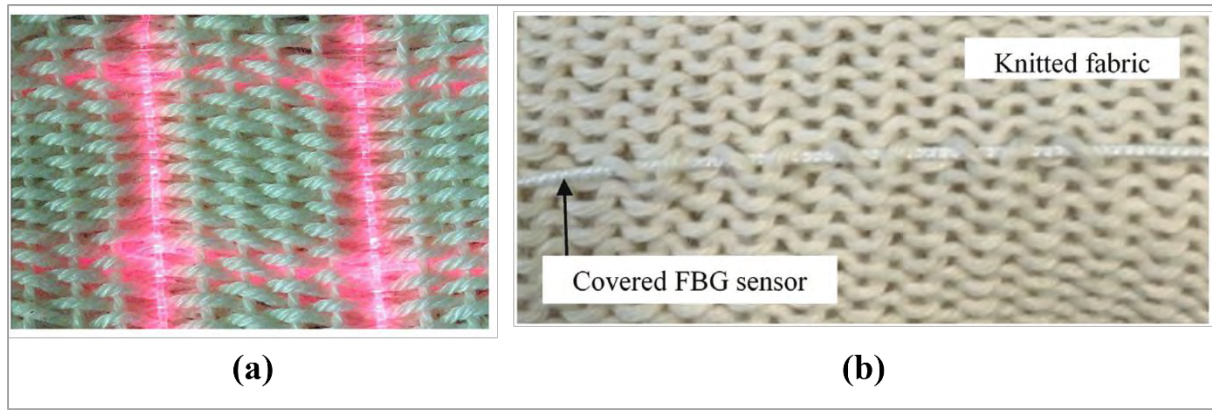
Embedding or layering is used to conceal a sensor between two or more material layers, thereby shielding the sensor from damage and preventing the sensor from protruding. This approach can be applied in the fabrication of insoles, gloves, and pressure pads to prevent the sensor from causing any discomfort to the user. For example, a wearable sensing glove had been constructed by embedding an FBG sensor within a three-layer structure to capture hand motions (da Silva et al., 2011) (Figure 3.12). Embedding is a commonly employed technique to secure and protect sensors, despite the possibility of increasing the thickness or bulkiness of the product, which may inhibit ease of mobility.



**Figure 3. 12** Three layered structure sensing glove (da Silva et al., 2011).

Inserting is regarded as the most complicated method because careful consideration of the fabric structure and properties of the textile yarns is necessary. Optical fibres are typically inserted into woven structures rather than knitting, owing to the ease of the manufacturing process and less likelihood of signal loss. In the weaving process, fibre optic sensors are used in a manner similar to that of textile yarns, which means that they are intersected with the warp or weft yarns in a predominantly linear configuration. Additionally, the placement of sensors can be secured at a predetermined intersection point, obviating the need for adhesive. Among the various weave patterns, the twill structure is the most compatible with inserting, owing to its reduced undulation (El-Sherif, 2005). For instance, Rothmaier et al. (2008a) inserted a POF sensor into a twill structure fabric (atlas pattern), with a  $\frac{1}{4}$  repeat to monitor the applied compressional force (Figure 3.13(a)). Furthermore, Li et al. (2012) created an FBG sensor that is sensitive to high temperatures by inserting the sensor into a woven fabric, which can be used to enable clinical monitoring of body temperature via the armpit. In knitting, fibre optic sensors serve as the inlaid yarns (El-Sherif, 2005; Koyama et al., 2017), which allows them to be obscured and laid straight among the knit loops. For instance, Koyama et al. (2017) employed the inlay method to insert a silk-covered FBG sensor into a knitted garment to produce a smart wristband for blood pressure monitoring (Figure 3.13(b)). However, this method may greatly affect the tensile properties and thickness of the knitted fabric. In addition to the fabric structure, the thickness and flexibility of the textile yarns, and spacing of the sensors can also ultimately influence the performance (Bai & Tan, 2013; Selm et al., 2010).





**Figure 3. 13** Inserting optical fibres into **(a)** a woven fabric (Rothmaier et al., 2008a), and **(b)** a knitted wrist band (Koyama et al., 2017).

### 3.4 Future trends and challenges

According to the knowledge structure in each domain, research in the domain of "Flexible sensors for vital signs monitoring" typically involves the integration of fibre optic sensors into clothing to enable overall body measurements. Studies within the "Strain sensors for motion monitoring" domain are primarily dedicated to the creation of wearable optical sensors that resemble skin, whereas those within the "TFOSs embedded in polymer substrate for lower monitoring" domain prioritise the compatibility of sensors with plastic materials, as well as their utility in monitoring the lower limbs. Hence, the current trend of research in this field is expected to shift towards the creation of smart textiles that are exceptionally flexible and comfortable to wear, which is ideal for continuous health monitoring applications, particularly for MRI and in homecare settings. Consequently, future TFOSs may need to possess characteristics such as portability, a lightweight design, stretchability, user-friendliness, and a high degree of compatibility with the elasticity of the skin.

Optical sensors offer superior electromagnetic immunity compared to electrical sensors, which makes them ideal for use during MRI procedures. With an increase in life expectancy, there is a growing demand for medical supplies and health-monitoring devices (Krehel et al., 2014b;



Leal-Junior et al., 2019a), including MRI-compatible systems that can monitor the instant status of patients. Therefore, some researchers have developed sensing belts or harnesses for vital sign monitoring during MRI (Grillet et al., 2008; Nedoma et al., 2019; Witt et al., 2012). Furthermore, as lifestyles continue to evolve, smart textiles have become increasingly integrated into daily use textiles (Van Langenhove, 2015), such as the Adidas Bluetooth Smart Heart Rate Monitor with Textile Strap (Hartmans, 2019). This demonstrates that even among healthy individuals, health is given high priority. Consequently, the development of daily use photonic sensing textiles for healthcare purposes is an emerging research trend.

Furthermore, advanced technologies such as biotechnology and nanotechnology are expected to facilitate the development of more flexible sensors (Hartmans, 2019), because they can substantially enhance wear comfort, health, and overall well-being, thus surpassing the offerings of conventional products (Future Markets Inc., 2018). For example, Zhang et al. (2020) and Pan et al. (2020) recently demonstrated the feasibility of producing skin-like wearable optical sensors with MNFs to measure movement. These sensors are highly compatible with the skin surface and exhibit high sensitivity, which make them suitable for long-term monitoring without causing irritation or inconvenience.

Although numerous TFOS prototypes have been produced, their commercialisation has yet to be realised. This means that they cannot replace currently used electronic devices (Castano & Flatau, 2014). The challenges include stability issues with the sensors and self-calibration problems that arise from the high variability of optical properties (Vanegas et al., 2020; Quandt et al., 2015). Additionally, integrating optical sensors into textiles seems to be a minor obstacle, given that conventional optical fibres tend to be fragile and inflexible, which restrict their stretchability (Gong et al., 2019). One feasible solution is to pre-bend the fibres into a curvilinear arrangement, thus enabling them to elongate in tandem with the textile. Once the

stability and reliability of fibre optic sensors can be ensured, they hold tremendous promise for future applications in textile technologies. 3.5 Limitations

This study has two primary methodological restrictions. First, the publications collected from the WoS core collection from 1959 to 2020 probably not be exhaustive. To the best of my understanding, diligent efforts have been made to incorporate all relevant keywords. However, it is possible that certain studies may employ alternative keywords that still relevance to the scope of the research. Secondly, certain journal papers might have been omitted because only the WoS was used to search for the related journals (Tang et al., 2018), which means journals may not comprehensively reflect the semantic of the field (Zhuge, 2016). Thirdly, although CNA is a comparatively objective approach for defining the research domain, the final screening of the relevant studies in the sample was still conducted by the research team, and this process may have included a certain degree of subjectivity (Fan et al., 2014).

### **3.5 Limitations**

This study has two primary methodological limitations. First, the publications collected from the WoS core collection from 1959 to 2020 might not be exhaustive. Although the inclusion of all relevant keywords has been ensured to the best of my knowledge, it is possible that some studies use different keywords that are still related to the research scope. Secondly, certain journal papers might have been omitted because only the WoS was used to search for the related journals (Tang et al., 2018), which means that the journals may not fully represent the semantics of the field (Zhuge, 2016). Thirdly, although CNA is a relatively objective method for defining the research domain, the final screening of the relevant studies in the sample was still conducted by the research team, and this process may have included a certain degree of subjectivity (Fan et al., 2014).

### 3.6 Summary

The exceptional performance of TFOSs have led to their increasing acceptance in healthcare for patient monitoring purposes. This chapter provides a systematic review of TFOSs for health-monitoring applications, and draws on 47 relevant articles. Three research domains are identified, namely "Flexible sensors for vital signs monitoring", "Strain sensors for motion monitoring", and "TFOSs embedded in polymer substrate for lower limb monitoring". Moreover, their knowledge structures are analysed to determine the main paths within each domain. The main paths are used to show the evolution of TFOSs for health-monitoring purposes and predict their potential future developments. The major research trend is now looking to develop highly flexible or skin-like strain sensors for the instant monitoring of vital signs and motion, including respiratory movement, heartbeat, blood pressure, and joint mobility. Additionally, it is likely that a larger number of TFOSs will be designed specifically for continuous health monitoring in MRI conditions or homecare. However, addressing the sensor stability and self-calibration challenges will be imperative in future research. The statistics extracted from TFOSs can serve as valuable information for a variety of applications, including training, rehabilitation, disease detection, accident prevention, and athletic performance assessment. Hence, researchers may deem it worthwhile to pursue similar studies and further refine related work in this direction.

## **CHAPTER 4 FACTORS THAT AFFECT WEAR COMFORT OF SUMMER UNDERGARMENT**

### **4.1 Introduction**

Hong Kong has a sub-tropical climate, characterised by high temperatures and humidity during the summer, with mid-day temperatures that can exceed 36°C (Grundy, 2021). As a result, air conditioning is crucial for maintaining indoor thermal comfort. Nevertheless, the large temperature differential between the indoor and outdoor environments can lead to a wide array of illnesses, especially among children who might be less vigilant of temperature changes and are less likely to have self-care ability. To maintain the thermal balance of the body, heat is transferred through perspiration (Qingqing et al., 2020). Therefore, the appropriate use of comfortable and suitable undergarments that regulate body temperature, effectively wick moisture, and prevent skin irritation is essential. Failure to do so may result in body odour, clinginess of the garment, and itchiness.

Thermal comfort is defined as perceived satisfaction with the thermal environment (Rupp et al., 2015). One of the important aspects of thermal comfort has to do with garments. Previous research has focused on thermal response based on garments worn during cold weather. Tang et al. (2020) examined the characteristics and thermal insulation properties of winter apparel for the elderly in China. Shaker (2018) focused on the material characteristics of protective clothing for extreme cold weather. However, the literature has neglected the importance of the thermal comfort of undergarments for those who frequently alternate between different environments with large temperature differences. This is an important area of study because the discomfort caused by undergarments can negatively affect productivity, mood, and overall well-being.

The tactile comfort of undergarments also affects consumer purchase intentions because it influences product quality and perceived comfort (Atalie et al., 2019; Broega et al., 2010; Jeguirim et al., 2010). In addition, undergarments are worn for hygiene purposes and comfort (Kar et al., 2011). However, the needs and expectations for undergarments can vary depending on the season. For instance, summer undergarments should be breathable and moisture-wicking, while winter undergarments need to provide warmth. Yet, most research has focused exclusively on the tactile comfort of winter fabrics. For example, McGregor et al. (2015) investigated perceived moisture levels of next-to-skin winter wear, while Speijers et al. (2015) compared the perceived comfort of wool and cashmere, which are usually found in winter garments, among Chinese and Australian users. Unfortunately, the importance of summer undergarments has been largely overlooked. To address this research gap, this study aims to investigate the factors that affect the thermal and tactile comfort of summer undergarments.

## **4.2 Materials and methods**

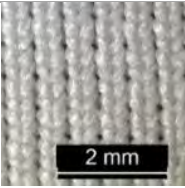
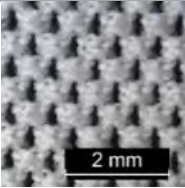
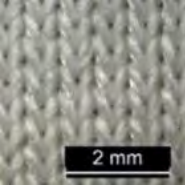
### **4.2.1 Materials and conditioning**

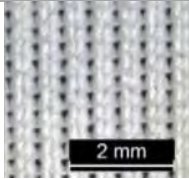
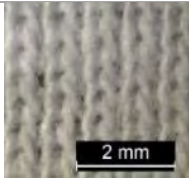

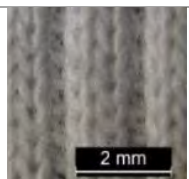
Typically, undergarments are fabricated from cotton due to its exceptional water absorbency, breathability, and softness, which are desirable features for the wearer (Rathore, 2018). However, AIS patients might be concerned with the cooling and moisture-wicking properties of undergarments, as some scoliotic braces are nearly impermeable to air and can trap body heat, thus resulting in perspiration-induced odour and discomfort. Moreover, these issues may be worsened in regions with hot and humid weather, such as Hong Kong. In response, the market has introduced a variety of cooling garments, such as Uniqlo's AIRism collection, which is made of cupro fibre and known for its breathability, ability to dry quickly, smoothness, lightweightness, and moisture-wicking properties (Uniqlo, 2021). Additionally, Chan (2019)

suggested that cooling effects can be attained by using cotton and regenerated fibres, and polyester.

Consequently, seven commercially available undergarments made of cotton and regenerated fibres, and polyester are used as samples in this study. These undergarments are knitted fabrics, which are commonly used for undergarments due to their excellent elasticity. Detailed descriptions are listed in Table 4.1, which include their fabric structure, areal and stitch densities, as well as fabric and yarn thicknesses. All of the specimens were conditioned at a temperature of  $20 \pm 1^\circ\text{C}$  and relative humidity (RH) of  $65 \pm 2\%$  for at least 24 hours before conducting the experiments.

**Table 4. 1** Specification of sample undergarments.

Sample	Structure	Materials	Areal density (g/m <sup>2</sup> )	Stitch density (per inch)	Thickness (micron)	Yarn thickness (micron)	Design details
U1	 Single jersey	66% Nylon 24% Cupro 10% Spandex	140	88 x 42	404	196	Seamless tank top Smooth, moisture wicking, fast drying, cool to the touch, stretchy, controls odour, and is anti-odour
U2	 Micro mesh	83% Nylon 17% Spandex	105	27 x 29	320	129	Tank top Smooth, moisture wicking, fast drying, cool to the touch, breathable, stretchy, controls odour, and is anti-odour
U3	 Single jersey	71% Cotton 25% Polyester 4% Spandex	167	48 x 38	480	234	Crew neck T-shirt Smooth, moisture wicking, fast drying, cool to the touch, stretchy, and controls odour

U4		88% Polyester 12% Spandex	107	80 x 46	260	135	Crew neck T-shirt Smooth, moisture wicking, fast drying, cool to the touch stretchy, and controls odour
	Single jersey						
U5		100% Cotton	173	50 x 30	780	190	Crew neck tank top, Anti-bacterial
	Single jersey						
U6		57% Cotton, 38% Polyester 5% Elastane (COOLMAX)	148	66 x 38	560	200	Tank top, Cool, dry, and comfortable to wear
	Single jersey						
U7		100% Cotton	182	40 x 26	880	246	Tank top
	Rib						

## 4.2.2 Thermal comfort

### 4.2.2.1 Air and water vapour permeability tests

Air and water vapour permeabilities are fabric properties that are closely linked to breathability. Specifically, air permeability measures the rate of airflow through a fabric, while water vapour permeability quantifies the amount of water vapour that passes through a material to the outside environment (Erdumlu & Saricam, 2017; Kulichenko, 2005; Lee et al., 2020). Given their role in regulating heat and moisture exchanges between the body and the environment, these properties are important determinants of thermal comfort.

Following the air permeability test in ASTM D737, a fabric specimen with dimensions of 100 x 100 mm was placed on the head of the KES-F8 air permeability tester, and air was released

to pass through the fabric in the perpendicular direction. The average air resistance (R) was then determined and expressed in kPa · s/m to denote the air permeability, with higher R values indicating lower air permeability.

As for the water vapour permeability test which was carried out in accordance with ASTM E96, the specimen was cut and sealed onto the open mouth of a dish filled with  $\frac{3}{4}$  distilled water. It was then placed in a controlled temperature room of 21°C with a humidity of 65% for 24 hours. The rate of water vapour transmission (WVT) was determined by using:

$$WVT = \frac{G}{TA} \quad (4.1)$$

where WVT denotes rate of water vapour transmission (g/h·m<sup>2</sup>), G denotes the weight change (g), T is time (h), and A is the test area of the dish (m)<sup>2</sup>.

#### **4.2.2.2 Thermal conductivity test**

The KES-F7 Thermos LABO II was utilised to conduct the thermal conductivity test. The experiment involved preparing a water box and a BT box, which were set to 25°C and 35°C, respectively. The fabric specimens, cut into dimensions of 50 x 50 mm, were inserted in-between the two boxes. The quantity of heat (watt) generated was determined by measuring the temperature when both boxes reached the same temperature. The thermal conductivity was then calculated using the following equation:

$$K = \frac{W \cdot D}{A \cdot \Delta T} \quad (4.2)$$

where K denotes the thermal conductivity (W/(cm·K)), W is the quantity of heat (watt), D is the thickness of the sample (cm), A = area of the BT box/heat plate (cm<sup>2</sup>) and  $\Delta T$  denotes the temperature difference between the BT and water boxes (°C).



#### 4.2.2.3 Maximum heat flux test (Qmax test)

The Qmax value, which represents the maximum heat transferred to a fabric sample upon initial skin contact, is a reliable indicator of the warm or cool feeling of the surface of a material. It is widely believed that undergarments with a cool feeling provide superior thermal comfort. To assess this sensation, the Thermos LABO II was utilised in the experiment. The fabric was placed on an insulated base, and a heated copper plate was subsequently placed on the top to transfer the stored heat to the fabric. This process mimics the immediate warm or cool sensation experienced by the skin upon contact with the fabric. The Qmax value, expressed in W/cm<sup>2</sup>, was used to quantify the sensation, with higher values indicating a cooler feeling.

#### 4.2.3 Tactile comfort

In addition, the KES-FB measurement system was used to obtain objective evaluations of the hand feel, and their parameters which are measured by using the KES-FB Auto system are found in Table 4.2.

**Table 4. 2** Parameters measured with KES FB-Auto system.

Parameter	Symbol	Description	Reading the data	Unit
<b>Tensile</b>	LT	Tensile rigidity	Values closer to 1 indicate higher tensile strength	-
	WT	Tensile energy	Higher values denote greater stretchability	gf.cm/cm <sup>2</sup>
	RT	Tensile resilience	Values closer to 100 denote better recoverability	%
<b>Shearing</b>	G	Shear rigidity	Higher values indicate more resistance to shearing	gf/cm. degree
	2HG	Elasticity for minute shear	Higher values denote lower recoverability from initial shear deformation	gf/cm
	2HG5	Elasticity for large shear	Higher values mean poorer recoverability	gf/cm
<b>Bending</b>	B	Bending rigidity	Higher values mean more resistance to bending	gf.cm <sup>2</sup> /cm <sup>2</sup>
	2HB	Bending moment	Higher values denote poor recoverability	gf. cm/cm <sup>2</sup>
<b>Compression</b>	LC	Compression linearity	Values closer to 1 mean greater compression	-

	WC	Compression energy		Higher value means higher susceptibility to compression	gf.cm/cm <sup>2</sup>
	RC	Compression resilience		Values closer to 100 denote higher resilience	%
<b>Surface Properties</b>	MIU	Coefficient of friction	of	Higher values mean less tendency to slip	-
	MMD	Mean deviation of coefficient of friction	of	Higher values mean less smoothness and more roughness	-
	SMD	Surface roughness		Higher values mean greater surface unevenness	μm

#### 4.2.3.1 Tensile and shear testing

The stiffness and anti-drop stiffness of fabrics are significantly influenced by tensile and shear strengths. Therefore, the KES-FB1-A tensile and shear tester was employed to measure the tensile and shear strengths. The former was tested by using a load-controlled method, while the latter was tested using a deformation-controlled method. Consequently, fabric properties, such as tensile linearity (LT), shear rigidity (G), tensile resilience (RT), tensile energy (WT), and small (2HG) and large (2HG5) shear hysteresis could be determined (Kato Tech, 2021a). For the experiment, fabric samples that measured 200 x 200 mm in dimensions with a maximum thickness of 2 mm were used. By controlling the sample slack with a motor, errors were minimised, thus resulting in improved accuracy. As shown in Table 4.2, higher WT, G, 2HG, and 2HG5 values indicate greater stretchability, more resistance to shearing, poor recoverability from initial shear deformation, and poor recoverability, respectively. In addition, LT values closer to 1 indicate higher tensile strength, while RT values closer to 100 indicate better recoverability.

#### **4.2.3.2 Bending test**

The bending rigidity (B) of fabrics is a crucial factor that affects tactile comfort and the range of motion of wearers. To measure fabric stiffness, the KES FB2-A pure bending tester was employed. This instrument can evaluate the B and bending moment (2HB), thus providing information on stiffness, fullness, softness, and anti-drape stiffness (Kato Tech, 2021b). Higher B values indicate more resistance to bending, while higher 2HB values indicate poor recoverability. Similar to the tensile and shear tests, the fabric samples were cut into dimensions of 200 x 200 mm with a maximum thickness of 1 mm.

#### **4.2.3.3 Compression test**

Material compressibility is a crucial property for the pressure monitoring undergarment in this study, as it should be soft and compressible to maximise its sensitivity. To determine the softness of the material used, the KES-FB3-A instrument was employed. The data extracted from the test, including compression linearity (LC), compression energy (WC), and compression resilience (RC), are important for assessing the fullness, softness, smoothness, and anti-drape stiffness of the fabric (Kato Tech, 2021c). LC values closer to 1 indicate greater compression, while higher WC values indicate higher susceptibility to compression. RC values closer to 100 indicate higher resilience. For the experiment, samples that measured 100 to 200 mm in width were cut into squares and compressed by using a sensor head of 2 cm<sup>2</sup>. The standard compression load was 50 gf/cm<sup>2</sup>, at a deformation rate of 0.02 (mm/sec).

#### **4.2.3.4 Surface properties test**

The smoothness of the fabric surface is a crucial factor in determining wear comfort. Since the undergarment comes into direct contact with bare skin, the material should be soft and smooth to avoid inducing tactile discomfort. Otherwise, AIS patients may be reluctant to wear the undergarment. To assess fabric fullness, softness, smoothness, and crispness (Kato Tech,

2021d), the KES FB4-A surface tester was employed. For the experiment, fabric samples that measured 200 x 200 mm in dimensions with a maximum thickness of 2 mm were used. A sensor was used to simulate human sensations, thus allowing for objective assessments of the hand feel. The mean coefficient of friction (MIU), mean deviation of the coefficient of friction (MMD), and surface roughness (SMD) were used to quantify these properties. Higher MIU and SMD values indicate higher friction or roughness (Kato Tech, 2021d; Shishoo, 2000; Tadesse et al., 2018).

#### **4.2.4 Wear trial**

A wear trial was subsequently carried out for the undergarment samples. The recruited subject is a 10-year-old female primary school student with a normal Body Mass Index (BMI). A temperature logger was positioned on her chest to record the RH and temperature of her skin. She was also instructed to walk (on a treadmill at 3 km/h at a 1% inclination) for an hour and rest alternately between donning each undergarment sample. The aim is to examine how the undergarments influence body temperature regulation under frequently changing temperatures. The trial was conducted in two conditioned rooms: (1) 32°C with an RH of 70% to simulate outdoor summer conditions in Hong Kong, and (2) 24°C with a RH of 60% to simulate an air-conditioned environment.

#### **4.3 Results**

With reference to Table 4.3, U2 is the most air permeable with an air resistance of 0.0148 kPa·s/m. Also, U3 and U4 show the highest thermal conductivity (0.0578W/(m·K)) and highest water vapour permeability (34.73g/h·m<sup>2</sup>), respectively. Furthermore, U1 has the highest Q<sub>max</sub> value (0.2486 W/m<sup>2</sup>).

**Table 4.3** Evaluation of thermal comfort.

	<b>Air resistance</b> (kPa·s/m)	<b>Water vapour</b> <b>permeability</b> (g/h·m <sup>2</sup> )	<b>Thermal</b> <b>conductivity</b> (W/(m·K))	<b>Q-Max value</b> (W/m <sup>2</sup> )
<b>U1</b>	0.1909	34.03	0.0558	<b>0.2486</b>
<b>U2</b>	<b>0.0148</b>	33.49	0.0427	0.1884
<b>U3</b>	0.2475	32.34	<b>0.0578</b>	0.2020
<b>U4</b>	0.0940	<b>34.73</b>	0.0371	0.1844
<b>U5</b>	0.1070	32.26	0.0563	0.1520
<b>U6</b>	0.1966	31.80	0.0551	0.2005
<b>U7</b>	0.1227	31.18	0.0489	0.1483

*\*Note: Yellow highlighted numbers denote highest value*

Besides, tactile comfort was objectively evaluated by using the KES-FB system, which included tensile, shearing, bending, compression, and surface properties tests. All samples are soft because their LT is less than 0.6 (Table 4.4). Among them, U1 is the softest material (mean LT = 0.09). Also, U2 and U3 have the highest RT and WT, respectively, which are 48.93% and 41.55 gf. cm/cm<sup>2</sup>. This implies that they are the most elastic and stretchable, respectively.

**Table 4.4** KES FB-Auto testing results.

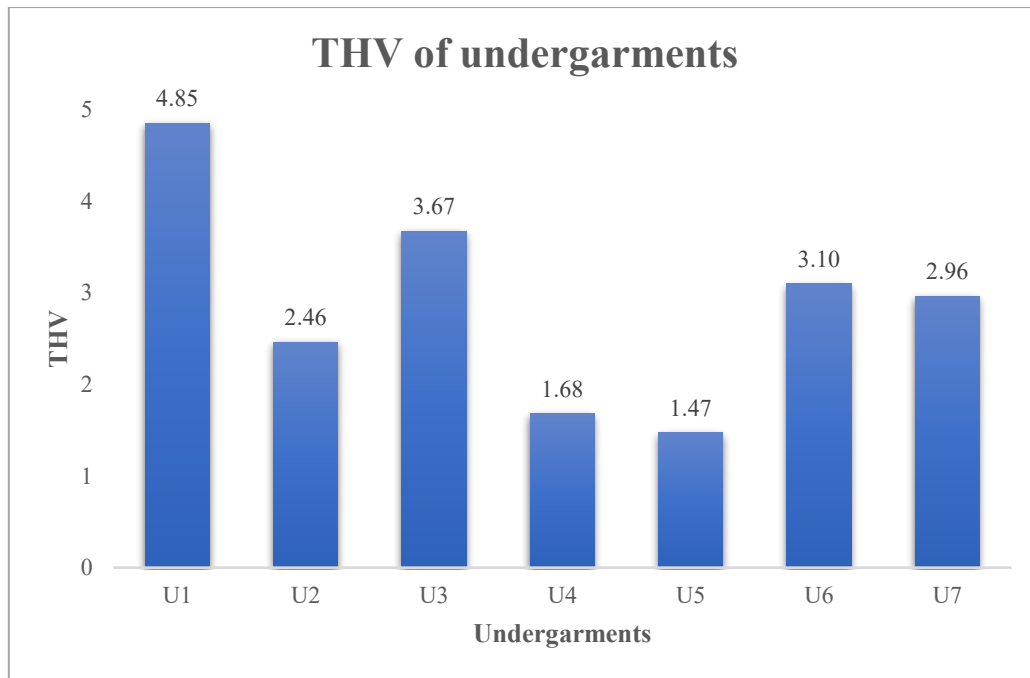
	U1		U2		U3		U4		U5		U6		U7	
	Wale; Course	Mean	Wale; Course	Mean	Wale; Course	Mean	Wale; Course	Mean	Wale; Course	Mean	Wale; Course	Mean	Wale; Course	Mean
<b>Tensile</b>														
LT	0.09; 0.10	0.09	0.17; 0.06	0.12	0.52; 0.56	0.54	0.34; 0.17	0.26	0.54; 0.14	0.34	0.20; 0.21	0.21	0.56; 0.20	0.38
WT	10.10; 11.93	11.02	20.10; 7.00	13.55	27.60; 55.50	41.55	40.50; 20.40	30.45	23.50; 17.20	20.35	23.90; 24.80	24.35	18.50; 23.10	20.80
RT	49.20; 42.67	45.94	44.28; 53.57	48.93	23.19; 20.63	21.91	32.80; 38.82	35.81	19.32; 19.77	19.55	33.33; 31.65	32.49	20.54; 17.53	19.04
<b>Shear</b>														
G	0.33; 0.42	0.38	0.61; 0.59	0.60	0.90; 0.88	0.89	0.54; 0.54	0.54	0.88; 1.02	0.95	0.63; 0.65	0.64	0.98; 1.19	1.09
2HG	0.53; 0.71	0.62	1.17; 1.22	1.20	3.43; 3.42	3.43	1.08; 0.97	1.03	2.90; 4.47	3.69	1.27; 1.85	1.56	4.25; 6.13	5.19
2HG5	0.53; 0.67	0.60	1.00; 1.13	1.07	3.22; 3.15	3.19	0.88; 0.88	0.88	2.58; 4.30	3.44	1.13; 1.63	1.38	3.83; 5.50	4.67
<b>Bending</b>														
B	0.0009; 0.0058	0.0034	0.0035; 0.0045	0.0040	0.0083; 0.0087	0.0085	0.0041; 0.0092	0.0067	0.0272; 0.0148	0.0210	0.0065; 0.0046	0.0056	0.0799; 0.0776	0.0788
2HB	0.0089; 0.0072	0.0081	0.0073; 0.0048	0.0061	0.0300; 0.0228	0.0264	0.0080; 0.0070	0.0075	0.0551; 0.0130	0.0341	0.0150; 0.0160	0.0155	0.1651; 0.1708	0.1680
<b>Compression</b>														
LC	-	0.57	-	0.65	-	0.39	-	0.52	-	0.31	-	0.37	-	0.38
WC	-	0.11	-	0.13	-	0.20	-	0.11	-	0.31	-	0.27	-	0.50
RC	-	39.08	-	34.02	-	35.68	-	44.97	-	56.08	-	35.04	-	33.19
<b>Surface</b>														
MIU	0.1440; 0.2060	0.1750	0.3180; 0.2520	0.2850	0.1820; 0.2130	0.1975	0.1780; 0.2410	0.2095	0.2330; 0.3300	0.2815	0.1890; 0.2220	0.2055	0.2180; 0.2430	0.2305
MMD	0.0030; 0.0062	0.0046	0.0230; 0.0078	0.0154	0.0061; 0.0082	0.0072	0.0043; 0.0332	0.0188	0.0071; 0.0101	0.0086	0.0052; 0.0066	0.0059	0.0072; 0.0146	0.0109
SMD	1.2220; 6.6850	3.9535	2.6470; 2.8550	2.7510	2.0020; 2.5680	2.2850	0.7720; 3.1620	1.9670	2.9700; 3.4750	3.2225	1.6820; 3.3570	2.5195	1.8880; 9.1530	5.5205

*\*Note: Yellow and blue highlighted numbers refer to the highest and lowest values, respectively.*

Irrespective whether in the warp or weft direction, U7 has the highest G, and largest 2HG and 2HG5, which contrasted with the results of U1. This means that U7 is more rigid, and has lower recoverability compared to U1. Moreover, U7 is the stiffest and the least elastic because it has the highest mean B of 0.0788 gf.cm<sup>2</sup>/cm and 2HB of 0.1680 gf. cm/cm.

Additionally, the compressional tests showed that the thinnest fabric, U2, has the highest LC of 0.65, while the thickest fabric, U7, has the highest WC of 0.50 gf. cm/cm<sup>2</sup>. Fabric thickness might be a contributing factor of the observed outcomes. Furthermore, the fabric warp appeared to be smoother than the fabric weft because the MIU, MMD, and SMD in the warp direction mostly have lower values than those in the weft direction in the surface properties tests. U1 has the smallest MIU (0.1750) and MMD (0.0046), which means that this sample has a higher tendency to slip and is smoother. On the other hand, U4 has the lowest mean SMD (1.9670  $\mu$ m), which implies a more even surface.

The data extracted from the tensile, shearing, bending, compression, and surface properties tests were inputted into the KES calculation software to measure the total hand value (THV) of each fabric. The THV gives the objective hand feel of fabric, where 1 and 5 represent the worst and the best hand feel, respectively. For the summer underwear, the Qmax value is also required, so it was considered in the calculation. Figure 4.1 shows that U1 and U5 have the best and worst hand feel, which are 4.85 and 1.47, respectively. Also, it is found that the THV of the summer underwear is correlated to the WT, RT, LC, and Qmax values at the 0.05 level. Their coefficients of correlation are -0.538, 0.630, 0.603 and 0.599, respectively (Table 4.5).



**Figure 4.1** Total hand values of undergarments.

**Table 4.5** Correlation among THV, tensile, shearing, bending, compression, surface properties, and Qmax

Tensile	THV	Shear	THV	Bending	THV	Com- pres- sion	THV	Surface properties	THV	Qmax	THV
LT	-0.432	G	-0.455	B	-0.163	LC	0.603*	MIU	-0.346	Qmax	0.599*
WT	-0.538*	2HG	-0.351	2HB	-0.098	WC	-0.358	MMD	-0.004		
RT	0.630*	2HG5	-0.337			RC	-0.42	SMD	0.16		

\*. Correlation is significant at the 0.05 level (2-tailed).

\*\*. Correlation is significant at the 0.01 level (2-tailed).

Table 4.6 provides the water vapour permeability, tensile, shearing, bending, and compression test results and shows that they are influenced by the areal density, and fabric and yarn thicknesses.

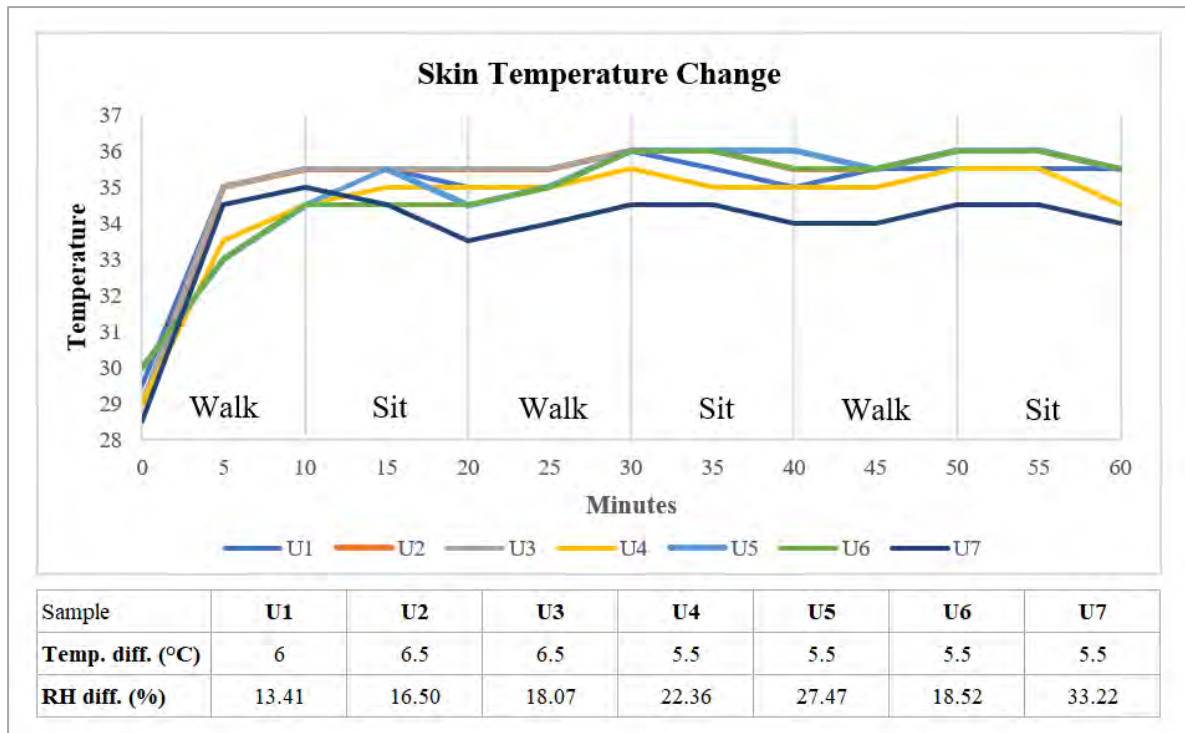


**Table 4.6** Correlation between wear comfort and various fabric specifications

Tested parameter	Symbol	Areal density	Sig.	Fabric thickness	Sig.	Yarn thickness	Sig.
Water vapour permeability	-	-0.825*	0.022	-0.860*	0.013	-0.764*	0.046
Qmax	-	-0.37	0.414	-0.636	0.125	-0.104	0.824
Tensile	RT	-0.826**	0.000	-0.765**	0.001	-0.684**	.0007
Shearing	G	0.765**	0.001	0.809**	0.000	0.607*	0.021
	2HG	0.810**	0.000	0.831**	0.000	0.690**	0.006
	2HG5	0.815**	0.000	0.827**	0.000	0.691**	0.006
Bending	2HB	0.638*	0.014	0.771**	0.001	0.633*	0.015
Compression	WC	0.796*	0.032	0.946**	0.001	0.688	0.088

Note: \*, \*\*denote significance at the 0.05 and 0.01 levels, respectively (2-tailed).

In the wear trial, the temperature of the skin immediately increased with the walking activity, and then gradually decreased when the subject sat down to rest. The temperature difference of the undergarments before and after the wear trial ranged from 5.5°C to 6.6°C (an 18.3% to 22.4% difference). Among them, U7 resulted in a comparatively lower skin temperature, which was often below 35°C (Figure 4.2). In addition, the RH of all the undergarments increased dramatically in the first 5 minutes of walking and then became relatively stable (all above 90%) after 10 minutes.



**Figure 4. 2** Changes in temperature of skin and RH during wear trial.

#### 4.4 Discussion

The wear comfort of fabrics is a critical attribute that affects the decision of customers when purchasing textile apparel, especially. undergarments Therefore, a number of different textile finishing treatments may be applied to fabrics to improve the hand feel, such as bio-polishing and softening (Jeguirim et al., 2010). Besides, the hand feel can be enhanced by using appropriate types of fibres, fabric structures, and yarn count (Atalie et al., 2019; Bivainyte et al., 2012; Siyao et al., 2020). Typically, undergarments are made of cotton due to the excellent water absorbency, breathability as well as softness of cotton (Rathmore, 2018). However, more people are concerned about cooling and moisture wicking effects nowadays because undergarments with poor breathability may trap body heat, induce odour and cause a clinging feeling during perspiration, especially during the summer when it is both hot and humid. Therefore, garments with cooling effects have become more popular recently. For example,

Uniqlo's AIRism collection made of cupro fibre is highly breathable, quick drying, smooth, and lightweight, and has good wicking moisture (Uniqlo, 2021). Chan (2019) also agreed that the cooling effect can be achieved by using cotton and regenerated fibres, and polyester. This implies that the raw materials of undergarments play a dominating role when evaluating overall textile comfort for summer weather.

#### 4.4.1 Thermal comfort

The experimental results in this study show that the main influential factors of material breathability are fabric porosity, areal density, fabric thickness, and yarn properties. Table 4.7 is a summary of the possible properties that affect the thermal comfort of the undergarments, which include areal density, fabric thickness, yarn properties, and stitch density. Apparently, lighter, thinner, and low stitch density fabrics that are made of neat and filament fibres provide better breathability and moisture wicking effect. Also, neat fibres that have higher thermal conductivity seem to offer a cooler feeling.

**Table 4.7** Possible factors that affect thermal comfort.

	Test	Properties				Result
		Areal density	Fabric Thickness	Yarn properties	Stitch density	
<b>Breathability</b>	Air permeability	-	-	-	Lower	More air permeable
	Water vapour permeability	Lighter	Thinner	Neat, filament, non-cotton	Lower	Transfers water vapour more effectively
<b>Cool feeling</b>	Thermal conductivity	-	-	Higher thermal conductivity fibres	-	Conducts heat faster
	Qmax values	-	-	Neat	Higher	Provides cool feelings

#### **4.4.1.1 Air permeability**

Usually, fabrics constructed with a lower stitch density or higher porosity are more air permeable because hot air can easily pass through the garments. For example, the pores of U2, a mesh fabric (stitch density = 27 x 29) are much larger than those of U3, a single jersey fabric (stitch density = 48x38) (Table 4.1), and therefore the former has a higher airflow rate and is more air permeable. This result is also supported in Chan (2019) and Yip and Ng (2008), who suggested that fabrics with high porosity have a higher air permeability. Therefore, it is likely that a lower stitch density can enhance air permeability and improve thermal comfort because heat can be easily transferred from the skin to the surrounding environment.

#### **4.4.1.2 Water vapour permeability**

Optimal water vapor transmission plays a significant role in enhancing thermal comfort, particularly during hot summers. This is attributed to the fact that perspiration serves as an effective mechanism for dissipating body heat and maintaining dryness (Qingqing et al., 2020; Lee et al., 2020). Conversely, inadequate water vapor transmission gives rise to a sense of clamminess and dampness as trapped heat and moisture become prevalent (Lee et al., 2020). The experimental findings of this study demonstrate that water vapor transmission is influenced by factors such as areal density, fabric thickness, and yarn thickness, with correlation coefficients of -0.825, -0.860, and -0.764, respectively (Table 4.6). For instance, U4, the lightest and thinnest sample (107 g/m<sup>2</sup>; 260 microns), and U7, the heaviest and thickest sample (182 g/m<sup>2</sup>; 880 microns) showed the highest and lowest water vapour permeability, respectively.

Besides, yarn properties in terms of hairiness and hydrophilic properties are crucial factors too. For example, U7 which was fabricated with pure cotton is hairier than U4, which was fabricated with synthetic fibres. The high water absorbency cotton and fibrils on U7 reduced the size of the pores after absorbing the water vapour and therefore inhibited moisture transportation. On the contrary, most of the synthetic fibres are hydrophobic, so they would not absorb as much moisture as cotton, and would not increase in thickness. Hence, undergarments made of light and thin synthetic materials which have low hairiness could provide higher water vapour permeability and breathability.

#### **4.4.1.3 Thermal conductivity**

Typically, fabrics with high conductivity conduct heat away from the body to the external environment efficiently and thus impart a cooling effect (Sumin et al., 2010; Tong et al., 2015). Making use of high thermal conductivity fibres or coating with metals can improve the thermal conductivity of fabrics.

Majumdar (2011) pointed out that this is related to the fabric thickness because thicker fabrics trap more still air in the fabric structure. However, this may not be an appropriate indicator for summer undergarments. For example, even though U3 is a thicker fabric made from thicker yarns, its thermal conductivity is higher than that of U4, which is a thinner material. The result showed the significance of the thermal conductivity of the fibres. U3 is mainly made of cotton, while U4 is polyester. The thermal conductivity of the fibres is 0.243 W/(m·K) and 0.157 W/(m·K), respectively (Zhang & Wang, 2020).

Additionally, it was found that the samples made from a natural material, such as cotton, have a higher thermal conductivity than those made of synthetic fibres. Their mean values are 0.055 W/(m·K) and 0.040 W/(m·K), respectively. Therefore, it is predicted that undergarments that consist of cotton have a higher thermal conductivity than those that consist of pure synthetic

fibres. This result is supported in Fujibo Holdings. INC. (2021), who indicated that cotton is the primary material in the market that provides a cooling feeling. Yip and Ng (2008) made a similar conclusion that the thermal conductivity of fabrics is affected by the thermal conductivity of the yarns.

#### **4.4.1.4 Q<sub>max</sub> value**

The main attribute that affects the Q<sub>max</sub> value are the material properties in terms of yarn hairiness and fineness, while a secondary contributor might be fabric thickness, which has a coefficient of correlation of -0.636 (Table 4.6). Both Park et al. (2018) and Vivekanadan et al. (2011) agreed that the Q<sub>max</sub> value is impacted by smoothness because smoothness increases the skin-to-fabric contact area, so the heat on the skin could be transferred to the fabric efficiently through conduction. For instance, the smoothest (U1 made of nylon, cupro, and spandex) and the roughest (U7 made of pure cotton) samples have the highest and lowest Q<sub>max</sub> values, respectively.

This result also implies that undergarments made of filament yarn are cooler than those made of staple yarn because the filament yarns are less hairy and finer than the staple yarns, so they can be packed tightly to form a smooth surface. Therefore, the surface area of U1 is larger and offers a cool feeling. Similarly, U1 to U4, and U6 that are made of synthetic yarns or blended yarns showed higher Q<sub>max</sub> values than U5 and U7 which are made of pure cotton. The thermal conductivity is 0.2048 W/m<sup>2</sup> and 0.1502 W/m<sup>2</sup>, respectively. Therefore, it is believed that the fibre properties in terms of hairiness and fineness play a dominant role when evaluating a perceived cool touch.

#### 4.4.2 Tactile comfort

The possible factors that affect tactile comfort are listed in Table 4.8. It can be observed that lighter and thinner undergarments that consist of a higher percentage of elastane, finer yarn, and neat and long fibres provide softer, smoother, and cooler hand feel and show better recoverability. However, the thicker fabrics show higher compression susceptibility.

**Table 4. 8** Possible factors that affect tactile comfort.

Test	Parameter					Result
	Areal density	Fabric Thickness	Elastane %	Yarn property	Stitch density	
<b>Tensile and shearing</b>	Lighter	Thinner	More	Finer	-	Softer and better recoverability
<b>Bending</b>	-	Thinner	-	Neat	-	Softer and better recoverability
<b>Compression</b>	-	Thicker	-	-	-	Better compression susceptibility
<b>Surface properties</b>	-	Thinner	-	Neat, long fibres	Higher	Smoother and cooler feeling

##### 4.4.2.1 Tensile and shear properties

The tensile and shear properties may be affected by the areal density, and fabric and yarn thicknesses, as well as the percentage of spandex. According to Table 4.6, RT is negatively proportional to the areal density, and fabric and yarn thicknesses, while G, 2HG, and 2HG5 show a positive correlation with them. This implies that lighter and thinner undergarments constructed with finer yarns are softer and have higher recoverability. For example, U2 is the lightest fabric, relatively thin, and fabricated with the finest yarn. This sample has the best tensile recoverability among all of the undergarments. In addition, U1 and U7 showed a distinct performance in the shearing test because of their large variation in areal density, and fabric and yarn thicknesses. Their differences are 42 g/m<sup>2</sup>, 480 microns and 50 microns, respectively (Table 4.1). This shows that heavier and thicker undergarments made of thick yarns tend to be

more rigid with less recoverability. Besides, it is predicted that fabrics with more spandex show higher tensile and shear recovery abilities. The spandex can be stretched 4 to 7 times its original size (TORAY Group, 2020b), which means only a small amount of spandex fibre can improve the fabric elasticity and maintain fabric softness at the same time. For example, U2 has the highest percentage of spandex (17%), and therefore it is reasonable that this sample has the highest RT. On the other hand, U7 is made of pure cotton and has poor shear recovery although it has a rib structure, which offers excellent width-wise extensibility and elasticity. The results indicate that spandex probably plays a dominant role when assessing recoverability.

#### **4.4.2.2 Bending properties**

Bending can act as an indicator of fabric stiffness and bending properties seem to be mainly affected by fabric thickness, fibre hairiness and fabric smoothness. A higher B and larger 2HB indicate more resistance to bending and poor recoverability, respectively.

U7 appeared to be far stiffer with poor bending recoverability than the other samples because it has the highest B, which is above 0.078, while U1 and U6 are below 0.005 (Table 4.4). This shows that U7 is much stiffer. Additionally, U7 has the highest 2HB, which is above 0.165, while U2 is below 0.007 in both the warp and weft directions. These distinct results might be due to fabric thickness, which is positively correlated to the bending hysteresis (0.771) (Table 4.6).

U5 and U7 are thicker pure cotton fabrics while the others are thinner fabrics made of synthetic fibres or cotton blend fibres. The mean fabric thickness of the pure cotton and synthetic fibre/cotton blend samples is 830 microns and 405 microns, respectively, while their 2HB is 0.0499 gf.cm/cm and 0.0127 gf.cm/cm, respectively. It appears that the thicker pure cotton fabric has a smaller 2HB which might be because the cotton fibres are hairier than the synthetic fibres, so they are more likely to be entangled, have higher friction, and show wrinkling problems. On



the other hand, most of the synthetic fibres are uniform, so the resultant fabric is smoother with better recoverability.

#### **4.4.2.3 Compressional properties**

The compressional properties are also greatly influenced by fabric thickness. Among the properties, WC is highly correlated with fabric thickness (0.946) (Table 4.6), which means that thicker fabrics are more susceptible to compression. It is fair to say that thicker fabric can be more compressed, and therefore its compression range can be wider. However, U7, the thickest fabric, could not recover back to its original bulk right away because its RC is the lowest (33.19%). This probably affects the fabric softness too. The aim of the pressure monitoring undergarment is to detect the bracing pressure, so it would be compressed frequently. Therefore, the RC is important because the undergarments should not deform easily. Otherwise, the fabric thickness may be uneven, which then affects the sensitivity of the FBG sensors.

#### **4.4.2.4 Surface properties**

Fabric smoothness could be affected by the fabric structure, stitch density, yarn properties in terms of fineness and hairiness, as well as length of the fibres. It is assumed that materials with a higher stitch density and made with fine filament yarns are smoother. Apparently, U1 and U2 are the smoothest and the roughest samples, respectively based on their distinct mean MIU and MMD. U1 is a single jersey fabric with the highest stitch density, made with fine and uniform filament yarns. This means that the yarns are packed tightly, so as to increase the surface area and provide a smoother hand feel. On the contrary, U2 is a high porosity micro mesh fabric, which has the lowest surface area, and thus has the highest friction and roughness. Besides, U7 showed an exceptionally high SMD in the weft direction because of its rib structure. These results show that materials with a higher stitch density and made with fine filament yarns are smoother.

#### 4.4.3 Total hand value and wear trial

The obtained results from the total hand value (THV) tests exhibited a high degree of consistency with those acquired during the wear trial. This implies that both the results from the objective and subjective experiments show that U1 is the most comfortable summer undergarment.

With reference to Figure 4.1, U1 has the best hand feel (THV = 4.85). Conversely, the remaining samples exhibit THV values below 3.7, thus indicating a worse hand feel. Although the THV results showed relatively high coefficients of correlation with WT, RT, LC, and Qmax values at the 0.05 significance level (Table 4.5), the Qmax value is deemed the most crucial factor that affects the wear comfort of an undergarment, particularly in the summertime. This is because the cool sensation of the fabric directly reduces the surface body temperature, thereby reducing the reliance on perspiration as the primary means of heat dissipation. The Qmax of U1 is approximately  $0.25 \text{ W/m}^2$ , while the others are close to or less than  $0.20 \text{ W/m}^2$ . Hence, it is believed that surface body heat can be conducted faster when wearing U1.

This result is also supported by the wear trial and water vapour permeability tests. U1 has the least difference in RH%, which is 13.41%, while the others range from 20% to 30% (Figure 4.2). Additionally, U1 is the second most water vapour permeable sample ( $34.03 \text{ g/h}\cdot\text{m}^2$ ) (Table 4.3). This implies that U1 traps the least amount of hot moisture, which can be easily transmitted from the body to the environment. On the other hand, U7, the thickest fabric made of pure cotton, has the highest difference in RH% (33.22%). Sweat may dampen this undergarment and cause clinging, especially since it is made of pure cotton, which has excellent water absorbency but does not dry quickly. Besides discomfort, the saturated fabric easily causes feelings of coldness due to the high latent heat of vaporisation ( $22.6 \times 10^5 \text{ J/kg}$ ).

However, U7 appears to have the highest thermoregulation because a comparatively lower skin temperature is obtained with its use, which is often below 35°C (Figure 4.2)

## **4.5 Summary**

The results suggest that U1 is the most comfortable summer underwear sample, as evidenced by both the physical experiments and a wear trial. The results show that the thermal and tactile comfort of the undergarments are affected by the fabric structure, areal and stitch densities, fabric and yarn thicknesses as well as fibre content. Overall, thinner, and higher porosity materials made of filament fibres are more breathable, dry quickly, and provide a cooler feeling than pure cotton undergarments. Yet, pure cotton undergarments can retain a lower body temperature because they cause more perspiration but also create discomfort at the same time. Therefore, compromise is needed when manufacturing summer undergarments because some of the desired properties are conflicting. For example, a high stitch density fabric that uses fine filament yarn is softer and smoother and provides a cooler feeling because of the larger surface area. However, it is also associated with less breathability.

## **CHAPTER 5 SMART TEXTILE: INSETING SILICONE-EMBEDDED FBG SENSORS INTO KNITTED UNDERGARMENT**

### **5.1. Introduction**

Monitoring force and pressure are critical for effective compression therapy, such as bracing, which is the most prevalent type of treatment for AIS patients with a Cobb's angle  $>25^\circ$  at Risser stages 0–2, with the aim to correct the spinal abnormality by passively exerting pressure (Bunge et al., 2010; Lonstein, 2006; Negrini et al., 2015; Schwieger et al., 2017; Weinstein et al., 2013). AIS patients are prescribed a rigid brace, which they must wear for at least 18 h each day (Konieczny et al., 2017; Schwieger et al., 2017) as tightly as they can tolerate, because the tightness and effectiveness of the brace are positively correlated (Tessadri et al., 2012; Weiss, 2010). However, no consensus has been reached on the optimal bracing pressure (Rigo et al., 2006), so the applied pressure mainly depends on the professional judgement of the orthotist (Chalmers et al., 2012). Additionally, many studies have proven that braces have a positive effect on trunk correction, but the mechanism behind this is still unclear (Fuss et al., 2021). Not only could this knowledge gap result in physical injury, but excessive pressure also affects compliance with bracing and quality of life, thus lowering treatment compliance and efficacy (Weinstein et al., 2013). For example, blood circulation, skin metabolism, and subcutaneous tissues could be affected if the pressure exceeds the typical capillary blood pressure (4.3 kPa) for an extended period of time (Mak et al., 2010). To tackle these issues, a more scientific approach should be developed to prevent excessive pressure by monitoring the forces applied by braces.

A variety of sensors are available to measure the force and pressure exerted by braces, but they all have limitations. For instance, Lou et al. (2010) designed a battery-powered wireless force sensor to measure the force exerted by a Boston brace for up to 6.78 N (60 kPa). However, some loggers showed a time delay, and the sensors could only be embedded in tailor-made engraved braces. Krištof et al. (2010) used a Pressurex® ultra-low pressure film to measure the relative pressure between an AIS patient and a Boston brace, and the maximum recorded pressure was 361.87 kPa. Although they obtained the overall pressure distribution, the exact amount of pressure on the film had to be further analysed with the Topaq® imaging system and a flatbed scanner that was specifically adapted to the study (Sensor Products Inc., 2023). Furthermore, attaching a large piece of pressure film on the inside of the brace could cause the film to pleat easily, which may affect the pressure distribution profile. Both methods are able to measure pressure, but no method has been developed to determine the instant pressure exerted by braces. Additionally, these two sensors cannot be easily applied to the torso and need to be embedded or cut beforehand. To overcome these challenges, Chan et al. (2018) used a Pliance®-xf-16 system with  $3 \times 3$  socket sensors to measure the pressure applied by a semi-rigid textile brace, for a pressure range of 0 to 200 kPa. While this is a instant flexible pressure sensor, it would be difficult to insert long-tailed sensors into a tightly fitting brace, especially as tape is needed to fix the sensor head to a specific location. Therefore, a flexible and user-friendly sensor with a instant pressure profile would be more suitable for measuring bracing pressure.

Smart textiles that use fibre optic sensors are one of the most appropriate means of obtaining close-to-body measurements, such as interface pressure, because they are very flexible and lightweight and have electromagnetic immunity while maintaining high strain sensitivity (Carmo et al., 2012; Mac-Thiong et al., 2004; Plümpe et al., 2017). Furthermore, they make up for the shortcomings of conductive sensors. For example, strain fibre optic sensors can be used

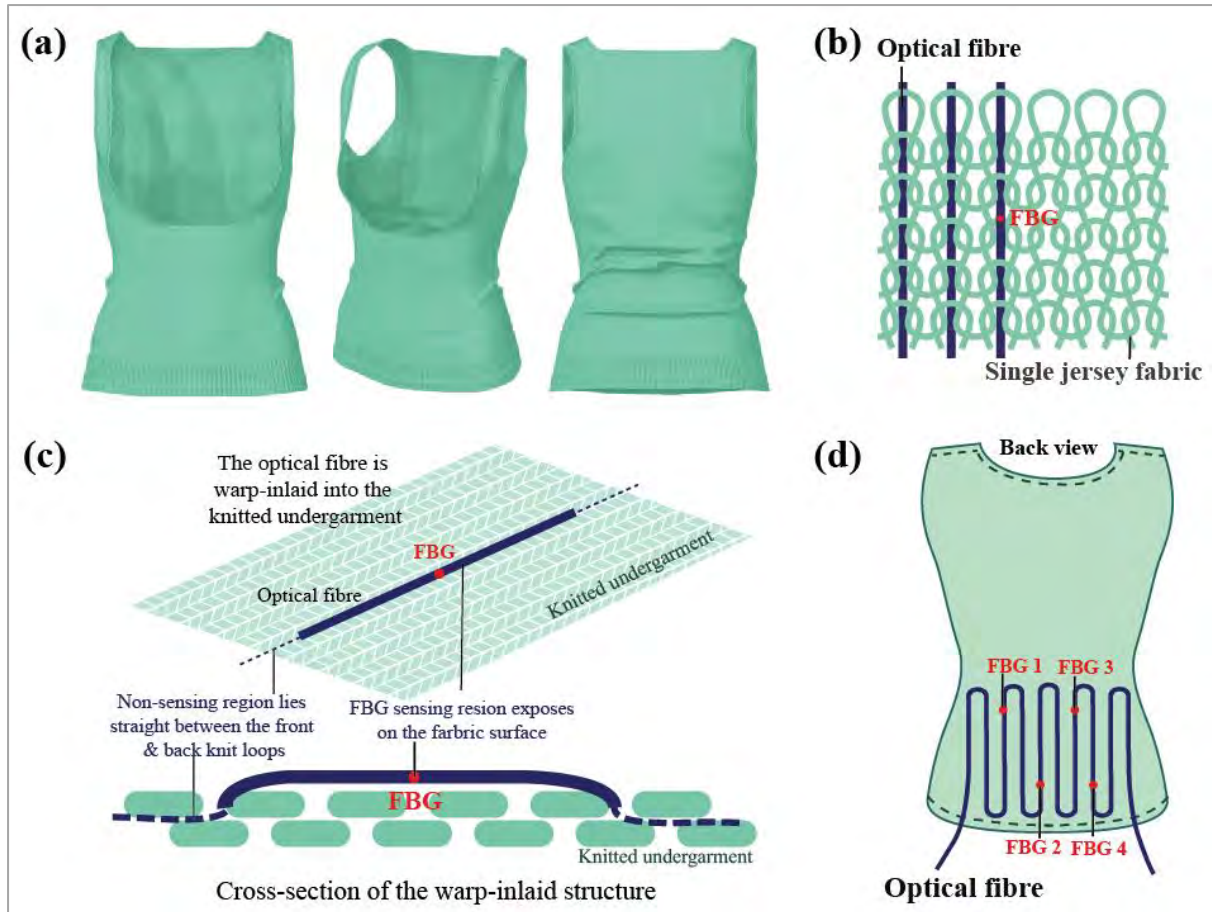
during MRI to monitor instant respiratory activity (Massaroni et al., 2015), while conductive sensors cannot. Additionally, fibre optic force sensors can be employed to monitor the blood flow of hospitalised patients who are immobile to prevent decubitus ulcers (Kanellos et al., 2010; Krehel et al., 2013; Quandt et al., 2017), examine plantar pressure and gait movement (Leal-Junior et al., 2018; 2019), and detect hand and joint movements (Koyama et al., 2013; Leber et al., 2019). The collected data are useful for detecting diseases and determining the required degree of rehabilitation or the level of athletic performance (Lee et al., 2022).

To address the inadequacies of conventional sensors, a smart textile capable of conveniently measuring bracing pressure is proposed in this study. This smart textile is not only easy to use, but can also accommodate adolescents of different body shapes, so no procedures are necessary before treatment. The smart textile also provides instant signal profiles and overall pressure distribution. This smart textile is constructed by inserting FBG sensors into a knitted undergarment via the inlay method. Additionally, the FBG sensing points are embedded into a thin silicone membrane with a curvilinear shape to enhance the fibre flexibility, robustness, and compatibility of the sensor with the surface of the skin. The smart textile can be applied directly to the body, and the tightly fitting design can prevent the formation of pleats or damage to the fibre optic sensors with compression textile or under braces. Instant data acquisition allows the tightness to be adjusted and monitored during the fitting process.

## **5.2. Methodology**

### **5.2.1 Construction of the smart textile: Inlaying FBG sensors into highly elastic knitted undergarment**

A perfectly fitting smart textile is desirable because pleat formation and optical fibre breakage would be less likely to occur. Therefore, pure PIMA cotton thread (4/80 Nm) was weft knitted by using a Shima Seiki knitting machine with a single jersey structure to ensure that the weft of the textile has high elasticity (Figure 5.1(a)). Then, optical fibres with 4 FBG sensors (wavelengths of 1550.09 nm, 1551.87 nm, 1554.12 nm, and 1555.90 nm, respectively) were warp-inlaid into the knitted undergarment manually to maintain widthwise elasticity (Figure 5.1(b)). Hence, the optical fibres were laid straight between the front and back knit loops, while the FBG area was exposed on the fabric surface to be embedded into a silicone membrane (Figure 5.1(c)). The sensing points were placed in the lumbar region, which is one of the main areas subjected to pressure during bracing (Figure 5.1(d)).



**Figure 5.1** (a) Three-dimensional illustration of smart textile, (b) structure of optical fibre warp-inlaid into single jersey fabric, (c) cross-section of warp-inlaid structure, and (d) configuration of optical fibre and allocation of FBG sensors 1 to 4.

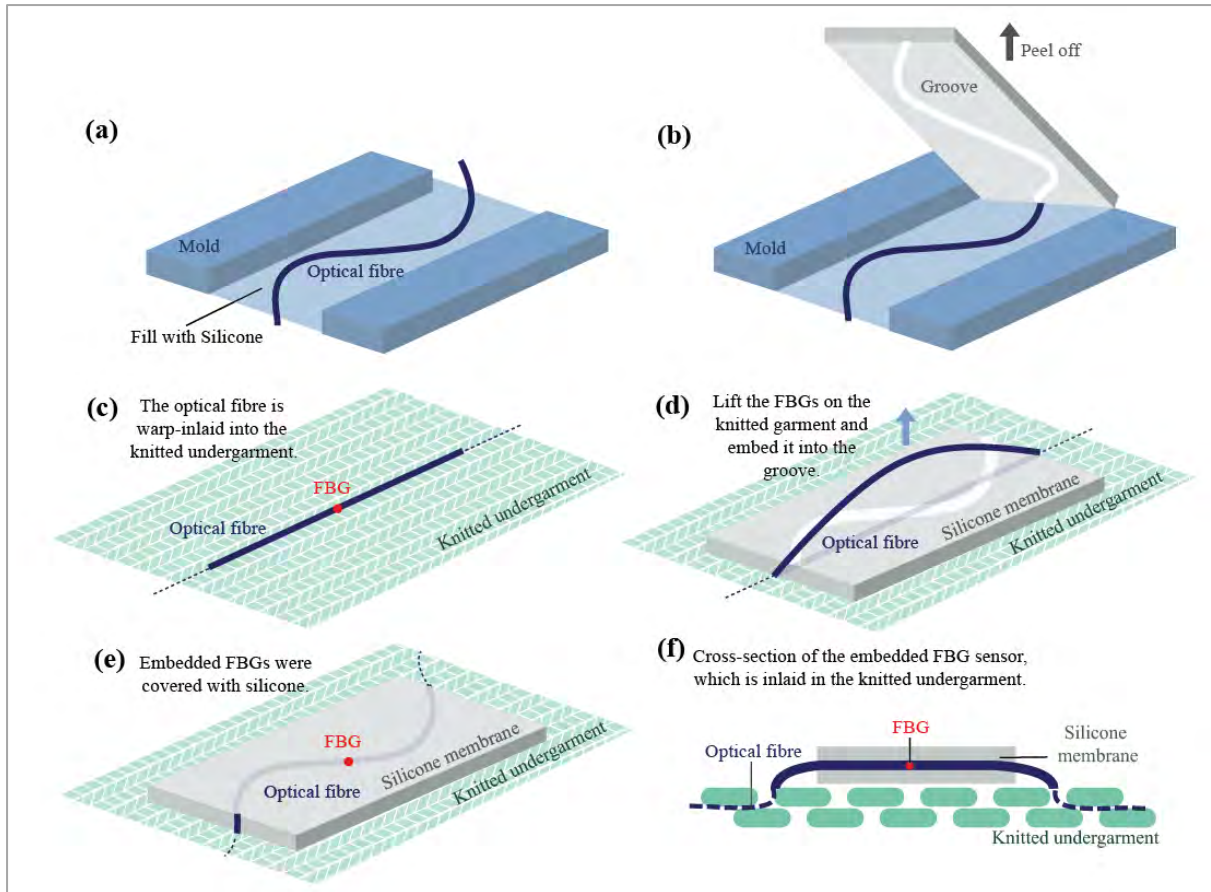
### 5.2.2 Embedding FBG sensors into silicone membranes

Embedding the FBG sensors into flexible silicone membranes not only enhances their flexibility and softness, and their susceptibility to compression, but also protects them more effectively. The moulding method in Guo et al. (2019) was used to embed the FBG sensors into a flexible PDMS membrane with a curvilinear shape. This improved the elasticity of the fibres during fabric stretching, compression, and twisting, as well as the strain sensitivity. However, Dragon Skin<sup>®</sup>20 silicone rubber is used instead of the PDMS membrane in this study because it does not require high-temperature curing, yet can be potentially integrated into textiles. For example, Presti et al. (2019) encapsulated a sensor in Dragon Skin<sup>®</sup>20 and



integrated this into an elastic band to monitor respiratory activity and heartbeat. This not only improved the sensor robustness and the compatibility of the sensor and the skin, but also the sensitivity of the physiological parameters.

For the embedding process, a mould with a depth of 1.5 mm was first prepared. Then, a bent optical fibre was placed in the middle of the mould, which was subsequently filled with Dragon Skin<sup>®</sup>20 (Figure 5.2 (a)). This was intended to create a groove in the silicone. After the silicone was dried at room temperature for 75 min, it was carefully peeled off to reveal a groove (Figure 5.2(b)). The optical fibre was warp-inlaid into the knitted undergarment, but the FBG sensing area was exposed on the fabric surface for embedding (Figure 5.2(c)). Then, the FBG sensors were lifted from the knitted undergarment and embedded into this groove (Figure 5.2(d)). Finally, the embedded FBG sensors were covered with silicone to secure them into position (Figure 5.2(e)). Figure 5.2 (f) shows a cross-section of an embedded FBG sensor warp-inlaid into the knitted structure. Aside from enhancing the sensor elasticity and sensitivity, the embedding of the FBG sensors also reduced the tendency of the sensors to shift. To integrate four FBG sensors into the silicone membranes, this process was repeated four times.



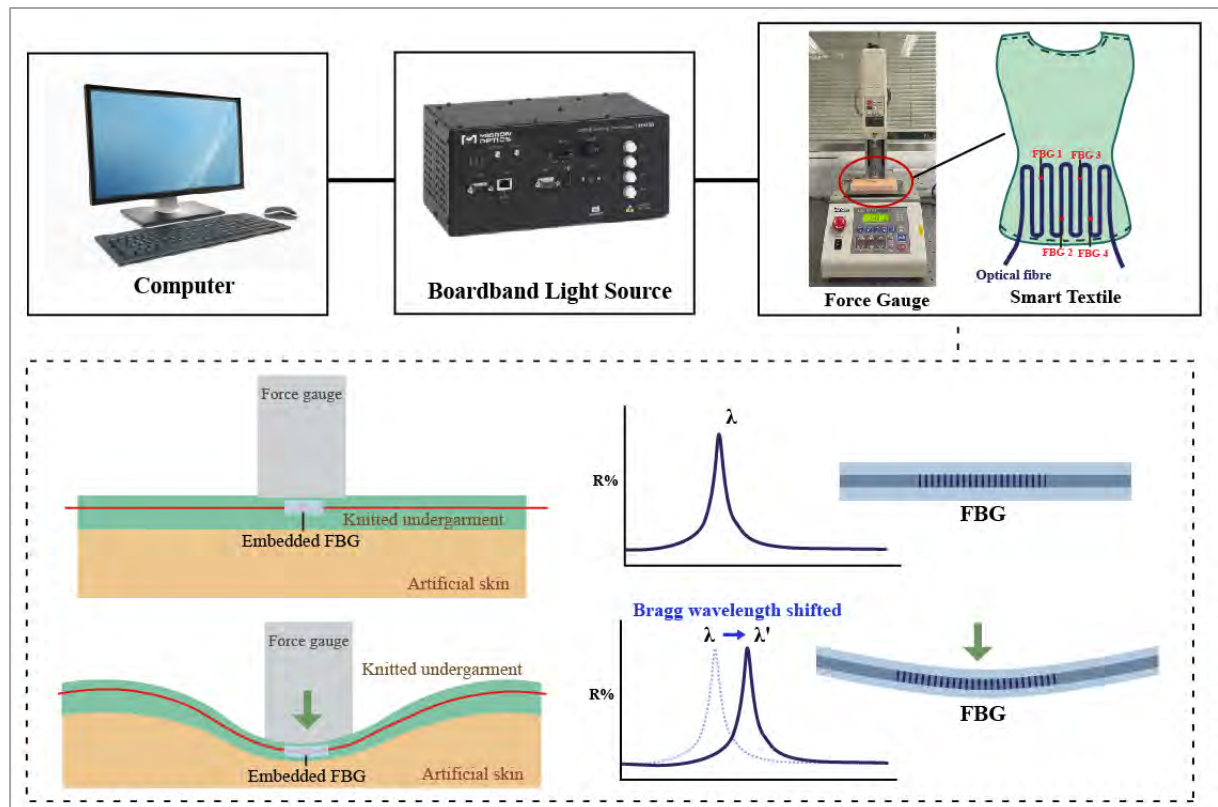
**Figure 5.2** Schematic of embedding FBG sensors into a silicone membrane: **(a)** filling mould with silicone, **(b)** peeling off resultant silicone membrane, **(c)** exposing FBG sensing area for embedding, **(d)** embedding FBG sensor into groove of silicone membrane, **(e)** covering embedded FBG sensor with silicone, and **(f)** cross-sectional view of an embedded FBG sensor warp-inlaid into knitted structure.

### 5.2.3 Wear trial to simulate bracing

#### 5.2.3.1 Smart textile

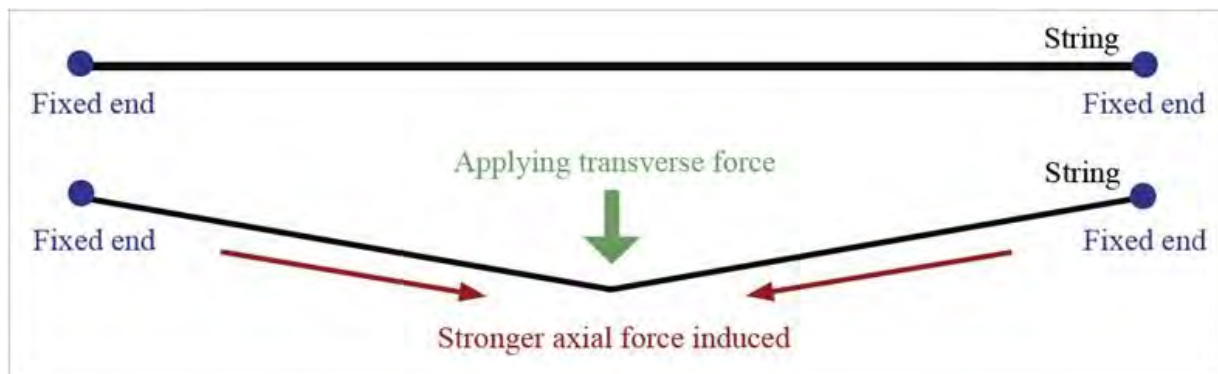
The applied forces could not be obtained by directly measuring the peak Bragg wavelength shifts, so it was necessary to understand the force–strain relationship. An experiment that simulated a bracing treatment was conducted to understand the relationship between the normal forces and strain sensed by the FBG sensors. In the experiment, artificial skin and a force gauge (model: JSV-H1000, Japan Instrumentation System) were used to model human skin and

bracing pressure, respectively. The artificial skin was 15 mm in thickness and made of Ecoflex<sup>®</sup> 0010 silicone rubber, which has a similar texture to the human torso. Chan (2019) indicated that the Young's modulus and Poisson's ratio of a soft mannequin made of Ecoflex<sup>®</sup> 0010 are 0.0768 MPa and 0.3, respectively. Furthermore, the pressure at the interface of a brace and a human torso is similar to that at the interface of a brace and a soft mannequin. Moreover, they have similar spinal corrective effects and were validated by using a finite element model. The embedded FBG sensors were inserted into the knitted garment and placed between the force gauge and the artificial skin (Figure 5.3). Every 5 s, the force gauge exerted a force onto the smart textile that rose by increments of 0.5 N until it reached 10 N.



**Figure 5.3** Equipment setup and schematic of transverse force applied to smart textile on artificial skin.

FBG sensors are sensitive to strain, which can be induced by axial and transverse forces. Typically, the strain of optical fibres is defined as axial force because they show prominent deformation. For example, FBG sensors increase in length when the fibres are stretched. However, transverse forces mainly change the fibre cross-section and slightly lengthen the fibres because of the positive Poisson's ratio of the fibres. Fixing the two ends of the FBG sensor could improve the transverse force sensitivity (Guo et al., 2019; Li et al., 2019). When the two ends of a flexible string are fixed and transverse force is applied to the string, higher axial forces result (Figure 5.4). This also implies that the corresponding deformation on the optical fibre caused by transverse forces will eventually convert to axial strain, which can be easily measured by calculating the peak Bragg wavelength shift. Therefore, the relationship between force and Bragg wavelength can be established, and it is predicted that a higher peak Bragg wavelength would shift to a higher force.

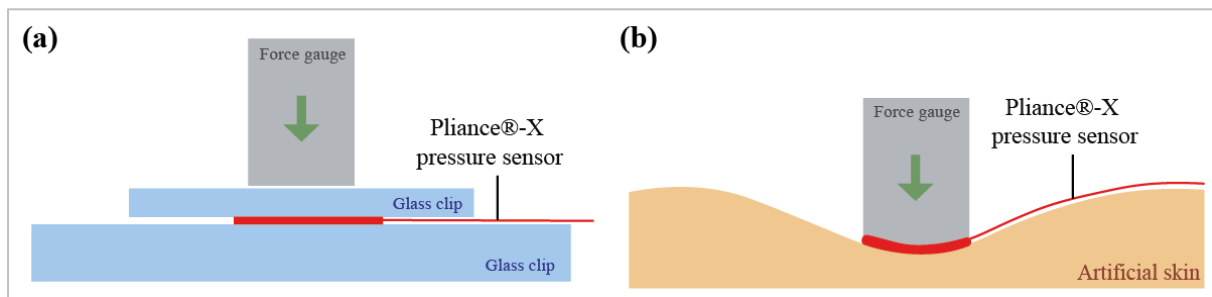


**Figure 5.4** Schematic of amplifying string axial and transverse forces.

### 5.2.3.2 Pliance®-X pressure sensor

The Pliance®-X pressure sensor was compared with conventional pressure sensors and used for a wear trial simulation. The sensor was tested under two conditions: (1) placed between two glass clips to simulate the calibration system (Figure 5.5(a)), and (2) placed on the artificial skin (Figure 5.5(b)). The Pliance®-X pressure sensor is a reliable tool for measuring low

interface pressure between textiles and skin under stationary conditions (Chan et al., 2018; Ghadikolaee et al., 2020; Lai & Li-Tsang, 2009; Wiseman et al., 2018). Its very small and ultra-thin sensing area is connected to an extended conductive strip, which makes it favorable for insertion underneath long-sleeved clothing. Moreover, due to the flexible sensor configuration, a single sensor or a matrix of sensors can be used for various measurements. Its high flexibility has captured much research interest, and studies have used this device to measure bracing pressure. For example, the Pliance®-X pressure sensor was used to measure the amount of pressure exerted by a posture correction girdle on AIS patients (Chan et al., 2018) and a functional brace on anterior cruciate ligament deficient (ACLD) subjects (Ghadikolaee et al., 2020).



**Figure 5.5** Schematic of transverse force applied to Pliance®-X pressure sensor: (a) between two glass clips and (b) on artificial skin.

#### 5.2.4 Data analysis

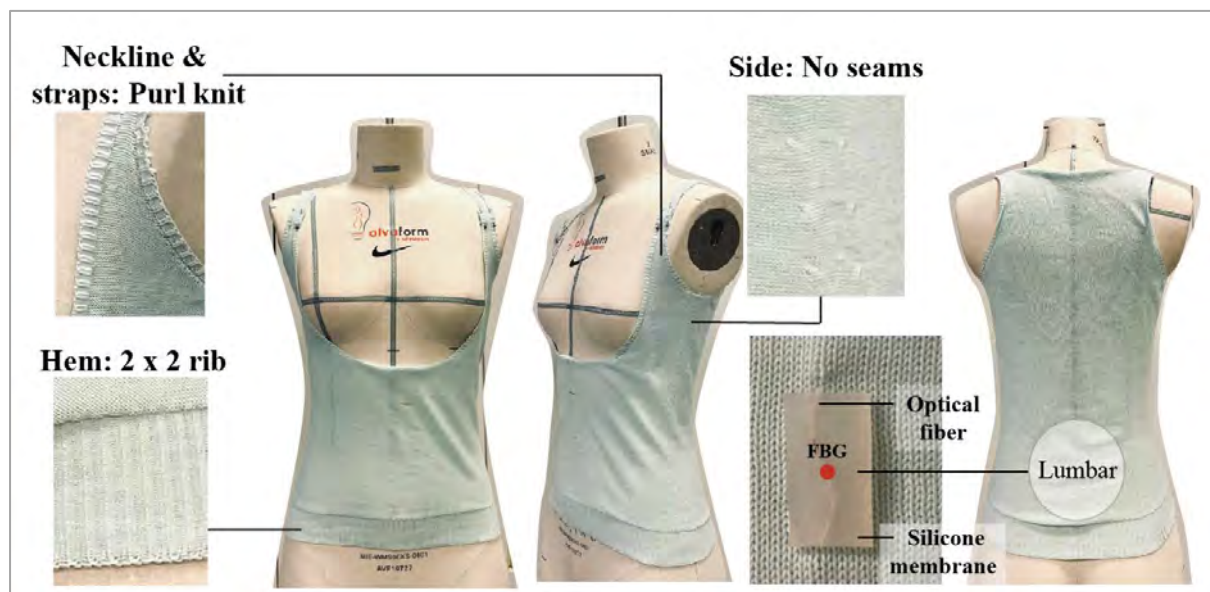
The data collected from the wear trials were used to examine the linearity ( $R^2$ ) of the smart textile by assessing the degree to which the FBG sensors responded to a range of standardised forces. The force gauge applied a loading force of 0.5 N every 5 s onto the smart textile until it reached 10 N, and 10 readings were recorded every second. In total, 50 readings were taken every 5 s, but only the peak Bragg wavelength shifts were extracted to analyse the linearities of the FBG sensors at 1550.09 nm (FBG 1), 1551.87 nm (FBG 2), 1554.12 nm (FBG 3), and

1555.90 nm (FBG 4). Furthermore, the linearity was compared to that of the Pliance®-X pressure sensor when tested on a soft surface. Moreover, to evaluate the test–retest reliability of the smart textile, an intraclass correlation coefficient (ICC) of a two-way random effects model with 95% confidence intervals was used.

## 5.3 Result and Discussion

### 5.3.1 Smart textile design

The knitted undergarment showed high elasticity and fit the dummy perfectly. The waistline was shaped, and an open chest design was adopted to prevent issues with the opening and compression (Figure 5.6). In addition, no side seam was used, thus maximising wear comfort. To avoid rolling edges, purl knit, and  $2 \times 2$  rib were applied for the strap edges and hemline, respectively.



**Figure 5.6** Seamless knitted undergarment created using Shima Seki knitting machine, and silicone-embedded FBG sensor inlaid in the warp direction.

Additionally, to meet the needs of AIS patients for wear comfort, pure cotton and a single jersey structure with relatively high porosity were chosen to knit the undergarment because

they are breathable, which means they are capable of maintaining a low body temperature and have high water absorbency (*please see Chapter 4*). These are believed to be the primary requirements of scoliotic braces because the issue of perspiration accumulation within the brace may increase the discomfort of AIS patients (Canavese & Kaelin, 2011). For instance, if the undergarment fails to absorb sweat efficiently, a clingy sensation may result, thus leading to discomfort and unpleasant odours, which may further intensify the sense of inferiority felt by AIS patients. Hence, while synthetic and ultra-fine undergarments may offer a cooling sensation, their inadequate breathability means that they are not used in this study.

Then, optical fibres with four FBG sensors were inlaid manually in the warp direction into the knitted undergarment at the lumbar region, which is one of the main areas subjected to pressure during bracing. Typically, straight configurations of optical fibres in a knitted structure reduce the fabric elasticity in the direction of the insertion (Yamada, 2020). Bending the optical fibres into a curvilinear shape along the warp direction solved this problem and preserved the widthwise elasticity of the fabric. Moreover, the sensor flexibility and softness were improved after the FBG sensors were embedded into the silicone membranes in a curvilinear shape.

### **5.3.2 Linearity of silicone-embedded FBG sensors and bare FBG sensors**

The results showed that the silicone-embedded FBG sensors are more stable and linear than the bare FBG sensors when force is applied. The Bragg wavelength delta difference indicated the force sensing range and force sensitivity; a larger delta difference denotes a higher sensitivity. For the embedded FBG sensors, the Bragg wavelength delta differences from 0 N to 10 N for FBG sensors 1 to 4 are 0.157 nm, 0.221 nm, 0.236 nm, and 0.175 nm, respectively (Figure 5.7(a)), while those for the bare FBG sensors are 0.196 nm, 0.253 nm, 0.233 nm, and 0.169 nm, respectively (Figure 5.7(b)). Although the bare FBG sensors have a higher sensing range, their linearity and stability are inferior to those of the embedded FBG sensors. For



example, the  $R^2$  values of the silicone-embedded and bare FBG sensors are 0.90-0.92. and 0.76–0.89, respectively. Their equations are:

$$\text{Embedded FBG 1: } y = 0.0145x + 0.0283 \quad (5.1)$$

$$\text{Embedded FBG 2: } y = 0.0208x + 0.0422 \quad (5.2)$$

$$\text{Embedded FBG 3: } y = 0.0216x + 0.0513 \quad (5.3)$$

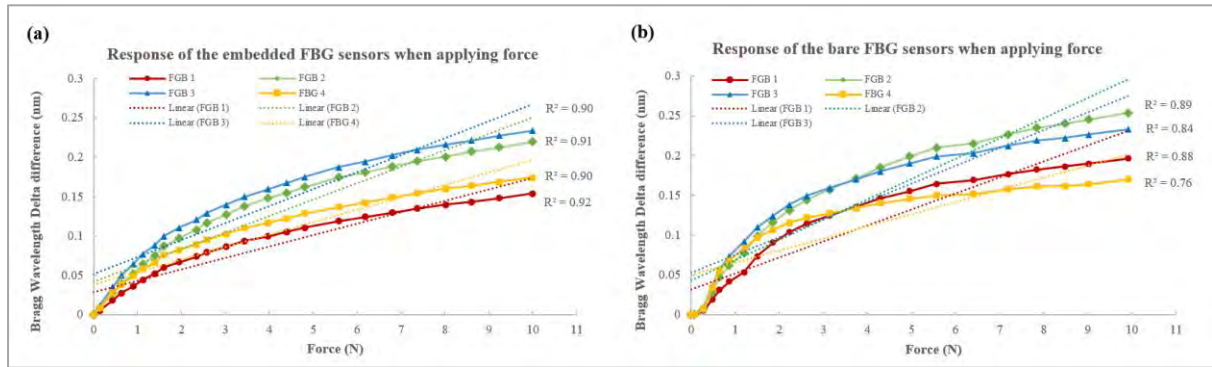
$$\text{Embedded FBG 4: } y = 0.0158x + 0.0386 \quad (5.4)$$

$$\text{Bare FBG 1: } y = 0.0201x + 0.0321 \quad (5.5)$$

$$\text{Bare FBG 2: } y = 0.0255x + 0.0433 \quad (5.6)$$

$$\text{Bare FBG 3: } y = 0.0223x + 0.0530 \quad (5.7)$$

$$\text{Bare FBG 4: } y = 0.0153x + 0.0499 \quad (5.8)$$



**Figure 5.7** Linearity of Bragg wavelength when applying force on **(a)** silicone-embedded FBG sensors, and **(b)** bare FBG sensors.

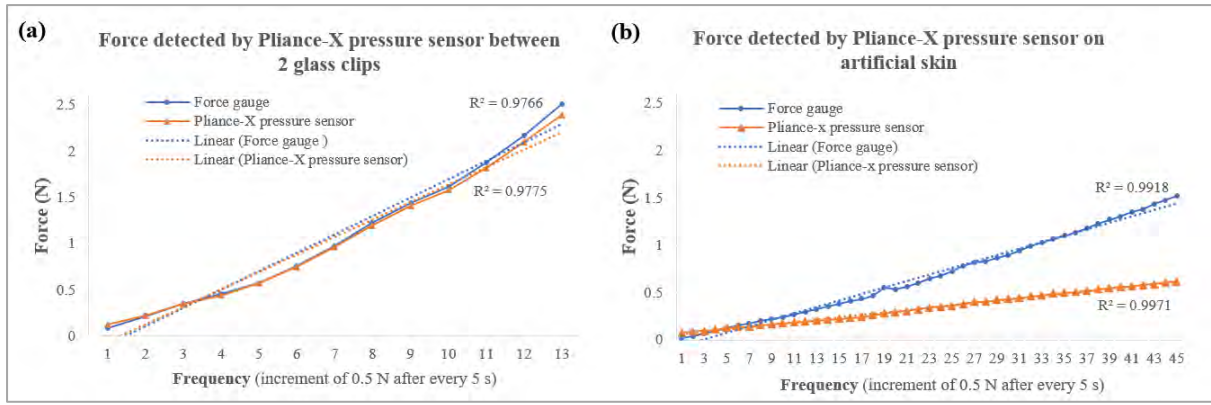
One of the reasons for this may be that the two ends of the FBG sensors were fixed in the silicone membranes, which minimised the shifting of the sensors and at the same time, maximised their sensitivity to the transverse force. Therefore, the signal could be transferred more efficiently and in a stable manner so that the silicone-embedded FBG sensors showed better linearity. Another reason for this could be the sensor flexibility, which is enhanced by its curvilinear shape and the silicone membrane. The former allows the optical fibre to bend



more without breaking, while the latter increases the compression susceptibility. A third possible reason is that the flat silicone membranes increase the sensing area and distribute the force more evenly. The FBG sensors are tiny points (125  $\mu\text{m}$  in diameter) on the optical fibre, so a minor displacement of the force gauge could have affected data acquisition. However, when the FBG sensors were embedded into the silicone membrane, the force applied near the FBG sensors could also be detected, which reduced the percentage of error. The pre-bent FBG sensors embedded into the silicone membranes eliminated shifting of the sensor and enhanced the sensor flexibility and compression resistance, as well as accuracy.

### **5.3.3 Linearity and reliability of silicone-embedded FBG sensors and Pliance®-X pressure sensor**

The Pliance®-X pressure sensor showed high linearity for both tests, with an  $R^2$  value above 0.97 (Figures 5.8(a) and 5.8(b)). However, its performance on hard and soft surfaces varied greatly. When tested between two glass clips, the detected forces were nearly identical to those of the force gauge, but their differences were more substantial when tested on artificial skin with increases in force. For example, when the force gauge applied a loading force of 1.5 N, the detected force was only 0.6 N, which implies that the force is absorbed by the artificial skin, and the sensor may not be suitable for use on a very soft surface with a high compression force. Moreover, the Pliance®-X sensor is only suitable for measuring forces up to 2.5 N (~30 kPa), while the FBG sensors could withstand a loading force of more than 10 N. This is in agreement with Lai and Li-Tsang (2009), who found that the Pliance®-X pressure sensor is a reliable tool when measuring low interface pressure. The experimental findings showed that the Pliance®-X pressure sensor has two main limitations, namely, low accuracy on soft surfaces and the inability to measure a high interface pressure.



**Figure 5.8** Force detected by Pliance®-X pressure sensor: **(a)** between two glass clips and **(b)** on artificial skin.

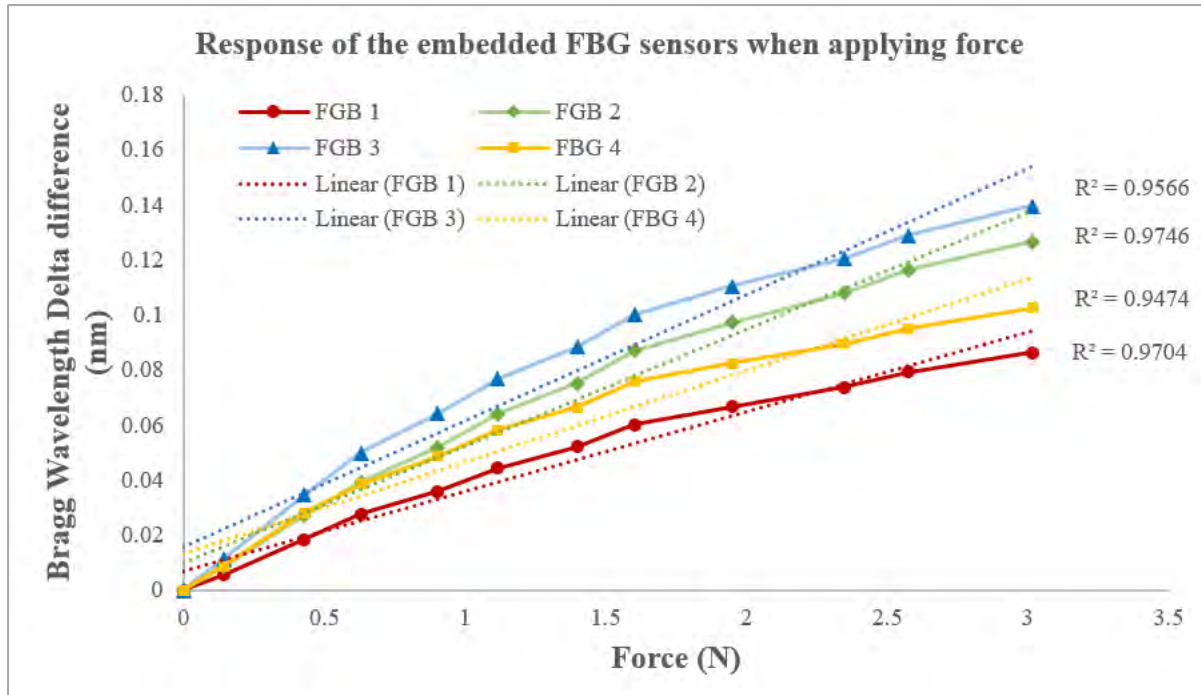
To compensate for the shortcomings of the Pliance®-X sensor, the smart textile was designed to measure the force on a soft elastic surface, such as human skin. All of the data were collected on soft artificial skin (with a Young's modulus of 0.0768 MPa), and the detected force was measured by using a force gauge. When the force applied ranged from 0 N to 10 N, all of the linearities between the peak-shifted Bragg wavelengths and forces of FBG sensors 1 to 4 showed a highly positive correlation, with an  $R^2$  of 0.90–0.92. When the scale of the force was 3 N, the  $R^2$  value was 0.95–0.97 (Figure 5.9), which approximates that of the Pliance®-X sensor when tested on soft material ( $R^2 = 0.9971$ ) (Figure 5.8(b)). Moreover, the FBG sensors have an intraclass correlation coefficient (ICC) of 0.97, which means that the smart textile is highly reliable when tested on a soft surface. Substituting the Bragg wavelength delta difference (y) into the equation, the corresponding force (x) within 3 N can be found as follows.

$$\text{FBG 1: } y = 0.0289x + 0.0070 \quad (5.9)$$

$$\text{FBG 2: } y = 0.0424x + 0.0099 \quad (5.10)$$

$$\text{FBG 3: } y = 0.0458x + 0.0157 \quad (5.11)$$

$$\text{FBG 4: } y = 0.0334x + 0.0131 \quad (5.12)$$



**Figure 5.9** Linear regression between Bragg wavelength delta difference and force when applying force to silicone-embedded FBG sensors 1 to 4.

### 5.3.4 Challenges of conventional integration methods

Besides their sensing abilities, compatibility between sensors and textiles may be the key to the success of smart textiles, because this factor greatly affects the final performance factors, such as flexibility and wear comfort. There are five main methods of integrating fibre optic sensors into textiles, namely, adhering; sewing; embroidering; embedding; and inserting (e.g., weaving and knitting) them (Lee et al., 2022). In the first generation of smart textiles that used fibre optic sensors, the sensing components were adhered and sewn onto the textile surface. Due to the simplicity of this method, the sensing component could be easily detached, which worked well for ongoing maintenance and laundering. For example, Grillet et al. (2008) sewed and glued fibre optic sensors onto elastic bandages in a curvilinear layout and applied them to the abdomen region to monitor respiratory movement during MRI. However, the protruding sensors may affect the aesthetics of the product.

The second generation of smart textiles used fibre optic sensors as textile yarn, i.e., the sensors were embroidered onto the textile surface, or woven, and knitted into the fabric. Similar to sewing, embroidering fixes the fibre optic sensors onto the fabric surface, but no sewing thread is used. This is because the fibre optic sensors can be directly used as thread and bent into a specific shape. For instance, Quandt et al. (2017) embroidered two rows of fibre optic sensors on a bed sheet in continuous loops to monitor heartbeat and blood flow for examining wound healing and preventing decubitus ulcers. However, the excessive bending of these fibres may affect signal transmission and even break the optical fibres. Inserting optical fibres into a textile structure seems to be a more effective solution, because the sensors are fully hidden in the fabric while maintaining high functionality. However, this method could be time-consuming, because the fabric structure and material properties must be considered before inserting the sensors. For example, Rothmaier et al. (2008) inserted a polymer fibre optic sensor into woven fabric with a twill structure to measure the applied compression forces. One of the most important factors may be the strength of the optical fibres, because they are subjected to a high degree of tension during the weaving process. Weak fibres may break or deform easily, and thus, lose their sensing ability. Knitting is an effective choice if elastic textiles are required, and the fibre optic sensors can be used in a similar manner to inlaid yarn, i.e., they can be laid straight between the front and back knit loops. Koyama et al. (2017) inserted silk-covered FBG sensors into a knitted wristband to monitor blood pressure. Although the silk-covered optical fibres contributed to the softness of the wristband, its elasticity could have been degraded, as the optical fibres have low stretchability.

The third generation of smart textiles focused on enhancing their flexibility. One of the common methods of embedding fibre optic sensors into polymer substrates is to bend them into curved lines. Not only can this protect the sensors, but they are also made more robust and compatible with the skin (Guo et al., 2019; Presti et al., 2019). For instance, Guo et al. (2019)

developed an ultra-flexible skin-like FBG strain sensor by embedding curvilinear FBG sensors into a thin PDMS membrane, and then, attaching the membrane onto kneepads and gloves. As these items are lightweight and flexible, they do not inhibit mobility, which is useful for measuring movement. Furthermore, Leal-Junior et al. (2019) developed a 3D-printed insole by embedding 15 macro-bending sensors into an insole in a curvilinear shape which was used to monitor plantar pressure and gait movement. Although the disadvantage of embedding is the increased bulkiness of the smart textile, this method is ideal for creating smart textiles that are subjected to compression forces due to its robustness to higher compression forces.

The novel method in this study for fabricating a force-sensing smart textile combines the advantages of the inlay and embedding techniques. The inlay approach fully conceals the fine optical fibres in the smart textile while maintaining the wear comfort of the material. Additionally, inserting optical fibres manually ensures that the FBG sensors are not overly stretched and prevents breakage during the manufacturing process. Moreover, the location of the FBG sensors could be determined without complicated calculations, therefore ensuring time-efficiency. Additionally, embedding FBG sensors into silicone membranes with a curvilinear shape enhances their flexibility, provides extra protection, and improves compatibility while maintaining sensitivity to force. However, the rigidity of optical fibres and textile yarn varies, so their integration would affect the softness and elasticity of the knitted undergarment to different extents.

#### **5.4. Limitations of experiment**

Several limitations of the current study are listed as follows. The results obtained by using a soft surface show that the smart textile in this study has less robustness than when a hard surface is used due to a cushioning effect, which indicates that the energy is absorbed. For example, the reliability of the Pliance<sup>®</sup>-X pressure sensor was assessed in Wiseman et al. (2018), who

reported an ICC of 0.998 on a hard surface, and an ICC of 0.87 on children's skin. This implies that the softness of the tested material may affect the reliability of sensors. In this project, the artificial skin is as soft and elastic as a human torso, so the energy is also absorbed. Although a force of 0.5 N is applied every 5 s to the smart textile and the Pliance<sup>®</sup>-X pressure sensor, the mean detected forces are approximately 0.45 N and 0.2 N, respectively. Therefore, the embedded FBG sensors require a longer time than the bare FBG sensors to reach 10 N (120 s and 105 s, respectively). Nevertheless, their sensitivity to force is not greatly affected. For example, the Bragg wavelength delta difference of the embedded and bare FBG sensors at 1552 nm is 0.221 nm and 0.253 nm, respectively. The overall results indicate that the bare FBG sensors have higher sensitivity to force but tend to become more stable and linear when embedded in silicone membranes.

Besides the deformation caused by applied force, the shifted Bragg wavelength is also affected by temperature. To minimise the error caused by body temperature, polarisation-maintaining fibres could be used to discriminate strain and temperature, for example, using highly birefringent FBG (Guo et al., 2020) and polarisation Brillouin reflectometry method (Barkov et al., 2020). Furthermore, the shifted Bragg wavelength could be affected by the deformation of the FBG sensors, as well as the temperature. The long tail of the optical fibre that is connected to the heavy sensing interrogator (Micron Optics SM130) may affect the wearability of the smart textile, so AIS subjects should wear these with caution. Developing a mini-interrogator would be the next step in enhancing the wearability of this smart textile, making it portable and more user-friendly.

## 5.5. Summary

A novel method for manufacturing a force-sensing smart textile by inlaying FBG sensors into a knitted structure along the warp direction and embedding FBG sensors into silicone membranes is discussed in this chapter. The results show that the silicone-embedded FBG sensors are more stable and linear than the bare FBG sensors when force is applied. Not only is the sensor flexibility enhanced, but the embedded FBG sensors eliminate the tendency of the sensor to shift, and enhance compressional susceptibility and accuracy. When the range of the force is 0–10 N, the linearity ( $R^2$ ) between the Bragg wavelengths and forces is above 0.90. However, the  $R^2$  ( $>0.95$ ) value is even higher when it is reduced to 3 N, which is comparable to the Pliance<sup>®</sup>-X sensor when evaluating a soft material. Furthermore, the FBG sensors have an ICC of 0.97, thus indicating that the smart fabric is highly reliable when evaluated on a soft surface. Since no consensus has been reached on the optimal bracing pressure, smart textiles could serve as a useful tool for tracking the forces exerted by a brace during the fitting process. Smart textiles could make the process of adjusting the brace simpler and more scientific for orthotists. The results can also be used to establish optimal bracing pressure levels, thus preventing AIS patients from having to endure excessive pressure, while maintaining an appropriate amount of bracing force in order to halt the progression of spinal curvature and reduce the risk of pressure-related injuries.

## **CHAPTER 6 DESIGN AND DEVELOPMENT OF SOFT MANNEQUIN**

### **6.1 Introduction**

Soft mannequins have been often used as substitutes for a human body for interface pressure measurements in experiments as it is more efficient, there is no risk of potential injury, and it is ethical because human subjects are not involved. Nevertheless, the accuracy of interface pressure readings of compression textiles can be significantly affected by the use of different types of soft mannequins and measurement devices to determine the interface pressure (Li et al., 2022). Consequently, an acceptable soft mannequin should have softness and flexibility comparable to those of the human body, and the sensors should be highly reliable. Several soft mannequins have been developed, but it appears that none of these models are specifically created to measure the pressure of braces on individuals with abnormal spinal curvature. Although these mannequins may have been useful in other areas of research, the lack of a specific model makes it challenging to accurately assess the pressure exerted by braces on individuals with spinal deformities. This highlights the need for the development of specific mannequins that can accurately simulate the abnormal curvature of the spine and body.

Among the different kinds of mannequins that have been used to measure the pressure of braces, one of the more well-known soft mannequins is developed in Yu et al. (2004), who used the mannequin for garment pressure testing. The mannequin is made of glass fibres, polyurethane (PU) foam, and silicone rubber to replicate the human bones, muscle tissues, and skin. Although the soft mannequin has a flexible means of support that can be used to simulate the spinal column, the skeleton and body contours of this soft mannequin do not apply to scoliotic cases. In view of this, Chan (2019) developed a soft mannequin for AIS with a thoracolumbar/lumbar spine to predict bracing effectiveness when the subject is wearing a posture correction girdle. The experimental results showed a similar performance as real-life



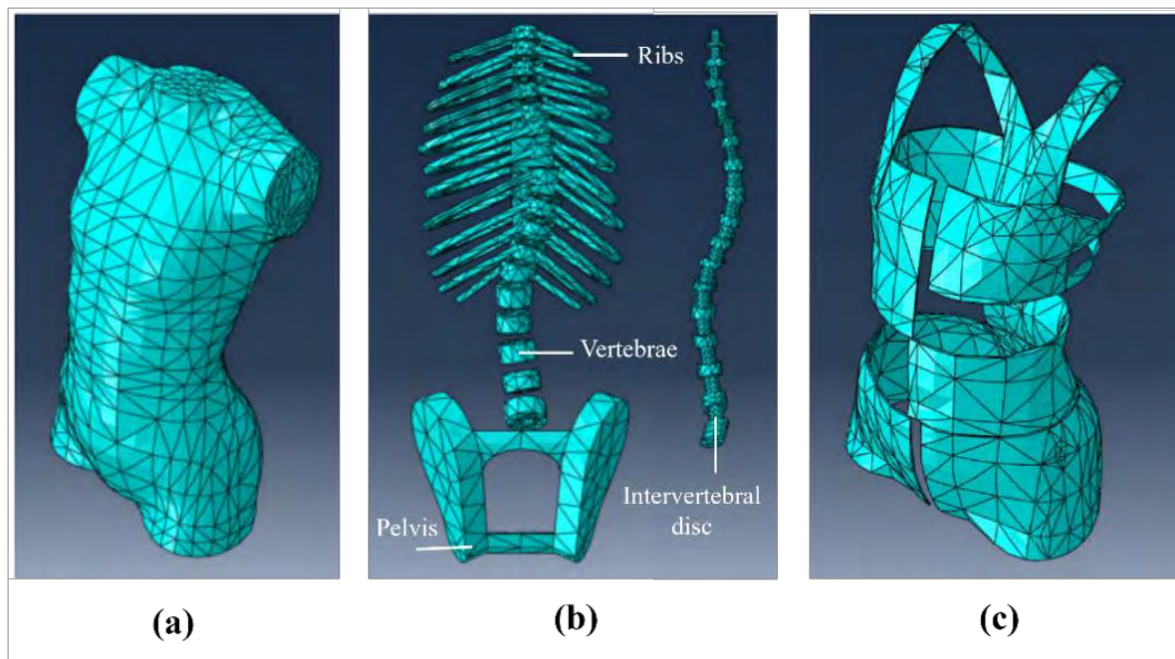
subjects. Unlike the soft mannequin in Yu et al. (2004), that in Chan (2019) used Ecoflex™ 0010 silicone for both the muscle tissues and skin. Additionally, the spine was further divided into vertebrae and intervertebral discs, which were 3D printed with polylactic acid (PLA) filament and composite material (Vero White and Tango printing materials), respectively. To clearly visualise the spinal movement with the girdle donned, each 3D printed vertebra was embedded with an LED light bulb at the centre. Therefore, the spinal curvature of the soft mannequin with AIS could be easily compared to the X-ray images of the subjects. However, both soft mannequins do not incorporate the thoracic spine and rib cage, which could potentially influence how the spine responds to pressure from the brace. Moreover, the mannequin in Chan (2019) appears to be quite costly and heavy, owing to the use of 22 lbs of silicone for one-third of the torso.

Therefore, this project proposes a soft mannequin that more closely resembles the torso of an AIS patient, including a full spine, muscle tissues, ribs, and skin. To achieve this, a previously validated FE model proposed by Fok (2020) is used as a reference to construct a geometrically identical soft mannequin as the torso of an AIS patient. Pressure measurement is then conducted to repeat the work in Fok (2020) and validate her clinical data of a female subject with AIS when using the FIA. This means that the same measurement system, amount of applied pressure, and FIA are used on the proposed mannequin. To evaluate its performance, the spinal curvature of the proposed mannequin is compared to radiographic images captured while a female subject with AIS is wearing the FIA.

## 6.2 Methodology

### 6.2.1 Construction of the proposed mannequin

The development of the proposed mannequin was based on an FE model developed by Fok (2020). A 12-year-old female with AIS characterised by an S-curve and a Risser grade of 2 was recruited in Fok (2020) to build the FE model, which included the models of the torso, skeletal structure, and FIA as well as their mechanical properties (Figure 6.1).

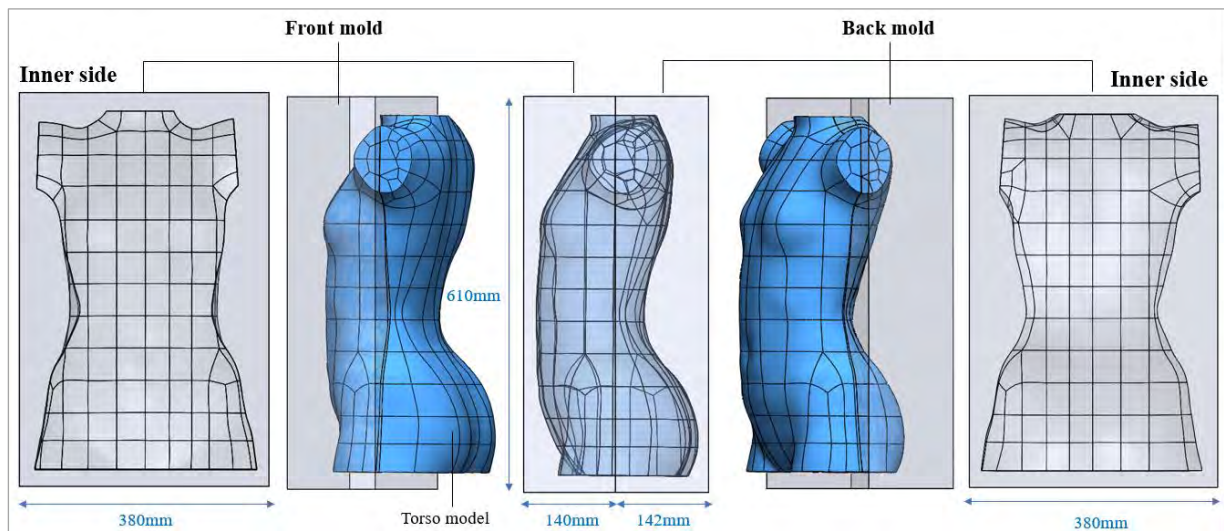


**Figure 6. 1** Meshed models of (a) torso, (b) skeletal structure, and (c) FIA (Fok, 2020).

#### 6.2.1.1 Skin

The surface contour of the proposed mannequin was designed to be geometrically equivalent (1:1) to the FE modelled torso (Figure 6.1(a)). The FE modelled torso was created based on 3D images of a female AIS patient, who was scanned with the Virtus Smart XXL 3D body scanner (Human Solution GmbH, Germany). For creating the moulds, the contours of the torso model were precisely extracted and transferred to the moulds by using Solidworks 2018 (64 Edition). As shown in Figure 6.2., the FE modelled torso and the 3D printed mould are seamlessly

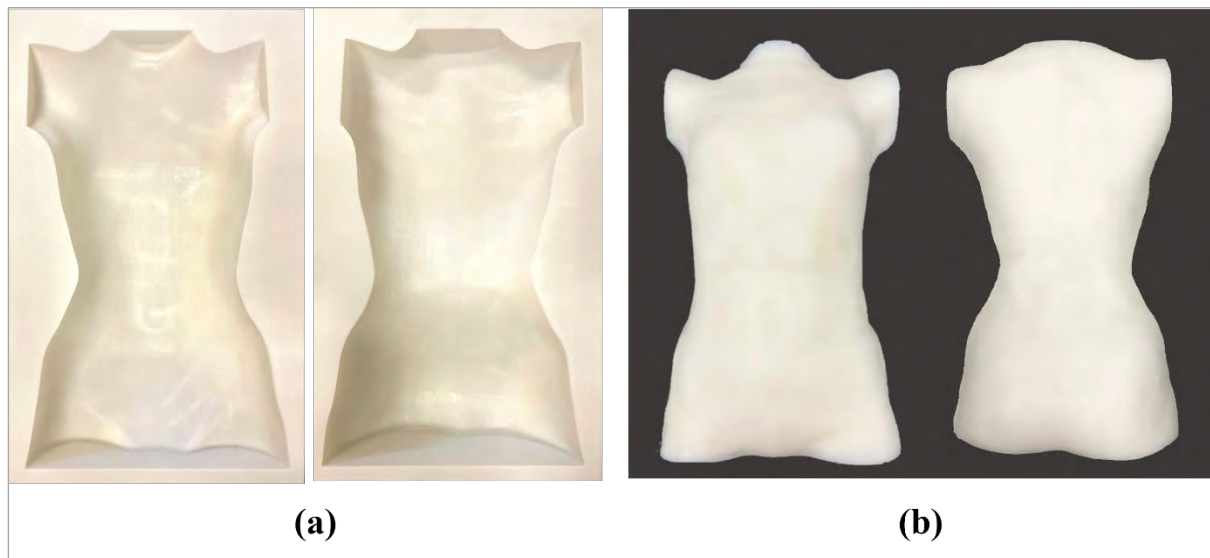
assembled. In addition, separate moulds are utilised to simplify the moulding process. The dimensions of the front and back moulds are 610 x 380 x 140 mm and 610 x 380 x 142 mm, respectively. To ensure congruity between the proposed mannequin and the FE modelled torso, the construction of the moulds was 3D printed.



**Figure 6. 2** FE modelled torso and 3D moulds for the torso.

Then, resin-based 3D printing (material with a Shore D hardness of 79) was used to construct the moulds for a high precision and a smooth surface finishing. The resulting 3D printed moulds are identical to the FE modelled torso (Figure 6.3(a)). The soft mannequin in Chan (2019) was also constructed by moulding but is relatively rigid because both the skin and muscle tissues are made of silicone. Therefore, silicone rubber is only used in this study to construct the skin to ensure optimal softness of the skin, while the muscles are made of flexible polyurethane (PU) and silicone foam. Dragon Skin™ 10 Very Fast Platinum Silicone was used for the skin material because it is elastic, soft, and quick-drying (within 30 minutes). Its superior performance is particularly suitable for creating a thin and uniform layer of soft material on curved surfaces due to its lower fluidity compared to commonly used silicone. To

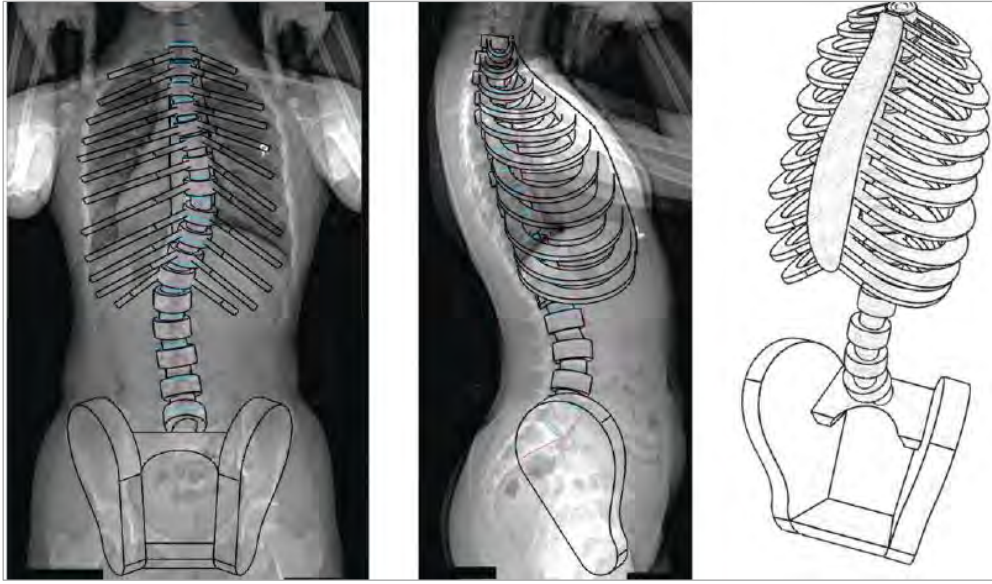
enhance the softness of the skin, Ecoflex™ 0010 Platinum Silicone was used as the second layer of skin. Figure 6.3(b)) shows the moulded skin, which is soft and smooth.



**Figure 6. 3 (a)** 3D printed moulds of skin and muscle tissues, and **(b)** moulded skin.

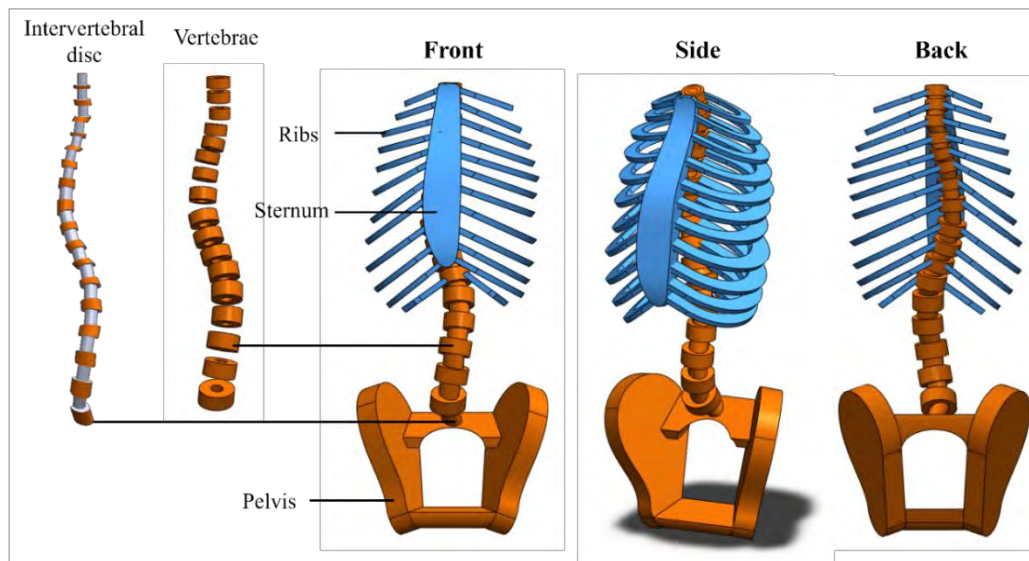
#### 6.2.1.2 Skeletal construction

To create a more realistic soft mannequin for AIS, the pelvis, ribs, sternum, intervertebral discs, and vertebrae from thoracic (T1 to T12) to lumbar (L1 to L5) were included in the model. The skeletal construction was based on Fok (2020) (Figure 6.1(b)). The model was developed by using bi-planar X-ray images of a female AIS patient with a Cobb's angle of  $25.3^\circ$  (T5 to T11) and  $21.8^\circ$  (T11 to L3), and a Risser grade of 2, which indicate that her skeletal bones are still soft enough to be modified by bracing. Figure 6.4 shows the construction of the FE skeletal model based on X-ray images of the back and side views (Fok, 2020).



**Figure 6. 4** FE skeletal model based on x-rays of back and side views (Fok, 2020).

Although the skeletal model is simplified due to the extremely long calculation time in the numerical simulation process, an FE analysis has validated its ability to exert a similar spinal corrective effect as that of the human body (Fok, 2020). To enhance the assembly process, the intervertebral discs, ribs, sternum, and vertebrae were modified to accommodate each other. The modified skeletal structure of the proposed mannequin is illustrated in Figure 6.5.

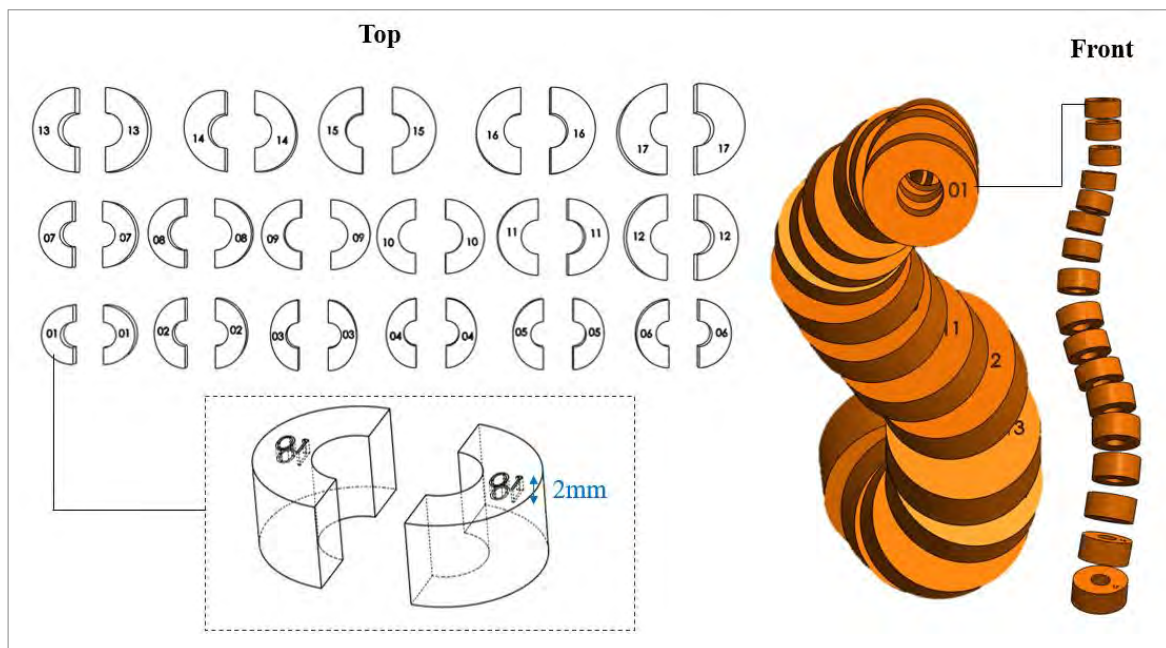


**Figure 6. 5** Skeletal construction of the proposed mannequin.

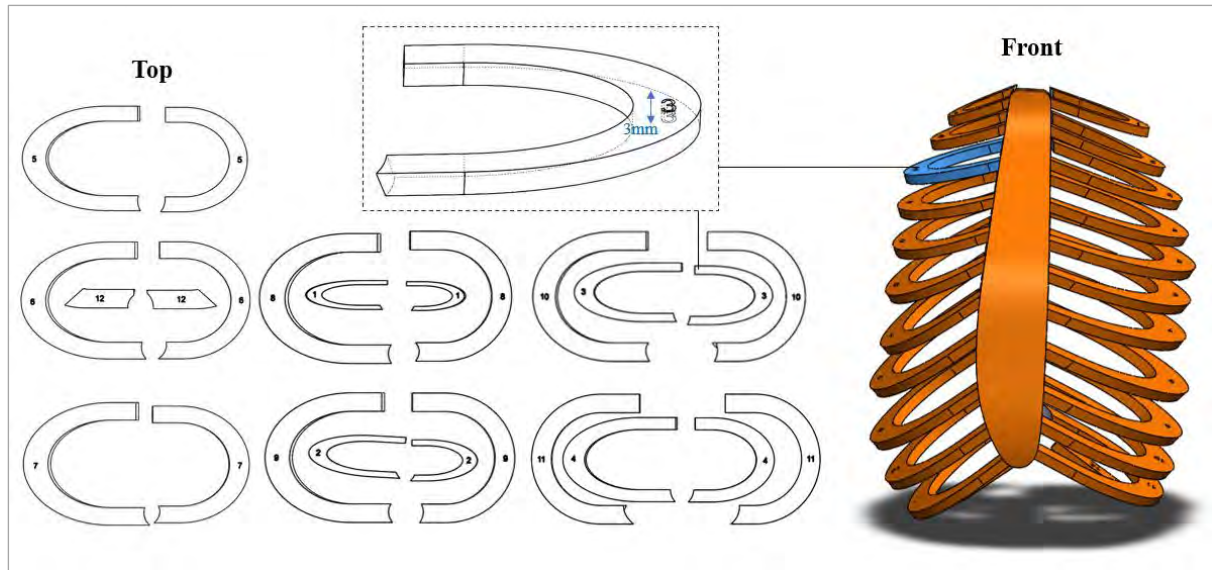


#### 6.2.1.2.1 Vertebrae, ribs, and pelvis

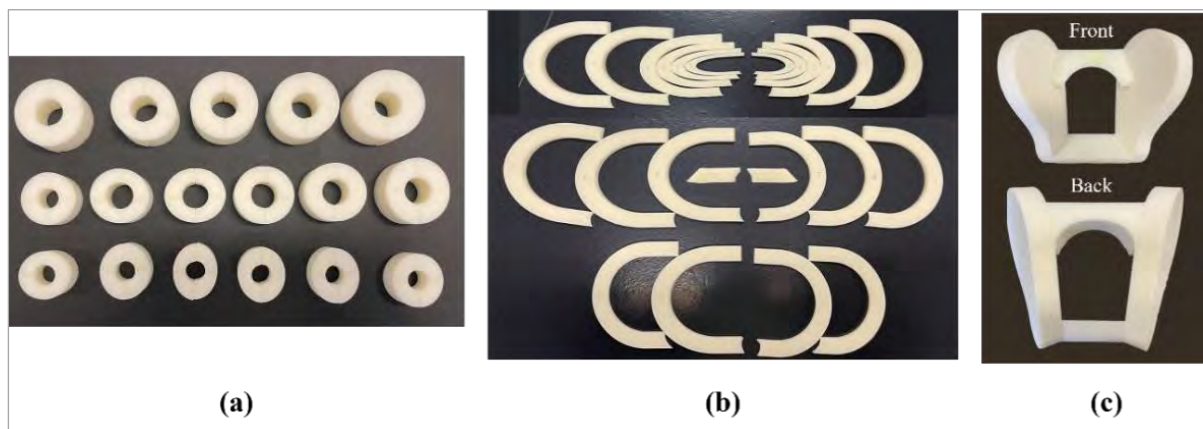
In total, there were 17 vertebrae and 24 ribs, and each vertebrae was segmented into two parts to facilitate better integration with the intervertebral disc model. Additionally, all parts of the vertebrae and ribs were labelled with a specific number for ease of recognition and matching with the corresponding parts (Figures 6.6 and 6.7). Then, the vertebrae, ribs, and pelvis were 3D printed with resin (Shore D hardness of 79), and their surface was polished for smoothness (Figure 6.8).



**Figure 6. 6** Segmented vertebrae for 3D printing.



**Figure 6. 7 Ribs for 3D printing.**

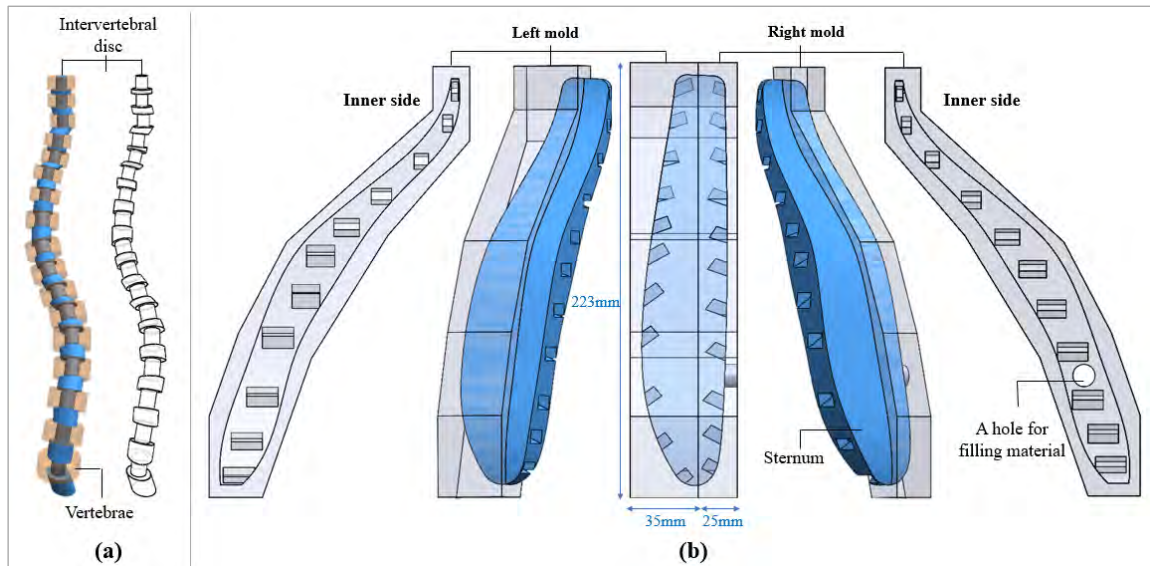


**Figure 6. 8 (a) 3D printed vertebrae, (b) ribs, and (c) pelvis.**

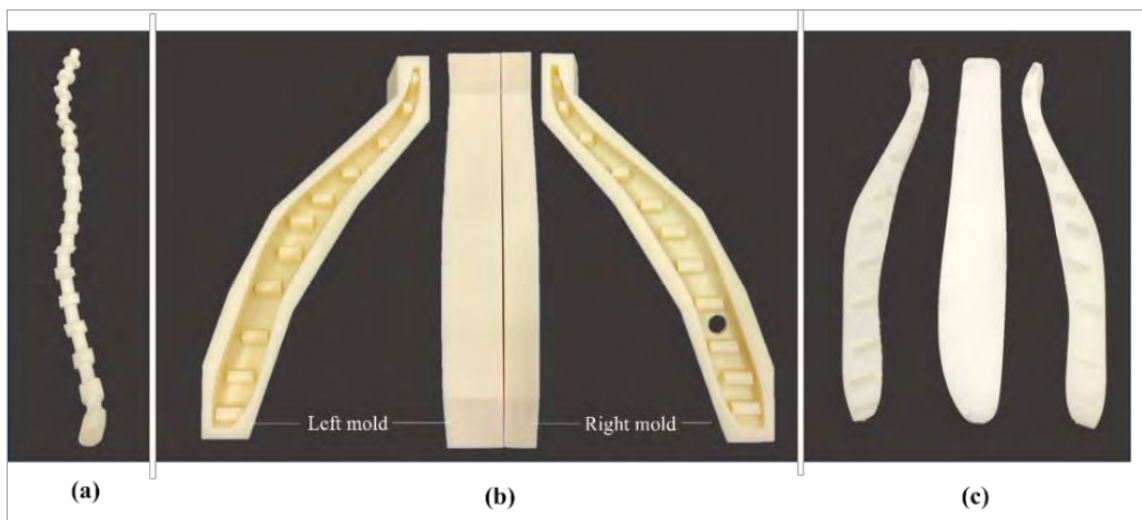
#### **6.2.1.2.2 Intervertebral discs and sternum**

To ensure that the flexibility of the proposed mannequin would resemble the skeletal bones of AIS patients, softer materials were used for the intervertebral discs and sternum. The intervertebral disc was 3D printed with Hei-Cast 8400 (Shore A hardness of 40), and this hardness had been previously validated to have similar flexibility to that of a human intervertebral disc (Chan, 2019) (Figure 6.9(a)). On the other hand, the sternum was moulded with Dragon Skin™ 10 NV Platinum Silicone (Figure 6.9(b)). The softness and flexibility of

the materials allow for the spine and ribs to shift along the spinal column in response to the pressure exerted by a brace, thereby facilitating spinal correction. Figure 6.10 shows the 3D printed intervertebral disc and mould for the sternum, and the moulded sternum.



**Figure 6. 9 (a) Intervertebral disc, and (b) moulds for sternum for 3D printing.**

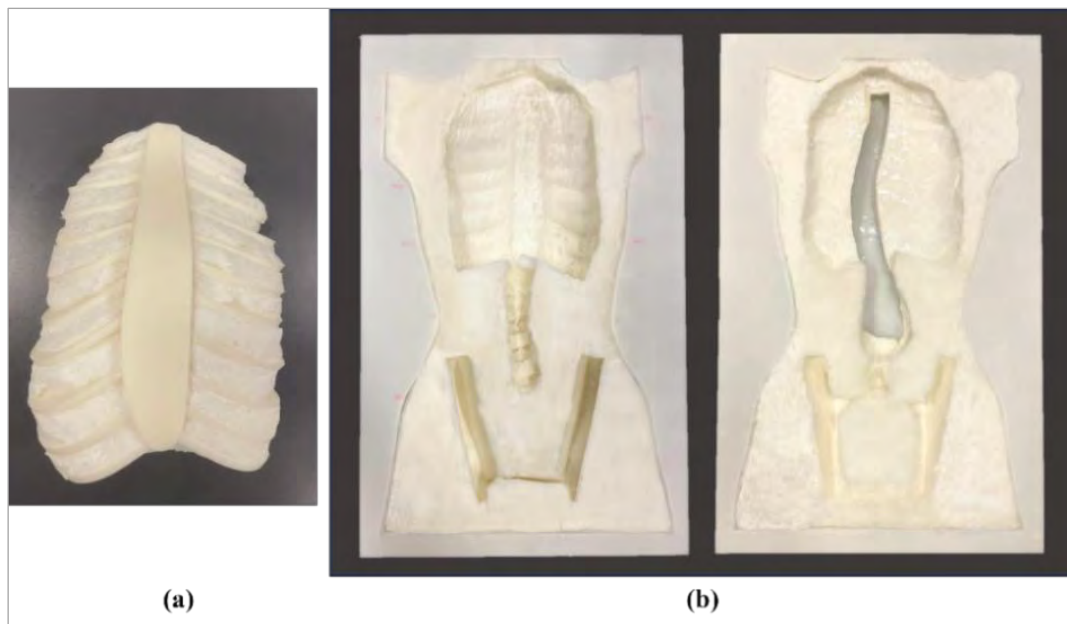


**Figure 6. 10 (a) 3D printed intervertebral disc, (b) the 3D printed mould for the sternum, and (c) the moulded sternum.**



### 6.2.1.3 Muscle tissues

The muscle tissues were composed of Soma Foama™ 15, and Flexible Polyurethane Foam 905 that is produced by Beijing Hai Bei Si Technology Limited Company. The Soma Foama™ 15, being softer in nature, was utilised for the softer regions such as the abdomen, breasts, and hips. Additionally, the rib cage was filled with Soma Foama™ 15 to ensure flexibility for bending purposes (Figure 6.11(a)). Following the precise placement of the rib cage, spine, and pelvis, the moulds were then carefully filled with foam, which formed the moulded muscles (Figure 6.11(b)). To facilitate the observation of spinal movement, an incision was made in the spine area.

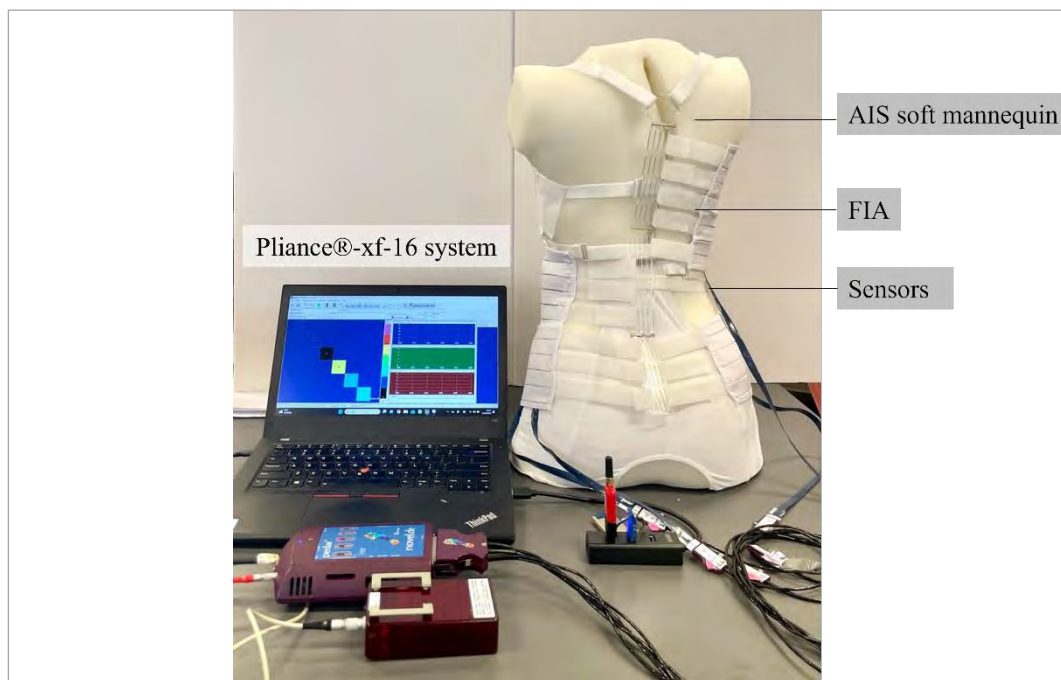


**Figure 6. 11 (a) Rib cage with filled foam, and (b) the moulded muscle.**

### 6.2.2 Validation of the proposed mannequin

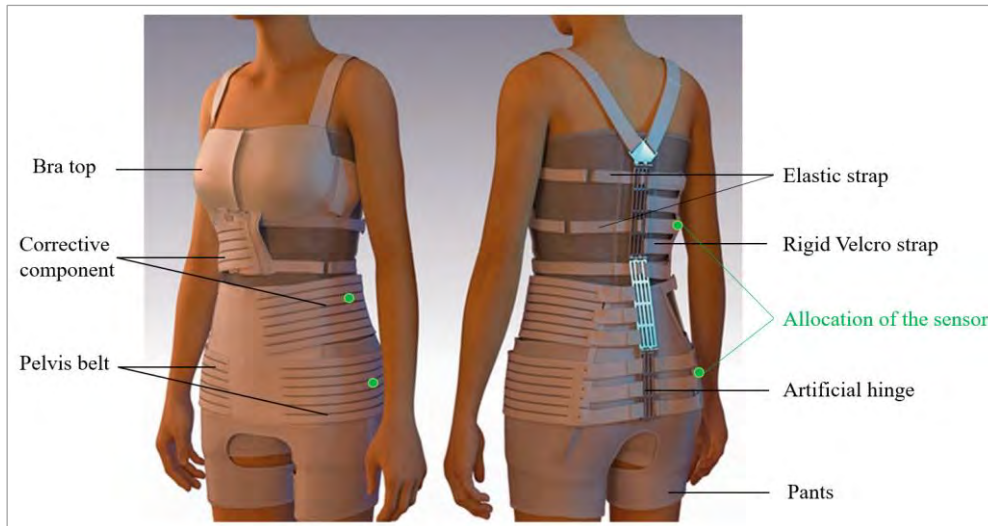
The objective of constructing the proposed mannequin in this study is to serve as a prototype of the human body for brace pressure measurements. Consequently, it is important to validate the ability of this mannequin to exert the same corrective effect on the spine as observed in human subjects when subjected to the same compression pressure conditions. To replicate the

clinical pressure measurement conducted by Fok (2020), the same measurement system, namely the Pliance®-xf-16 system with 3x3 socket sensors, and FIA, was employed on the proposed mannequin. However, to facilitate visual observation of the spinal changes, the hinged bones were replaced with a transparent material. Figure 6.12 shows the equipment setup of the experiment. The FIA is donned on the soft mannequin, and four sensors are fixed in between the soft mannequin and FIA.



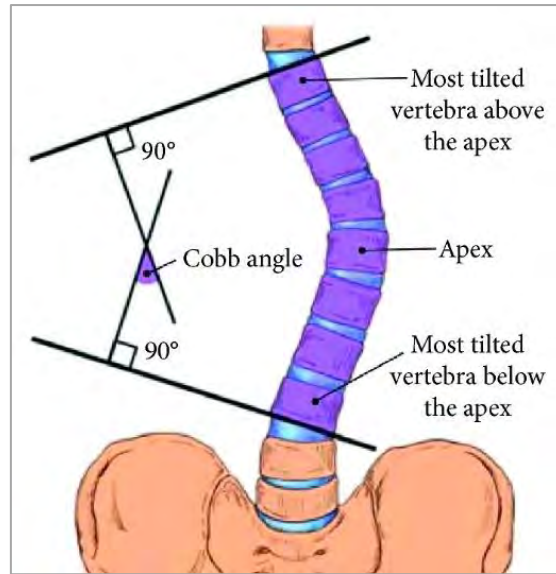
**Figure 6. 12** Equipment setup of the experiment.

The measurements were taken along the middle axillary line at the under-bust, waist, and pelvis levels, with interface pressure recorded at least once per minute. This means that the interface pressure was exerted by the FIA on the AIS subject at the thoracic and lumbar pad regions and left and right pelvis (Figure 6.13). The pressure ranged from 1.8 kPa to 24.4 kPa, and this range is comparable to that of a standard Boston brace, which exerts pressure between 10 kPa and 30 kPa (Mac-Thiong et al., 2004).



**Figure 6. 13** FIA design and placement of sensors (Fok et al., 2021).

Upon the correct application of the FIA and the specified pressure, the spinal curvature was recorded. Then, the correlation coefficient between the spinal curvature as depicted on the mannequin and that on the X-ray images was calculated, which provided an objective assessment of the mannequin's ability to accurately mimic the spinal curvature seen in the X-ray images. Moreover, the Cobb's angles on the proposed mannequin and X-ray images were measured by Solidworks 2018 (64 Edition) and RadiAnt DICOM Viewer (64-bit). The process of measuring the Cobb angle includes the estimation of the angle formed by the two tangents drawn on the upper and lower endplates of the most tilted upper and lower end vertebrae (Hornig et. al., 2019) (Figure 6.14). These assessments are crucial in determining the effectiveness of the FIA and its potential for use in clinical settings.

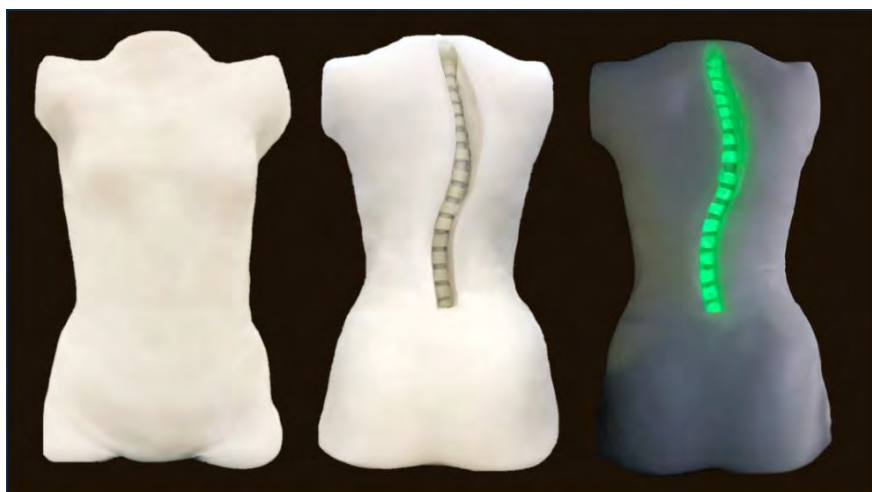


**Figure 6. 14** Cobb's angle measurement method (Horng et. al., 2019)

## 6.3 Result and Discussion

### 6.3.1 Body contour of proposed mannequin

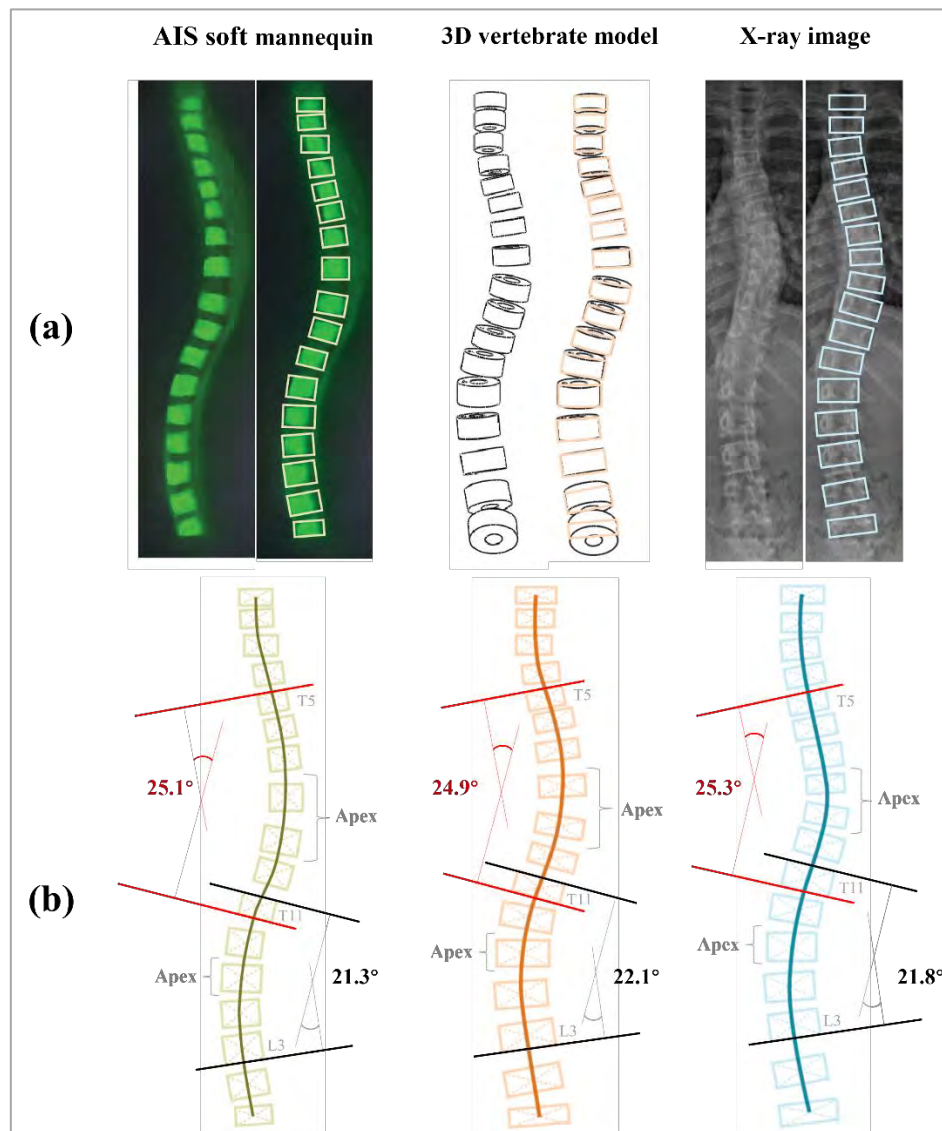
The assembled mannequin in this study has body contours that closely resemble those of the FE modelled torso. To visualise the instant effects of spinal correction, the back of the mannequin is deliberately cut open, and the vertebrae are coated with fluorescent pigment. As a result, the spinal curvature becomes visible in the dark, as shown in Figure 6.15.



**Figure 6. 15** Back of mannequin cut open with fluorescent pigment.

### 6.3.2 Spinal curvature of proposed mannequin

In addition to closely resembling the contours of the FE modelled torso, it has been observed that the Cobb's angle and spinal curvature of the assembled mannequin also closely match those of the 3D vertebrate model and the X-ray image of the AIS subject. In Figure 6.16 (a), rectangles are used to represent the position of the vertebrae. After identifying the centre point of the vertebrae, the spinal curvature and Cobb's angles are depicted in Figure 6.16 (b).

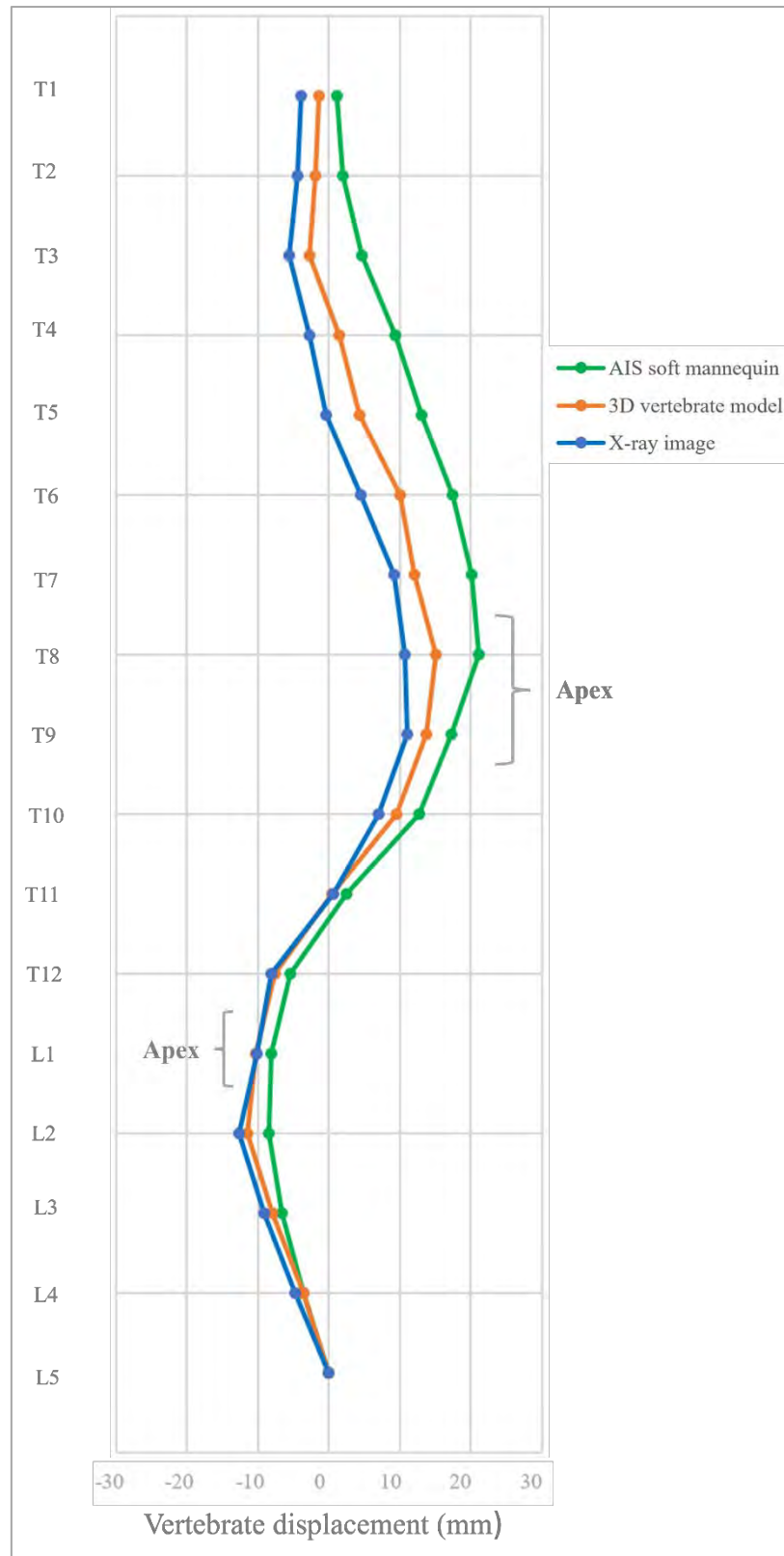


*\*Note: Cobb's angles depicted in the graph are not drawn to scale.*

**Figure 6. 16 (a)** Vertebrae position, and **(b)** comparison of initial spinal curves and Cobb's angles on AIS soft mannequin, 3D vertebrate model, and X-ray image.

For thoracic region, all the apexes of the angles are located at T8 to T9, and they have similar Cobb's angles, which range from approximately  $25^{\circ}$  at T5 to T11. However, a major difference arises in the lumbar region, with the proposed mannequin showing a difference of  $-0.8^{\circ}$  and  $-0.5^{\circ}$  compared to the 3D vertebrate model and X-ray images, respectively. This variance may be attributed to the fact that T12 to L5 rely on the support provided by the flexible foam. This may result in displacement due to gravitational forces when assuming an upright posture. On the other hand, the rib cage plays a crucial role in stabilising the positioning of the vertebrae from T1 to T11. As a result, the proposed mannequin exhibits a thoracic curve that is nearly identical to that of the 3D vertebrate model and X-ray image.

Furthermore, to facilitate a more comprehensive comparison of the spinal curves, each vertebral position is represented on a graph by measuring the horizontal distance between the vertebral body and the CSVL as shown in Figure 6.17. The results indicate a close proximity between the plotted positions.



**Figure 6. 17** Graphical comparison of spinal curves.

### 6.3.3 Pressure test on proposed mannequin

During the pressure test, the FIA was adjusted until the pressure reached the required pressure at the thoracic, lumbar pad areas, and left and right pelvis. Table 6.1 compares the interface pressure when FIA is donned on the proposed mannequin and AIS body. The results indicate that the proposed mannequin exhibits a pressure pattern similar to that of the human torso, whereas the subject generates considerably higher pressure readings except for the left pelvis. This may be because the pelvis of the proposed mannequin is softer than that of the human torso, so it absorbs a certain amount of energy.

**Table 6. 1** Interface pressure exerted by FIA on proposed mannequin and AIS subject.

	Sensor locations	Proposed mannequin	AIS body
<b>Interface pressure (kPa)</b>	Thoracic pad	24.1	24.4
	Lumbar pad	9.4	9.6
	Left pelvis	2.1	1.8
	Right pelvis	7.4	7.5

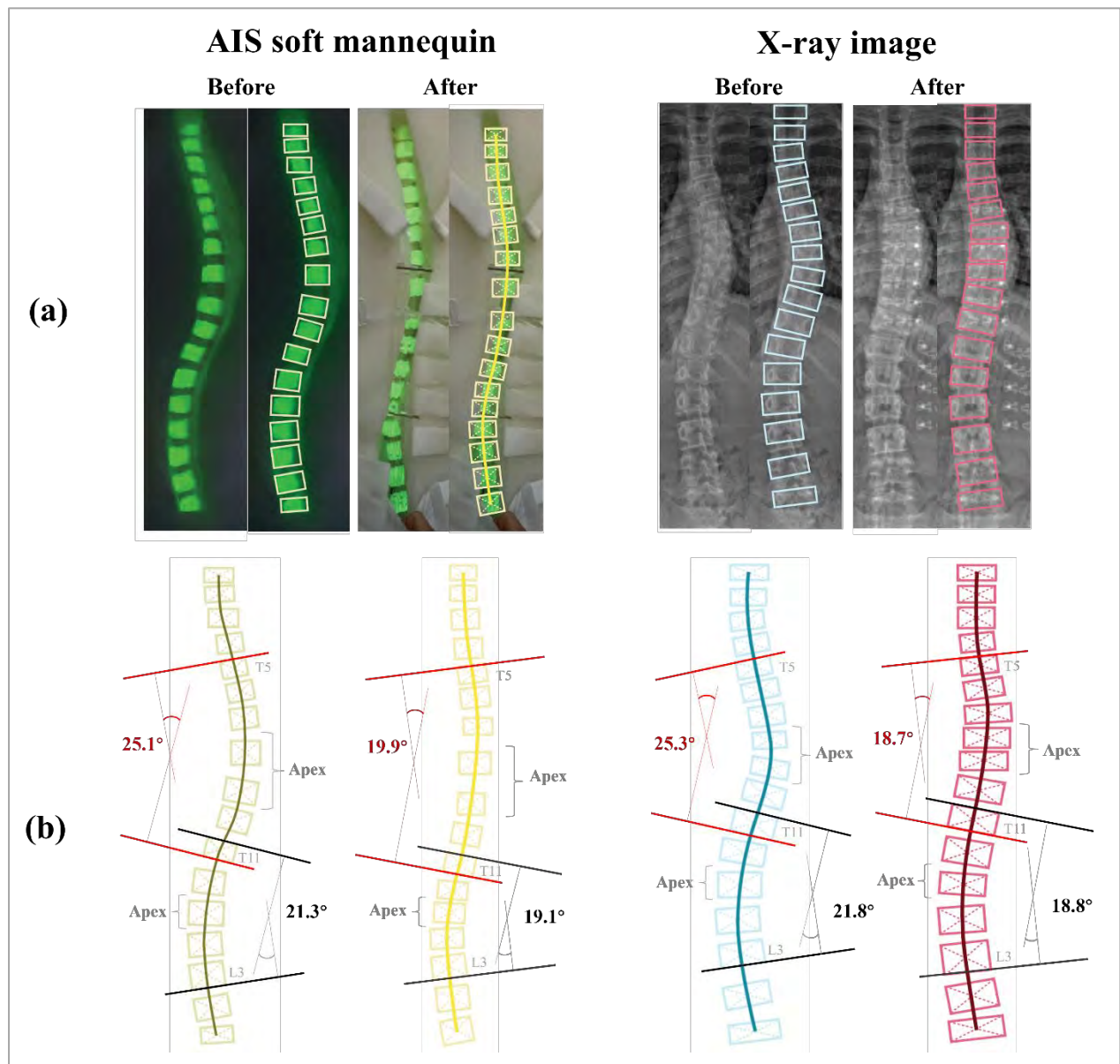
### 6.3.4 Spinal corrective effect on proposed mannequin

Upon adjusting the pressure to 1.8 kPa and 24.4 kPa, as per Fok (2020), a notable improvement in the spinal alignment of the proposed mannequin is observed. This corrective effect on the spine is comparable to the findings of a clinical trial under similar pressure conditions.

Figure 6.18 shows an obvious shift of the apex of the spine towards the concave sides after the intervention of the FIA, which means that T8 to T9 shift to the left, while L1 shifts to the right. Notably, upon comparing these findings with the X-ray images, a similar trend in spinal shift at the apex is found. To provide a more comprehensive visual comparison of the spinal corrective effect on the proposed mannequin and X-ray images, Figure 6.19 graphically illustrates the displacement of the vertebrae before and after the intervention of FIA. Furthermore, the correlation coefficient of 0.95 between the positions of the vertebral bodies

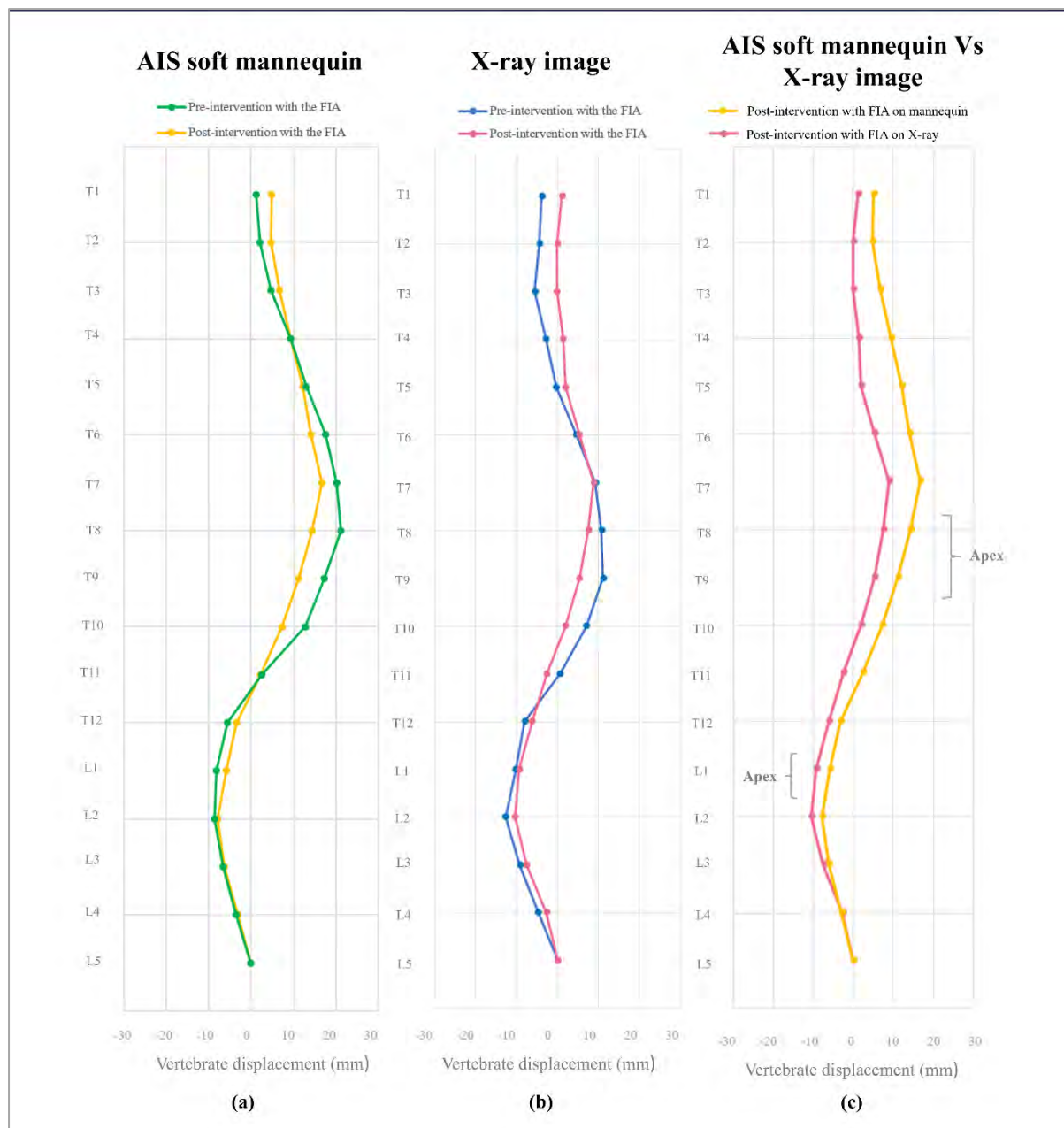


derived from the mannequin and those on the X-ray images suggests a high degree of similarity in their curvature and corrective effects.



*\*Note: Cobb's angles depicted in the graph are not drawn to scale.*

**Figure 6. 18 (a) Vertebrate position, and (b) comparison of spinal curves and Cobb's angles on AIS soft mannequin and X-ray images.**



**Figure 6. 19** Comparison of the spinal corrective effects.

However, it is important to note that the range of the observed shifts differs. Consequently, a thorough assessment of Cobb's angles is necessary to determine whether these shifts indeed correspond to similar spinal corrective effects.

Table 6.2 shows that both the thoracic region (T5 to T11) and the lumbar region (T11 to L3) of the proposed mannequin exhibit a reduction in their respective Cobb's angles, thus resulting

in a decrease of 5.2° and 2.2°, respectively. These findings closely align with the results obtained from a comparative analysis of the X-ray images pre- and post-intervention with the FIA, which reveals a reduction in Cobb's angles of 6.6° and 3° in the thoracic and lumbar regions, respectively.

**Table 6. 2** Comparison of Cobb's angle on proposed mannequin and X-ray before and after the intervention of FIA.

FIA intervention	Proposed mannequin		X-ray image	
	Before	After	Before	After
Cobb's angle at T5-T11 (°)	25.1	19.9	25.3	18.7
Cobb's angle at T11-L3 (°)	21.3	19.1	21.8	18.8
Apex	T8-9, L1	T8-9, L1	T8-9, L1	T8-9, L1

While there exists minor difference in the Cobb's angle, it is crucial to note that the proposed mannequin shows a comparable trend to that of humans. Hence, it can be assumed that the corrective effects observed in the proposed mannequin are comparable to those observed in humans. This finding establishes that the proposed mannequin can serve as a valuable reference tool for enhancing current understanding of spinal movement following bracing. Also, the proposed mannequin has the ability to yield results consistent with those obtained from human subjects.

#### 6.4 Challenges and Limitations

Constructing the proposed mannequin in this study which can exactly replicate the properties of a human is a challenging task, primarily due to the differential factors that influence their softness. Unlike the softness of human tissues, which arises from a combination of intrinsic factors, like the properties of the skin, subcutaneous tissues, muscles, and underlying structure, the softness of a mannequin primarily relies on the characteristics of the materials employed.

However, various factors can influence the overall softness of a mannequin, including the type and density of foam or silicone utilised, as well as the composition and formulation of the materials. To obtain a softer and more pliable texture, specialised foams or elastomers with lower stiffness or durometer ratings are often employed in the construction of soft mannequins. In the context of this study, silicone, silicone foam, and PU foam are selected as the materials to replicate the softness and flexibility observed in the AIS subject, owing to their popularity in creating skin-like texture and elasticity. Although the proposed mannequin exhibits a comparable spinal corrective trend to that of the human subject, its softness and flexibility may degrade over time. Consequently, the proposed mannequin may no longer produce results consistent with those obtained from human subjects. It is important to note that although it is possible to replicate the softness of human tissues in a mannequin, achieving an exact match is challenging due to the inherent complexities and instant nature of biological tissue.

## **6.5 Summary**

A proposed mannequin that closely resembles the torso of individuals with AIS is proposed in this chapter. This endeavour addresses a research gap where the lack of specialised mannequins has made it challenging to accurately assess the pressure exerted by braces on individuals with spinal deformities. The project utilises a previously validated FE model as a reference to construct a proposed mannequin that shares the same geometric features as an AIS torso, including a full spine, muscle tissues, rib cage, and skin.

The constructed mannequin matches the body contours, spinal curvature, and spinal corrective effect observed in the X-ray images of an AIS subject. When adjusting the pressure on the proposed mannequin according to the methodology used in Fok (2020), the results show that there is a significant improvement in the alignment of the spine. Also, this corrective effect closely resembles the outcomes observed in the clinical trial. Then, the performance of the

proposed mannequin is evaluated by comparing its spinal curvature to X-ray images of the AIS subject wearing the FIA. Both the X-ray images and the proposed mannequin show a reduction in the Cobb's angles in the thoracic (T5 to T11) and lumbar (T11 to L3) regions. While there is a difference in the Cobb's angle and spinal curvature between the proposed mannequin and the human subject, it is important to note that the mannequin shows a similar overall trend in corrective effect.

These findings establish the potential of the proposed mannequin as a valuable tool for studying spinal movement following brace application. The proposed mannequin can serve as a reference tool and provide insights consistent with those obtained from human subjects. The development of such a specialised mannequin represents a significant advancement in accurately assessing pressure from bracing for individuals with AIS and enhancing current understanding of the treatment outcomes of using a brace.

## CHAPTER 7 BIOMECHANICAL SIMULATION MODEL

### 7.1 Introduction

Examining how the spine responds to brace force necessitates a comprehensive and reliable methodology. While the conventional approach of recruiting human subjects offers direct insight, it is accompanied by significant time consumption and inherent risks due to the unknown effects of various forces applied to the human body. Additionally, conducting such studies requires multiple X-ray images, which can expose individuals to harmful radiation. As a result, researchers have been actively investigating alternative approaches, notably FEA, to study the spine response efficiently and safely.

FEA is a numerical method to address engineering and physical problems without repetitive experiments and wear trials (Chan, 2019; Fok, 2020). Due to its time-saving nature and ability to mitigate unexpected hazards to subjects, it is not surprising that FEA has gained widespread acceptance as an approach for evaluating the effectiveness of orthopedic devices and optimising their biomechanical designs (Yahyaiee et al., 2020). For instance, Chan (2019) utilised FEA to predict the effectiveness of a posture corrective girdle by inputting clinical pressure data. Similarly, Fok (2020) employed a similar method to predict the efficacy of FIA, and identified the optimal corrective force by applying different loading conditions to the FE models. In addition to correcting spinal deformities, Gignac et al. (2000) employed FEA to determine the optimal force for correcting rib cage deformities. Previous studies have demonstrated the potential of FEA in predicting the efficacy of bracing and determining the optimal force. However, it is crucial to note that the successful operation of FEA relies on the use of reliable sensors; otherwise, its feasibility may be compromised. Furthermore, it is essential to validate the outcomes derived from these simulations by comparing them with empirical data. One approach to validation is comparing the estimated corrective effects on the

spine obtained through FEA with actual observations from X-ray images. This validation step ensures the accuracy, reliability, and overall credibility of the simulated results, enhancing the robustness of the research findings.

Although Fok (2020)'s FE model has been validated to have a similar effect as the AIS subject, only two loading areas were used. It implies that the loading condition could not fully represent the pressure exerted by the brace. Therefore, this chapter is aimed to examine how the overall pressure distribution affects the spinal corrective effect based on Fok (2020)'s FE model. Besides adjusting the material properties to align with those of the proposed mannequin, the load condition of the new FE model was revised based on the pressure data obtained from the pressure monitoring undergarment when the FIA was worn on the proposed mannequin. After the FE model has been validated, it can provide more comprehensive data to determine the required optimal force. This not only helps to prevent physical injuries induced by excessive force, but also improves bracing compliance and success.

## **7.2 Methodology**

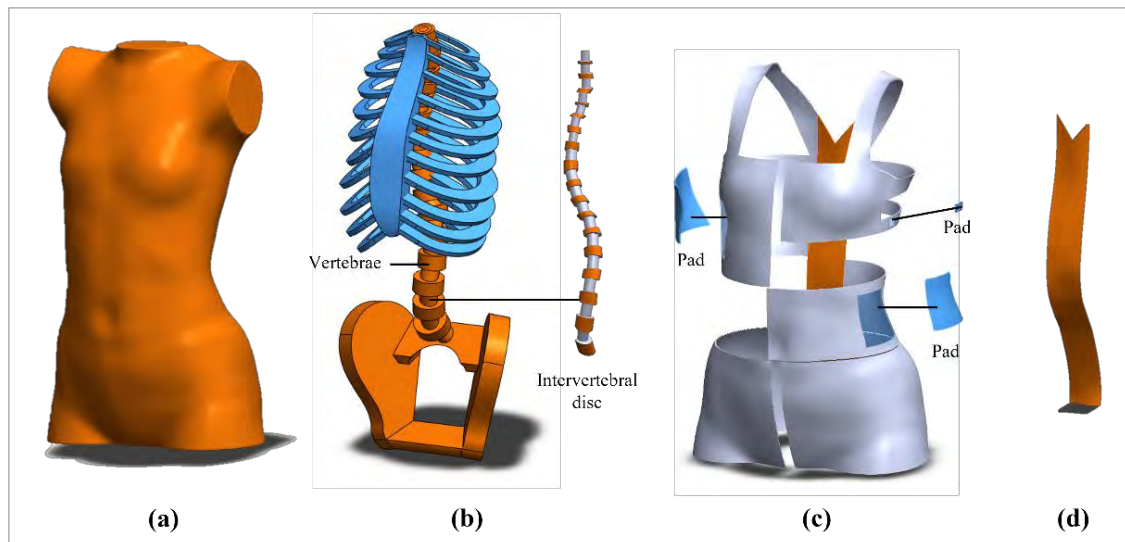
### **7.2.1 FE model construction**

In this study, the FE model was constructed by modelling three main components: the torso, skeletal structure, and FIA. These components were benchmarked against a validated FE model that Fok (2020) developed. The estimated Cobb's angles of the validated FE model were in close agreement with the actual measurements, indicating the effectiveness of the FIA (Fok & Yip, 2021). Table 7.1 shows the demographic data of the recruited AIS subject and the FE-estimated Cobb's angles obtained from the FEA developed by Fok (2020).

**Table 7. 1** Demographic data of the AIS subject and the FEA predicted Cobb's angle.

	Pre-intervention	Post-intervention	FE-estimation
Age	12	13	/
Weight (kg)	45.4	/	/
Height (cm)	150	/	/
Date of taken X-ray	12/2/2018	26/7/2018	/
Risser grade	2	2	/
Cobb's angle at T5-T11 (°)	25.3	18.7	20.8
Cobb's angle at T11-L3 (°)	21.8	18.8	19.4
Apex	T8-9, L1	T8-9, L1	T8-9, L1

To conduct the FEA, the first step is constructing geometric models, which include models of the torso, skeletal structure, textile, and hinge material of the FIA (Figure 7.1). The torso model was constructed according to the 3D body scanned AIS subject using Geomagic Studio 2012 (4-bit) and Solidworks 2018 (64 Edition). The model accurately represented the body contour, although the cross-sectional details were not included. Additionally, the FIA model was developed based on the 3D body images when the brace was worn, while the skeletal structure model was developed based on the X-ray images.



**Figure 7. 1** Models of (a) torso, (b) skeletal structure, (c) textile materials, and (d) hinge material of FIA.



Then, these constructed models were implemented into MSC Marc 2020 Edition, and their material properties were defined (Table 7.2). The determination of Young's modulus for the textile material was based on the results of stretch and recovery tests conducted using an Instron 4411 tensile strength tester (Fok & Yip, 2021). Additionally, the Poisson's ratio was obtained from a study by Zhou et al. (2010). These properties play a crucial role in accurately simulating the behaviour of the spine under various loading conditions. By incorporating these properties into the FE model, researchers can obtain more reliable and accurate results, leading to a better understanding of the factors influencing spinal correction.

**Table 7. 2** Mechanical properties of the FE models.

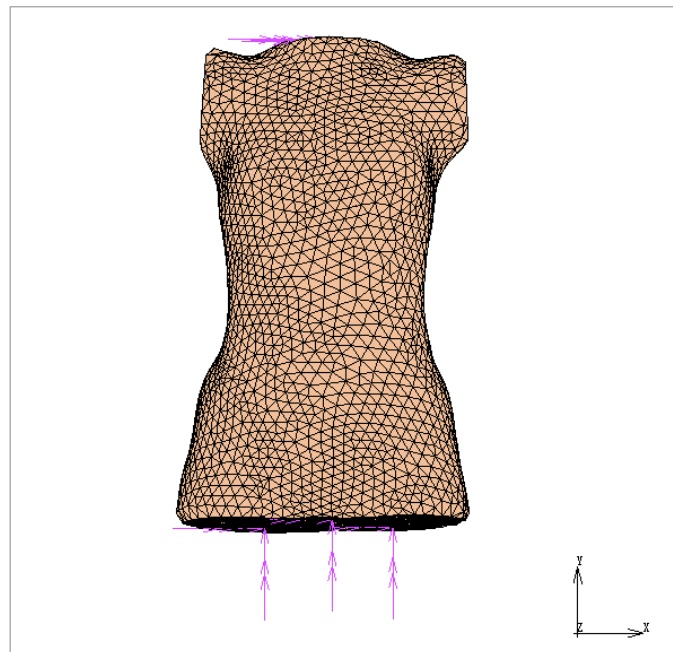
	Young's modulus (MPa)	Poisson's ratio
<b>Torso body</b>	0.1 ~ 20	0.4 ~ 0.45
<b>Rib &amp; pelvis</b>	2,790 ~ 30,000	0.2 ~ 0.4
<b>Vertebrate</b>	3,000 ~ 12,000	0.4
<b>Intervertebral disc</b>	30 ~ 300	0.2 ~ 0.3
<b>Textile material of FIA</b>	0.56	0.4
<b>Hinge material of FIA</b>	2070	0.3
<b>Padding of FIA</b>	300 ~ 3000	0.35

Subsequently, the meshing process was conducted. The FE model employed 3-node triangle, 4 and 10-node linear quadratic tetrahedral elements with three degrees of freedom at each node for meshing purposes (Figure 7.2). Table 7.3 summarises the types and sizes of the mesh, as well as the element numbers. The FE model comprised a total of 405,155 elements, with the following allocation: 359,334 elements for the torso model, 25,333 elements for the ribs and pelvis, 15,846 elements for the vertebrae, 2,156 elements for the intervertebral disc, and 2,486 elements for the textile and hinge materials of the FIA. Once the mesh elements were defined, a numerical simulation was conducted to assess the process of donning the FIA on the torso.

**Table 7. 3** Mesh elements of the FE models.

Model	Element type	Element size (mm)	Element number
<b>Torso body</b>	4-node quadratic tetrahedral	12	359,334
<b>Ribs, pelvis</b>	10-node quadratic tetrahedral	5	25,333
<b>Vertebrae</b>	10-node quadratic tetrahedral	9	15,846
<b>Intervertebral disc</b>	4-node quadratic tetrahedral	9	2,156
<b>FIA</b>	3-node triangle	12	2,486

After that, it was necessary to define the initial and boundary conditions (Figure 7.3), including the displacement conditions of the FIA and the loading conditions on the surface of the torso. These boundary conditions for the FE model were established to reflect real-life scenarios. Since the primary objective of this model was to examine the spinal effects while wearing the brace, so only the torso and skeletal structure were included. It was assumed that the forces exerted by the FIA on the torso did not induce any displacement of the head and legs. As a result, the top surface of the T1 vertebra and the bottom surface of the torso body were fixed by restricting all degrees of freedom.



**Figure 7. 2** Boundary conditions of torso model.

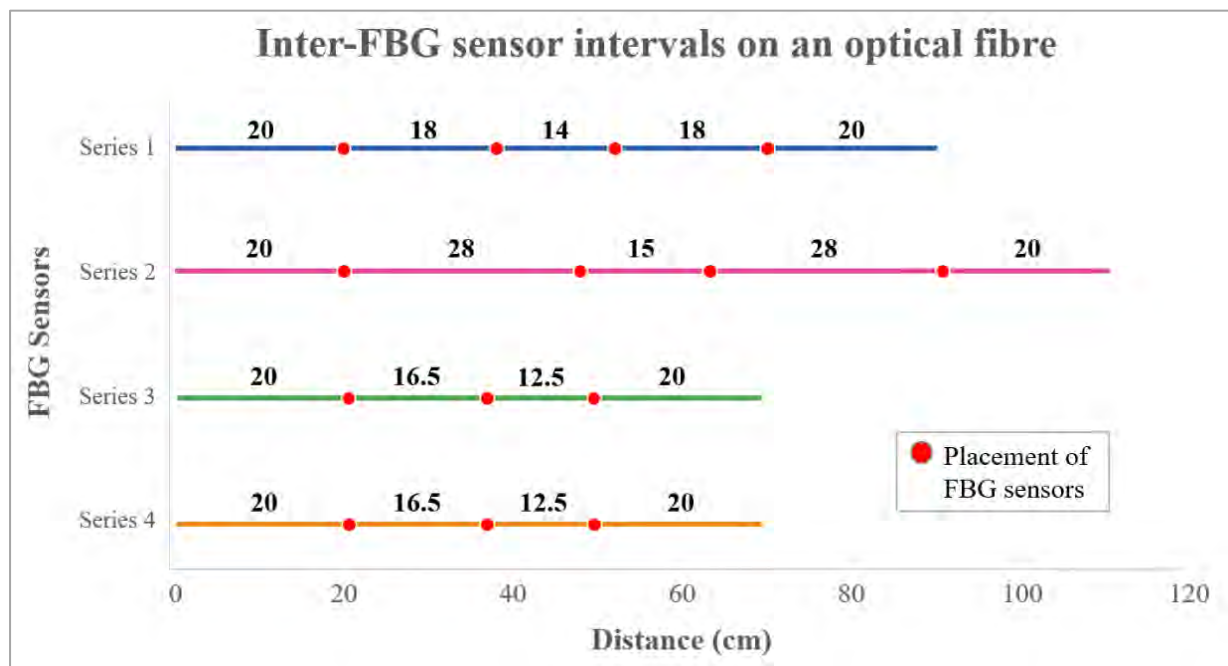
Subsequently, the obtained results were subjected to post-processing and validation. Given that Fok (2020)'s FE model had already undergone validation, modifications were mainly made on the re-meshing of the model, while the material properties and loading conditions, aligning them with those of the proposed mannequin and the data collected from the pressure monitoring undergarment, respectively.

### **7.2.2 Pressure measurement on a proposed mannequin**

The loading conditions employed in Fok (2020)'s FEA were based on clinical pressure measurements obtained from an AIS subject using Pliance® pressure sensors. However, it is not feasible to recruit the same subject to compare the data collected from the Pliance® pressure sensor and the pressure monitoring undergarment due to changes in the subject's Cobb's angle and skeletal maturity. To overcome this limitation, a validated mannequin, as discussed in Chapter 6, was utilised as a substitute for the AIS body. Using a soft mannequin helps to minimise interference caused by body movements and respiratory activity, thereby reducing measurement duration. Furthermore, it confirmed that the corrective effect on the spine resulted from compressional force rather than axial force induced by bodily movements.

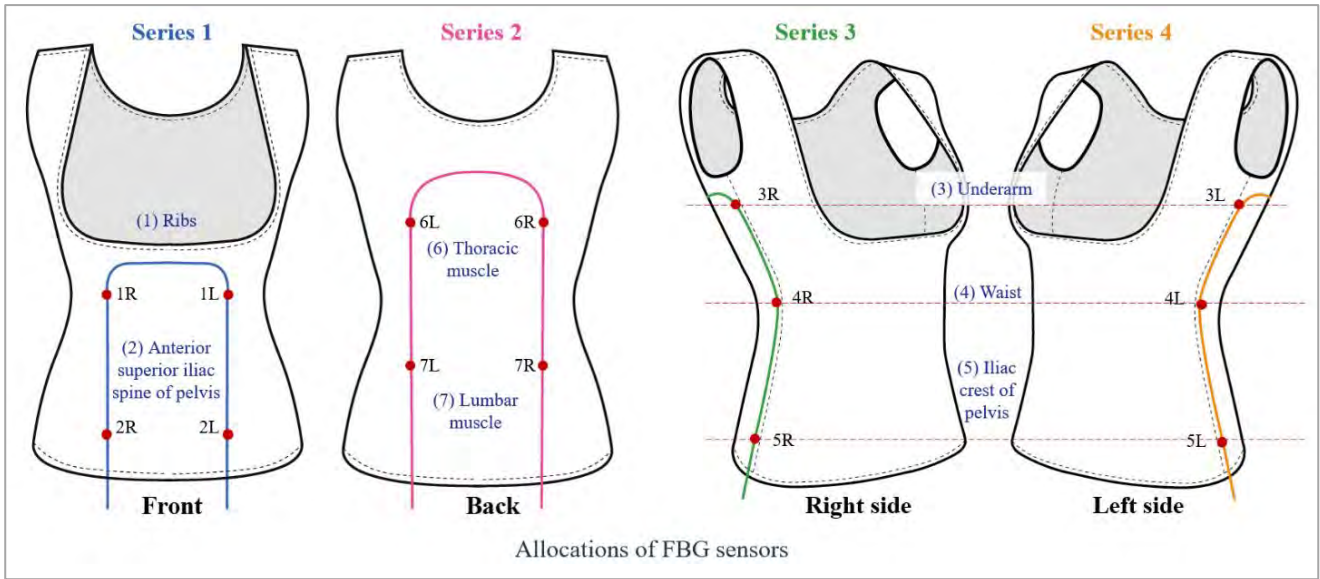
This study used the pressure monitoring undergarment instead of the Pliance® pressure sensors because it provided both instant and overall pressure distribution. Also, a previous experimental result has shown that it was more stable and linear when testing on a soft surface (Lee et al., 2023) (*please see Chapter 5.3*). Instead of 4 FBG sensors, the modified pressure monitoring undergarment was equipped with 14 embedded FBG sensors to obtain more comprehensive data. However, due to the inherent challenges, costs, and time required in manufacturing 14 FBG sensors on a single optical fibre, a decision was made to distribute them among four optical fibres. The objective behind this division was to alleviate the difficulties

associated with the production process and enhance efficiency. The interval between each FBG sensor was measured before inscribing the sensors into the optical fibres (Figure 7.3).



**Figure 7. 3** Inter-FBG sensor intervals on an optical fibre.

Referring to Figure 7.4, 14 FBG sensors are allocated at the common brace pad areas: (1) ribs, (2) anterior superior iliac spine of the pelvis, (3) underarm, (4) waist, (5) iliac crest of pelvis, (6) thoracic muscle, and (7) lumbar muscle. Since the FBG sensors were arranged in pairs, they were also labelled as “R” and “L”, which denoted right and left sensors, respectively. Also, the specifications of the FBG sensors are listed in Table 7.4.



**Figure 7. 4** Placement of the FBG sensors.

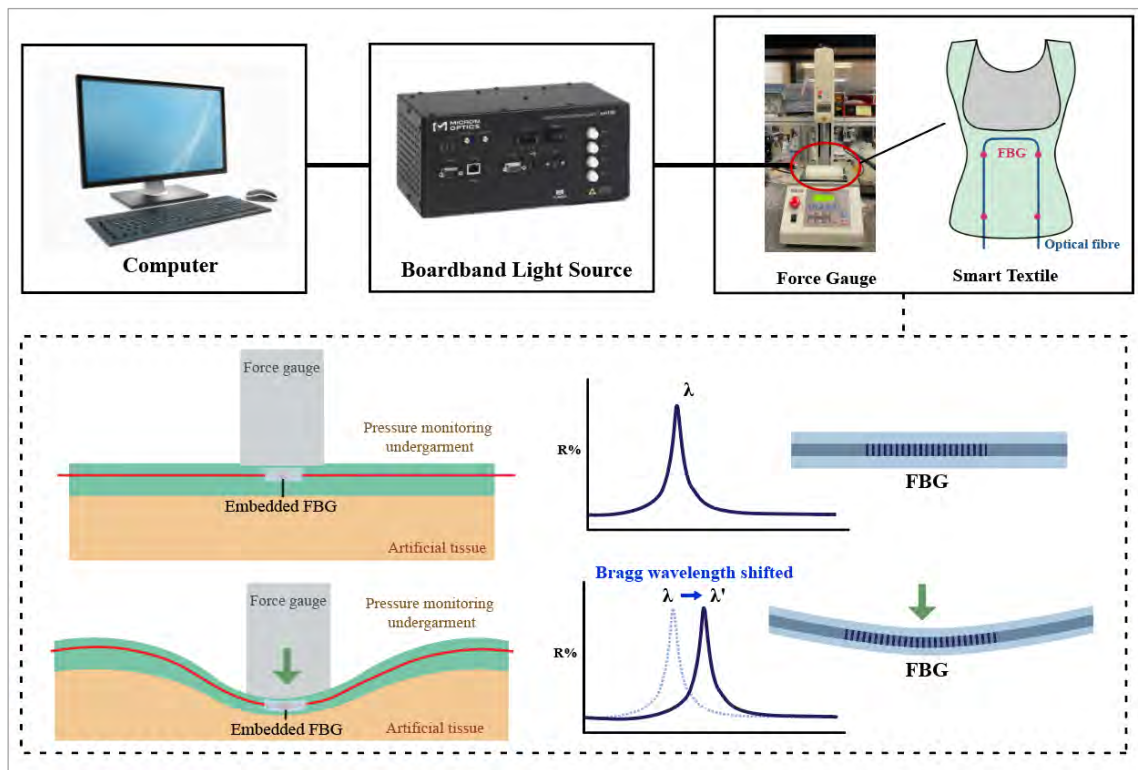
**Table 7. 4** Specifications of the FBG sensors.

FBG series 1 (Front)		FBG series 2 (Back)		FBG series 3 (Right side)		FBG series 4 (Left side)	
Location	$\lambda$ (nm)	Location	$\lambda$ (nm)	Location	$\lambda$ (nm)	Location	$\lambda$ (nm)
2R	1550.113	7R	1549.738	3R	1550.127	3L	1549.997
1R	1552.090	6R	1551.852	4R	1551.797	4L	1551.901
1L	1554.117	6L	1553.915	5R	1553.980	5L	1553.995
2L	1555.799	7L	1555.996				

Afterwards, they were inserted into the pure PIMA cotton knitted undergarment by the warp-inlaid method and embedded into the silicone membrane. The details of the manufacturing process of the FBG sensors can be referred to in *Chapter 5.2*.

Since the peak Bragg wavelength shifts could not directly measure the applied forces, it was necessary to establish the force-strain relationship as a prerequisite. A stimulated wear trial was conducted to achieve this, and the equipment setup is shown in Figure 7.5. The experimental

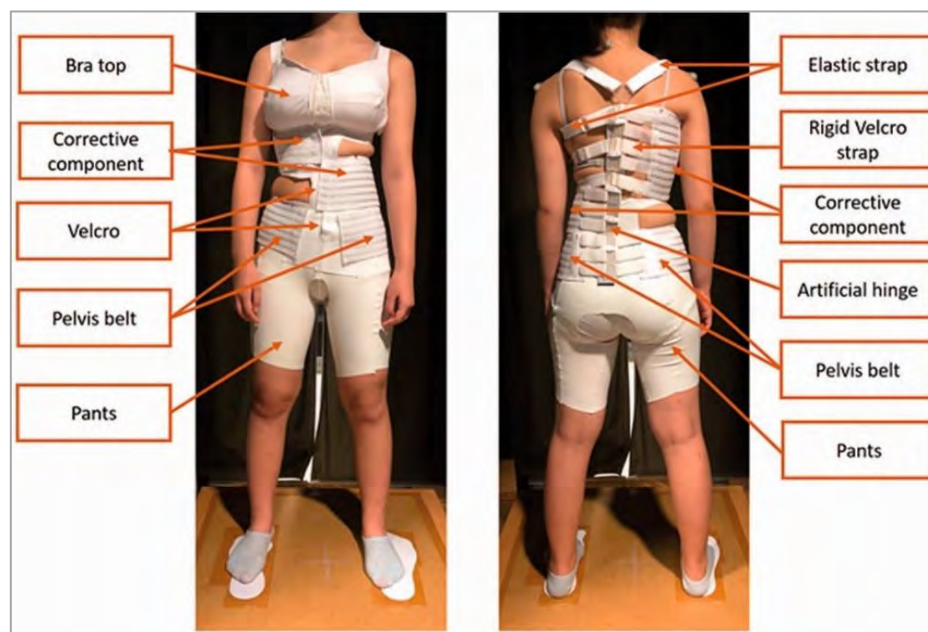
setup involved the application of artificial tissue and a force gauge (model: JSV-H1000, Japan Instrumentation System) to mimic human tissue and bracing force, respectively. To replicate the characteristics of human skin and muscle tissue, a 20 mm thick artificial tissue was fabricated using Ecoflex® 0010 silicone rubber and PU foam. The tissue served as a simulation medium for skin and muscle, respectively. The FBG sensors embedded in the pressure monitoring undergarment were placed between the force gauge and the artificial tissue, enabling precise measurements of applied pressure. The force gauge consistently applied incremental force on the FBG sensors at intervals of 1 second, augmenting by 0.5 N until it reached a threshold of 10 N. As a result, 14 equations were generated, and the applied force (x) at a specific location can be calculated by inputting the shifted Bragg wavelength (y) into a corresponding equation.



**Figure 7. 5** Equipment setup and schematic of transverse force applied to smart textile on artificial tissue.

To perform pressure measurements, the pressure monitoring undergarment was placed on the mannequin, which was then fitted with the FIA. This process involved adjusting the compressional force of the brace until the FIA was appropriately worn on the mannequin. The pressure test was conducted for approximately one minute, allowing sufficient time for the signals to stabilise.

The FIA consists of breathable textiles, elastic bands and straps, semi-rigid pads, and 3D printed artificial bone (Figure 7.6). The pressure applied by the brace can be adjusted by modifying the tightness of the elastic bands and straps, with pressures reaching up to 25 kPa. Moreover, the study discovered that the FIA could achieve an initial spine correction of up to 87.0%, and 60% of the subjects demonstrated an improvement of more than 5° after treatment. By employing the FIA in conjunction with the pressure monitoring undergarment, it becomes possible to measure the pressure distribution on the spine and acquire instant feedback regarding the efficacy of the brace. This information can be utilised to optimise the design of spinal braces and enhance treatment outcomes for patients with AIS.



**Figure 7. 6** The functional intimate apparel (Fok, 2020).



### 7.2.3 Validation

Validation is a crucial aspect of simulation work because it determines the degree to which simulation results correspond to the actual situation and the accuracy of the simulation model. Given that the in-brace correction is recognised as a robust predictor of the effectiveness of brace treatment, it was deemed necessary to calculate the displacement of the spine by inputting the force data acquired from the pressure monitoring undergarment to the FEA.

To enable a comprehensive comparison between FEA and clinical findings, Cobb's angles and spinal curvatures were evaluated, with a specific focus on the frontal plane of the spine as the chosen parameter of interest. When comparing the spinal curvatures, a plot was generated by associating the position of each vertebral body, which was determined by measuring the horizontal distance between the vertebral body and the CSVL using Solidworks 2018 (64 Edition). Through the utilisation of Equation 7.1, it becomes possible to calculate the correlation coefficient between the vertebral body derived from the FE estimations and the corresponding measurements obtained from in-brace X-ray images. It means that a curve resembling the actual curve on the X-ray would demonstrate a higher correlation coefficient, with a value closer to 1. It has been known that the correlation coefficient of the vertebral body displacement of Fok (2020)'s FEA was 0.74, which indicated a high correlation.

$$\text{Correlation coefficient} = \frac{\sum_{i=1}^{17} [(T_i - \bar{T}) \cdot (E_i - \bar{E})]}{\sqrt{\sum_{i=1}^{17} (T_i - \bar{T})^2} \cdot \sqrt{\sum_{i=1}^{17} (E_i - \bar{E})^2}} \quad (7.1)$$

where:  $T_i$  = vertebral displacement measured from the radiographic image;  $E_i$  = vertebral displacement estimated from the FEM;  $\bar{T}$  = average vertebral displacement measured from the radiographic image;  $\bar{E}$  = average vertebral displacement estimated from the FEM



## 7.3 Result and discussion

### 7.3.1 Brace force detected by the pressure monitoring undergarment

Upon increasing the applied force from 0 N to 10 N, the results revealed a range of linearity ( $R^2$ ) values between force and shifted Bragg wavelength, spanning from 0.83 to 0.99 (Figure 7.7). This range of linearity values highlights the high level of reliability of the FBG sensors when measuring brace force on a soft surface. By substituting the difference in Bragg wavelength (y) into the equation, the corresponding force (x) within the range of 10 N can be determined as follows.

$$2R: y = 0.0134x + 0.0190 \quad (7.2)$$

$$1R: y = 0.0078x + 0.0125 \quad (7.3)$$

$$1L: y = 0.0093x + 0.0152 \quad (7.4)$$

$$2L: y = 0.0086x - 0.0032 \quad (7.5)$$

$$7R: y = 0.0183x + 0.0340 \quad (7.6)$$

$$6R: y = 0.0169x + 0.0295 \quad (7.7)$$

$$6L: y = 0.0118x + 0.0185 \quad (7.8)$$

$$7L: y = 0.0133x - 0.0143 \quad (7.9)$$

$$3R: y = 0.0113x + 0.0366 \quad (7.10)$$

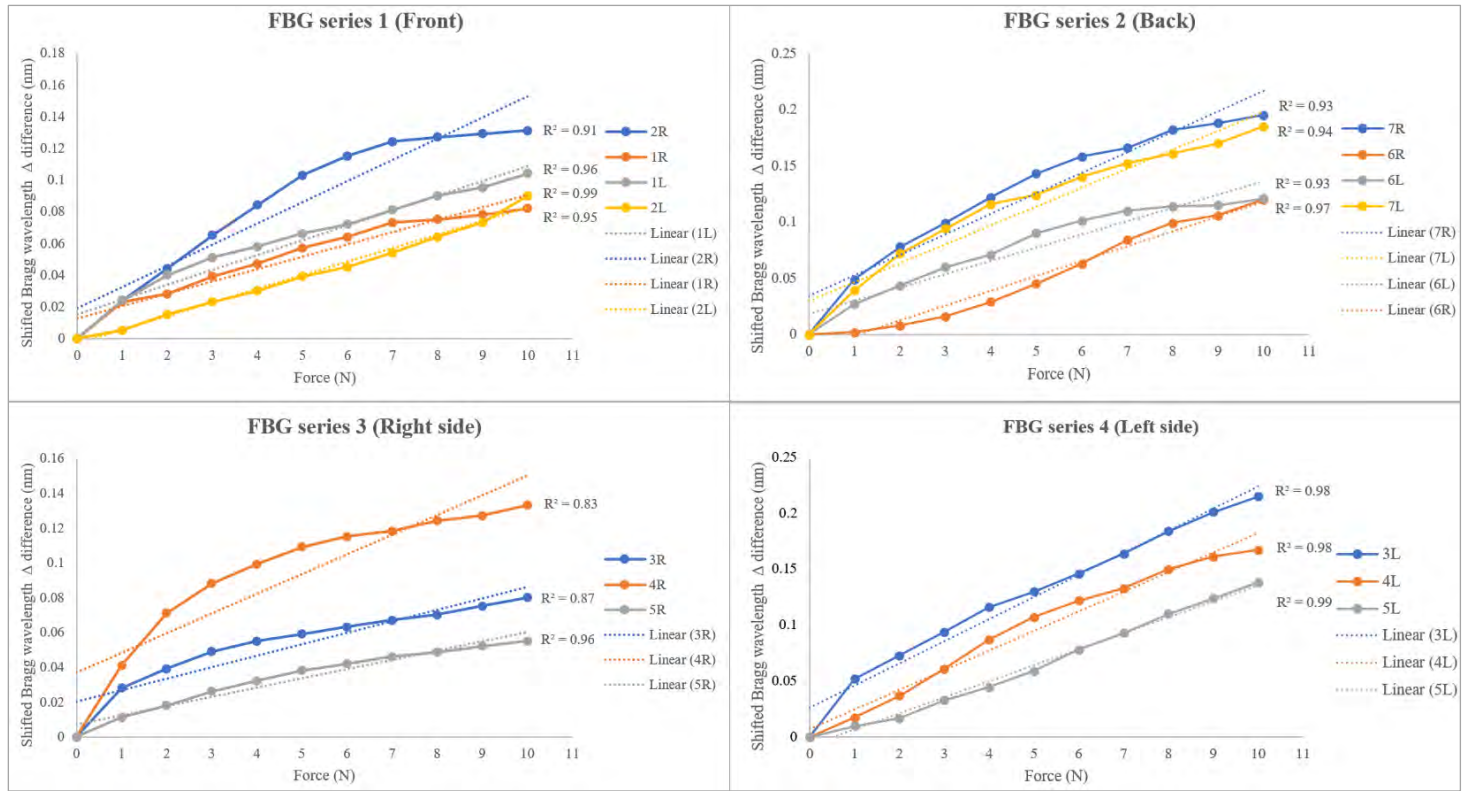
$$4R: y = 0.0066x + 0.0202 \quad (7.11)$$

$$5R: y = 0.0053x + 0.0071 \quad (7.12)$$

$$3L: y = 0.0198x + 0.0262 \quad (7.13)$$

$$4L: y = 0.0175x + 0.0072 \quad (7.14)$$

$$5L: y = 0.0144x - 0.0075 \quad (7.15)$$

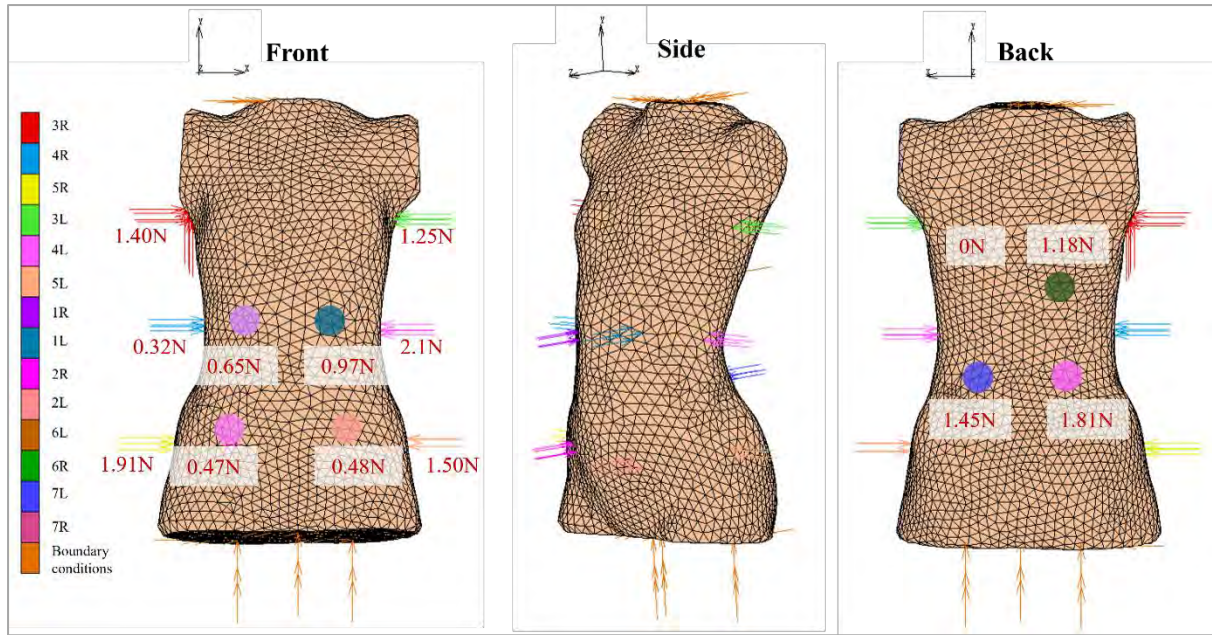


**Figure 7. 7** Linear regression between Bragg wavelength delta difference and force when applying force to FBG series 1 to 4.

Based on these equations, the force exerted by the FIA on the mannequin was found, and the corresponding force was calculated (Table 7.5). Subsequently, these data were input into the FEA (Figure 7.8).

**Table 7. 5** Force exerted by the FIA.

FBG series 1 (Front)		FBG series 2 (Back)		FBG series 3 (Right side)		FBG series 4 (Left side)	
Location	Force (N)	Location	Force (N)	Location	Force (N)	Location	Force (N)
2R	0.471	7R	1.810	3R	1.400	3L	1.250
1R	0.648	6R	1.178	4R	0.324	4L	2.107
1L	0.965	6L	0.000	5R	1.905	5L	1.494
2L	0.481	7L	1.453				



**Figure 7. 8** Loading conditions on the surface of the torso.

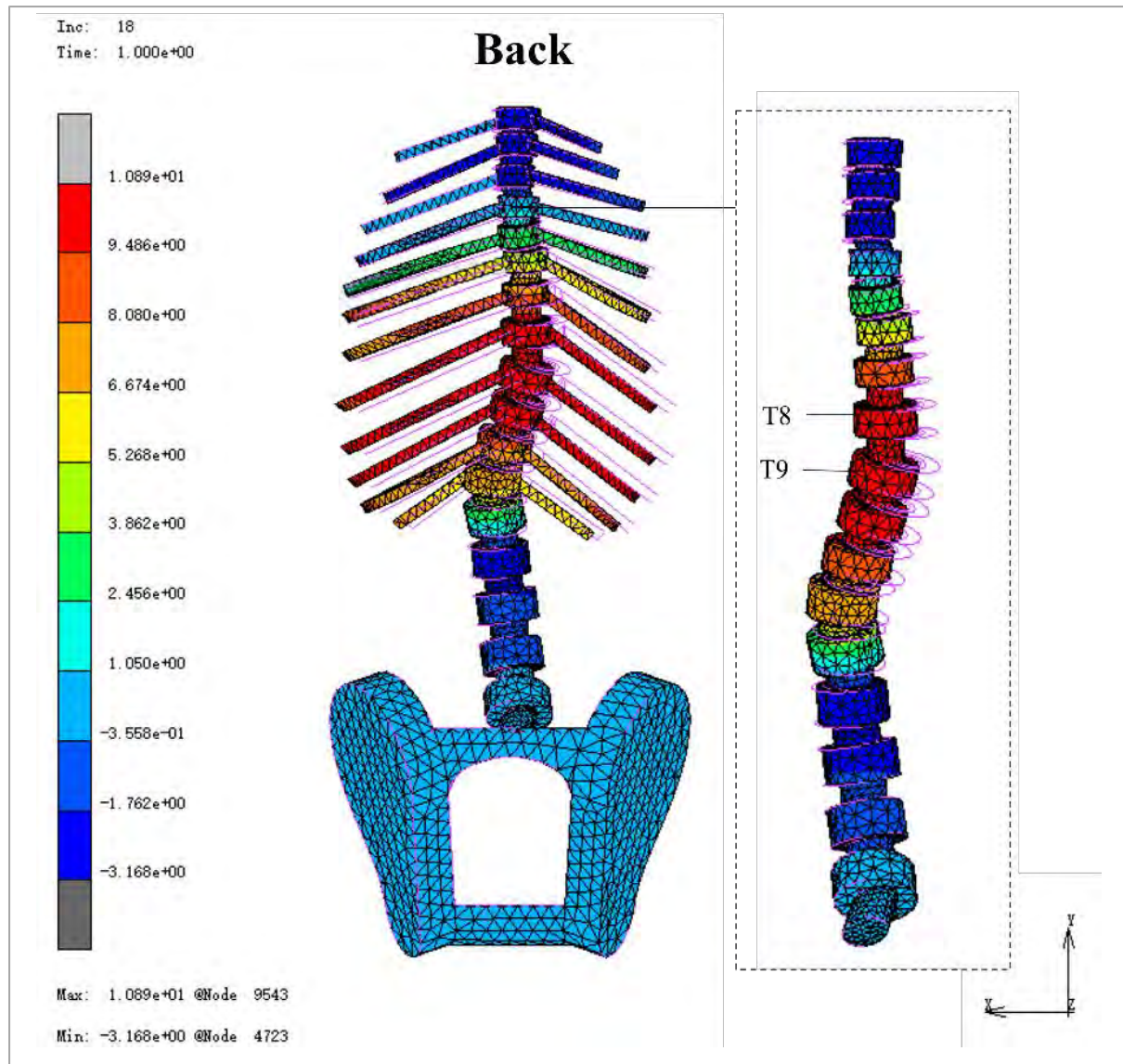
However, it is important to note that the results revealed a significant disparity in FBG sensor sensitivity. The difference in Bragg wavelength delta served as an indicator of the force sensing range and sensitivity, with a greater delta difference indicating higher sensitivity (Lee et al., 2023). While most FBG sensors exhibited high sensitivity to force on the soft surface, few displayed significantly lower sensitivity. For instance, the FBG sensor at 3L exhibited a Bragg wavelength delta difference of 0.215 nm, whereas the sensor at 5R only showed a difference of 0.055 nm (Table 7.6). This discrepancy in sensitivity may be attributed to factors related to the manufacturing process involved in inscribing the FBG into the optical fibre or potential variations that can arise during the inlay process. Moreover, different fabric structure, and thickness on the pressure monitoring undergarment may affect their sensitivity.

**Table 7. 6** Bragg wavelength delta differences of the FBG sensors from 0 N to 10 N.

FBG series 1 (Front)		FBG series 2 (Back)		FBG series 3 (Right side)		FBG series 4 (Left side)	
Location	$\Delta$ Bragg wavelength (nm)	Location	$\Delta$ Bragg wavelength (nm)	Location	$\Delta$ Bragg wavelength (nm)	Location	$\Delta$ Bragg wavelength (nm)
2R	0.131	7R	0.195	3R	0.080	3L	0.215
1R	0.082	6R	0.120	4R	0.133	4L	0.167
1L	0.104	6L	0.121	5R	0.055	5L	0.138
2L	0.090	7L	0.185				

### 7.3.2 Comparison of the spinal corrective effect between FEA and clinical study

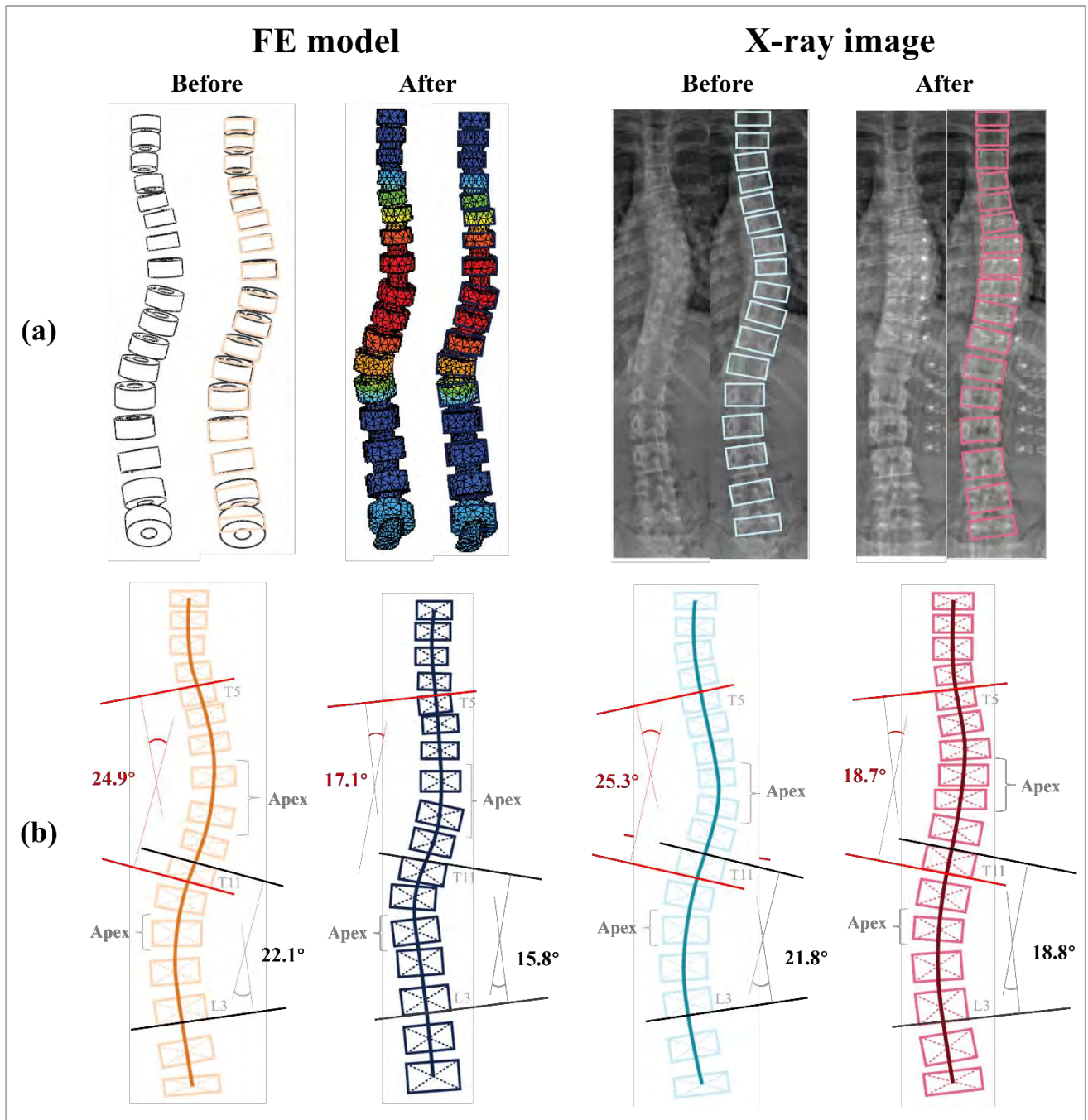
The displacement of the skeletal model after the analysis is shown in Figure 7.9. The purple outlines indicated the initial positions of the vertebrates. The red and blue regions represented significant and minimal displacement deformations, respectively. In the back view, it can be observed that the thoracic and lumbar vertebrae shifted to the left and right, respectively. Notably, T8 and T9, which formed the apex of the thoracic curve, displayed the most pronounced degree of displacement. The results indicate a tendency for the spine to straighten, which is consistent with the findings of the clinical study.



**Figure 7. 9** Displacement of skeletal model.

To validate the FE model employed in this study, it is necessary to identify the centre of each vertebra (Figure 7.10 (a)), followed by a thorough comparison of spinal curvature and Cobb's angles (Figure 7.10 (b)) after the intervention of FIA.

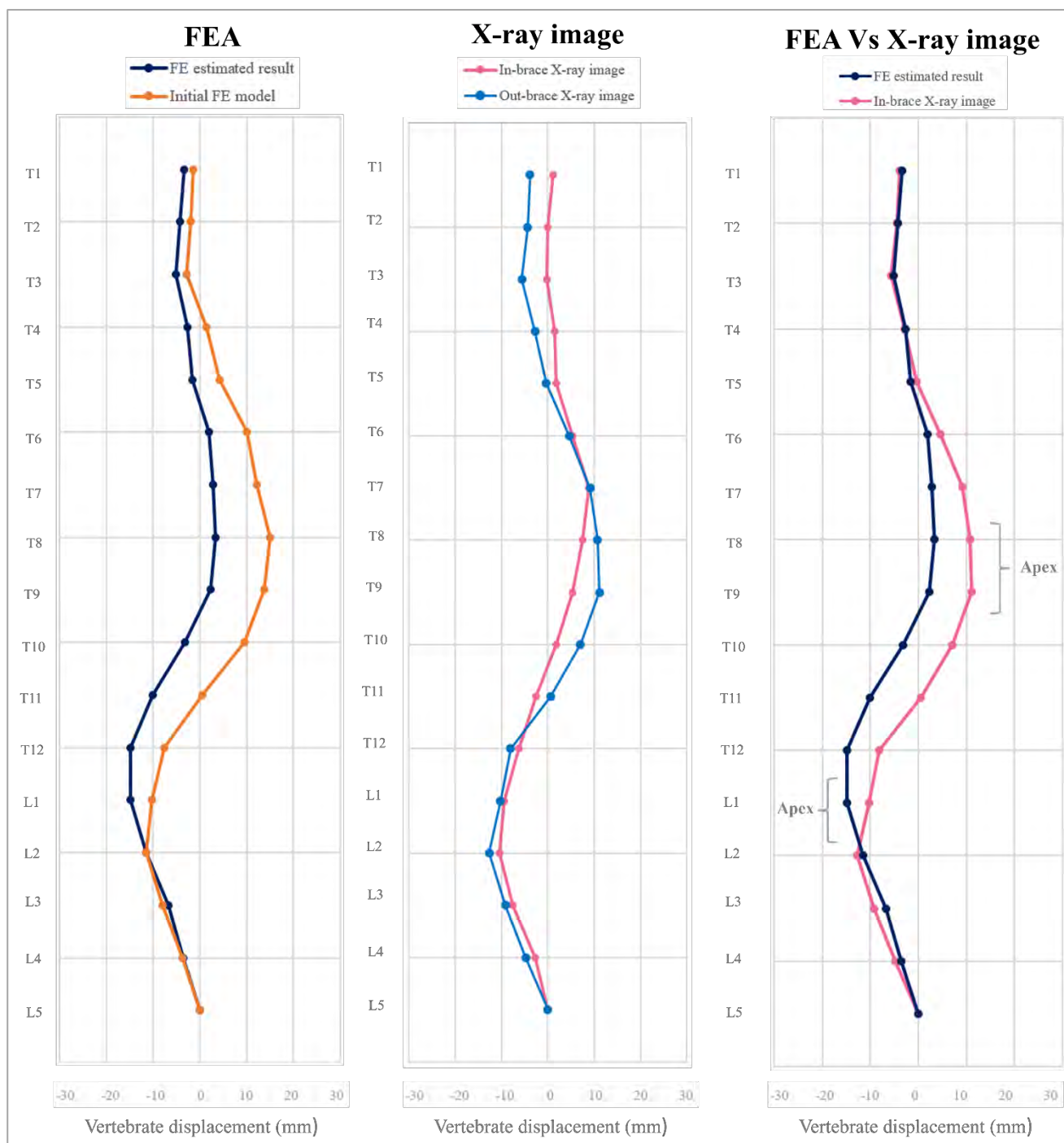




*\*Note: Cobb's angles depicted in the graph are not drawn to scale.*

**Figure 7. 10 (a)** Vertebrate position, and **(b)** spinal curvatures and Cobb's angles on the FE model and X-ray images.

In addition, to enable a more thorough visual analysis, the FE estimated spinal curve is graphically compared with the actual curvatures identified from X-ray images (Figure 7.11). This comparison is achieved by measuring the horizontal distance between the vertebral body and the CSVL. Referring to Figure 7.11, it is observed that T7 to T11 of both the FE-estimated and in-brace spinal curves shifted towards the left, while L2 to L4 of both curves shifted towards the right. It means that the shift exhibited by the FE estimated spinal curve demonstrates a consistent trend with that of the in-brace X-ray image. Furthermore, the correlation coefficient between the vertebral body derived from the FE estimation and the X-ray image is 0.90, which is significantly higher than the 0.74 reported in Fok's study (Fok, 2020). This may be attributed to the close estimation of the thoracic (T1 to T5) and lower lumbar (L2 to L4) movement.



**Figure 7. 11** Comparison of the spinal curves.

In addition to analysing vertebral displacement and spinal curves, a comparison was made regarding Cobb's angles after the intervention of FIA. Table 7.7 provides insights into this comparison, indicating a decrease in Cobb's angles for both thoracic and lumbar curves as observed in the FE model and the in-brace X-ray image.



**Table 7. 7** Comparison of Cobb's angles on FE modelling and X-ray.

	FE modelling		X-ray images	
	FE initial model	FE-estimated result	Pre-intervention	Post-intervention
<b>Cobb's angle at T5-T11 (°)</b>	24.9	17.1	25.3	18.7
<b>Cobb's angle at T11-L3 (°)</b>	22.1	15.8	21.8	18.8
<b>Apex</b>	T8-9, L1	T8-9, L1	T8-9, L1	T8-9, L1

However, it is worth noting that the FE model appears to slightly overestimate the degree of vertebral movement. The estimated Cobb's angles at T5 to T11 and T11 to L3 were 17.1° and 15.8°, respectively, displaying minor deviations of -1.6° and -3.0° compared to the post-intervention X-ray images, respectively. Overall, this finding aligns with the results obtained from the clinical study, and thus it is believed that this FE model can be validated to have a similar spinal corrective effect as a human subject.

#### 7.4 Limitations

Despite the FEA neglecting the brace compliance of AIS subjects, and their habitual activities and spinal growth, it remains a favourable method for predicting the corrective effect on the spine without causing harm to the human body.

The FE model developed in this study and the previously established FEA model by Fok (2020) demonstrated comparable spinal curvature and corrective effects when subjected to similar pressure conditions, as observed in clinical outcomes. Nevertheless, there were notable distinctions that warrant consideration. Firstly, the loading position differs between the two models. Secondly, the new FEA model incorporated an overall pressure distribution with 14 loading points, whereas the previous one only incorporated 2 loading points. These differences in the loading approach resulted in divergent outcomes, thus careful interpretation and analysis of the respective findings may be needed.

## 7.5 Summary

In this chapter, a simulation model is developed to simulate the overall pressure distribution exerted by the FIA on the body and investigate its biomechanics on the spine. The FE model incorporates a human torso, skeletal structure, textile materials, and the hinge material of the FIA. Moreover, a validated soft mannequin is utilised as a substitute for the AIS body to measure the forces exerted by the FIA. A pressure monitoring undergarment is also employed to capture the overall pressure distribution data. The findings revealed a linear relationship ( $R^2 > 0.83$ ) between Bragg wavelengths and forces within 0 to 10 N, indicating the potential of the pressure monitoring undergarment as a valuable tool for monitoring brace forces during the fitting process.

The forces calculated are then inputted into the FEA, leading to the identification of vertebrate displacement: the thoracic and lumbar vertebrae underwent a leftward and rightward shift, respectively. Notably, T8 and T9, which constituted the apex of the thoracic curve, exhibit the most prominent degree of displacement. Moreover, the correlation coefficient between the vertebral body derived from the FE estimation and the X-ray image is 0.90, which is highly correlated. Besides, it is found that the FE estimated Cobb's angles are comparable to the clinical study conducted by Fok (2020). The FE estimated Cobb's angles are also found to be comparable to the clinical study conducted by Fok (2020). Therefore, it is concluded that the implementation of the FE model in this study effectively addresses the challenges associated with conducting human wear trials to assess the efficacy of bracing, providing a radiation-free methodology for predicting the spinal corrective effect.

## **CHAPTER 8 CONCLUSIONS AND SUGGESTIONS FOR FUTURE RESEARCH**

### **8.1 Conclusions**

AIS is a three-dimensional spinal deformity in adolescents aged 10 to 16 (Altaf et al., 2013). If Cobb's angle is at least  $10^{\circ}$  and there is vertebral rotation, it indicates an abnormal shift or rotation of the spine (Spoonamore, 2023; Weinstein et al., 2013b). The decision of the treatment approach for patients with AIS is based on their type of curve, age, and severity of spinal curvature. Bracing is the most used conservative treatment to halt the progression of spinal deformity and restore normal spinal alignment by applying pressure to the problematic areas of the spine (Bunge et al., 2010; Schwieger et al., 2017; Weinstein et al., 2013b). However, wearing the brace may cause several notable side effects, including temporary vital capacity reduction, mild chest wall and inferior rib deformation, skin irritation, and psychological distress (Canavese & Kaelin, 2011). These side effects are often due to prolonged exposure to high pressure and the unpleasant appearance of the brace.

Because of ambiguous brace effectiveness without standardised pressure, the applied pressure depends on the judgment of the orthotist (Chalmers et al., 2012). To prevent excessive brace pressure, one of the scientific methods is employing sensors to monitor the forces exerted by the braces. However, it is found that market available force and pressure sensors possess certain limitations, such as inflexibility, a narrow measurement range, lack of instant and overall pressure distribution, and application challenges. Considering the factors above, a pressure monitoring undergarment that addresses the inadequacies of conventional sensors is developed in this study. Aside from evaluating the existing sensors used to measure the force exerted by a brace, this study also elaborates on the design and development of this novel force-sensing undergarment for scoliosis brace treatment. The primary intention of this pressure

monitoring undergarment is to provide reliable sensor readings while prioritising wear comfort. By carefully examining and analysing these forces, it is possible to optimise the design parameters and ensure that the pressure exerted by the braces remains within acceptable limits. Additionally, this approach is crucial to minimise the potential risks associated with bracing while providing the desired corrective measures for spinal deformities.

The research objectives of this study are to (1) review the development of TFOSs for health monitoring purposes regarding their features, applications, and integration methods; (2) investigate the main factors that affect the wear comfort of health-monitoring undergarments in terms of tactile and thermal comfort by conducting physical experiments; (3) investigate the relationship between normal force and strain sensed by using FBG sensors; (4) develop a flexible pressure monitoring undergarment by inserting FBG sensors into the knitted garment, so the overall and instant pressure exerted by braces on AIS patients can be measured; and (5) formulate a biomechanical model that simulates the forces from a brace and examine how the spine responds to the exerted pressure. The outlined research objectives have been accomplished, and the results of this study can be summarised as follows.

(1) Smart textiles with fibre optic sensors offer a promising solution to address the limitations of conventional sensors in measuring brace pressure. They are flexible, lightweight, and immune to electromagnetic interference. A comprehensive review of TFOSs for health monitoring was conducted in the Web of Science Core Collection, and 47 relevant studies were identified. The analysis reveals a trend toward developing highly flexible and comfortable smart textiles for continuous health monitoring, particularly respiratory monitoring. Embedding FBG sensors into flexible silicone with a curvilinear shape is a popular method, which enhances flexibility, robustness, and compatibility with the skin's surface.

(2) To achieve optimal comfort in the design of an undergarment, it is essential to investigate the key factors influencing wear comfort, particularly in terms of tactile and thermal sensations. A series of experiments, including physical experiments, KES-FB measurements, and a wear trial, were performed on seven conventional undergarments. The results indicated that breathability and moisture wicking could be improved by using lighter, thinner, and low stitch density fabrics constructed with uniform filaments. Furthermore, lighter and thinner materials containing a higher percentage of elastane, finer yarn, and uniform, long fibres provide a softer, smoother, and cooler sensation. Notably, undergarments made of pure cotton produce better body temperature regulation by facilitating a higher perspiration rate despite clinging. These results serve as valuable guidelines for developing a pressure-monitoring undergarment.

(3) and (4) The pressure-monitoring undergarment is developed by embedding silicone-embedded FBG sensors into a knitted undergarment using the inlay method. This design offers several advantages over existing methods, including ease of use and adaptability to individuals with different body shapes, without requiring additional procedures before treatment. Additionally, instant data acquisition and overall pressure distribution enable adjustment and monitoring of tightness during the fitting process. To evaluate the reliability of the undergarment and understand the response of FBG sensors to force, a simulated bracing treatment experiment was conducted using artificial skin and a force gauge. The results demonstrate that the sensors embedded in silicone membranes improve sensitivity, flexibility, and softness when subjected to applied forces. The linearity ( $R^2$ ) between the shift in Bragg wavelength and force is assessed using standardised forces on artificial skin, and it is found to be above 0.95 with an ICC of 0.97. Since no consensus has been reached on the optimal bracing pressure, it is believed that instant data acquisition of the pressure monitoring undergarment can facilitate the adjustment and monitoring of force during the fitting processes.

(5) A soft mannequin is developed to simulate the AIS subject's abnormal body and spine curvature and examine how the spine responds to the exerted pressure. A previously validated FE model developed by Fok (2020) serves as a reference for constructing the soft mannequin, which includes a 3D printed spine and ribs, as well as moulded muscle tissues, skin, and sternum. The constructed soft mannequin successfully matches the body contour, spinal curve, and spinal corrective effect observed in the X-ray images of the AIS subjects. Both demonstrate a reduction in Cobb's angles in the thoracic (T5 to T11) and lumbar region (T11 to L3) under similar pressure. However, there is a differentiation in Cobb's angle between the mannequin and the human subject. The mannequin shows a  $1.4^{\circ}$  and  $0.8^{\circ}$  difference in thoracic and lumbar corrective effects, respectively. Nevertheless, it is important to note that the mannequin exhibits a similar overall trend in corrective effects. The results of this study underscore the value of the soft mannequin as a significant tool for examining spinal movement following brace application.

A biomechanical model is also constructed based on Fok (2020)'s FE model. It stimulates the overall pressure of FIA that detected by the pressure monitoring undergarment and facilitates the evaluation of the spinal corrective effect induced by the brace. Like the soft mannequin, the FE model incorporates a body torso, ribs, a spine, and a sternum, however, skin is excluded. To validate the model, the in-brace vertebrae position and Cobb's angle on the FE model are compared to that on X-rays. The actual and simulated spinal curvatures exhibit a consistent trend, with a 0.90 correlation coefficient between their vertebrae bodies. It indicates that the results obtained from the FE model are comparable to the clinical findings. The output could be further extended to determine ideal bracing pressure levels by adjusting the load condition, thus preventing AIS patients from having to endure excessive pressure, while maintaining an appropriate amount of bracing force to halt curve progression and reduce the risk of pressure-related injuries.

## 8.2 Limitations of the study

The following discussion highlights certain limitations of this study that restrict the generalizability of the results.

(1) Regarding the CNA, there are several methodological limitations. Firstly, despite efforts to include all relevant keywords, it is possible that some studies employing different but related keywords are not captured. Secondly, relying solely on the WoS Core Collection for searching related journals may have resulted in the omission of certain journal papers, and thus the journals may not fully represent the semantics of the field (Tang et al., 2018; Zhuge, 2016). Thirdly, although CNA is used to define the research domain objectively, the final screening of studies involves some subjective judgment by the research team (Fan et al., 2014).

(2) As for the wear trial on the conventional undergarments, the short-term nature of wear trials may restrict the estimation of how the product performs over extended periods. Secondly, the absence of a comparison group limits the ability to make meaningful comparisons about the performance of the undergarments being tested. Thirdly, with only one subject, it can be challenging to determine whether the observed effects are attributable to the product itself or other factors specific to that individual. Therefore, the findings may not generalize to a larger population because individual responses and experiences can vary significantly. To alleviate these issues, several physical experiments, including a hand feel system and temperature logger, are used to verify the results.

(3) Similar to the Pliance®-X pressure sensor, the pressure monitoring undergarment on a soft surface produces less robust outcomes than on a hard surface, primarily due to the cushioning effect. For instance, the embedded FBG sensors exhibit a longer time to reach a force of 10 N when compared to the bare FBG sensors, despite their force sensitivity not being significantly affected. Secondly, apart from the deformation induced by applied forces, the shifted Bragg

wavelength is also influenced by temperature variations, potentially introducing errors into the measurements. Thirdly, it is important to note that the extended length of the optical fibre connected to the interrogator may have implications for the wearability of the smart textile.

(4) Constructing a soft mannequin that accurately replicates the softness of human tissue is challenging. Unlike human softness, which is influenced by various intrinsic factors such as skin properties and underlying structures, the softness of a mannequin primarily depends on the materials used. Factors such as the type of foam or silicone, density, and composition affect the overall softness of the mannequin. Furthermore, even though it is possible to construct a soft mannequin that approximates the complexities and instant nature of humans, it is critical to note that the softness and flexibility of the mannequin may deteriorate over time, leading to results that diverge from those obtained with human subjects.

(5) In constructing the biomechanical simulation model, certain restrictions arise because of equipment limitations and the challenge of handling large file sizes. As a result, a simplified skeletal model is utilised. For instance, the torso model is created as a single component, disregarding elements like blood vessels, ligaments, muscles, skin, tendons, and organs. Similarly, the FIA model is simplified to incorporate only a textile and hinge component, neglecting material properties like those of the bra cup, seams, accessories, and hinge pin. Secondly, certain material properties utilised in the study are based on previous literature, which may not precisely match the characteristics of the subjects and the brace used in this study. These limitations explain the observed difference in the magnitude of vertebral displacement between the predicted spinal curve and the experimental results, despite demonstrating a similar trend.



### **8.3 Suggestions for future research**

Based on the established research findings, the following suggestions are offered for future work.

(1) A larger sample size should be employed to alleviate participant bias in wear trials. Increasing the number of participants can help mitigate the influence of individual differences and provide more reliable and representative data. Moreover, it is favourable for determining the factors that affect the wear comfort of health-monitoring undergarments in terms of tactile and thermal comfort.

(2) To improve the accuracy and wearability of the pressure monitoring undergarment for AIS subjects, the application of polarization-maintaining fibres and the development of a mini-interrogator are possible solutions. These improvements can contribute to more reliable and effective monitoring of pressure distribution, allowing for better assessment and management of spinal deformities in AIS patients.

(3) In future research, developing a more comprehensive torso model is recommended to include detailed components such as the skin, blood vessels, muscles, tendons, ligaments, and organs. Similarly, a more intricate brace model should be constructed to capture its complexity accurately. It is believed that researchers can better understand the mechanical interactions between the brace and the body by developing precise FE models of the torso and brace. Additionally, this approach helps to obtain valuable insights for optimising the brace's design by considering different material properties and loading conditions.

## References

- Abro, Z. A., Hong, C., Chen, N., Zhang, Y., Lakho, R. A., & Yasin, S. (2019). A fiber Bragg grating-based smart wearable belt for monitoring knee joint postures. *Textile research journal*, 90(3-4), 386-394. <https://doi.org/10.1177/0040517519868168>
- Adidas. (2023). *Adidas Men's Workout Climalite Pants*. Retrieved 7 April 2023 from [https://www.adidas.com.hk/item/CG1509?rt=pdp&locale=en\\_GB](https://www.adidas.com.hk/item/CG1509?rt=pdp&locale=en_GB)
- Ameri Research Inc. (2017). *Smart Textiles Market To 2024: Key Product Categories (Active, Passive, Ultra Smart), Application (Sensing, Thermo-Electricity, Energy Harvesting, Luminescence & Aesthetics), End-Use, Regional Segmentation, Competitive Dynamics, M&A Insights, Pricing Analysis (OPP, IPP, RAP) And Segment Forecast*. Retrieved 7 August 2020 from <https://www.ameriresearch.com/product/smart-textiles-market/>
- Allsop, T., Bhamber, R., Lloyd, G., Miller, M. R., Dixon, A., Webb, D., Ania Castañón, J. D., & Bennion, I. (2012). Respiratory function monitoring using a real-time three-dimensional fiber-optic shaping sensing scheme based upon fiber Bragg gratings. *Journal of biomedical optics*, 17(11), 117001-117001. <https://doi.org/10.1117/1.JBO.17.11.117001>
- Altaf, F., Gibson, A., Dannawi, Z., & Noordeen, H. (2013). Adolescent idiopathic scoliosis. *BMJ*, 346(7906), 30-34. <https://doi.org/10.1136/bmj.f2508>
- An, H., & Lee, I. (2015). A conceptual framework for Asian women's emotional needs in fashion design. *International Journal of Fashion Design, Technology and Education*, 8(3), 206-213. <https://doi.org/10.1080/17543266.2015.1053421>
- Asher, M., Min Lai, S., Burton, D., & Manna, B. (2003). The Reliability and Concurrent Validity of the Scoliosis Research Society-22 Patient Questionnaire for Idiopathic Scoliosis. *Spine (Phila Pa 1976)*, 28(1), 63-69. <https://doi.org/10.1097/00007632-200301010-00015>
- Atalie, D., Gideon, R. K., Ferede, A., Tesinova, P., & Lenfeldova, I. (2019). Tactile Comfort and Low-Stress Mechanical Properties of Half-Bleached Knitted Fabrics Made from Cotton Yarns with Different Parameters. *Journal of natural fibers*, 1-13. <https://doi.org/10.1080/15440478.2019.1697989>
- Aulisa, A. G., Giordano, M., Falciglia, F., Marzetti, E., Poscia, A., & Guzzanti, V. (2014). Correlation between compliance and brace treatment in juvenile and adolescent idiopathic scoliosis: SOSORT 2014 award winner. *Scoliosis*, 9(1), 6-6. <https://doi.org/10.1186/1748-7161-9-6>

- Bai, Z.-Q., & Tan, J. (2013). Innovative Design of Polymeric Optical Fiber Fabric for Interior Textiles. *Research Journal of Textile and Apparel*, 17(2), 10-15. <https://doi.org/10.1108/RJTA-17-02-2013-B002>
- Barkov, F. L., Konstantinov, Y. A., Burdin, V. V., & Krivosheev, A. I. (2020). Theoretical and Experimental Estimation of the Accuracy in Simultaneous Distributed Measurements of Temperatures and Strains in Anisotropic Optical Fibers Using Polarization-Brillouin Reflectometry. *Instruments & Experimental Techniques*, 63(4), 487-493. <https://doi.org/10.1134/S0020441220040223>
- Bartie, B. J., Lonstein, J. E., & Winter, R. B. (2009). Long-term follow-up of adolescent idiopathic scoliosis patients who had Harrington instrumentation and fusion to the lower lumbar vertebrae: is low back pain a problem? *Spine*, 34(24), E873-E878.
- Behera, B. K., & Hari, P. K. (2010). 1 - The basics of woven fabric structure. In B. K. Behera & P. K. Hari (Eds.), *Woven Textile Structure* (pp. 3-8). Woodhead Publishing. <https://doi.org/https://doi.org/10.1533/9781845697815.1.3>
- Behera, B. K., Hari, P. K., & Textile Institute, S. (2010). *Woven Textile Structure: Theory and Applications* (Vol. 115) <https://doi.org/10.1533/9781845697815>
- Bell, D. (2019). *Nike smart shoe is a giant leap forward for wearable tech that could redefine the sneaker*. Retrieved 7 August 2021 from <https://www.t3.com/news/nike-adapt-bb-self-lacing-smart-shoes-are-a-giant-leap-back-to-the-future>
- Bennett, A., Beiderman, Y., Agdarov, S., Beiderman, Y., Hendel, R., Straussman, B., & Zalevsky, Z. (2020). Monitoring of vital bio-signs by analysis of speckle patterns in a fabric-integrated multimode optical fiber sensor. *Optics express*, 28(14), 20830-20844. <https://doi.org/10.1364/OE.384423>
- Bivainyte, A., Mikučionienė, D., & Kerpauskas, P. (2012). Investigation on thermal properties of double-layered weft knitted fabrics. *Medžiagotyra*, 18(2), 167-171. <https://doi.org/10.5755/j01.ms.18.2.1921>
- BodiTrak. (2023). *BodiTrak Pressure Mat*. Retrieved 11 April 2023 from <https://boditrakbiometrics.com/pressure-mapping-technology/>
- Boston Orthotics & Prosthetics. (2017). *The Boston T*. Retrieved 28 April 2020 from <https://www.bostonoandp.com/products/scoliosis-and-spine/boston-t/>
- Botens-Helmus, C., Klein, R., & Stephan, C. (2006). The reliability of the Bad Sobernheim Stress Questionnaire (BSSQbrace) in adolescents with scoliosis during brace treatment. *Scoliosis*, 1(1), 22-22. <https://doi.org/10.1186/1748-7161-1-22>

- Brigham, E. M. M. D., & Armstrong, D. G. M. D. (2016). Motivations for Compliance With Bracing in Adolescent Idiopathic Scoliosis. *Spine Deform*, 5(1), 46-51. <https://doi.org/10.1016/j.jspd.2016.09.004>
- Broega, A., Nogueira, C., Silva, M. E., & Lima, M. (2010). *Sensory comfort evaluation of wool fabrics by objective assessment of surface mechanical properties* AUTEX 2010 World Textile Conference, Vilnius. <https://repositorium.uminho.pt/bitstream/1822/12941/1/SENSORY%20COMFORT%20EVALUATION%20OF%20WOOL%20FABRICS%20BY%20OBJECTIVE%20ASSESSMENT.pdf>
- Bunge, E. M., de Bekker-Grob, E. W., van Biezen, F. C., Essink-Bot, M.-L., & de Koning, H. J. (2010). Patients' Preferences for Scoliosis Brace Treatment A Discrete Choice Experiment. *Spine (Phila Pa 1976)*, 35(1), 57-63. <https://doi.org/10.1097/BRS.0b013e3181bdeaa6>
- Busscher, I., Wapstra, F. H., & Veldhuizen, A. G. (2010). Predicting growth and curve progression in the individual patient with adolescent idiopathic scoliosis: design of a prospective longitudinal cohort study. *BMC Musculoskelet Disord*, 11(1), 93-93. <https://doi.org/10.1186/1471-2474-11-93>
- Canavese, F., & Kaelin, A. (2011). Adolescent idiopathic scoliosis: Indications and efficacy of nonoperative treatment. *Indian J Orthop*, 45(1), 7-14. <https://doi.org/10.4103/0019-5413.73655>
- Cao, H., Branson, D. H., Peksoz, S., Nam, J., & Farr, C. A. (2016). Fabric Selection for a Liquid Cooling Garment. *Textile research journal*, 76(7), 587-595. <https://doi.org/10.1177/0040517506067375>
- Carmo, J. P., Da Silva, A. M. F., Rocha, R. P., & Correia, J. H. (2012). Application of Fiber Bragg Gratings to Wearable Garments. *IEEE Sensors Journal*, 12(1), 261-266. <https://doi.org/10.1109/JSEN.2011.2161281>
- Castano, L. M., & Flatau, A. B. (2014). Smart fabric sensors and e-textile technologies: a review. *Smart Materials and Structures*, 23(5), 053001. <https://doi.org/10.1088/0964-1726/23/5/053001>
- Chalmers, E., Lou, E., Hill, D., Zhao, V. H., & Man-Sang, W. (2012). Development of a Pressure Control System for Brace Treatment of Scoliosis. *IEEE Trans Neural Syst Rehabil Eng*, 20(4), 557-563. <https://doi.org/10.1109/TNSRE.2012.2192483>

- Chan, S. L., Cheung, K. M. C., Luk, K. D. K., Wong, K. W. H., & Wong, M. S. (2014). A correlation study between in-brace correction, compliance to spinal orthosis and health-related quality of life of patients with Adolescent Idiopathic Scoliosis. *PolyU IRA*, 12. <https://doi.org/10.1186/1748-7161-9-1>
- Chan, W.Y., Yip, J., Yick, K.-L., Ng, S.-P., Lu, L., Cheung, K. M.-C., Kwan, K. Y.-H., Cheung, J. P.-Y., Yeung, K. W.-K., & Tse, C.-Y. (2018). Mechanical and Clinical Evaluation of a Shape Memory Alloy and Conventional Struts in a Flexible Scoliotic Brace. *Annals of Biomedical Engineering*, 46(8), 1194-1205. <https://doi.org/10.1007/s10439-018-2016-8>
- Chan, W. Y. (2019). *Evaluation and enhancement of thermal and mechanical performance of posture correction girdle for adolescent idiopathic scoliosis (AIS)*. [Doctoral dissertation, The Hong Kong Polytechnic University]. <https://theses.lib.polyu.edu.hk/handle/200/10231>
- Chan, W. Y., Yip, J., Yick, K.-L., Ng, S.-P., Lu, L., Cheung, K. M.-C., Kwan, K. Y.-H., Cheung, J. P.-Y., Yeung, K. W.-K., & Tse, C.-Y. (2018). Mechanical and Clinical Evaluation of a Shape Memory Alloy and Conventional Struts in a Flexible Scoliotic Brace. *Annals of Biomedical Engineering*, 46(8), 1194-1205. <https://doi.org/https://doi.org/10.1007/s10439-018-2016-8>
- Chen, Y.-C., Chen, L.-W., & Lu, W.-H. (2011). Power loss characteristics of a sensing element based on a polymer optical fiber under cyclic tensile elongation. *Sensors*, 11(9), 8741-8750. <https://doi.org/10.3390/s110908741>
- Chong, H. K. S. (2013). Study the relationship between UV protection and knitted fabric structure. In.
- Clin, J., Aubin, C.-E., Parent, S., Sangole, A., & Labelle, H. (2010). Comparison of the biomechanical 3D efficiency of different brace designs for the treatment of scoliosis using a finite element model. *Eur Spine J*, 19(7), 1169-1178. <https://doi.org/10.1007/s00586-009-1268-2>
- Clin, J., Aubin, C.-E., Sangole, A., Labelle, H., & Parent, S. (2010). Correlation Between Immediate In-Brace Correction and Biomechanical Effectiveness of Brace Treatment in Adolescent Idiopathic Scoliosis. *Spine (Phila Pa 1976)*, 35(18), 1706-1713. <https://doi.org/10.1097/BRS.0b013e3181cb46f6>

- Coillard, C., Leroux, M. A., Zabjek, K. F., & Rivard, C. (2003). SpineCor – a non-rigid brace for the treatment of idiopathic scoliosis: post-treatment results. *Eur Spine J*, 12(2), 141-148. <https://doi.org/10.1007/s00586-002-0467-x>
- Colicchia, C., & Strozzi, F. (2012). Supply chain risk management: a new methodology for a systematic literature review. *Supply Chain Management: An International Journal*, 17(4), 403-418.
- Corning Incorporated. (2013). Fiber 101. [https://www.youtube.com/watch?v=N\\_kA8EpCUQo](https://www.youtube.com/watch?v=N_kA8EpCUQo)
- Costa, J. C., Spina, F., Lugoda, P., Garcia-Garcia, L., Roggen, D., & Münzenrieder, N. (2019). Flexible Sensors—From Materials to Applications. *Technologies (Basel)*, 7(2), 35. <https://doi.org/10.3390/technologies7020035>
- Da Silva, A. F., Goncalves, A. F., Mendes, P. M., & Correia, J. H. (2011). FBG Sensing Glove for Monitoring Hand Posture. *IEEE Sensors Journal*, 11(10), 2442-2448. <https://doi.org/10.1109/JSEN.2011.2138132>
- Da Silva, A.F., Rocha. R. P.,Carmo, J.P., & Correia, J.H. (2013). Photonic Sensors Based on Flexible Materials with FBGs for Use on Biomedical Applications. In Current trends in short-and long-period fiber gratings. IntechOpen. <https://www.intechopen.com/books/current-trends-in-short-and-long-period-fiber-gratings/photonic-sensors-based-on-flexible-materials-with-fbgs-for-use-on-biomedical-applications>
- Das, S., Paul, D., Hasan, S., Chowdhury, N., & Nizam, M. E. H. (2013). Smart Textiles-New Possibilities in Textile Engineering. *Journal of Polymer and Textile Engineering*, 1(1), 1-4.
- Dewald, R. L. (2003). *Spinal deformities: the comprehensive text*. Thieme.
- Diab, M., Smith, A. R., & Kuklo, T. R. (2007). Neural Complications in the Surgical Treatment of Adolescent Idiopathic Scoliosis. *Spine (Phila Pa 1976)*, 32(24), 2759-2763. <https://doi.org/10.1097/brs.0b013e31815a5970>
- Dolan, L. A., Donnelly, M. J., Spratt, K. F., & Weinstein, S. L. (2007). Professional Opinion Concerning the Effectiveness of Bracing Relative to Observation in Adolescent Idiopathic Scoliosis. *J Pediatr Orthop*, 27(3), 270-276. <https://doi.org/10.1097/01.bpb.0000248579.11864.47>

- Dublin. (2023). *Global Smart Fabrics Strategic Markets Report 2023: Market to Reach \$20.6 Billion by 2030 - Industry Evolves from Passive to Active to Ultra-Smart Textiles*. Globe Newswire. Retrieved 11 April 2023 from <https://www.globenewswire.com/en/news-release/2023/02/09/2605396/28124/en/Global-Smart-Fabrics-Strategic-Markets-Report-2023-Market-to-Reach-20-6-Billion-by-2030-Industry-Evolves-from-Passive-to-Active-to-Ultra-Smart-Textiles.html>
- Dziuda, Ł., Skibniewski, F. W., Krej, M., & Baran, P. M. (2013). Fiber Bragg grating-based sensor for monitoring respiration and heart activity during magnetic resonance imaging examinations. *J. Biomed. Opt.*, 18(5), 057006-057006. <https://doi.org/10.1117/1.JBO.18.5.057006>
- El-Sherif, M. (2005). *6 - Integration of fibre optic sensors and sensing networks into textile structures*. Woodhead Publishing. <https://doi.org/10.1533/9781845690441.105>
- Emans, J., Hedequist, D., Miller, R., Cassella, M., Hresko, M., Karlin, L., Magin, M., Ryan, K., Hall, J., & Miller, J. (2003). Reference manual for the Boston scoliosis brace. *Milwaukee, WI: Scoliosis Research Society*.
- Embraced in Comfort. (2021). *A Scoliosis Brace T-Shirt*. Retrieved 28 April 2023 from <https://embracedincomfort.com/home%2Fshop/ols/products/scoliosis-brace-t-shirt>
- Erdumlu, N., & Saricam, C. (2017). Investigating the effect of some fabric parameters on the thermal comfort properties of flat knitted acrylic fabrics for winter wear. *Textile research journal*, 87(11), 1349-1359.
- Fajkus, M., Nedoma, J., Martinek, R., Vasinek, V., Nazeran, H., & Siska, P. (2017). A Non-Invasive Multichannel Hybrid Fiber-Optic Sensor System for Vital Sign Monitoring. *Sensors*, 17(1), 111. <https://doi.org/10.3390/s17010111>
- Fan, D., Lo, C. K. Y., Ching, V., & Kan, C. W. (2014). Occupational health and safety issues in operations management: A systematic and citation network analysis review. *International journal of production economics*, 158, 334-344. <https://doi.org/10.1016/j.ijpe.2014.07.025>
- Fayssoux, R. S., Cho, R. H., & Herman, M. J. (2010). A History of Bracing for Idiopathic Scoliosis in North America. *Clin Orthop Relat Res*, 468(3), 654-664. <https://doi.org/10.1007/s11999-009-0888-5>
- Fok, L. H. (2020). *Functional intimate apparel for adolescents with scoliosis*. [Doctoral dissertation, The Hong Kong Polytechnic University]. PolyU e-Theses. <https://theses.lib.polyu.edu.hk/handle/200/10816>

- Fok, Q., Yip, J., Yick, K.-l., & Ng, S.-p. (2021). Design and fabrication of an anisotropic textile brace for exerting corrective forces on spinal curvature. *Journal of Industrial Textiles*, 51(1\_suppl), 1682S-1702S.  
<https://doi.org/10.1177/15280837211032619>
- Fok, Q., & Yip, J. (2021). *Applying Numerical Simulation to Predict Effect of Brace Wear for Scoliosis*. International Conference on Applied Human Factors and Ergonomics.
- Forney, K. J., Keel, P. K., apos, Connor, S., Sisk, C., Burt, S. A., & Klump, K. L. (2019). Interaction of hormonal and social environments in understanding body image concerns in adolescent girls. *J Psychiatr Res*, 109, 178-184.  
<https://doi.org/10.1016/j.jpsychires.2018.12.008>
- Fujiibo. Holdings. INC. (2021). *Life Style Apparel Business*. Retrieved 20 May 2021 from <http://www.fujiibo.co.jp/division/textile/product06.html>
- Fujiwara, E., Ferreira Marques Dos Santos, M., & Suzuki, C. K. (2014). Flexible Optical Fiber Bending Transducer for Application in Glove-Based Sensors. *JSEN*, 14(10), 3631-3636.  
<https://doi.org/10.1109/jsen.2014.2330998>
- Fuss, F. K., Ahmad, A., Tan, A. M., Razman, R., & Weizman, Y. (2021). Pressure Sensor System for Customized Scoliosis Braces. *Sensors*, 21(4).  
<https://doi.org/10.3390/s21041153>
- Fung, H. Y. (2020). Ergonomic brace wear for adolescent idiopathic scoliosis (AIS). In J. Yip, K.-l. Yick, T. Institute of, & Clothing (Eds.).
- Future Markets Inc. (2018). *The Global Market for Wearables and Smart Textiles to 2027*. Retrieved 7 August 2020 from <https://www.researchandmarkets.com/reports/4429956/the-global-market-for-wearables-and-smart>
- Ghadikolaee, M. S., Sharifmoradi, K., Karimi, M. T., & Tafti, N. (2020). Evaluation of a Functional Brace in ACL-Deficient Subjects Measuring Ground Reaction Forces and Contact Pressure: A Pilot Study. *JPO: Journal of Prosthetics and Orthotics*, 32(2).  
[https://journals.lww.com/jpojournl/Fulltext/2020/04000/Evaluation\\_of\\_a\\_Functional Brace\\_in\\_ACL\\_Deficient.10.aspx](https://journals.lww.com/jpojournl/Fulltext/2020/04000/Evaluation_of_a_Functional_Brace_in_ACL_Deficient.10.aspx)
- Gignac, D., Aubin, C. É., Dansereau, J., & Labelle, H. (2000). Optimization method for 3D bracing correction of scoliosis using a finite element model. *Eur Spine J*, 9(3), 185-190.  
<https://doi.org/10.1007/s005860000135>



- Gong, Z., Xiang, Z., OuYang, X., Zhang, J., Lau, N., Zhou, J., & Chan, C. C. (2019). Wearable Fiber Optic Technology Based on Smart Textile: A Review. *Materials*, 12(20), 3311. <https://doi.org/10.3390/ma12203311>
- Grillet, A., Kinet, D., Witt, J., Schukar, M., Krebber, K., Pirotte, F., & Depre, A. (2008). Optical Fiber Sensors Embedded Into Medical Textiles for Healthcare Monitoring. *JSEN*, 8(7), 1215-1222. <https://doi.org/10.1109/JSEN.2008.926518>
- Grivas, T. B., de Mauroy, J. C., Wood, G., Rigo, M., Hresko, M. T., Kotwicki, T., & Negrini, S. (2018). Retraction Note: Brace classification study group (BCSG): part one - definitions and atlas. *Scoliosis Spinal Disord*, 13(1), 25. <https://doi.org/10.1186/s13013-018-0171-1>
- Grivas, T. B., Vasiliadis, E., Mouzakis, V., Mihas, C., & Koufopoulos, G. (2006). Association between adolescent idiopathic scoliosis prevalence and age at menarche in different geographic latitudes. *Scoliosis*, 1(1), 9-9. <https://doi.org/10.1186/1748-7161-1-9>
- Grundy, T. (2021). *Hong Kong records hottest day in May since records began, as mercury hits 36.1°C on Sunday*. Retrieved 16 August 2021 from <https://hongkongfp.com/2021/05/23/hong-kong-records-hottest-day-in-may-since-records-began-as-mercury-hits-36-7%E2%84%83-on-sunday/>
- Guo, J., Zhao, K., Zhou, B., Ning, W., Jiang, K., Yang, C., Kong, L., & Dai, Q. (2019a). Wearable and Skin-Mountable Fiber-Optic Strain Sensors Interrogated by a Free-Running, Dual-Comb Fiber Laser. *Advanced optical materials*, 7(12), 1900086-n/a. <https://doi.org/10.1002/adom.201900086>
- Guo, J., Zhou, B., Yang, C., Dai, Q., & Kong, L. (2019b). Stretchable and Temperature-Sensitive Polymer Optical Fibers for Wearable Health Monitoring. *Advanced functional materials*, 29(33), 1902898-n/a. <https://doi.org/10.1002/adfm.201902898>
- Guo, K., He, J., Shao, L., Xu, G., & Wang, Y. (2020). Simultaneous measurement of strain and temperature by a sawtooth stressor-assisted highly birefringent fiber Bragg grating. *Journal of Lightwave Technology*, 38(7), 2060-2066.
- Hartmans, A. (2019). *Levi's and Google are launching new denim jackets that can answer phone calls and control your music*. Retrieved 7 August 2020 from <https://www.businessinsider.com/levis-google-jacquard-smart-denim-jacket-price-photos-2019-9>
- Harvard Medical School. (2016). *Harvard Medical School health topics A-Z*. Harvard Health Publications.

- Havey, R., Gavin, T., Patwardhan, A., Pawelczak, S., Ibrahim, K., Andersson, G. B. J., & Lavender, S. (2002). A reliable and accurate method for measuring orthosis wearing time. *Spine (Phila Pa 1976)*, 27(2), 211-214. <https://doi.org/10.1097/00007632-200201150-00018>
- Health Care & Co. (2020). *BodiTrak Pressure Mapping System*. Retrieved 11 August 2020 from <https://www.healthcarehk.com/product/boditrak-pressure-mapping-system/>
- Hill, K. O., & Meltz, G. (1997). Fiber Bragg grating technology fundamentals and overview. *Journal of Lightwave Technology*, 15(8), 1263-1276. <https://doi.org/10.1109/50.618320>
- Horng, M.-H., Kuok, C.-P., Fu, M.-J., Lin, C.-J., & Sun, Y.-N. (2019). Cobb angle measurement of spine from X-ray images using convolutional neural network. *Computational and mathematical methods in medicine*, 2019.
- Hresko, M. T. (2013). Clinical practice. Idiopathic scoliosis in adolescents. *N Engl J Med*, 368(9), 834.
- Hummon, N. P., & Dereian, P. (1989). Connectivity in a citation network: The development of DNA theory. *Social networks*, 11(1), 39-63. [https://doi.org/10.1016/0378-8733\(89\)90017-8](https://doi.org/10.1016/0378-8733(89)90017-8)
- International Schroth Three Dimensional Scoliosis Therapy. (2023). *Schroth method*. Retrieved 11 April 2023 from <https://www.scoliosis-rehabilitation.com/schroth-method/>
- Jayaraman, S., & Park, S. (2010). Georgia Tech Wearable Motherboard: The Intelligent Garment for the 21st Century. *Retrieved*, 6, 18.
- Jeguirim, S. E.-G., Dhouib, A. B., Sahnoun, M., Cheikhrouhou, M., Njeugna, N., Schacher, L., & Adolphe, D. (2010). The Tactile Sensory Evaluation of Knitted Fabrics: Effect of Some Finishing Treatments. *Journal of sensory studies*, 25(2), 201-215. <https://doi.org/10.1111/j.1745-459X.2009.00251.x>
- Jha, C. K., Agarwal, S., Chakraborty, A. L., & Shirpurkar, C. (2019). An FBG-Based Sensing Glove to Measure Dynamic Finger Flexure with an Angular Resolution of 0.1 degrees up to Speeds of 80 degrees/s. *Journal of lightwave technology*, 37(18), 4734-4740. <https://doi.org/10.1109/JLT.2019.2919496>
- Jonghun, L. (2011). Characteristics of Fiber Bragg Grating Temperature Sensor using Thermal Strain of an External Tube. *J. Korean Phys. Soc.*, 59(51), 3188. <https://doi.org/10.3938/jkps.59.3188>

- Kanellos, G. T., Papaioannou, G., Tsiokos, D., Mitrogiannis, C., Nianios, G., & Pleros, N. (2010). Two dimensional polymer-embedded quasi-distributed FBG pressure sensor for biomedical applications. *Opt Express*, 18(1), 179-186. <https://doi.org/10.1364/OE.18.000179>
- Kar, J., Fan, J., & Yu, W. (2011). 10 - Women's apparel: knitted underwear. In K. F. Au (Ed.), *Advances in Knitting Technology* (pp. 235-261). Woodhead Publishing. <https://doi.org/https://doi.org/10.1533/9780857090621.3.235>
- Katayama, K., Chino, S., Koyama, S., Ishizawa, H., & Fujimoto, K. (2020). Verification of Blood Pressure Monitoring System Using Optical Fiber Sensor: Tracing Sudden Blood Pressure Changes. *JFST*, 76(2), 79-87. <https://doi.org/10.2115/fiberst.2020-0008>
- Kato Tech. (2021a). KES-FB1-A/AW Tensile and Shear Tester. In: Kato Tech Co. Ltd.
- Kato Tech. (2021b). KES-FB2-A Pure Bending Tester. In: Kato Tech Co. Ltd.
- Kato Tech. (2021c). KES-FB3-A Compression Tester. In: Kato Tech Co. Ltd.
- Kato Tech. (2021d). KES-FB4-A Surface Tester. In: Kato Tech Co. Ltd.
- Katz, D. E., & Durrani, A. A. (2001). Factors That Influence Outcome in Bracing Large Curves in Patients with Adolescent Idiopathic Scoliosis. *Spine (Phila Pa 1976)*, 26(21), 2354-2361. <https://doi.org/10.1097/00007632-200111010-00012>
- Kennedy, J. D., Robertson, C. F., Olinsky, A., Dickens, D. R., & Phelan, P. D. (1987). Pulmonary restrictive effect of bracing in mild idiopathic scoliosis. *Thorax*, 42(12), 959-961. <https://doi.org/10.1136/thx.42.12.959>
- Khoddam-Khorasani, P., Arjmand, N., & Shirazi-Adl, A. (2018). Trunk Hybrid Passive–Active Musculoskeletal Modeling to Determine the Detailed T12–S1 Response Under In Vivo Loads. *Ann Biomed Eng*, 46(11), 1830-1843. <https://doi.org/10.1007/s10439-018-2078-7>
- Kim, H. J., Kleuver, M. d., & Luk, K. (2013). *Lenke Classification*. Retrieved 19 August 2020 from <https://surgeryreference.aofoundation.org/spine/deformities/adolescent-idiopathic-scoliosis/further-reading/lenke-classification#introduction>
- Ko, E., Sung, H., & Yun, H. (2009). Comparative Analysis of Purchase Intentions Toward Smart Clothing Between Korean and U.S. Consumers. *Clothing and Textiles Research Journal*, 27(4), 259-273. <https://doi.org/10.1177/0887302X08327086>

- Koncar, V. (2016). *1 - Introduction to smart textiles and their applications*. Woodhead Publishing. <https://doi.org/10.1016/B978-0-08-100574-3.00001-1>
- Konieczny, M. R., Hieronymus, P., & Krauspe, R. (2017). Time in brace: where are the limits and how can we improve compliance and reduce negative psychosocial impact in patients with scoliosis? A retrospective analysis. *Spine J*, 17(11), 1658-1664. <https://doi.org/10.1016/j.spinee.2017.05.010>
- Kotwicki, T., Kinel, E., Stryła, W., & Szulc, A. (2007). Estimation of the stress related to conservative scoliosis therapy: an analysis based on BSSQ questionnaires. *Scoliosis*, 2(1), 1-1. <https://doi.org/10.1186/1748-7161-2-1>
- Kotwicki, T., Pietrzak, S., & Szulc, A. (2002). Three-dimensional action of Cheneau brace on thoracolumbar scoliosis. *Studies in health technology and informatics*, 226-229.
- Koyama, S., Sakaguchi, A., Ishizawa, H., Yasue, K., Oshiro, H., & Kimura, H. (2017). Vital Sign Measurement Using Covered FBG Sensor Embedded into Knitted Fabric for Smart Textile. *JFST*, 73(11), 300-308. <https://doi.org/10.2115/fiberst.2017-0046>
- Koyama, Y., Nishiyama, M., & Watanabe, K. (2013). A Motion Monitor Using Hetero-Core Optical Fiber Sensors Sewed in Sportswear to Trace Trunk Motion. *IEEE transactions on instrumentation and measurement*, 62(4), 828-836. <https://doi.org/10.1109/TIM.2013.2241534>
- Koyama, Y., Nishiyama, M., & Watanabe, K. (2018). Behavior Monitoring Based on Intensity Matrix Distribution in Output Plane of Single-Mode Fiber Bundle. *IEEE transactions on instrumentation and measurement*, 67(4), 930-937. <https://doi.org/10.1109/TIM.2017.2786676>
- Krehel, M., Rossi, R. M., Bona, G.-L., & Scherer, L. J. (2013). Characterization of flexible copolymer optical fibers for force sensing applications. *Sensors*, 13(9), 11956-11968. <https://doi.org/10.3390/s130911956>
- Krehel, M., Schmid, M., Rossi, R., Boesel, L., Bona, G.-L., & Scherer, L. (2014a). An Optical Fibre-Based Sensor for Respiratory Monitoring. *Sensors*, 14(7), 13088-13101. <https://doi.org/10.3390/s140713088>
- Krehel, M., Wolf, M., Boesel, L. F., Rossi, R. M., Bona, G.-L., & Scherer, L. J. (2014b). Development of a luminous textile for reflective pulse oximetry measurements. *Biomed Opt Express*, 5(8), 2537-2547. <https://doi.org/10.1364/BOE.5.002537>

- Krishna, S. (2017). *Modal Fiber, It's Properties (Chemical and Physical) and Uses in Apparel Industry*. Slide Share. Retrieved 7 September 2020 from <https://www.slideshare.net/SwathiKrishna21/modal-fiber>
- Křištof, M., Hudák, R., Takáčová, A., Zivčák, J., Fialka, L., & Takáč, R. (2010). Contact pressure measurement in trunk orthoses. In (pp. 175-179).
- Kulichenko, A. (2005). Theoretical analysis, calculation, and prediction of the air permeability of textiles. *Fibre Chemistry*, 37(5), 371-380.
- Lai, C. H. Y., & Li-Tsang, C. W. P. (2009). Validation of the Pliance X System in measuring interface pressure generated by pressure garment. *Burns*, 35(6), 845-851. <https://doi.org/https://doi.org/10.1016/j.burns.2008.09.013>
- Lam, P. T. S. (2007). Recent developments in flexible wearable electronics for monitoring applications. *Transactions of the Institute of Measurement & Control*, 29(3-4), 283-300. <https://doi.org/10.1177/0142331207070389>
- Lakho, R. A., Yi-Fan, Z., Jin-Hua, J., Cheng-Yu, H., & Ahmed Abro, Z. (2019). A smart insole for monitoring plantar pressure based on the fiber Bragg grating sensing technique. *Textile Research Journal*, 89(17), 3433-3446. <https://doi.org/10.1177/0040517519833977>
- Landauer, F., Wimmer, C., & Behensky, H. (2003). Estimating the final outcome of brace treatment for idiopathic thoracic scoliosis at 6-month follow-up. *Pediatr Rehabil*, 6(3-4), 201-207. <https://doi.org/10.1080/13638490310001636817>
- Leal-Junior, A. G., Diaz, C. A. R., Avellar, L. M., Pontes, M. J., Marques, C., & Frizera, A. (2019a). Polymer Optical Fiber Sensors in Healthcare Applications: A Comprehensive Review. *Sensors*, 19(14), 3156. <https://doi.org/10.3390/s19143156>
- Leal-Junior, A. G., Díaz, C. R., Leitão, C., Pontes, M. J., Marques, C., & Frizera, A. (2019b). Polymer optical fiber-based sensor for simultaneous measurement of breath and heart rate under dynamic movements. *Optics and laser technology*, 109, 429-436. <https://doi.org/10.1016/j.optlastec.2018.08.036>
- Leal-Junior, A. G., Díaz, C. R., Marques, C., Pontes, M. J., & Frizera, A. (2019c). 3D-printed POF insole: Development and applications of a low-cost, highly customizable device for plantar pressure and ground reaction forces monitoring. *Optics and laser technology*, 116, 256-264. <https://doi.org/10.1016/j.optlastec.2019.03.035>

- Leal-Junior, A. G., Frizera, A., Vargas-Valencia, L., dos Santos, W. M., Bo, A. P. L., Siqueira, A. A. G., & Pontes, M. J. (2018). Polymer Optical Fiber Sensors in Wearable Devices: Toward Novel Instrumentation Approaches for Gait Assistance Devices. *JSEN*, 18(17), 7085-7092. <https://doi.org/10.1109/jsen.2018.2852363>
- Leber, A., Cholst, B., Sandt, J., Vogel, N., & Kolle, M. (2019). Stretchable Optical Fibers: Stretchable Thermoplastic Elastomer Optical Fibers for Sensing of Extreme Deformations (Adv. Funct. Mater. 5/2019). *Advanced functional materials*, 29(5), 1970030-n/a. <https://doi.org/10.1002/adfm.201970030>
- Lee, K.-P., Yip, J., Kan, C.-W., Chiou, J.-C., & Yung, K.-F. (2020). Reusable Face Masks as Alternative for Disposable Medical Masks: Factors that Affect their Wear-Comfort. *International Journal of Environmental Research and Public Health*, 17(18), 6623. <https://www.mdpi.com/1660-4601/17/18/6623>
- Lee, K.-P., Yip, J., Yick, K.-L., Lu, C., & Lo, C. K. (2022). Textile-based fiber optic sensors for health monitoring: A systematic and citation network analysis review. *Textile Research Journal*, 92(15-16), 2922-2934. <https://doi.org/10.1177/00405175211036206>
- Lenke, L. G., Betz, R. R., Haher, T. R., Lapp, M. A., Merola, A. A., Harms, J., & Shufflebarger, H. L. (2001). Multisurgeon assessment of surgical decision-making in adolescent idiopathic scoliosis: curve classification, operative approach, and fusion levels. *Spine (Phila Pa 1976)*, 26(21), 2347-2353. <https://doi.org/10.1097/00007632-200111010-00011>
- Li, H., Yang, H., Li, E., Liu, Z., & Wei, K. (2012). Wearable sensors in intelligent clothing for measuring human body temperature based on optical fiber Bragg grating. *Opt Express*, 20(11), 11740-11752. <https://doi.org/10.1364/oe.20.011740>
- Li, J., Liu, J., Li, C., Zhang, H., & Li, Y. (2020). Wearable Wrist Movement Monitoring Using Dual Surface-Treated Plastic Optical Fibers. *Materials*, 13(15), 3291. <https://doi.org/10.3390/ma13153291>
- Li, J. h., Chen, J. h., & Xu, F. (2018). Sensitive and Wearable Optical Microfiber Sensor for Human Health Monitoring. *Advanced materials technologies*, 3(12), 1800296-n/a. <https://doi.org/10.1002/admt.201800296>
- Li, K., Chan, T. H., Yau, M. H., Thambiratnam, D. P., & Tam, H. Y. (2019). Maximum amplification of a string transverse-force amplifier in fiber Bragg grating accelerometers. *OSA Continuum*, 2(3), 938-945.

- Li, Q., Sun, G., Chen, Y., Chen, X., Shen, Y., Xie, H., & Li, Y. (2022). Fabricated leg mannequin for the pressure measurement of compression stockings. *Textile Research Journal*, 92(19-20), 3500-3510.
- Lo Presti, D., Romano, C., Massaroni, C., D'Abbraccio, J., Massari, L., Caponero, M. A., Oddo, C. M., Formica, D., & Schena, E. (2019). Cardio-Respiratory Monitoring in Archery Using a Smart Textile Based on Flexible Fiber Bragg Grating Sensors. *Sensors*, 19(16), 3581. <https://doi.org/10.3390/s19163581>
- Lonstein, D. (1994). Adolescent idiopathic scoliosis. *Lancet*, 344(8934), 1407-1412. [https://doi.org/10.1016/s0140-6736\(94\)90572-x](https://doi.org/10.1016/s0140-6736(94)90572-x)
- Lonstein, J. E. (2006). Scoliosis: surgical versus nonsurgical treatment. *Clinical Orthopaedics and Related Research (1976-2007)*, 443, 248-259.
- Lou, E., Hill, D., Hedden, D., Mahood, J., Moreau, M., & Raso, J. (2010a). An objective measurement of brace usage for the treatment of adolescent idiopathic scoliosis. *Med Eng Phys*, 33(3), 290-294. <https://doi.org/10.1016/j.medengphy.2010.10.016>
- Lou, E., Hill, D. L., & Raso, J. V. (2010b). A wireless sensor network system to determine biomechanics of spinal braces during daily living. *Med Biol Eng Comput*, 48(3), 235-243. <https://doi.org/10.1007/s11517-010-0575-4>
- Lou, E., Raso, J. V., Hill, D. L., Durdle, N. G., Mahood, J. K., & Moreau, M. J. (2002). The daily force pattern of spinal orthoses in subjects with adolescent idiopathic scoliosis. *Prosthet Orthot Int*, 26(1), 58-63. <https://doi.org/10.1080/03093640208726622>
- Lu, L. (2017). Development of an adaptive corset for children with spinal deformities. In K.-l. Yick, J. Yip, S.-p. Ng, T. Institute of, & Clothing (Eds.): Hong Kong Polytechnic University.
- Mac-Thiong, J.-M., Petit, Y., Aubin, C.-É., Delorme, S., Dansereau, J., & Labelle, H. (2004). Biomechanical Evaluation of the Boston Brace System for the Treatment of Adolescent Idiopathic Scoliosis: Relationship between Strap Tension and Brace Interface Forces. *Spine*, 29(1), 26-32. <https://doi.org/10.1097/01.BRS.0000103943.25412.E9>
- Majumdar, A. (2011). Modelling of thermal conductivity of knitted fabrics made of cotton–bamboo yarns using artificial neural network. *The Journal of The Textile Institute*, 102(9), 752-762. <https://doi.org/10.1080/00405000.2010.516929>
- Mak, A. F. T., Zhang, M., & Tam, E. W. C. (2010). Biomechanics of pressure ulcer in body tissues interacting with external forces during locomotion. *Annu Rev Biomed Eng*, 12(1), 29-53. <https://doi.org/10.1146/annurev-bioeng-070909-105223>

- Martínez-Llorens, J., Ramírez, M., Colomina, M. J., Bagó, J., Molina, A., Cáceres, E., & Gea, J. (2010). Muscle dysfunction and exercise limitation in adolescent idiopathic scoliosis. *Eur Respir J*, 36(2), 393-400. <https://doi.org/10.1183/09031936.00025509>
- Massaroni, C., Saccomandi, P., Formica, D., Lo Presti, D., Caponero, M. A., Di Tomaso, G., Giurazza, F., Muto, M., & Schena, E. (2016). Design and Feasibility Assessment of a Magnetic Resonance-Compatible Smart Textile Based on Fiber Bragg Grating Sensors for Respiratory Monitoring. *JSEN*, 16(22), 8103-8110. <https://doi.org/10.1109/jsen.2016.2606487>
- Massaroni, C., Saccomandi, P., & Schena, E. (2015). Medical Smart Textiles Based on Fiber Optic Technology: An Overview. *Journal of Functional Biomaterials*, 6(2), 204-221. <https://www.mdpi.com/2079-4983/6/2/204>
- Massaroni, C., Venanzi, C., Silvatti, A. P., Lo Presti, D., Saccomandi, P., Formica, D., Giurazza, F., Caponero, M. A., & Schena, E. (2018). Smart textile for respiratory monitoring and thoraco-abdominal motion pattern evaluation. *J Biophotonics*, 11(5), e201700263-n/a. <https://doi.org/10.1002/jbio.201700263>
- McGregor, B. A., Stanton, J., Beilby, J., Speijers, J., & Tester, D. (2015). The influence of fiber diameter, fabric attributes and environmental conditions on wetness sensations of next-to-skin knitwear. *Textile research journal*, 85(9), 912-928. <https://doi.org/10.1177/0040517514555800>
- Misterska, E., Głowacki, J., Głowacki, M., & Okręt, A. (2018). Long-term effects of conservative treatment of Milwaukee brace on body image and mental health of patients with idiopathic scoliosis. *PLoS One*, 13(2), e0193447. <https://doi.org/10.1371/journal.pone.0193447>
- Morton, A., Riddle, R., Buchanan, R., Katz, D., & Birch, J. (2008). Accuracy in the Prediction and Estimation of Adherence to Bracewear Before and During Treatment of Adolescent Idiopathic Scoliosis. *J Pediatr Orthop*, 28(3), 336-341. <https://doi.org/10.1097/BPO.0b013e318168d154>
- Nedoma, J., Fajkus, M., Martinek, R., & Nazeran, H. (2019). Vital Sign Monitoring and Cardiac Triggering at 1.5 Tesla: A Practical Solution by an MR-Ballistocardiography Fiber-Optic Sensor. *Sensors*, 19(3), 470. <https://doi.org/10.3390/s19030470>



- Negrini, S., Aulisa, A. G., Aulisa, L., Circo, A. B., de Mauroy, J. C., Durmala, J., Grivas, T. B., Knott, P., Kotwicki, T., Maruyama, T., Minozzi, S., apos, Brien, J. P., Papadopoulos, D., Rigo, M., Rivard, C. H., Romano, M., Wynne, J. H., Villagrasa, M., Weiss, H.-R., & Zaina, F. (2012). 2011 SOSORT guidelines: Orthopaedic and Rehabilitation treatment of idiopathic scoliosis during growth. *Scoliosis*, 7(1), 3-3. <https://doi.org/10.1186/1748-7161-7-3>
- Negrini, S., Minozzi, S., Bettany-Saltikov, J., Chockalingam, N., Grivas, T. B., Kotwicki, T., Maruyama, T., Romano, M., & Zaina, F. (2015). Braces for idiopathic scoliosis in adolescents. *Cochrane Database Syst Rev*, 2015(6), CD006850. <https://doi.org/10.1002/14651858.cd006850.pub3>
- Nishiyama, M., & Watanabe, K. (2009). Wearable Sensing Glove With Embedded Hetero-Core Fiber-Optic Nerves for Unconstrained Hand Motion Capture. *IEEE Transactions on Instrumentation and Measurement*, 58(12), 3995-4000. <https://doi.org/10.1109/TIM.2009.2021640>
- North Orthotics & Prosthetics Inc. (2020). *Scoliosis bracing systems*. Retrieved 24 August 2020 from <http://www.northeastoandp.com/scoliosis-bracing-systems>
- Novel GmbH. (2020). *Texsens®: mobile load measurement in the textile and garment industry*. Retrieved 11 August 2020 from <https://www.novel.de/products/texsens>
- Orlando Liposuction Specialty Clinic. (2023). *Scoliosis in Children*. Retrieved 19 April 2023 from <https://www.uscspine.com/childrens-spine-surgery/scoliosis/>
- Ovadia, D. (2013). Classification of adolescent idiopathic scoliosis (AIS). *J Child Orthop*, 7(1), 25-28. <https://doi.org/10.1007/s11832-012-0459-2>
- Pan, J., Zhang, Z., Jiang, C., Zhang, L., & Tong, L. (2020). A multifunctional skin-like wearable optical sensor based on an optical micro-/nanofibre. *Nanoscale*, 12(33), 17538-17544.
- Park, J., Yoo, H.-S., Hong, K. H., & Kim, E. (2018). Knitted fabric properties influencing coolness to the touch and the relationship between subjective and objective coolness measurements. *Textile research journal*, 88(17), 1931-1942. <https://doi.org/10.1177/0040517517715079>
- Périé, D., Aubin, C.-E., Petit, Y., Beauséjour, M., Dansereau, J., & Labelle, H. (2003). Boston brace correction in idiopathic scoliosis: A biomechanical study. *Spine (Philadelphia, Pa. 1976)*, 28(15), 1672-1677. <https://doi.org/10.1097/00007632-200308010-00008>

- Périé, D., Aubin, C. E., Petit, Y., Labelle, H., & Dansereau, J. (2004). Personalized biomechanical simulations of orthotic treatment in idiopathic scoliosis. *Clin Biomech (Bristol, Avon)*, 19(2), 190-195. <https://doi.org/10.1016/j.clinbiomech.2003.11.003>
- Peters, K. (2011). Polymer optical fiber sensors: a review. In (Vol. 20, pp. 013002).
- Philippine Daily Inquirer. (2016). *Adidas uses smart textiles for new fitness training collection*. Retrieved 7 August 2020 from <https://lifestyle.inquirer.net/234846/adidas-uses-smart-textiles-for-new-fitness-training-collection/>
- Plaszewski, M., & Bettany-Saltikov, J. (2014). Non-surgical interventions for adolescents with idiopathic scoliosis: an overview of systematic reviews. *PLoS One*, 9(10), e110254. <https://doi.org/10.1371/journal.pone.0110254>
- Plümpe, M., Beckers, M., Mecnika, V., Seide, G., Gries, T., & Bunge, C. A. (2017). 9 - Applications of polymer-optical fibres in sensor technology, lighting and further applications. In C.-A. Bunge, T. Gries, & M. Beckers (Eds.), *Polymer Optical Fibres* (pp. 311-335). Woodhead Publishing. <https://doi.org/https://doi.org/10.1016/B978-0-08-100039-7.00009-9>
- Presti, D. L., Massaroni, C., D'Abbraccio, J., Massari, L., Caponero, M., Longo, U. G., Formica, D., Oddo, C. M., & Schena, E. (2019). Wearable system based on flexible FBG for respiratory and cardiac monitoring. *IEEE Sensors Journal*, 19(17), 7391-7398.
- Qingqing, W., Jianhua, L., Liang, Z., Jiawen, Z., & Linlin, J. (2020). Effect of temperature and clothing thermal resistance on human sweat at low activity levels. *Building and Environment*, 183, 107117. <https://doi.org/https://doi.org/10.1016/j.buildenv.2020.107117>
- Qu, Y., Nguyen-Dang, T., Page, A. G., Yan, W., Das Gupta, T., Rotaru, G. M., Rossi, R. M., Favrod, V. D., Bartolomei, N., & Sorin, F. (2018). Superelastic Multimaterial Electronic and Photonic Fibers and Devices via Thermal Drawing. *Adv Mater*, 30(27), e1707251-n/a. <https://doi.org/10.1002/adma.201707251>
- Quandt, B. M., Boesel, L. F., & Rossi, R. M. (2018). Polymer optical fibres in healthcare: solutions, applications and implications. A perspective: Polymer optical fibres in healthcare. *Polymer international*, 67(9), 1150-1154. <https://doi.org/10.1002/pi.5511>
- Quandt, B. M., Braun, F., Ferrario, D., Rossi, R. M., Scheel-Sailer, A., Wolf, M., Bona, G.-L., Hufenus, R., Scherer, L. J., & Boesel, L. F. (2017). Body-monitoring with photonic textiles: a reflective heartbeat sensor based on polymer optical fibres. *Journal of the Royal Society interface*, 14(128), 20170060. <https://doi.org/10.1098/rsif.2017.0060>

- Quandt, B. M., Scherer, L. J., Boesel, L. F., Wolf, M., Bona, G.-L., & Rossi, R. M. (2015). Body-Monitoring and Health Supervision by Means of Optical Fiber-Based Sensing Systems in Medical Textiles. *Adv Healthc Mater*, 4(3), 330-355. <https://doi.org/10.1002/adhm.201400463>
- Rantala, J., Hännikäinen, J., & Vanhala, J. (2011). Fiber optic sensors for wearable applications. *Pers Ubiquit Comput*, 15(1), 85-96. <https://doi.org/10.1007/s00779-010-0303-y>
- Rathore, A. (2018). *Cotton Fibers and its Properties*. Textiles School. Retrieved 8 September 2020 from <https://www.textileschool.com/164/cotton-fibers-and-its-properties/>
- Rigo, M., Negrini, S., Weiss, H. R., Grivas, T. B., Maruyama, T., & Kotwicki, T. (2006). SOSORT consensus paper on brace action: TLSO biomechanics of correction (investigating the rationale for force vector selection). *Scoliosis*, 1(1), 11-11. <https://doi.org/10.1186/1748-7161-1-11>
- Rigo, M. D., Villagrasa, M., & Gallo, D. (2010). A specific scoliosis classification correlating with brace treatment: description and reliability. *Scoliosis*, 5(1), 1-1. <https://doi.org/10.1186/1748-7161-5-1>
- Rothmaier, M., Luong, M. P., & Clemens, F. (2008a). Textile Pressure Sensor Made of Flexible Plastic Optical Fibers. *Sensors*, 8(7), 4318-4329. <https://doi.org/10.3390/s8074318>
- Rothmaier, M., Selm, B., Spichtig, S., Haensse, D., & Wolf, M. (2008b). Photonic textiles for pulse oximetry. *Opt Express*, 16(17), 12973-12986. <https://doi.org/10.1364/oe.16.012973>
- Roudjane, M., Khalil, M., Miled, A., & Messaddeq, Y. (2018). New Generation Wearable Antenna Based on Multimaterial Fiber for Wireless Communication and Real-Time Breath Detection. *Photonics*, 5(4), 33. <https://doi.org/10.3390/photonics5040033>
- Rupp, R. F., Vásquez, N. G., & Lamberts, R. (2015). A review of human thermal comfort in the built environment. *Energy and Buildings*, 105, 178-205. <https://doi.org/https://doi.org/10.1016/j.enbuild.2015.07.047>
- Schlösser, T. P. C., van der Heijden, G. J. M. G., Versteeg, A. L., & Castelein, R. M. (2014). How 'Idiopathic' Is Adolescent Idiopathic Scoliosis? A Systematic Review on Associated Abnormalities. *PLoS One*, 9(5), e97461. <https://doi.org/10.1371/journal.pone.0097461>
- Schneegass, S. (2017). *Smart Textiles: Fundamentals, Design, and Interaction*. Springer. <https://doi.org/10.1007/978-3-319-50124-6>

- Schrank, V., Beer, M., Beckers, M., & Gries, T. (2017). 10 - Polymer-optical fibre (POF) integration into textile fabric structures. In C.-A. Bunge, T. Gries, & M. Beckers (Eds.), *Polymer Optical Fibres* (pp. 337-348). Woodhead Publishing. <https://doi.org/https://doi.org/10.1016/B978-0-08-100039-7.00010-5>
- Schwarz-Pfeiffer, A., Mecnika, V., Beckers, M., Gries, T., & Jockenhoevel, S. (2015). Optical Fibers. In X. Tao (Ed.), *Handbook of Smart Textiles* (pp. 79-108). Springer Singapore. [https://doi.org/10.1007/978-981-4451-45-1\\_4](https://doi.org/10.1007/978-981-4451-45-1_4)
- Schwieger, T., Campo, S., Weinstein, S. L., Dolan, L. A., Ashida, S., & Steuber, K. R. (2017). Body Image and Quality of Life and Brace Wear Adherence in Females With Adolescent Idiopathic Scoliosis. *J Pediatr Orthop*, 37(8), e519-e523. <https://doi.org/10.1097/BPO.0000000000000734>
- Selm, B., Gürel, E. A., Rothmaier, M., Rossi, R. M., & Scherer, L. J. (2010). Polymeric Optical Fiber Fabrics for Illumination and Sensorial Applications in Textiles. *Journal of Intelligent Material Systems and Structures*, 21(11), 1061-1071. <https://doi.org/10.1177/1045389X10377676>
- Sensor Products Inc. (2023). *Surface Pressure Mapping Sensors*. Retrieved 12 August 2023 from [https://www.sensorprod.com/pressurex\\_micro.php](https://www.sensorprod.com/pressurex_micro.php)
- Shaker, K. (2018). Clothing for Extreme Cold Weather. *Material, Properties, Production and Testing. National Textile University*, (1), 1-12.
- Shishoo, R. (2000). *Objective measurement of fabric handle: Dream or reality*. Proceedings of Avantex, International Symposium for High-Tech Apparel Textiles and Fashion Engineering with Innovation-Forum, Frankfurt, Germany. [https://www.researchgate.net/publication/271642451\\_Objective\\_Measurement\\_of\\_Fabric\\_Handle\\_Dream\\_or\\_Reality](https://www.researchgate.net/publication/271642451_Objective_Measurement_of_Fabric_Handle_Dream_or_Reality)
- Shmerling, R. H. (2017). *Health reference series: Harvard Medical School health topics A-Z*. Harvard Health Publications. Retrieved 19 April 2020 from <https://search.credoreference.com/content/entry/hhphealth/scoliosis/0>
- Silva, A., Catarino, A., Correia, M., & Frazão, O. (2013). Design and characterization of a wearable macrobending fiber optic sensor for human joint angle determination. *Optical Engineering*, 52, 126106-126106. <https://doi.org/10.1117/1.OE.52.12.126106>
- Sirkis, T., Beiderman, Y., Agdarov, S., Beiderman, Y., & Zalevsky, Z. (2017). Fiber sensor for non-contact estimation of vital bio-signs. *Optics communications*, 391, 63-67. <https://doi.org/10.1016/j.optcom.2017.01.013>

- Siyao, M., Liu, S., Peihua, Z., & Hairu, L. (2020). Functional investigation on automotive interior materials based on variable knitted structural parameters. *Polymers*, 12(11), 1-20. <https://doi.org/10.3390/polym12112455>
- Smania, N., Picelli, A., Romano, M., & Negrini, S. (2008). Neurophysiological basis of rehabilitation of adolescent idiopathic scoliosis. *Disabil Rehabil*, 30(10), 763-771. <https://doi.org/10.1080/17483100801921311>
- Smith, J. S., Shaffrey, C. I., Kuntz, C., & Mummaneni, P. V. (2008). CLASSIFICATION SYSTEMS FOR ADOLESCENT AND ADULT SCOLIOSIS. *Neurosurgery*, 63(suppl\_3), A16-A24. <https://doi.org/10.1227/01.neu.0000320447.61835.ea>
- Speijers, J., Stanton, J. H., Naylor, G. R., Ramankutty, P., & Tester, D. (2015). Skin comfort of base layer wool garments. Part 3: The effect of ethnicity on perceptions of comfort using Chinese and Australian wearers. *Textile research journal*, 85(11), 1167-1180.
- Spoonamore, M. J. (2023). *Scoliosis in Children*. Univesity of Southern California. Retrieved 19 April 2023 from <https://www.uscspine.com/childrens-spine-surgery/scoliosis/>
- SportingTex. (2021). *Cooling Fabrics*. Retrieved 4 April 2020 from <https://www.sportingtex.com/cooling-fabric>
- Stokes, I. A., Sangole, A. P., & Aubin, C.-E. (2009). Classification of scoliosis deformity 3-d spinal shape by cluster analysis. *Spine*, 34(6), 584.
- Stoppa, M., & Chiolerio, A. (2014). Wearable Electronics and Smart Textiles: A Critical Review. *Sensors*, 14(7), 11957-11992. <https://doi.org/10.3390/s140711957>
- Sumin, L., Kimura, D., Keun Hyung, L., Park, J. C., & Ick Soo, K. (2010). The Effect of Laundering on the Thermal and Water Transfer Properties of Mass-produced Laminated Nanofiber Web for Use in Wear. *Textile research journal*, 80(2), 99-105. <https://doi.org/10.1177/0040517508102308>
- Tadesse, M. G., Chen, Y., Wang, L., Nierstrasz, V., & Loghin, C. (2018). Tactile Comfort Evaluation of Conductive Knitted Fabric Using KES-FB. *IOP Conference Series: Materials Science and Engineering*, 374, 012056. <https://doi.org/10.1088/1757-899x/374/1/012056>
- Tang, A. Y., Lo, C. K., & Kan, C. w. (2018). Textile dyes and human health: A systematic and citation network analysis review. *Coloration Technology*, 134(4), 245-257.

- Tang, Y., Yu, H., Wang, Z., Luo, M., Zhang, K., Jiao, Y., & Li, C. (2020). Typical winter clothing characteristics and thermal insulation of ensembles for older people in China. *Building and Environment*, 182, 107127. <https://doi.org/https://doi.org/10.1016/j.buildenv.2020.107127>
- Tao, X. (2005). 7 - Wearable photonics based on integrative polymeric photonic fibres. In X. Tao (Ed.), *Wearable Electronics and Photonics* (pp. 136-154). Woodhead Publishing. <https://doi.org/https://doi.org/10.1533/9781845690441.136>
- Tencel. (2020). *About Tencel fibers*. Tencel. Retrieved 24 September 2020 from <https://www.tencel.com/about>
- Tessadri, F., Pellegrini, A., Tavernaro, M., Zonta, A., & Negrini, S. (2012). Importance of team to increase compliance in adolescent spinal deformities brace treatment: a cross-sectional study of two different settings. *Scoliosis*, 7(S1), O5-O5. <https://doi.org/10.1186/1748-7161-7-S1-O5>
- The Insight Partners. (2020). *Smart Textile Market is expected to reach US\$ 13.63 Bn in 2027*. Retrieved 11 April 2020 from <https://www.theinsightpartners.com/pr/smart-textile-market>
- Thiele, E. (2003). Gewirkte lichtnetze-ein leuchtendes beispiel textiler innovation (Knitted light nets - a shining example of textile innovation). *Kettenwirk-Praxis*, 37, 24.
- Tong, S.-f., Yip, J., Yick, K.-l., & Yuen, C.-w. M. (2015). Exploring use of warp-knitted spacer fabric as a substitute for the absorbent layer for advanced wound dressing. *Textile research journal*, 85(12), 1258-1268. <https://doi.org/10.1177/0040517514561922>
- TORAY Group. (2020a). *CEOα™*. Retrieved 4 September 2020 from [https://www.toray.com/products/fibers/fib\\_0040.html#](https://www.toray.com/products/fibers/fib_0040.html#/)
- TORAY Group. (2020b). *LYCRA®*. Retrieved 4 September 2020 from [https://www.toray.com/products/fibers/fib\\_0140.html](https://www.toray.com/products/fibers/fib_0140.html)
- Uniqlo. (2021). *Women's AIRism Innerwear*. Retrieved 28 April 2021 from <https://www.uniqlo.com/feature/airism/eu/en/inner/women/>
- Van Eck, N. J., & Waltman, L. (2014). CitNetExplorer: A new software tool for analyzing and visualizing citation networks. *Journal of informetrics*, 8(4), 802-823.

- Van Langenhove, L. (2015). Smart Textiles: Past, Present, and Future. In X. Tao (Ed.), *Handbook of Smart Textiles* (pp. 1035-1058). Springer. [https://doi.org/10.1007/978-981-4451-45-1\\_15](https://doi.org/10.1007/978-981-4451-45-1_15)
- Van Langenhove, L., Puers, R., & Matthys, D. (2005). 7 - Intelligent textiles for protection. In R. A. Scott (Ed.), *Textiles for Protection* (pp. 176-195). Woodhead Publishing. <https://doi.org/https://doi.org/10.1533/9781845690977.1.176>
- Vanegas, E., Igual, R., & Plaza, I. (2020). Sensing systems for respiration monitoring: A technical systematic review. *Sensors*, 20(18), 5446.
- Verma, P. (2010). *Modal: Fibre to Fabric*. Fibre 2 Fasion. Retrieved 7 September 2020 from <https://www.fibre2fashion.com/industry-article/5169/modal-fibre-to-fabric>
- Vivekanadana, M. V., Raj, S., Suffixeenivasan, S., & Nachane, R. P. (2011). Parameters affecting warm-cool feeling in cotton denim fabrics. *Indian journal of fibre and textile research*, 36(2), 117-121.
- Weinstein, S. L., Dolan, L. A., Wright, J. G., & Dobbs, M. B. (2013a). Design of the Bracing in Adolescent Idiopathic Scoliosis Trial (BrAIST). *Spine (Phila Pa 1976)*, 38(21), 1832-1841. <https://doi.org/10.1097/01.brs.0000435048.23726.3e>
- Weinstein, S. L., Dolan, L. A., Wright, J. G., & Dobbs, M. B. (2013b). Effects of Bracing in Adolescents with Idiopathic Scoliosis. *N Engl J Med*, 369(16), 1512-1521. <https://doi.org/10.1056/NEJMoa1307337>
- Weiss, H. R., Negrini, S., Hawes, M. C., Rigo, M., Kotwicki, T., Grivas, T. B., & Maruyama, T. (2006). Physical exercises in the treatment of idiopathic scoliosis at risk of brace treatment -- SOSORT consensus paper 2005. *Scoliosis*, 1(1), 6-6. <https://doi.org/10.1186/1748-7161-1-6>
- Weiss, H. R., Werkmann, M., & Stephan, C. (2007). Brace related stress in scoliosis patients - Comparison of different concepts of bracing. *Scoliosis*, 2(1), 10-10. <https://doi.org/10.1186/1748-7161-2-10>
- Weiss, H. R. (2003). Conservative treatment of idiopathic scoliosis with physical therapy and orthoses. *Orthopade*, 32(2), 146.
- Weiss, H. R. (2010). Spinal deformities rehabilitation - state of the art review. *Scoliosis*, 5(1), 28-28. <https://doi.org/10.1186/1748-7161-5-28>
- Werneck, M. M., Allil, R., Ribeiro, B. A., & De Nazare, F. V. (2013). A guide to fiber Bragg grating sensors. *Current trends in short-and long-period fiber gratings*, 1-24.

- Wiseman, J., Simons, M., Kimble, R., & Tyack, Z. (2018). Reliability and clinical utility of the Pliance X for measuring pressure at the interface of pressure garments and burn scars in children. *Burns*, 44(7), 1820-1828. <https://doi.org/https://doi.org/10.1016/j.burns.2018.05.002>
- Witt, J., Narbonneau, F., Schukar, M., Krebber, K., De Jonckheere, J., Jeanne, M., Kinet, D., Paquet, B., Depre, A., D'Angelo, L. T., Thiel, T., & Logier, R. (2012). Medical Textiles With Embedded Fiber Optic Sensors for Monitoring of Respiratory Movement. *IEEE Sensors Journal*, 12(1), 246-254. <https://doi.org/10.1109/JSEN.2011.2158416>
- Wong, M. S., Cheng, J. C. Y., Lam, T. P., Ng, B. K. W., Sin, S. W., Lee-Shum, S. L. F., Chow, D. H. K., & Tam, S. Y. P. (2008). The effect of rigid versus flexible spinal orthosis on the clinical efficacy and acceptance of the patients with adolescent idiopathic scoliosis. *Spine (Phila Pa 1976)*, 33(12), 1360-1365. <https://doi.org/10.1097/BRS.0b013e31817329d9>
- Wong, M. S., Mak, A. F. T., Luk, K. D. K., Evans, J. H., & Brown, B. (2016). Effectiveness and biomechanics of spinal orthoses in the treatment of adolescent idiopathic scoliosis (AIS). *Prosthet Orthot Int*, 24(2), 148-162. <https://doi.org/10.1080/03093640008726538>
- Yahyaiee Babil, A., & Rouhi, G. (2020). The biomechanical performance of the night-time Providence brace: experimental and finite element investigations. *Heliyon*, 6(10), e05210-e05210. <https://doi.org/10.1016/j.heliyon.2020.e05210>
- Yamada, Y. (2020). Textile-integrated polymer optical fibers for healthcare and medical applications. *Biomed Phys Eng Express*, 6(6). <https://doi.org/10.1088/2057-1976/abbf5f>
- Yip, J., & Chan, W.-Y. (2020). 3 - Textile fibers and fabrics. In (pp. 47-72): Elsevier Ltd.
- Yip, J., & Ng, S.-P. (2008). Study of three-dimensional spacer fabrics: Physical and mechanical properties. *Journal of materials processing technology*, 206(1-3), 359-364. <https://doi.org/10.1016/j.jmatprotec.2007.12.073>
- Yu, W., Fan, J.-t., & Qian, X.-m. (2004). A Soft Mannequin for the Evaluation of Pressure Garments on the Human Body. *Journal of Fiber Science and Technology* 60(2), 57-64. <https://doi.org/10.2115/fiber.60.57>



- Zaborowska-Sapeta, K., Kowalski, I. M., Kotwicki, T., Protasiewicz-Fałdowska, H., & Kiebzak, W. (2011). Effectiveness of Chêneau brace treatment for idiopathic scoliosis: prospective study in 79 patients followed to skeletal maturity. *Scoliosis*, 6(1), 2-2. <https://doi.org/10.1186/1748-7161-6-2>
- Zaina, F., De Mauroy, J., Grivas, T., Hresko, M., Kotwizki, T., Maruyama, T., Price, N., Rigo, M., Stikeleather, L., & Wynne, J. (2014). Bracing for scoliosis in 2014: state of the art. *Eur J Phys Rehabil Med*, 50(1), 93-110.
- Zaina, F., Romano, M., Knott, P., de Mauroy, J. C., Grivas, T. B., Kotwicki, T., Maruyama, T., O'Brien, J., Rigo, M., & Negrini, S. (2015). Research quality in scoliosis conservative treatment: state of the art. *Scoliosis*, 10(1), 21. <https://doi.org/10.1186/s13013-015-0046-7>
- Zendehnam, A., Mirzaei, M., Farashiani, A., & Horabadi Farahani, L. (2010). Investigation of bending loss in a single-mode optical fibre. *Pramana - J Phys*, 74(4), 591-603. <https://doi.org/10.1007/s12043-010-0052-5>
- Zhang, C., & Wang, F. (2020). Comfort Management of Fibrous Materials. *Handbook of fibrous materials*, 857-887.
- Zhang, L., Pan, J., Zhang, Z., Wu, H., Yao, N., Cai, D., Xu, Y., Zhang, J., Sun, G., Wang, L., Geng, W., Jin, W., Fang, W., Di, D., & Tong, L. (2020). Ultrasensitive skin-like wearable optical sensors based on glass micro/nanofibers. *Opto-Electronic Advances*, 3(3), 19002201-19002207. <https://doi.org/10.29026/oea.2020.190022>
- Zheng, W. (2014). *Light intensity-based wearable polymer optical fiber (POF) sensors: design, fabrication and characterization*. [Doctoral dissertation, The Hong Kong Polytechnic University]. PolyU e-Theses. <https://theses.lib.polyu.edu.hk/handle/200/7450>
- Zheng, W., Tao, X., Zhu, B., Wang, G., & Hui, C. (2014). Fabrication and evaluation of a notched polymer optical fiber fabric strain sensor and its application in human respiration monitoring. *Textile research journal*, 84(17), 1791-1802. <https://doi.org/10.1177/0040517514528560>
- Zhou, J., Li, Y., Lam, J., & Cao, X. (2010). The Poisson ratio and modulus of elastic knitted fabrics. *Textile Research Journal*, 80(18), 1965-1969.
- Zhuge, H. (2016). *Multi-Dimensional Summarization in Cyber-Physical Society* (1 ed.). Elsevier.
- Zubia, J., & Arrue, J. (2001). Plastic Optical Fibers: An Introduction to Their Technological Processes and Applications. *Optical Fiber Technology*, 7(2), 101-140. <https://doi.org/10.1006/ofte.2000.0355>